Istituto Universitario
di Studi Superiori di Pavia

Università degli Studi
di Pavia

EUROPEAN SCHOOL OF ADVANCED STUDIES IN REDUCTION OF SEISMIC RISK

ROSE SCHOOL

SEISMOLOGICAL CRITERIA FOR SELECTING AND SCALING REAL ACCELEROGRAMS FOR USE IN ENGINEERING ANALYSIS AND DESIGN

A Dissertation Submitted in Partial Fulfilment of the Requirements for the Master Degree in

EARTHQUAKE ENGINEERING

By

ANA BEATRIZ ACEVEDO JARAMILLO

Supervisor: Dr JULIAN J. BOMMER

June, 2003

The dissertation entitled “Seismological criteria for selecting and scaling real accelerograms for use in engineering analysis and design”, by Ana Beatriz Acevedo Jaramillo, has been approved in partial fulfilment of the requirements for the Master Degree in Earthquake Engineering.

Julian J. Bommer

David M. Boore

ABSTRACT

When dynamic analysis is needed, seismic actions need to be defined in terms of accelerograms. There are three fundamental types of accelerograms available: artificial records compatible with the design response spectrum, synthetic records obtained from seismological models and real accelerograms recorded in earthquakes. This work focuses on the most accessible solution for engineering applications: the selection, and when needed scaling, of real accelerograms.

The first issue addressed is the criteria used to select real records. The two basic options are to select records that match some specified feature of the ground motion, such as the elastic response spectrum, or to select on the basis of an earthquake scenario. The latter is shown to be a preferable approach, with the minimum parameters being the magnitude, distance and site classification.

Once the records are selected, it will generally be necessary to scale them to match the elastic response spectrum of acceleration. Matching criteria must be established to judge the degree to which the scaled records are compatible with the design criteria, for which it is judged that at least two of the following should be considered: divergence, over a given period range, between the mean of the scaled records and the design spectrum; covariance of the scaled spectra; maximum residual between a scaled record and the design spectrum.

When the criteria for matching are chosen, the final issue is to choose a scaling technique to achieve the required adjustment to the real records. Based on the premise that the scaled records should retian the characteristics of real records, options based on spectral amplitudes and intensities are explored to derive linear scaling factors to be applied to amplitudes; scaling of the time axis is discouraged because it changes the frequency content and duration without altering the number of cycles and is hence unlikely to result in realistic motions. An important issue that is addressed is the maximum scaling factor that can be applied, since the limit of two established by Vanmarcke (1979) has been widely adopted in practice without any rigorous re-evaluation. The conclusion is that provided the selection criteria outlined above are used to obtain the suite of real accelerograms, scaling factors

significantly outside the range of 0.5 to 2.0 can be applied to obtain acceptable input to dynamic analyses.

ACKNOWLEDGEMENTS

Thanks a lot for the guidance, support and good advise of the professors and professionals that have influenced and helped me pursuit my studies: Josef Farbiarz F., Dr. Elkín Castrillón O. and Luis Gonzalo Mejía C.

Special gratitude to my adviser, Dr. Julian J. Bommer for being an excellent guide and having the patience to take on somebody without any knowledge in seismology and sharing through the work a lot of his knowledge on the subject.

Thanks to Prof. Gian Michele Calvi and to ROSE School for giving me the great opportunity of being part of this excellent school, and for the financial support during the year of my master.

An special acknowledgment to Dr. David M. Boore for being a referee of this work and his useful comments.

Finally, the most important thanks to my family: my mom, my dad, my brother and my sister. You have been a great support and a perfect example to follow in everything I have done.

SEISMOLOGICAL CRITERIA FOR SELECTING AND SCALING REAL ACCELEROGRAMS FOR USE IN ENGINEERING ANALYSIS AND DESIGN

INDEX

	page
ABSTRACT …….	i
ACKNOWLEDGEMENTS …….	iii
INDEX ……..	iv
LIST OF TABLES ……	viii
LIST OF FIGURES ……..	x
1. INTRODUCTION ……	1
1.1. The need for accelerograms ……	1
1.2. Types of accelerograms ……...	1
1.2.1. Real accelerograms ……	2
1.2.2. Artificial accelerograms …….	2
1.2.3. Synthetic accelerograms …….	2
1.3. Objectives of the thesis ……..	4
2. ACCELEROGRAMS ……..	6
2.1. Accelerographs and accelerograms …….	6

page

2.2. Characterisation of accelerograms …….. 7

2.2.1. Peak ground motions …….. 7
2.2.2. Arias intensity …… 8
2.2.3. Root-mean-square (RMS) acceleration …….. 9
2.2.4. Duration ……. 10
2.2.5. Equivalent number of uniform stress cycles (N) …….. 12
2.2.5. Response spectra …… 12
2.2.6. Spectrum intensity (SI) …….. 13
2.2.7. Iv index …….. 13

3. FACTORS INFLUENCING ACCELEROGRAMS …… 15

3.1. Source …… 15

3.1.1. Magnitude …….. 15
3.1.2. Rupture mechanism …… 17
3.1.3. Directivity …….. 18
3.1.4. Focal depth ……. 20

3.2. Path ……. 20

3.2.1. Distance …….. 21
3.2.2. Crustal structure ……. 22

3.2. Site …….. 22

3.3.1. Surface geology ……. 22
3.3.2. Topography …… 25
3.3.3. Structures …… 26

4. ATTENUATION RELATIONSHIPS ……. 28

4.1. General …… 28

4.2. Relationships for spectral ordinates …… 32

4.2.1. Magnitude …….. 32
4.2.2. Distance ……. 33
4.2.3. Site condition ……. 35
4.2.4. Fault mechanism …… 36
4.2.5. Focal depth ……. 39
4.2.6. Directivity …….. 40

4.3. Relationships for Arias intensity ……. 41

4.4. Relationships for duration ……... 43

4.5. Relationships for the equivalent number of uniform stress cycles (N) ……... 45

4.6. Uncertainty in attenuation relationships …….. 46

page

5. INFLUENCE OF DIFFERENT FACTORS AFFECTING STRONG-MOTION ……... 48

5.1. Relationships for Spectral Ordinates ……... 48

5.1.1. Magnitude …….. 48
5.1.2. Distance ……. 49
5.1.3. Soil condition ……. 51
5.1.4. Fault mechanism …… 53
5.1.5. Focal depth ……. 54
5.1.6. Directivity …….. 56

5.2. Relationships for Arias intensity ……. 57

5.3. Relationships for duration ……... 58

5.4. Relationships for the equivalent number of uniform stress cycles (N) ……... 59

5.5. Relative influence of explanatory parameters on response parameters …….. 60

5.6. Examples of variation of parameters with scaling …….. 67

6. REVIEW OF SELECTION AND SCALING PROCEDURES …….. 72

6.1. SELECTION PROCEDURES …… 73

6.2. SCALING PROCEDURES ……. 79

6.2.1. Scaling on the basis of strong-motion parameters ……. 80
6.2.1.1. Scaling to the peak ground parameters (PGA and PGV) …….. 80
6.2.1.2. Scaling to AI (Arias intensity) …….. 81
6.2.1.3. Scaling to the RMS (root-mean-square) acceleration …….. 81
6.2.1.4. Scaling to the SI (spectrum intensity) ……... 82
6.2.1.5. Scaling to the Iv index …….. 82
6.2.1.6. Scaling to Sa (spectral acceleration) ……. 83
6.2.1.7. Scaling in time ……... 84
6.2.2. Scaling by wavelets or Fourier transform ……. 87
6.2.3. Scaling on the basis of seismological parameters…….. 92

7. DEFINITION OF SELECTION AND SCALING CRITERIA …….. 93

7.1. Selection of real records …….. 93

7.2. Criteria for judging effectiveness of scaling procedures ……. 95

7.3. Scaling on the basis of seismological parameters ……... 95

7.4. Scaling in amplitude …… 97

7.5. Scaling in time and amplitude …… 98

7.6. Limits on scaling ……. 98

page

8. EXPLORATORY ANALYSES ……... 100

8.1. Scaling performance …… 100

8.1.1. Different recorded earthquakes …….. 101
8.1.2. Multiply-recorded earthquakes …… 110
8.1.3. Bins scaled to a smaller distance ……... 115

8.2. Exploration of limits on scaling …….. 121

9. DISCUSSION and CONCLUSIONS ……... 129

10. BIBLIOGRAPHY …… 134

ANNEX 1 Attenuation equations for response spectral ordinates

ANNEX 2 Attenuation equations for PGA including explicit treatment of focal depth

ANNEX 3 Attenuation equations for Arias intensity

ANNEX 4 Attenuation equations for duration and equivalent number of uniform stress cycles(N)

ANNEX 5 McGuire et al (2001) strong-motion database

LIST OF TABLES

3.1. Simplified geotechnical site categories (Rodríguez-Marek et al., 2001).
4.1. Parameters included in some attenuation relationship for spectral ordinates.
4.2. Parameters included on some attenuation relationship for Arias Intensity.
5.1. Comparison of the maximum ratio of the Sa(T) values for the normalised spectra considered in Figures 4.5 and 4.6 with the scenarios of Figures 4.7 and 4.8.
5.2. Time-histories selected.
5.3. Variation of the strong-motion parameters with scaling on amplitude and time for the 1984 Morgan Hill earthquake.
5.4. Variation of the strong-motion parameters with scaling on amplitude and time for the 1983 Coalinga earthquake.
5.5. Variation of the strong-motion parameters with scaling on amplitude and time for the 1971 San Fernando earthquake.
6.1. Variation of the duration and Equivalent Number of Uniform Stress Cycles (N) for the 1984 Morgan Hill earthquake (magnitude 6.2).
6.2. Variation of the duration and Equivalent Number of Uniform Stress Cycles (N) for the 1983 Coalinga earthquake (magnitude 6.4).
6.3. Variation of the duration and Equivalent Number of Uniform Stress Cycles (N) for the 1971 San Fernando earthquake (magnitude 6.6).
8.1. Characteristics of the bins.
8.2. Scaling factors for bin BA.
8.3. Scaling factors for bin BB.
8.4. Scaling factors for bin BC.
8.5. Scaling factors for bin BD.
8.6. Scaling factors for bin BE.
8.7. Convention to indicate scaling performance.
8.8. Scaling factors for bin BF.
8.9. Scaling factors for bin BG.
8.10. Scaling factors for bin BH.
8.11. Characteristics of bins BA*, BC* and BE*.
8.12. Scaling factors for bin BA*.
8.13. Scaling factors for bin BC*.
8.14. Scaling factors for bin BE*.
8.15. Characteristics of the bins.
8.16. Characteristics of bins BI (Whittier Narrows earthquake)
8.17. Characteristics of bins BJ (Loma Prieta earthquake)
8.18. Characteristics of bins BK (Northridge earthquake)
8.19. Scaling factors for bin BI.

8.20. Scaling factors for bin BJ.
8.21. Scaling factors for bin BK.
8.22. Strong-motion parameters for the Whittier Narrows records (bin BI).
8.23. Strong-motion parameters for the Loma Prieta records (bin BJ).
8.24. Strong-motion parameters for the Northridge records (bin BK).

LIST OF FIGURES

2.1. Accelerograms with identical values of PGA (Bommer, 1991).
2.2. Accelerogram from the 1978 Tabas earthquake in Iran, with velocity and displacement time-histories (Bommer and Elnashai, 1999).
2.3. Husid plots for combined horizontal components for two accelerograms recorded in San Salvador, with the same total energy but at different periods of time. $M_s = 7.3$ for the offshore earthquake in 1982 (solid line) and $M_s = 5.4$ for the local earthquake in 1986 (dashed line). (Bommer, 2001)
2.4. Integration of squared acceleration. Curves represent the sum of the three components of motion in centimetre-second units. (Housner and Jennings, 1977)
2.5. The definition of bracketed duration, D_b (Bommer and Martínez-Pereira, 1999).
2.6. The definition of uniform duration, D_u (Bommer and Martínez-Pereira, 1999).
2.7. The definition of significant duration, D_s (Bommer and Martínez-Pereira, 1999).
2.8. Definition of the response spectrum (Tsangaris, 1996).
3.1. Comparison of moment magnitude scale with other magnitude scales (Reiter, 1990). Figure originally derived by Hiroo Kanamori.
3.2. Mechanisms of fault rupture (Reiter, 1990).
3.3. Definition of the dip (δ), strike (ϕ) and rake (λ) angles of a fault rupture (Shearer, 1999).
3.4. Near-field velocity time-histories from accelerograms of the 1992 Landers earthquake in California, showing the effect of rupture directivity on the recorded motion (Somerville *et al*., 1997).
3.5. Near-field directivity parameters (Somerville *et al*., 1997).
3.6. Definitions of source-to-site distance used in attenuation studies (Abrahamson and Shedlock, 1997).
3.7. Acceleration response spectra of records from the 1985 Michoacán earthquake recorded in Mexico City on rock (UNAM) and soft soil (SCT) sites (Kramer, 1996).
3.8. Relationship between structural damage intensity and soil depth for the 1967 Caracas earthquake (Seed *et al*., 1972).
3.9. Generalized 2D geometries of irregular surface topography (Stewart *et al*., 2001).
3.10. Acceleration spectra (2% damping) of transverse components of accelerograms obtained at Hollywood Storage Building during the San Fernando (California) earthquake of 1971, from instruments located in the basement of the 15-storey building (solid) and from a free-field instrument in the car park (dotted).
4.1 Attenuation of PGA with distance from earthquakes with M 5.5 and 6.5. *Left* - from the attenuation relationships for active tectonics regions (Ambraseys *et al*., 1996) with $M_s \sim M_w$ and stable continental regions for Mid-continent (Toro *et al*., 1997), *right* - from the attenuation relationship for subduction zones for interface earthquakes (Youngs *et al*, 1997).

4.2. Response spectral acceleration at 10 km from earthquakes of M = 5.5 and 6.5. *Left* - from the attenuation relationships for active tectonics regions (Ambraseys *et al*., 1996) with $M_s \sim M_w$ and stable continental regions for Mid-continent (Toro *et al*., 1997), right – from the attenuation relationship for subduction zones for interface earthquakes (Youngs *et al*, 1997).
4.3. Comparison of the PGA values for earthquakes with M 5.5, 6.5 and 7.5 ($M_s \sim M_w$) for rock sites from the attenuation relationships of Ambraseys *et al*. (1996) for Europe and Middle East and Boore *et al*. (1997) for Western North America with V_s = 620 m/s.
4.4. Comparison of the acceleration response spectra for earthquakes with M 5.5, 6.5 and 7.5 ($M_s \sim M_w$) for rock sites from the attenuation relationships of Ambraseys *et al*. (1996) for Europe and Middle East and Boore *et al*. (1997) for Western North America with V_s = 620 m/s.
4.5. Normalised spectral shapes for rock sites at 10 km from earthquakes of M 5, 6 and 7. *Left* - from the attenuation equations of Ambraseys *et al*. (1996), *right* – from the attenuation equations of Abrahamson and Silva (1997).
4.6. Normalised spectral shapes for rock sites at 10 km. *Left* - from earthquakes of M_w 5.5, 6 and 7 from the attenuation equations of Boore *et al*. (1997) with V_s = 620 m/s, *right* – from earthquakes of M_w 5, 6 and 7 from the attenuation equations of Campbell (1997).
4.7. Normalised spectral shapes for rock sites at 5, 20 and 50 km from a M 7 earthquake. *Left* - from the attenuation equations of Ambraseys *et al*. (1996), right – from the attenuation equations of Campbell (1997).
4.8. Normalised spectral shapes for rock sites at 5, 20 and 50 km from a M_w 7 earthquake. *Left* - from the attenuation equations of Boore *et al*. (1996) with V_s = 620 m/s, *right* – from the attenuation equations of Abrahamson and Silva (1997).
4.9. Acceleration response spectra predicted for a M_s 5.5 earthquake at 10 km according to the European equations of Ambraseys *et al*. (1996) for rock, stiff soil and soft soil sites.
4.10. Ratios of the soil ordinates to the rock spectrum for the attenuation relationship of Ambraseys *et al*. (1996) for stiff soil (solid line) and soft soil (dashed line).
4.11. Acceleration response spectra predicted for a M_w 5.5 earthquake at 10 km. *Left* – from the attenuation relationships of Campbell (1997) for hard rock, alluvium or firm soil and soft soil, *right* – from the attenuation relationships of Abrahamson and Silva (1997) for rock and deep soil.
4.12. Scaling of PGA with magnitude, distance and source mechanism form the attenuation relationship of Campbell (1997) for rock.
4.13. Scaling of PGA with magnitude, distance and source mechanism form the attenuation relationship of Abrahamson and Silva (1997) for rock.
4.14. Pseudo-absolute acceleration response spectra for an earthquake of magnitude M_w 7 at 5 and 20 km for strike-slip and reverse mechanisms. *Left* – from the attenuation relationship of Campbell (1997) for firm soil, *right* – from the attenuation relationship of Abrahamson and Silva (1997) for rock.
4.15. Attenuation of PGA with distance for an event of magnitude M_w 6.5 for a strike-slip event and a reverse event from the attenuation relationship of Abrahamson and Silva (1997) for rock with and without the hanging wall effect.
4.16. Acceleration response spectra for an earthquake at 10 km for rock sites with a magnitude M_w 6.5 for a strike-slip event and a reverse event from the attenuation relationship of Abrahamson and Silva (1997) with and without the hanging wall effect.
4.17. Attenuation of PGA with distance for an M_s 5 using the equations of Ambraseys and Bommer (1991) with constant depth (dashed) and explicit focal depth (solid lines).
4.18. Empirical modification factors for acceleration response spectrum ordinates (Somerville *et al*., 1997)
4.19. Median value of Arias Intensity for rock sites using the equations of Travasarou *et al*. (2002) for earthquakes with magnitude M_w = 5.5, 6.5 and 7.5.
4.20. Predicted values of bracketed duration (a_0 = 0.05g) as a function of distance for a magnitude 6.5 earthquake according to the attenuation relationships of McGuire and Barnhard (1979) and Papazachos *et al*. (1992) for rock sites, and Kawasima and Aizawa (1989), which is independent of site condition.

4.21. Prediction of 5-75% significant duration for rock sites using the equations of Abrahamson and Silva (1996).
4.22. Prediction of 5-95% significant duration for rock sites using the equations of Trifunac and Brady (1975), McGuire and Barnhard (1979) and the Kamiyama (1984) for focal depth of 10 km.
4.23. Equivalent number of uniform stress cycles for rock sites, using the equations of Liu *et al*. (2001).
4.24. Response spectra for rock sites at 10 km for earthquakes of magnitude M_w 6 and 7 from the attenuation relationships of Boore *et al*. (1997) with V_s = 620 m/s and the equation of Abrahamson and Silva (1997).
5.1. Spectral shapes for rock sites at 10 km from earthquakes of M 6, 6.5 and 7 for median values (solid lines) and median plus/minus the standard deviation for the earthquake of M = 6 (dashed). *Left* - from the attenuation equations of Ambraseys *et al*. (1996), *right* – from the attenuation equations of Abrahamson and Silva (1997).
5.2. Spectral shapes for rock sites at 10 km from earthquakes of M_w 6, 6.5 and 7. *Left* - for median values (solid lines) and median*$10^{\sigma logy}$ and median/$10^{\sigma logy}$ for the earthquake of M_w = 6 (dashed) from the attenuation equations of Boore *et al*. (1997) with V_s = 620 m/s, *right* - for median values (solid lines) and median plus/minus the standard deviation for the earthquake of M_w = 6 (dashed) from the attenuation equations of Campbell (1997).
5.3. Spectral shapes for rock sites from a M 7 earthquake at 5, 10 and 20 km for median values (solid lines) and median plus/minus the standard deviation at 10 km (dashed). *Left* - from the attenuation equations of Ambraseys *et al*. (1996), *right* – from the attenuation equations of Campbell (1997).
5.4. Spectral shapes for rock sites from a M_w 7 earthquake at 5, 10 and 20 km. *Left* - for median values (solid lines) and median*$10^{\sigma logy}$ and median/$10^{\sigma logy}$ at 10 km (dashed) from the attenuation equations of Boore *et al*. (1997) with V_s = 620 m/s, *right* - for median values (solid lines) and median plus/minus the standard deviation at 10 km (dashed) from the attenuation equations of Abrahamson and Silva (1997).
5.5. Response spectra for earthquakes at 10 km sites of magnitude M 5.5 and 6 for rock sites (solid lines) and for an earthquake of magnitude M 5.5 for stiff and soft sites (dashed lines). *Left* - from the attenuation relationship of Ambraseys *et al*. (1996), *right* - from the attenuation relationship of Boore *et al*. (1997).
5.6. Response spectra for earthquakes at 10 km sites of magnitude M_w 5.5 and 6 for rock sites (solid lines) and for an earthquake of magnitude M_w 5.5 for soil sites (dashed lines). *Left* – from the attenuation relationship of Campbell (1997), *right* – from the attenuation relationship of Abrahamson and Silva (1997).
5.7. Spectral shapes of an earthquake with magnitude M 5.5 at 10 km sites for the median values for rock and soil sites and median plus/minus the standard deviation for rock sites. *Left* – from the attenuation equations of Ambraseys *et al*. (1996), *right* – from the attenuation equations of Abrahamson and Silva (1997).
5.8. Pseudo-absolute acceleration response spectra for earthquakes of magnitudes M_w 5.5 and 6.5 *Left* - from the attenuation equations of Campbell (1997) for firm soil at 5 km with strike slip and reverse faults, *right* – from the attenuation equations of Abrahamson and Silva (1997) for rock soil at 5 km sites and reverse faults.
5.9. Influence of the standard error on pseudo-absolute acceleration response spectra for earthquakes of magnitude M_w 7 for rock soils at 5 km sites. *Left* - from the attenuation relationship of Campbell (1997), *right* – from the attenuation relationship of Abrahamson and Silva (1997).
5.10. Attenuation of PGA with distance for earthquakes with M_s 5, 6 and 7 using the equations of Ambraseys and Bommer (1991) with a focal depth of 5 (solid lines) and 20 km (dashed lines).
5.11. Attenuation of PGA with distance for earthquakes with M_s 5 using the equations of Ambraseys and Bommer (1991) for the median values for focal depths of 2, 5, 10 and 20 km (solid lines) and the median plus/minus one standard deviation for a focal depth of 5 km (dashed lines).

5.12. Effect of rupture directivity on the acceleration response spectra for an earthquake of magnitude M_w = 6.5 for rock soil at 10 km sites form the attenuation relationship of Abrahamson and Silva (1997). *Left* – for strike-slip faulting, *right* – for dip-slip faulting.
5.13. Median value of Arias intensity from earthquakes of M_w 5.5, 6.5 and 7.5 using the equations of Travasarou *et al*. for site category B (rock) and for strike slip and reverse faults.
5.14. Median value of Arias intensity from earthquakes of M_w 5.5, 6.5 and 7.5 using the equations of Travasarou *et al*. for strike-slip faults and for site category B (rock) and C (deep stiff soil).
5.15. Median value of the bracketed duration (a_0 = 0.05g) for earthquakes with magnitude 5, 6 and 7 and rock sites. *Left* – from the attenuation relationship of McGuire and Barnhard (1979), *right* – from the attenuation relationship of Papazachos *et al*. (1992)
5.16. Median value of the bracketed duration (a_0 = 0.05g) for earthquakes with magnitude 5, 6 and 7 from the attenuation relationship of Kawasima and Aizawa (1989).
5.17. Median values for the prediction of 5-95% significant duration for rock sites for earthquakes with magnitude 5, 6 and 7 and rock sites. *Left* – McGuire and Barnhard (1979), *right* – Trifunac and Brady (1975).
5.18. Median values for the prediction of 5-95% significant duration for rock sites for earthquakes with magnitude 5, 6 and 7 and rock sites from the attenuation relationship of Kamiyama (1984) for a focal depth of 10 km.
5.19. Equivalent number of uniform stress cycles using the equations of Liu *et al*. (2001) for earthquakes of magnitude 5, 6, 7 and 8 for deep soil sites (dashed lines) and shallow stiff soil or rock sites (solid lines).
5.20. Relative influence of explanatory parameters on response parameters by the attenuation relationship of Ambraseys *et al*. (1996).
5.21. Relative influence of explanatory parameters on response parameters by the attenuation relationship of Campbell. (1997).
5.22. Relative influence of explanatory parameters on response parameters by the attenuation relationship of Abrahamson and Silva. (1997).
5.23. Relative influence of explanatory parameters on response parameters by the attenuation relationship of Boore *et al*. (1997).
5.24. Comparison of the acceleration response spectra for the 1984 Morgan Hill, 1983 Coalinga and 1971 San Fernando earthquakes with the acceleration response spectra given by the attenuation relationship of Ambraseys *et al*. (1996) for rock sites for an event of magnitude 6.5 and source-site distance 30 km.
5.25. Variation of the acceleration response spectra with scaling for the 1984 Morgan Hill earthquake. *Left* - by scaling on amplitude, *right* – by scaling on time.
5.26. Variation of the acceleration response spectra with scaling for the 1983 Coalinga earthquake. *Left* - by scaling on amplitude, *right* – by scaling on time.
5.27. Variation of the acceleration response spectra with scaling for the 1971 San Fernando earthquake. *Left* - by scaling on amplitude, *right* – by scaling on time.
6.1. Selection procedures for strong-motion records.
6.2. Contributions to the 100,000-year seismic hazard at Colorado (USA) by magnitude, distance and e for the ordinate of spectral acceleration at a period of 0.1 second (top) and at 1.0 second (bottom) (McGuire, 1995).
6.3. Magnification factor required on basic search window (0.1 M_s and 4 km distance) for each magnitude-distance pair in order to obtain at least three accelerograms (Bommer and Scott, 2000).
6.4. Amplification factor required on basic search window (0.1 M_s and 4 km distance) for each magnitude-distance pair in order to obtain at least three accelerograms from rock sites (Bommer and Scott, 2000).
6.5. Actual scaling procedures for strong-motion records.
6.6. Variation of the time-history of the 1984 Morgan Hill earthquake when scaling in time axis.
6.7. Variation of the time-history of the 1983 Coalinga earthquake when scaling in time axis.
6.8. Variation of the time-history of the 1971 San Fernando earthquake when scaling in time axis.

6.9. Variation of the response spectra when adjusting by RASCAL and RSPMATCH programs is performed for the 1984 Morgan Hill earthquake. *Left* – acceleration response spectra, *right* – velocity response spectra.
6.10. Variation of the response spectra when adjusting by RASCAL and RSPMATCH programs is performed for the 1983 Coalinga earthquake. *Left* – acceleration response spectra, *right* – velocity response spectra.
6.11. Variation of the response spectra when adjusting by RASCAL and RSPMATCH programs is performed for the 1971 San Fernando earthquake. *Left* – acceleration response spectra, *right* – velocity response spectra.
6.12. Variation of the time-history of the 1984 Morgan Hill earthquake when adjusting by RASCAL and RSPMATCH programs is performed.
6.13. Variation of the Arias intesity of the 1984 Morgan Hill earthquake when adjusting by RASCAL and RSPMATCH programs is performed. *Left* – Husid plots, *right* – ratio between adjusted records and original record.
6.14. Variation of the time-history of the 1983 Coalinga earthquake when adjusting by RASCAL and RSPMATCH programs is performed.
6.15. Variation of the Arias intensity of the 1983 Coalinga earthquake when adjusting by RASCAL and RSPMATCH programs is performed. *Left* – Husid plots, *right* – ratio between adjusted records and original record.
6.16. Variation of the time-history of the 1971 San Fernando earthquake when adjusting by RASCAL and RSPMATCH programs is performed.
6.17. Variation of the Arias intensity of the 1971 San Fernando earthquake when adjusting by RASCAL and RSPMATCH programs is performed. *Left* – Husid plots, *right* – ratio between adjusted records and original record.
7.1. Scaling procedures studied in this work.
7.2. Scaling factor for a target earthquake with magnitude M = 6.5 and distance d = 30 km. *Left* – for the 1984 Morgan Hill earthquake (M = 6.2, d = 22.7 km), *right* – for the 1983 Coalinga earthquake (M = 6.4, d = 38.8 km).
7.3. Scaling factor for a target earthquake with magnitude M = 6.5 and distance d = 30 km for the 1971 San Fernando earthquake (M = 6.6, d = 24.2 km).
8.1. Scaled records for bin BA.
8.2. Performance of the scaling factors for bin BA. *Left* – considering the scatter among the scaled records, *right* – considering the relative error with respect to the target spectrum.
8.3. Scaled records for bin BB.
8.4. Performance of the scaling factors for bin BB. *Left* – considering the scatter among the scaled records, *right* – considering the relative error with respect to the target spectrum.
8.5. Scaled records for bin BC. Scatter among the records (COV) and relative error for the average.
8.6. Performance of the scaling factors for bin BC. *Left* – considering the scatter among the scaled records, *right* – considering the relative error with respect to the target spectrum.
8.7. Scaled records for bin BD.
8.8. Performance of the scaling factors for bin BD. *Left* – considering the scatter among the scaled records, *right* – considering the relative error with respect to the target spectrum.
8.9 Scaled records for bin BE.
8.10. Performance of the scaling factors for bin BE. *Left* – considering the scatter among the scaled records, *right* – considering the relative error with respect to the target spectrum.
8.11. Scaled records for bin BF.
8.12. Performance of the scaling factors for bin BF. *Left* – considering the scatter among the scaled records, *right* – considering the relative error with respect to the target spectrum.
8.13. Scaled records for bin BG.
8.14. Performance of the scaling factors for bin BG. *Left* – considering the scatter among the scaled records, *right* – considering the relative error with respect to the target spectrum.
8.15. Scaled records for bin BH.
8.16. Performance of the scaling factors for bin BH. *Left* – considering the scatter among the scaled records, *right* – considering the relative error with respect to the target spectrum.

8.17. Scaled records for bin BA*.
8.18. Performance of the scaling factors for bin BA*. *Left* – considering the scatter among the scaled records, *right* – considering the relative error with respect to the target spectrum.
8.19. Scaled records for bin BC*.
8.20. Performance of the scaling factors for bin BC*. *Left* – considering the scatter among the scaled records, *right* – considering the relative error with respect to the target spectrum.
8.21. Scaled records for bin BE*.
8.22. Performance of the scaling factors for bin BE*. *Left* – considering the scatter among the scaled records, *right* – considering the relative error with respect to the target spectrum.
8.23. Husid plot for the records of bin BI (Whittier Narrows earthquake). *Left* – relative value of AI, *right* – absolute value of AI
8.24. Scaled records for bin BI (Whittier Narrows earthquake).
8.25. Husid plot for the records of bin BJ (Loma Prieta earthquake). *Left* – relative value of AI, *right* – absolute value of AI
8.26. Scaled records for bin BJ (Loma Prieta earthquake).
8.27. Husid plot for the records of bin BK (Northridge earthquake). *Left* – relative value of AI, *right* – absolute value of AI
8.28. Scaled records for bin BK (Northridge earthquake).

1. INTRODUCTION

1.1. The need for accelerograms

According to the type of structure under analysis, different earthquake loading representation is needed. In most of the codes and for the majority of structures, a pseudo-static analysis is required (either the equivalent lateral force method or spectral modal analysis); for this type of analysis a smooth response spectra characterises the earthquake actions. However, for some specific design situations dynamic analysis is required or recommended, hence the selection of one or more representative time-histories is needed. These situations include the design of buildings with irregularities, those for which higher modes are likely to be excited, or those designed for high levels of ductility. Time-histories are sometimes also required to evaluate the response of earth structures in terms of stability, deformation, liquefaction potential and dynamic site response.

Accelerograms are the most detailed representation of earthquake ground motion and contain a wealth of information about the nature of the ground shaking. When time-histories are needed, they can be selected from databanks of real accelerograms or they can be generated synthetically. In all the cases, the accelerograms used in earthquake-resistant design should be compatible with the level of seismic hazard defined and they should reflect the nature of the expected ground motion at the site.

1.2. Types of accelerograms

Three different types of accelerograms are available: real, synthetic and artificial.

1.2.1. Real accelerograms

The advantage of using *real* accelerograms is that they are genuine records of shaking produced by earthquakes. Therefore, they carry all the ground-motion characteristics (amplitude, frequency and energy content, duration and phase characteristics), and reflect all the factors that influence accelerograms (characteristics of the source, path and site). The disadvantages of *real* accelerograms are that not all M-*d*-soil combinations are covered, and the spectra are generally not smoothed.

1.2.2. Artificial accelerograms

Artificial accelerograms are generated to match a target response spectrum. Amongst the methods available is the SIMQKE program of Gasparini & Vanmarcke (1976). The use of these methods tends to generate artificial records that do not have the appearance of real earthquake accelerograms, with unrealistically high numbers of cycles of motion. This is due to the fact that the code spectrum is a uniform hazard spectrum (UHS), which is an envelope of the spectra corresponding to earthquakes in different seismic sources and the conservative scenario of earthquakes occurring in different seismic sources simultaneously is implicitly taken into account. The artificial records are problematic because they have to match the smooth code spectrum at all response periods.

Additionally, in order to get other characteristics of artificial spectrum-compatible record, such as duration, it is necessary to obtain supplementary information about the expected earthquake motion apart from the response spectrum.

1.2.3. Synthetic accelerograms

The number of real accelerograms has increased significantly in the last years, but a couple of decades ago there was a lack of records obtained a short distances from the causative fault ruptures of significant earthquakes. The use of *synthetic* records was necessary in order to overcome this lack of real records. Even today, with the large number of accelerograms recorded during the past three decades, it may still be difficult to find accelerograms that fulfil

the requirements of certain magnitude and distance bins, especially for large magnitudes and close distances.

The generation of synthetic accelerograms is mainly made by either deterministic or stochastic ground-motion modelling methods. Long-period motions behave mainly in a deterministic manner, while short-period motions behave stochastically. The period of transition from deterministic to stochastic behaviour is uncertain, but is often taken as about T ~ 1s (Stewart, *et al*. 2001). One example of a successful match with a recorded ground-motion by a deterministic model is giving by Somerville *et al*. (1995) for the motion recorded at Arleta during the 1994 Northridge earthquake. For applications of the stochastic method some references can be found in the work of Boore (2003a), like those of Atkinson and Boore (1997b), Silva and Darragh (1995) and Toro *et al*. (1997), among many others. These generation methods are able to approximate the effects of the physical processes on observed ground motions (earthquake source process, wave propagation and shallow soil response).

The earthquake source process denotes the generation of seismic waves as part of the strain energy released from the rupture of an active geologic fault. In the simulation procedure, a kinematic source model is typically used to describe the fault slip process. The fault slip can be modelled as a point or a finite source. When a site is close to the source of a large-magnitude earthquake, a finite source is necessary for the simulation of the near-fault effects. At distances far from the fault, a finite source can be simplified to a point source model, which reduces considerably the amount of computational work and the number of input parameters required.

After the rupture of the fault, seismic waves propagate through the Earth's crust. This is called the path effect. Green's functions can be used to simulate the typical path effects, which include attenuation of wave amplitude, reflection and refraction at the interface of different rock types and wave scattering from small-scale heterogeneities in the crust. At the moment when the seismic waves approach the surface of the Earth, they undergo further modifications while propagating through shallow soils. These site effects are discussed further in Section 3.3.

1.3. Objectives of the thesis

This work is focused on the use of real accelerograms, not only because they are the most detailed representation of earthquake ground motion but because while working with real accelerograms (instead of artificial or synthetic) less input is required for the dynamic analysis (often the selection of the input is undertaken by engineers with limited knowledge of engineering seismology). Furthermore, in current engineering practice this is the option most commonly used. Once an unique earthquake scenario is defined, either by a deterministic seismic hazard analysis (DSHA) or by deaggregation of a probabilistic seismic hazard analysis (PSHA), the selection of records has to be made. The records selected must agree with the characteristics of the design earthquake scenario specified and should match the site conditions. Alternatively, records from rock sites can be chosen and site response analyses can be performed.

The selection of the ground motions will be primarily based on the site conditions and the two dominant parameters: magnitude, M, and distance, *d*. Due to the current lack of data, ground motion records matching the exact values of M and *d* are not easy to find. Therefore, the use of M-*d* bins becomes necessary in the data selection.

There are cases where a unique earthquake scenario cannot be specified, either because deaggregation of the probabilistic seismic hazard assessment cannot be performed, due to the lack of information, or because the earthquake actions are characterised only by a response spectrum. In this situation, the selection criterion cannot be based on the seismological parameters discussed previously. Therefore, the selection has to be done by choosing records to directly match the spectral shape.

In order to obtain sufficient records for analysis, it will often be required to use a relatively poor match with magnitude and/or distance. The records selected should then be scaled to compensate for the mismatch of M, *d* or other factors, or to obtain a better match with the design spectrum. Even if scaling is done on the basis of any M, *d* mismatch, it will generally still be necessary to check the agreement or otherwise with the design spectrum.

The limits on the scaling amplitude factor are an important issue. Vanmarcke (1979) proposed that scaling on amplitude should not exceed certain limits according to the type of problem to

which the resulting motion is to be applied. For analysis of linear elastic structures an upper limit of 4 could be accepted, but for liquefaction a scaling factor no greater than 2 should be used. Nevertheless, the spectral shape is relatively insensitive to distances, suggesting that scaling amplitude by factor much higher than 2 for mismatched distances may be acceptable (Bommer and Ruggeri, 2002). However, these approximate limits, proposed by Vanmarcke (1979) almost 25 years ago and based on limited data, have worked their way into engineering practice and become generally accepted rules-of-thumb.

The key issue addressed in this work is the limits on scaling factors that can be applied, in terms of strong motion parameters and seismological criteria, in order to obtain realistic ground-motions from the scaling. When the scaling is done on the basis of seismological parameters, the resultant scaled records are checked against the design ground motion in terms of response spectrum, duration and other parameters. For both types of scaling, the scaled ground motions have to be consistent with the design scenario. The aim of this work is to provide coherent guidance on allowable scaling factors and procedures, including careful consideration of the treatment of uncertainties.

2. ACCELEROGRAMS

2.1. Accelerographs and accelerograms

Strong ground-motion is recorded by accelerographs, which are instruments that record the acceleration as a function of time. The first accelerographs were developed and installed in California in 1932 and recorded the strong ground-motion generated by the Long Beach earthquake in the following year.

The first generation of accelerographs are analogue instruments recording on film or paper. They do not record continuously, instead they remain on stand-by until triggered by a certain threshold level of acceleration. Therefore, the first wave arrivals that do not exceed the threshold value are not recorded. Since accelerographs only record strong shaking, they must be installed in those areas where earthquakes are expected. For this generation of instruments, there is the necessity of digitising the analogue record, which creates problems associated with the introduction of short- and long-period noise.

The second generation of accelerographs operates with a force-balance transducer and record digitally on to solid state or magnetic media. They are able to operate continuously and hence the first motions of the earthquake shaking are retained.

Accelerographs usually record three mutually perpendicular components of motion in the vertical and two horizontal directions. The records obtained from the accelerographs are accelerograms, which are the most detailed representation of earthquake ground motion. They contain a wealth of information about the nature of the ground shaking in strong earthquakes and also about the highly varied characteristics that different earthquakes can produce at different locations.

2.2. Characterisation of accelerograms

2.2.1. Peak ground motions

One of the parameters most widely associated with the severity of the ground motion is the peak ground acceleration (PGA), which is obtained directly from the recorded data; it is the maximum absolute value of acceleration in a time-history. PGA is generally recognised as a poor parameter for characterising the damage potential. Both a short-duration impulse of high-frequency and a long-duration impulse of low-frequency may have the same peak ground acceleration value, producing very different response in structures. This can be observed in Figure 2.1.

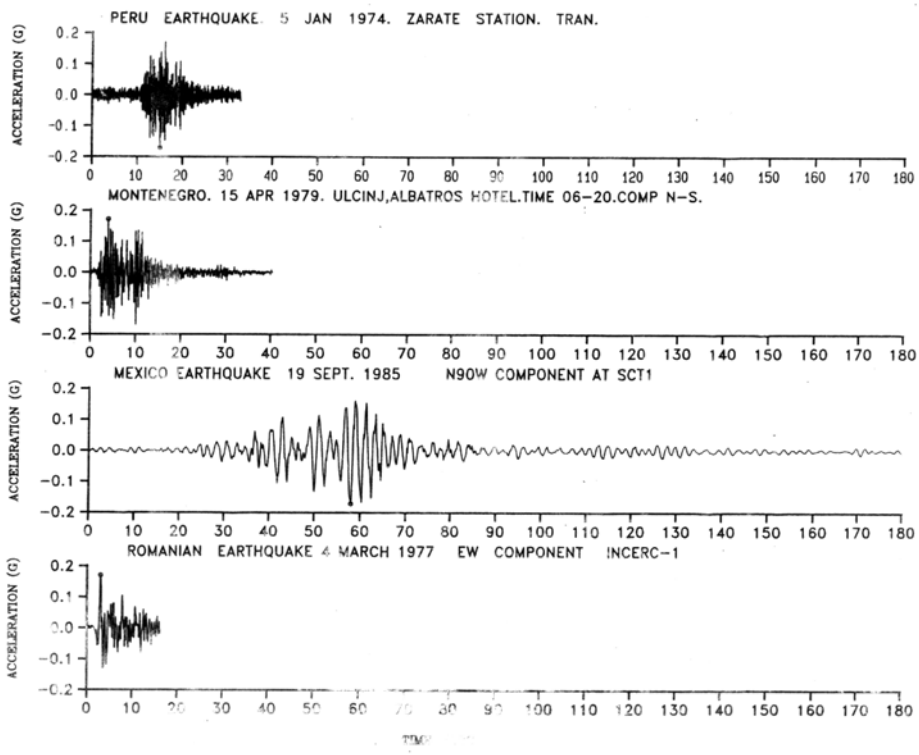

Figure 2.1. Accelerograms with identical values of PGA (Bommer, 1991).

Two other parameters also obtained directly from integration of the recorded data are the peak ground velocity (PGV) and the peak ground displacement (PGD). However, the integrated motions, especially the displacements, are highly sensitive to the processing applied to remove the digitisation noise from the record, which tends to dilute high-frequency components of the motion and enhance low-frequency components. The reported values of velocity and displacements must always be interpreted

with some caution, particularly the latter. Figure 2.2 presents an accelerogram with velocity and displacement time-histories for a specific earthquake.

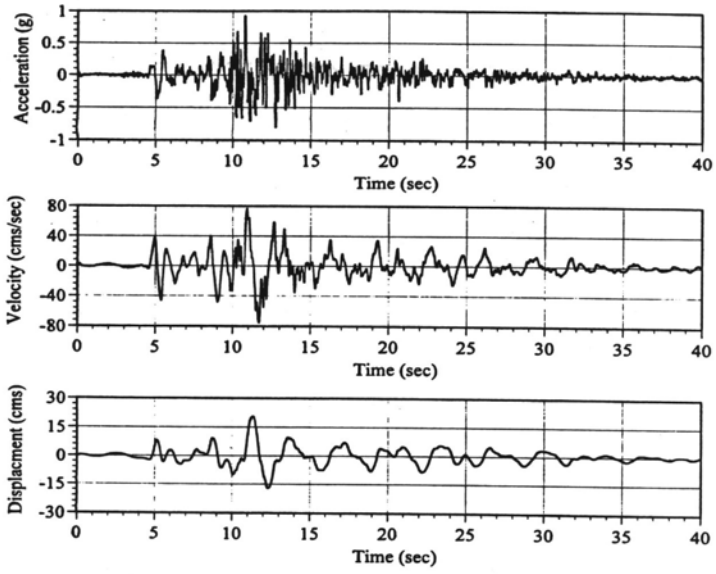

Figure 2.2. Accelerogram from the 1978 Tabas earthquake in Iran, with velocity and displacement time-histories (Bommer and Elnashai, 1999).

2.2.2. Arias intensity

Arias intensity, AI, is a ground motion parameter that has been used to evaluate damage potential. It is defined as:

$$AI = \frac{\pi}{2g}\int_0^T a^2(t)dt \tag{2.1}$$

where a(t) is the acceleration time history of total duration T. The energy in the accelerogram can be quantified by the Arias intensity (Arias, 1969).

A Husid plot is a graph of the build-up of AI with time as can be observed in Figure 2.3. It shows both the total amount of energy carried by the shaking and the rate at which it is imparted to structures. The rate of energy input over any interval t_1 to t_2 is related to another parameter called the root-mean-square acceleration, a_{rms}:

$$a_{rms}^{2} = \frac{1}{(t_2 - t_1)^2} \int_{t_1}^{t_2} a^2(t)dt \tag{2.2}$$

The level of damage produced by a ground motion will depend on both the total amount of energy and on the rate at which this energy is carried (Bommer, 2001).

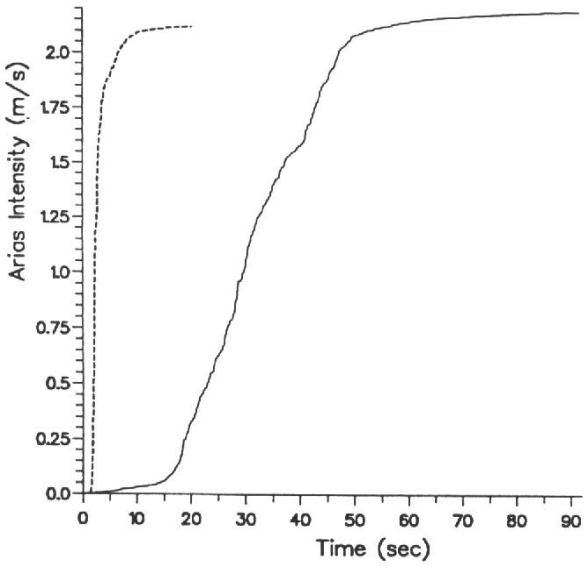

Figure 2.3. Husid plots for combined horizontal components for two accelerograms recorded in San Salvador, with the same total energy but at different periods of time. M_s = 7.3 for the offshore earthquake in 1982 (solid line) and M_s = 5.4 for the local earthquake in 1986 (dashed line). (Bommer, 2001)

2.2.3. Root-mean-square (RMS) acceleration

Another ground motion parameter that has been used to estimate the damage potential is the integral of the squared ground acceleration, which is a measure of the energy input capacity of the ground motion. Nevertheless, a strong short-duration ground motion could have the same RMS acceleration value than a weaker ground shaking of a very long duration.

a_{rms} is defined in equation 2.2, where ($t_2 - t_1$) denotes the significant duration and a denotes the ground acceleration. For the significant duration defined by Trifunac and Brady (1975) $t_2 - t_1$ corresponds to $t_{95} - t_5$.

Figure 2.4 shows the RMS acceleration for four different accelerograms from the San Fernando earthquake of 1971. It can be observed that the initial phase of shaking was followed by and extended period of weaker, decreasing motion.

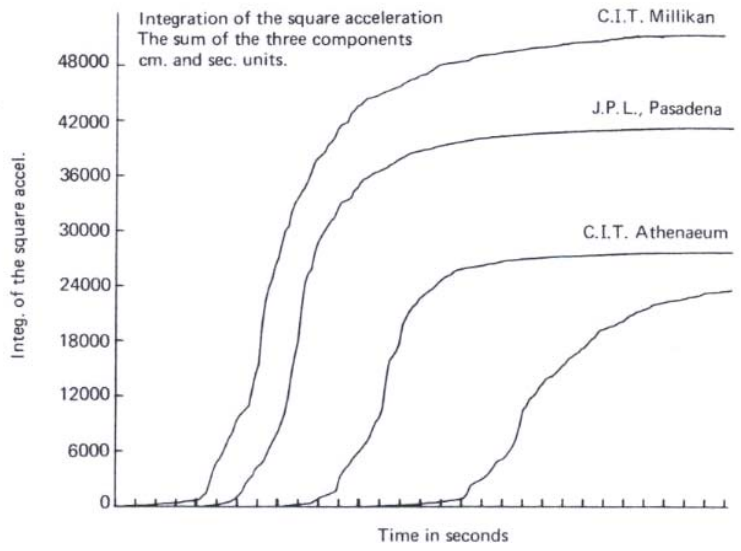

Figure 2.4. Integration of squared acceleration. Curves represent the sum of the three components of motion in centimetre-second units. (Housner and Jennings, 1977)

2.2.4. Duration

The duration of the ground motion is related to the time required for rupture to spread across the fault surface, which is a function of the seismic moment or the magnitude. There is a wide number of duration measures commonly used. The value of the duration differs according to the measure used.

All the duration definitions can be grouped into three categories: bracketed, uniform and significant durations (Bommer and Martínez-Pereira, 1999). The most common measure is the bracketed duration, D_b, which is defined as the time between the first and the last exceedances of a defined threshold level of acceleration (usually 0.05g). The uniform duration, D_u, is defined as the sum of the intervals during which the acceleration exceeds a threshold level. Another measure is the significant duration, defined as the time interval across which a specified amount of energy in the accelerogram is distributed. A common measure of significant duration, D_s, is the duration defined by Trifunac and Brady (1975), related to the interval between 5% and 95% of AI. The time interval between 5% and 75% of AI is also commonly used.

The differences between the durations defined previously can be observed in Figures 2.5, 2.6 and 2.7.

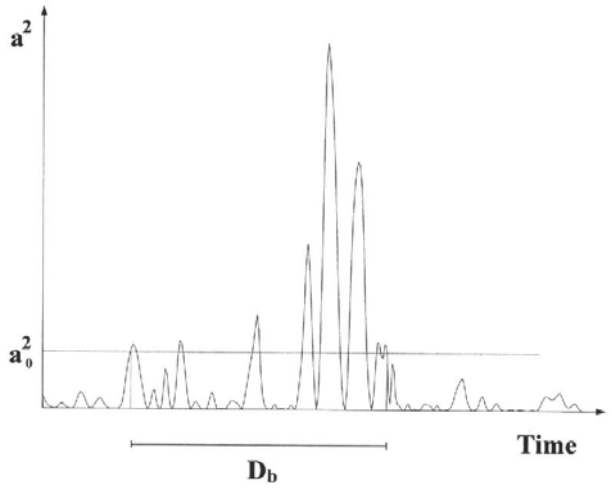

Figure 2.5. The definition of bracketed duration, D_b (Bommer and Martínez-Pereira, 1999).

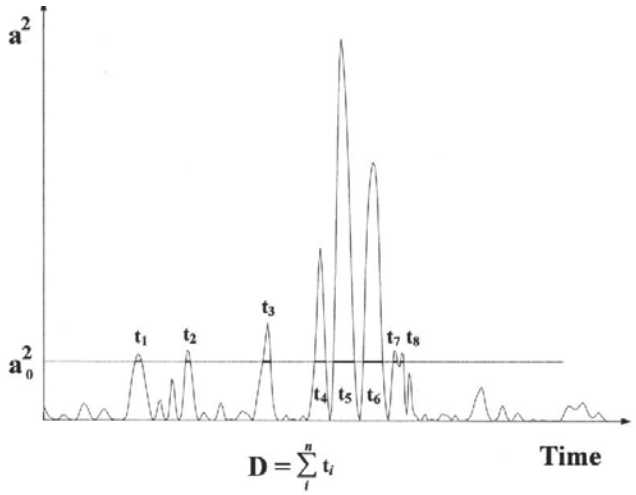

Figure 2.6. The definition of uniform duration, D_u (Bommer and Martínez-Pereira, 1999).

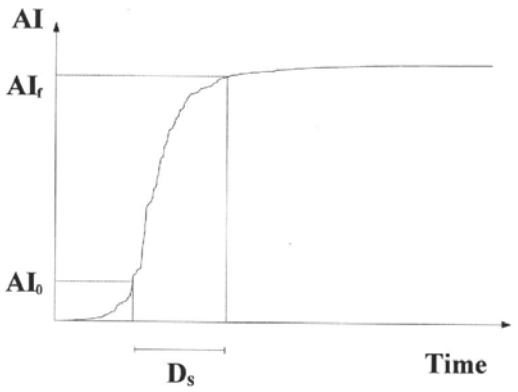

Figure 2.7. The definition of significant duration, D_s (Bommer and Martínez-Pereira, 1999).

2.2.5. Equivalent number of uniform stress cycles (N)

A quantity sometimes used as a substitute of duration is equivalent number of uniform stress cycles (N). Parameter N is obtained by counting a weighted number of cycles in an accelerogram, with the weighting factors being application-dependent. One common application is soil liquefaction analysis in which it is required to convert an irregular time-history of shear stress to an equivalent series of uniform stress cycles (N) that would produce an increase in pore pressure equivalent to that of the irregular time-history. Different relations have been developed for different stress levels, the 65% level being the most commonly used (Kramer, 1996). Procedures for the evaluation of N for liquefaction applications have been developed by Liu *et al*. (2001), in which the process of converting an irregular time history of earthquake-induced cyclic stresses to an equivalent number of uniform stress cycles (N) consist of counting a weighted number of local minimum and maximum points in a normalized accelerogram.

2.2.6. Response spectra

The response spectrum is the most important characterisation of seismic ground-motion in earthquake engineering. This parameter is obtained by passing the recorded data through a single-degree-of-freedom (SDOF) oscillator.

Acceleration response spectral ordinates represent the period-dependent peak acceleration response of a SDOF elastic structure with a specified level of equivalent viscous damping. Acceleration response spectra are widely used in structural engineering, as the product of the spectral ordinate at the building period and the structural mass can be used to approximate the base shear in elastic structures. A limitation of response spectral ordinates is that they do not provide information on the duration of strong shaking.

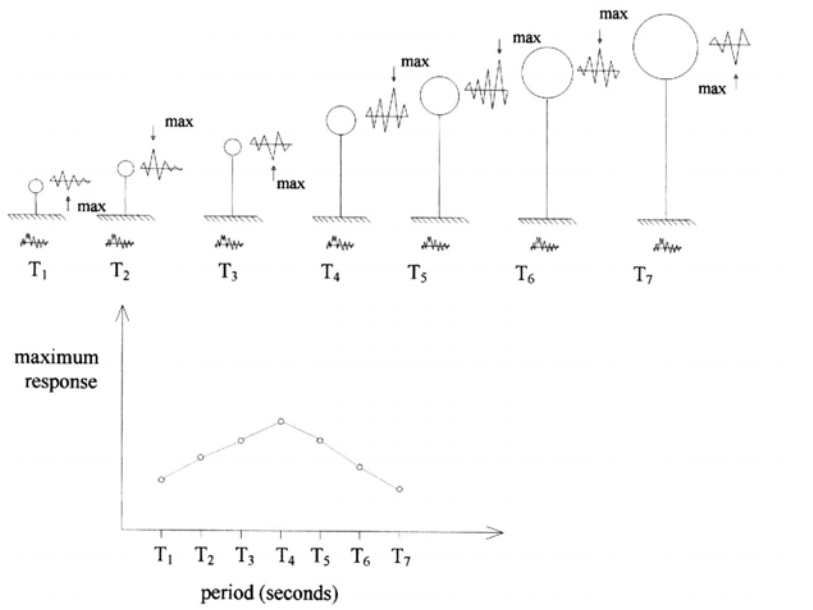

Figure 2.8. Definition of the response spectrum (Tsangaris, 1996).

2.2.7. Spectrum intensity (SI)

The spectrum intensity, SI, is a measure of the intensity of shaking of an earthquake at a given site. The Housner spectrum intensity, SI is defined as:

$$SI = \int_{0.1}^{2.5} SV(T,\xi)dT \tag{2.3}$$

where SV is the velocity spectrum curve and ξ is the damping coefficient.

The limits of the integral were chosen by Housner because they include a range of typical periods of vibration of urban buildings.

2.2.8. I_v index

Fajfar *et al*. (1990) proposed a new intensity parameter for structures with fundamental periods in the medium-period range. This parameter, I_v, is defined as:

$$I_v = PGV \cdot D_s^{0.25} \tag{2.4}$$

where D_s is the significant duration defined by Trifunac and Brady (1975).

The medium-period range is the region where the smoothed pseudo-velocity spectrum has its maximum values. This region has a lower and upper bound that varies for different ground motions and depend on the magnitude of the earthquake, the distance from the epicentre, and on the local soil condition.

3. FACTORS INFLUENCING ACCELEROGRAMS

The parameters that characterise a ground motion analysis are the earthquake source, the travel path and the site effects.

3.1. Source

Earthquakes are caused by the sudden release of elastic strain energy in the Earth's crust because of the rupture on a geological fault. The rupture begins at one particular point and then propagates along the fault plane very rapidly. As the size of an earthquake increases, so does the size of the fault rupture area.

The fault rupture is characterised by a plane or a volume corresponding to that part of the crust from which strain energy is released.

Magnitude, rupture mechanisms, directivity and focal depth are parameters that define the nature of the resulting motion.

3.1.1. Magnitude

Magnitude is a measure of the amount of seismic energy released in an earthquake. It is the most familiar measure.

There are different magnitude scales. The local magnitude, M_L, was the first scale. It was introduced by Richter to quantify the size of earthquakes in southern California and it is determined from the amplitudes of seismograms obtained from a Wood-Anderson seismograph.

The body-wave magnitude, m_b, is a teleseismic magnitude scale. It is rarely used in attenuation studies, partly because it saturates at lower values than other magnitude scales. The m_B scale is similar to m_b, but calculated a slightly longer periods. Another teleseismic magnitude scale is based on measurements of surface-waves, M_s.

The M_{JMA}, which is the scale of the Japanese Meteorological Society, is calculated from the ground-motion amplitudes measured from medium period seismographs.

Empirical relationships have been developed to relate values from different scales, such as the equations obtained by Ambraseys and Bommer (1990) by orthogonal regression on European data.

All of these magnitude scales are unable to distinguish the relative size of the largest earthquakes, a phenomenon known as saturation (Figure 3.1). Seismic moment has the advantage that it does not saturate and therefore it is really the only suitable measure for the largest earthquakes.

The seismic moment, M_o, is defined as:

$$M_o = \mu.A.U \tag{3.1}$$

where A is the area of the fault rupture, μ is the rigidity of the Earth's crust and U is the slip. Seismic moment is directly related to the physical properties of the earthquake source.

A moment magnitude scale, M_w, provides moment values in a format that is more easily interpreted:

$$M_w = \frac{2}{3}\log(M_0) - 6.03 \tag{3.2}$$

where M_0 has units of N·m.

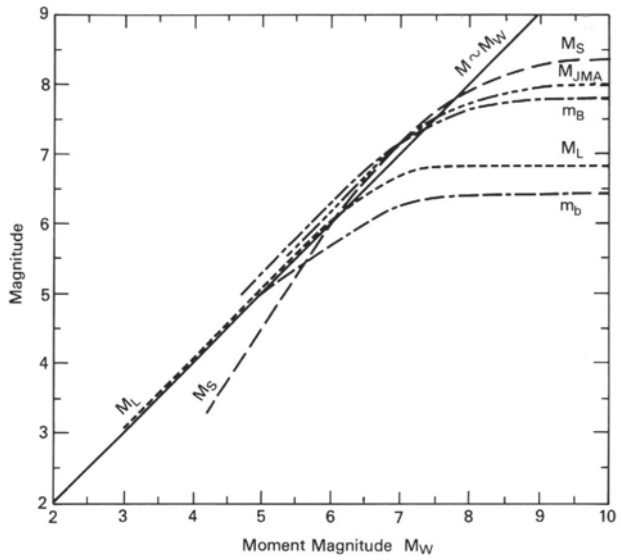

Figure 3.1. Comparison of moment magnitude scale with other magnitude scales (Reiter, 1990). Figure originally derived by Hiroo Kanamori.

3.1.2. Rupture mechanism

One of the factors affecting the near-fault zone (distances of up to about 20-60 km from a rupture fault) is the rupture mechanism. Although the fault ruptures associated with earthquakes are often very complex, it is usual to model the fault rupture as a rectangular plane.

According to the fault mechanism, ruptures are classified as strike-slip, which involves only horizontal motion (they can be either right-lateral or left-lateral), or as dip-slip, when the movement of the fault is purely vertical (they can be either normal or reverse); and oblique ruptures, when they are a combination of both horizontal and vertical slip (Figure 3.2).

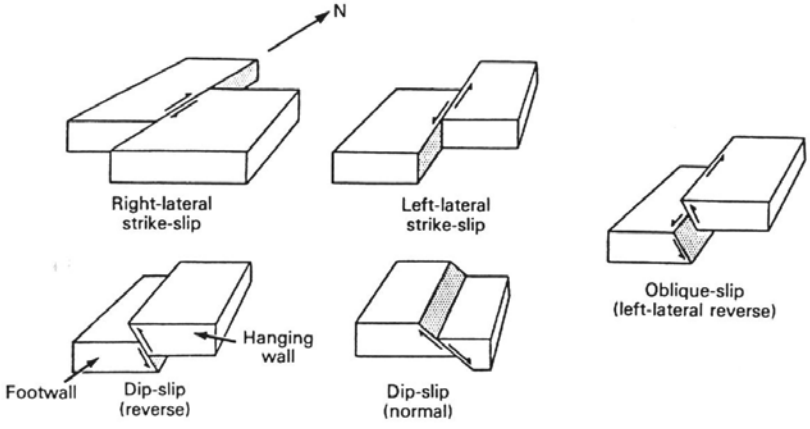

Figure 3.2. Mechanisms of fault rupture (Reiter, 1990).

The crustal block above the fault plane is referred to as the hanging wall, the block below the fault plane the footwall. There are differences between the motion on the hanging wall and footwall of dipping faults since sites located over the hanging wall are closer to a larger area of source than footwall sites.

The angle of the maximum slope of the fault plane, measured downwards from the horizontal in the vertical plane is referred to as the dip and is generally represented by δ°. The strike, ϕ°, is the angle made by the line of intersection between the fault plane and the ground surface, measured clockwise from north in the horizontal plane. The angle between the strike direction and the vector of the slip of the hanging wall with respect to the fault wall is the rake or slipe, λ°, which is measured in the plane of the fault, positive upwards. The rake angle defines unambiguously the direction of slip on a rupture. A normal fault rupture has a rake of -90° and a reverse rupture a rake of +90°.

The dip, strike and rake angles are illustrated in Figure 3.3.

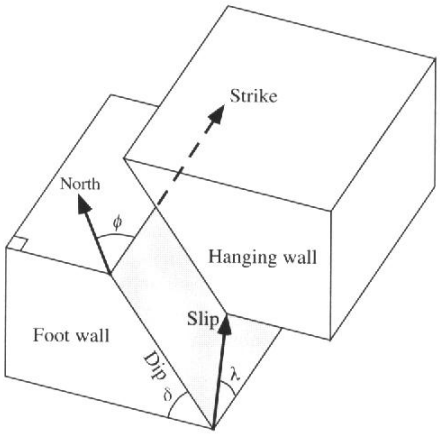

Figure 3.3. Definition of the dip (δ), strike (ϕ) and rake (λ) angles of a fault rupture (Shearer, 1999).

3.1.3. Directivity

Another important factor that affects the near-fault zone is the rupture directivity, which causes spatial variations in ground motion amplitude and durations. The estimation of ground motions close to an active fault should account for both the directivity and the rupture mechanism.

Forward directivity occurs when the rupture propagates toward a site and the direction of slip on the fault is also toward the site. It takes place when the velocity of fault rupture is almost as large as the

shear wave velocity of the rock near the source. In this situation the wave front arrives as a large pulse of motion oriented in the direction perpendicular to the fault. It occurs at the beginning of the record and it is polarized in the strike-normal direction. The pulse of motion is typically characterised by large amplitude at intermediate to long periods and the overall motion is generally of short duration.

Backward directivity occurs when a site is located near the epicentre and it is the condition in which the rupture propagates away from the site. It is characterised by motions with relatively long duration and low amplitude at long periods.

Figure 3.4 shows two near-fault recordings of the Landers earthquake of 1992 in which the effects of forward and backward directivity is clearly appreciated.

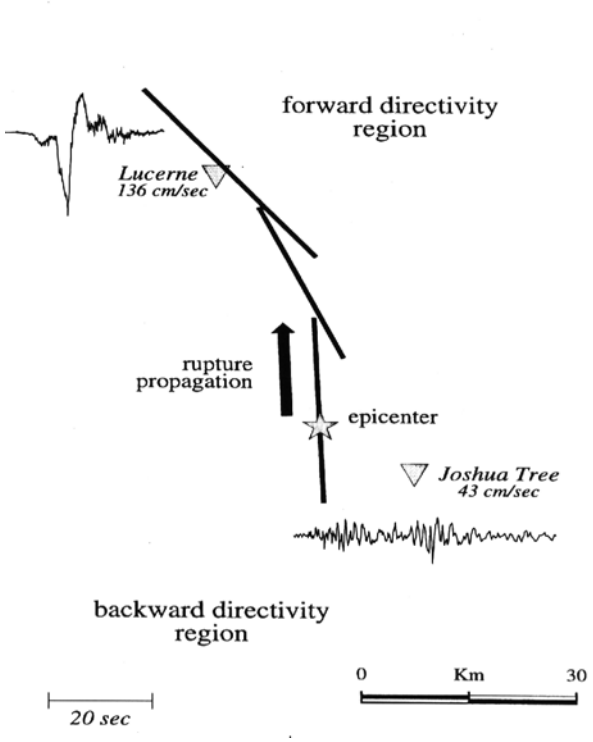

Figure 3.4. Near-field velocity time-histories from accelerograms of the 1992 Landers earthquake in California, showing the effect of rupture directivity on the recorded motion (Somerville *et al*., 1997).

Somerville *et al*. (1997) correlated the response spectrum ordinates to geometric parameters of the near-field directivity. These parameters are illustrated in Figure 3.5.

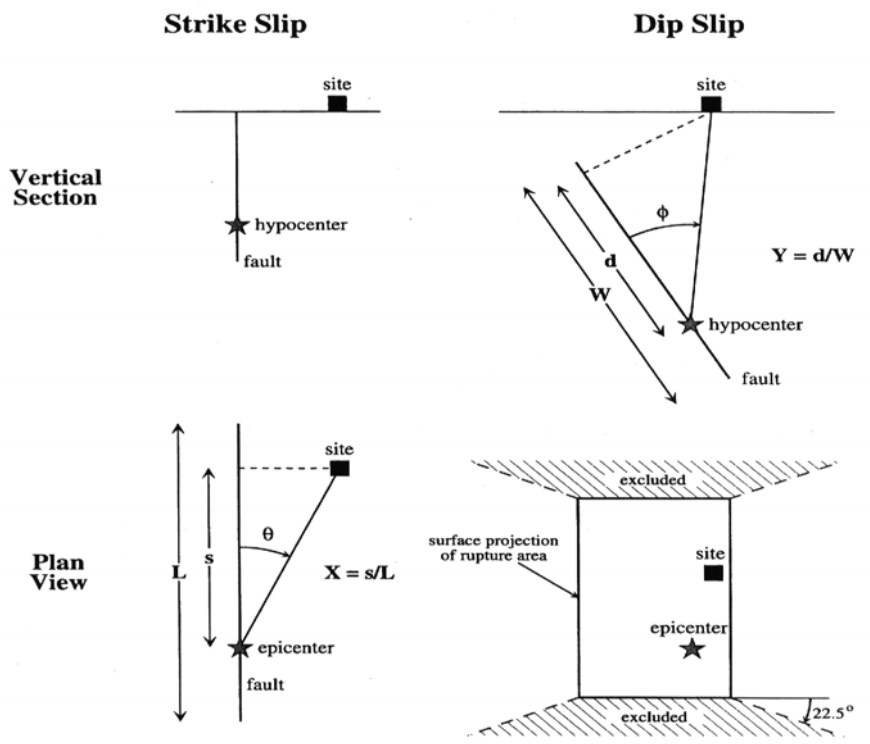

Figure 3.5. Near-field directivity parameters (Somerville *et al.*, 1997).

3.1.4. Focal depth

The focal depth is only important for small magnitude earthquakes, where the rupture dimensions are small compared to the thickness of the seismogenic layer of the crust, in which the focal depth is the parameter that controls how far below the surface the source of energy is located. It is also only significant at short distances from the source, at least for crustal earthquakes, as indicated by the attenuation relationships of Ambraseys and Bommer (1991).

3.2. Path

The path is the particular route that the energy released at the earthquake source will travel along to arrive at a particular site. The path effects include attenuation of wave amplitude, reflection and refraction at the interface of different rock types and wave scattering from small-scale heterogeneities in the crust. The main parameters that characterise the path are the distance and the crustal structure.

3.2.1. Distance

The source-site distance reflects how far the waves carrying the seismic energy have travelled when reaching a particular point. As waves travel away from a seismic source, geometric spreading reduces their amplitude.

Source-site distance is measured differently by different investigators. Figure 3.6 shows graphically these distances for a vertical and for a dipping fault. The simplest measure of distance is the hypocentral distance, r_{hyp}, which is the distance from the site to the hypocentre. For this distance, the fault is represented as a point, without taking into account the length of the fault rupture. Other measures of distance are the r_{rup}, which is the shortest distance to the fault rupture, r_{seis}, which is the distance to the closest part of the rupture whitin the seismogenic layer and the r_{jb} distance ("Joyner-Boore" distance), which is the shortest horizontal distance to the surface projection of the fault rupture. The distance definitions most widely used in attenuation relationships are the r_{jb} and r_{rup} distances.

It is important to use the appropriate distance measure with each attenuation relationship, particularly for short distances where the main variations among the different distance definitions become apparent.

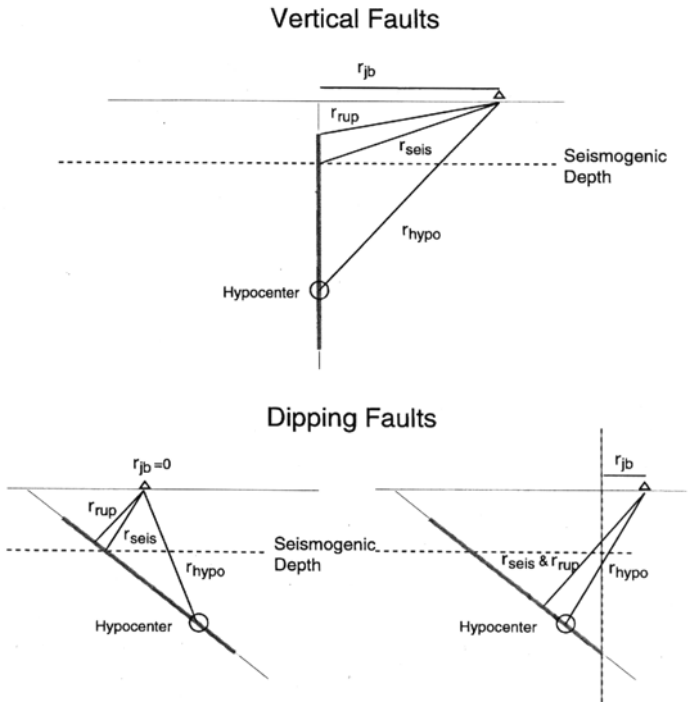

Figure 3.6. Definitions of source-to-site distance used in attenuation studies (Abrahamson and Shedlock, 1997).

3.2.2. Crustal structure

Another parameter that characterises the path is the physical composition of the crust and its tendency to transmit and absorb the energy in the seismic waves. When the body waves travel through the crust and into the mantle, they encounter boundaries or discontinuities in which they can experience both reflection and refraction.

The tectonic environment is an important factor in strong-motion generation. In seismic hazard usually three categories of regional ground motion are used: shallow crustal earthquakes in active tectonic regions, shallow crustal earthquakes in stable continental regions and subduction zone earthquakes, which are sub-divided into inter-face and intra-slab earthquakes. Each tectonic environment gives rise to different ground-motion attenuation relationships, as will be addressed in Section 4. Data collected within each of the different tectonic environments are often inadequate to uniquely characterise the distance attenuation and magnitude scaling for a region, therefore there are significant differences even amongst attenuation models for the same tectonic category.

3.3. Site

At the moment when the seismic waves approach the surface of the Earth, they undergo further modifications while propagating through surface deposits. The site effects represent local ground response and the influence of surface topography, which are the main characteristics that influence the nature of the motion at the ground surface (Stewart *et al*., 2001). Local ground response refers to the influence of relatively shallow geologic material on vertically propagating body waves.

3.3.1. Surface geology

When a soil deposit lies above the bedrock, the motion experienced at the ground surface will be the response of the soil layer to the input motion at the bedrock-soil interface. Generally, the effect to the soil deposit is to amplify the ground motion, commonly by the phenomenon of impedance. Resonance can also cause significant amplification.

Impedance takes place when there is a significant difference in the wave propagation velocity between the bedrock and the soil, being much greater in the bedrock. Therefore, the wave energy that is transmitted into the soil layer will be retarded. In order to maintain the flow of energy, the amplitude of the waves in the soil layer must increase, amplifying the ground motion. Resonance occurs when

there is a clearly defined velocity contrast between the soil layer and the bedrock. Waves passing into the soil layer are repeatedly reflected at the ground surface and the soil-rock interface. The seismic energy becomes trapped in the soil layer, increasing appreciably the duration of the shaking. When the natural period of the soil deposit, T_n ($T_n = 4H/V_s$, where H is the soil depth and V_s is the average shear-wave velocity), is similar to the predominant period of the ground motion, resonance takes place leading to very large amplifications (Figure 3.7).

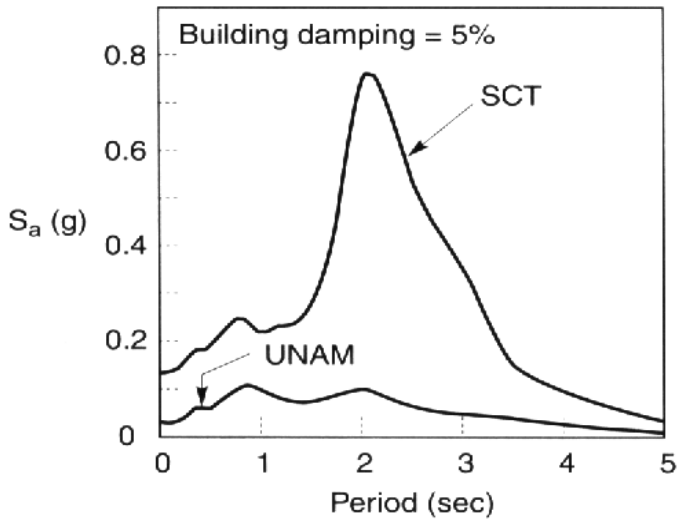

Figure 3.7. Acceleration response spectra of records from the 1985 Michoacán earthquake recorded in Mexico City on rock (UNAM) and soft soil (SCT) sites (Kramer, 1996).

Site effects have been introduced into most current attenuation relationships. All of them separate "rock" (rock and shallow stiff soil) from "soil" (intermediate to deep stiff soil). An additional "soft soil" category has not been included in most of the spectral attenuation relationships due to the few number of soft-soil strong motion recordings. In addition, the response of soft-soil sites is strongly site specific. This site condition is usually addressed with a site response analysis. One attenuation relationship that includes this "soft soil" category is the relationship of Abrahamson and Silva (1997).

Although in general soft soil will amplify the ground motion, high frequency motion will also be more rapidly attenuated in soft soils. Because of this, different attenuation relationships that include the soil conditions on peak ground acceleration have different outcomes, although nearly all predict higher amplitudes of motion at soft soil sites.

There are various soil classification systems. The simplest one divides sites into 'rock' and 'soil' and it is based purely on the description of the surface geology. The classification systems that have been used in recent studies are based on measurements of the average shear-wave velocity over the upper 30 metres at the site. The attenuation studies of Boore *et al*. (1993) and Ambraseys *et al*. (1996) use this second system, which defines four site classes: rock, A (V_s > 750 m/s); stiff soil, B (360 < V_s < 750 m/s); soft soil, C (180 < V_s < 360) and very soft soil, D (V_s < 180 m/s). The average shear-wave velocity over a set of 30 m depth to classify a site has the advantage of uniformity. The 30 metres is used because for the majority of site investigations the depth reached is not greater than this value. Using the $V_{s,30}$ value introduces a measure of stiffness. Nevertheless, seismic site response is also a function of soil depth, as can be observed in Figure 3.8 for the 1967 Caracas earthquake, in which significantly more damage occurred when the natural period of the building "matched" that of the soil deposit. For a soil layer to influence the ground motions, a rule-of-thumb is that the thickness must be equal to at least one quarter of a wavelength. Both dynamic stiffness and soil depth are important.

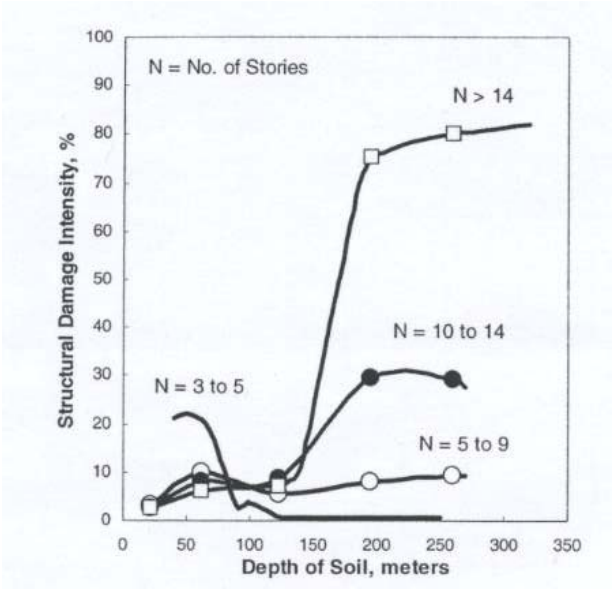

Figure 3.8. Relationship between structural damage intensity and soil depth for the 1967 Caracas earthquake (Seed *et al*., 1972).

The most recent classification systems define more site classes, with a tendency to move towards six classes, such as the classification proposed by Rodriguez-Marek *et al*. (2001). This last classification is made according to the type of deposit (hard rock, A; competent rock, B; weathered rock, C; stiff soil, D; soft soil, E; and potentially liquefiable sand, F) and the depth to bedrock ($V_s \geq 760$ m/s) or to a significant impedance contrast between surficial soil deposits and material with $V_s \approx 760$ m/s. These

soil types are subdivided according to the depositional age and soil type. Table 3.1 summarises the site classification scheme.

Table 3.1. Simplified geotechnical site categories (Rodríguez-Marek *et al*., 2001).

Site	Description	Site Period	Comments
A	Hard Rock	≤ 0.1 s	Hard, strong, intact rock; V_s ≥1500 m/s.
B	Rock	≤ 0.2 s	Most "unweathered" California rock cases (V_s ≥760 m/s or < 6 m of soil).
C-1	Weathered / Soft Rock	≤ 0.4 s	Weathered zone > 6 m and < 30 m (V_s > 360 m/s increasing to > 700 m/s).
-2	Shallow Stiff Soil	≤ 0.5 s	Soil depth > 6 m and < 30 m.
-3	Intermediate Depth Stiff Soil	≤ 0.8 s	Soil depth > 30 m and < 60 m.
D-1	Deep Stiff Holocene Soil, either **S** (Sand) or **C** (Clay)	≤ 1.4 s	Soil depth > 60 m and < 200 m. Sand has low fines content (< 15%) or nonplastic fines (PI < 5). Clay has high fines content (> 15%) and plastic fines (PI > 5).
-2	Deep Stiff Pleistocene Soil, **S** (Sand) or **C** (Clay)	≤ 1.4 s	Soil depth > 60 m and < 200 m. See D_1 for S or C sub-categorization.
-3	Very Deep Stiff Soil	≤ 2 s	Soil depth > 200 m.
E-1	Medium Depth Soft Clay	≤ 0.7 s	Thickness of soft clay layer 3 m to 12 m.
-2	Deep Soft Clay Layer	≤ 1.4 s	Thickness of soft clay layer > 12 m.
F	Special, e.g., Potentially Liquefiable Sand or Peat	≈ 1 s	Holocene loose sand with high water table (z_w ≤ 6 m) or organic peat.

3.3.2. Topography

The presence of topographic features can have a significant influence on the nature of the ground motion. However, no attenuation relationship has included topography explicitly, partly because of the complexity of the effects and the difficulties in defining simple parameters to model them (Bommer, 2001).

Many geometries can give rise to topographic effects on ground motion. Two-dimensional geometries can be generally categorised as ridges, canyons or slopes (shown in Figure 3.9). Studies done on these geometries are described by Stewart *et al*. (2001). Significant numbers of parameters affect model predictions of topographic effects but most of them have not been appropriately verified with observation.

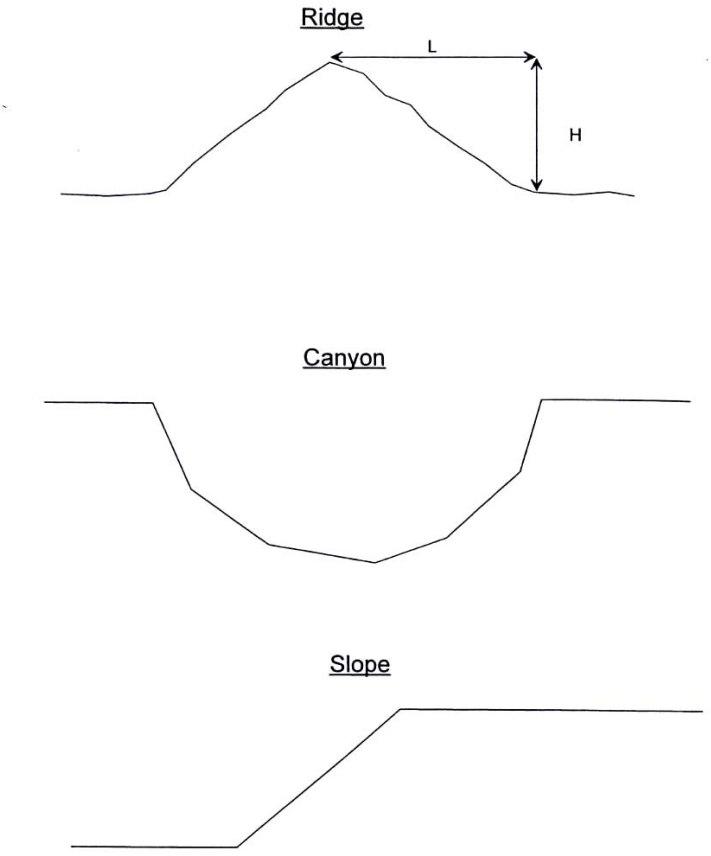

Figure 3.9. Generalized 2D geometries of irregular surface topography (Stewart *et al*., 2001).

3.3.3. Structures

The presence of large structures can modify the ground motion through interaction with the soil and foundations. If the recording instrument is in the basement or ground storey of a structure, the recorded motion will be different from the free-field motion (where there are no structures of any kind) as observed in Figure 3.10. Some reports suggest peak ground acceleration decreases with embedment depth, as those of Darragh and Campbell (1981), McCann and Boore (1983) and Campbell (1979, 1983, 1984).

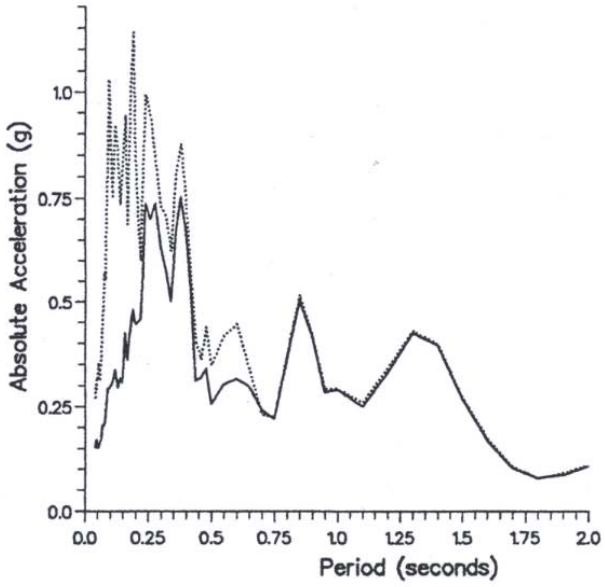

Figure 3.10. Acceleration spectra (2% damping) of transverse components of accelerograms obtained at Hollywood Storage Building during the San Fernando (California) earthquake of 1971, from instruments located in the basement of the 15-storey building (solid) and from a free-field instrument in the car park (dotted).

4. ATTENUATION RELATIONSHIPS

4.1. General

Attenuation relationships are equations that can be used to estimate the values of strong-motion parameters as functions of independent parameters that characterise the earthquake and the site of interest. They are generally derived through regression on empirical data. The parameters included in the attenuation relationships are always magnitude and distance. Other seismological parameters such as type of faulting, focal depth and directivity are sometimes included by different authors.

The general formulation of the attenuation for median values is as follows:

$$\ln(y) = c_1 + c_2 m + c_3 m^{c_4} + c_5 \ln r + f(F) + f(HW) + f(S) \tag{4.1}$$

where y is the parameter being predicted, m is the magnitude, r is the source-site distance (see section 3.2.1), F is a factor related to the source rupture mechanism, HW is a hanging wall factor for dip-slip faults, S is a site factor and c_1 to c_5 are constants to be determined by the regression (Stewart *et al.*, 2001).

The attenuation relationship depends on the tectonic environment, as described by Abrahmson and Shedlock (1997). The tectonic regimes where earthquakes more commonly occur are the active tectonic regions and the subduction zones, but they can also occur within stable continental regions.

Since shallow crustal earthquakes in *active tectonic regions* have produced the largest number of ground motion records, several attenuation relationships have been developed for these regions. Since

there is enough data, other parameters beside magnitude, distance and soil condition can be evaluated (Abrahmson and Shedlock, 1997).

The number of shallow crustal earthquakes records in *stable continental regions* is few. Therefore, the majority of the attenuation relationships are based on numerically simulated ground motion, such as the equations developed by Toro *et al*. (1997) for earthquakes in Central and Eastern North America. Atkinson and Boore (1997a) also developed attenuation relationship by simulated ground motion for Eastern North America.

For the *subduction zones*, the majority of the attenuation relationships are developed primarily based on recordings from Japan and South America (Abrahamson and Shedlock, 1997) like those of Youngs *et al*. (1997). Atkinson and Boore (1997b, 2003) developed equations for the Cascadia Region (USA) and other regions based on simulated ground motions. In the study of Youngs *et al*. (1997) it was found that the peak ground motions from subduction zones earthquakes attenuate more slowly than those from shallow crustal earthquakes in active tectonic areas, as shown in Figure 4.1.

For the shallow crustal events the attenuation relationship of Toro *et al*. (1997) for stable continental regions gives bigger values of PGA than the attenuation relationship of Ambraseys *et al*. (1996) for active tectonic regions (Figure 4.1). Significant part of this difference is probably due to differences in site conditions affecting high frequencies; in Europe, rock is defined as $V_s > 750$ m/s, but for Eastern North America, ENA, Toro *et al*. (1997) used $V_s = 2800$ m/s.

For a horizontal distance of 10 km the ratio of the PGA values given by the two attenuation relationships used for shallow crustal earthquakes assuming $M_s \sim M_{w,}$ is of 1.9 for M = 5.5, 2.4 for M = 6.5 and 2.9 for M = 7.5. As stated before, significant part of this difference is probably due to the very different site conditions. Figure 4.2 contains the response spectral acceleration at a horizontal distance of 10 km and M = 5.5 and 6.5.

Attenuation relationships have been developed for different regions. The influence of regional differences in strong-motion can be observed by the comparison of the equations for active tectonic regions of Ambraseys *et al*. (1996) for Europe and Middle East and Boore *et al*. (1997) for Western North America (Figures 4.3 and 4.4).

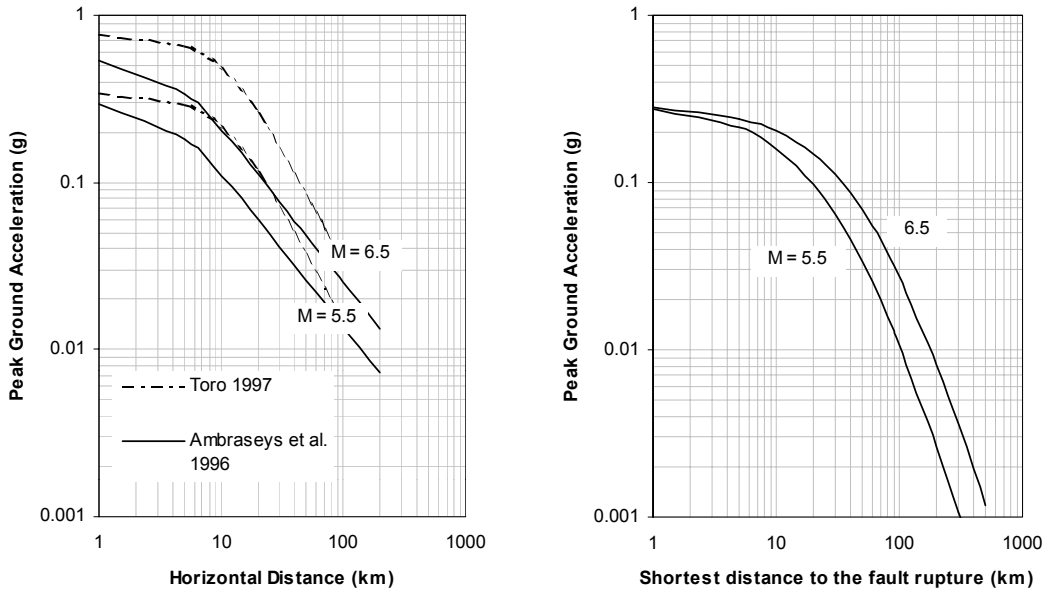

Figure 4.1 Attenuation of PGA with distance from earthquakes with M 5.5 and 6.5. *Left* - from the attenuation relationships for active tectonics regions (Ambraseys *et al.*, 1996) with $M_s \sim M_w$ and stable continental regions for Mid-continent (Toro *et al.*, 1997), *right* - from the attenuation relationship for subduction zones for interface earthquakes (Youngs *et al*, 1997).

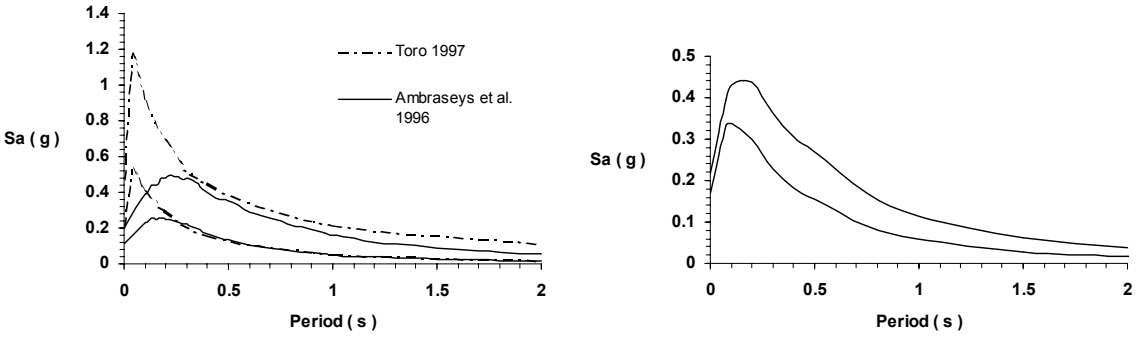

Figure 4.2. Response spectral acceleration at 10 km from earthquakes of M = 5.5 and 6.5. *Left* - from the attenuation relationships for active tectonics regions (Ambraseys *et al.*, 1996) with $M_s \sim M_w$ and stable continental regions for Mid-continent (Toro *et al.*, 1997), *right* – from the attenuation relationship for subduction zones for interface earthquakes (Youngs *et al*, 1997).

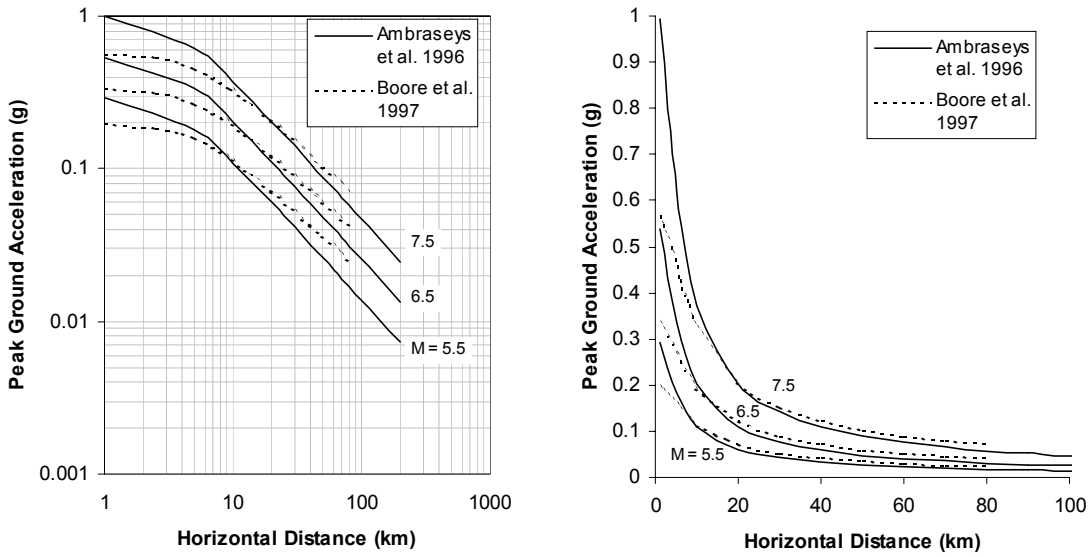

Figure 4.3. Comparison of the PGA values for earthquakes with M 5.5, 6.5 and 7.5 ($M_s \sim M_w$) for rock sites from the attenuation relationships of Ambraseys *et al.* (1996) for Europe and Middle East and Boore *et al.* (1997) for Western North America with V_s = 620 m/s.

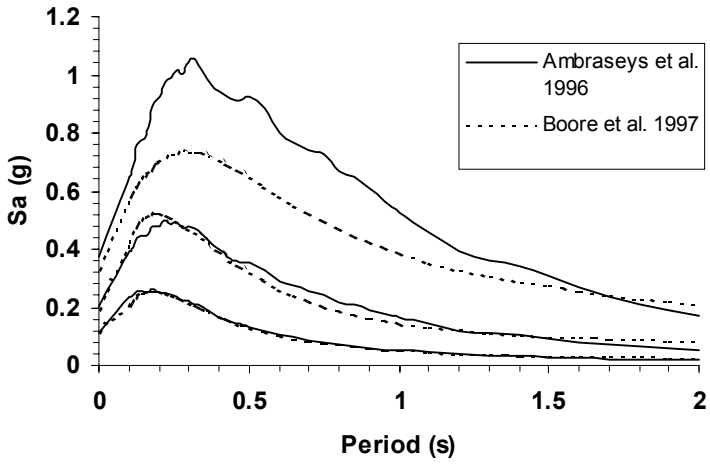

Figure 4.4. Comparison of the acceleration response spectra for earthquakes with M 5.5, 6.5 and 7.5 ($M_s \sim M_w$) for rock sites from the attenuation relationships of Ambraseys *et al.* (1996) for Europe and Middle East and Boore *et al.* (1997) for Western North America with V_s = 620 m/s.

The relationships included in the following sections are those for active tectonic regions, since they are based on recorded ground motion and they introduce other parameters beside magnitude, distance and site conditions.

4.2. Relationships for spectral ordinates

Table 4.1. Parameters included in some attenuation relationship for spectral ordinates.

Equation	Area	Magnitude	Distance (km)	Number of site parameters	Fault mechanism	Others
Ambraseys *et al*. (1996)	Europe and Middle East	$4.0 < M_s < 7.5$	$r_{jb} \leq 200$	3 ($V_{s,30}$)	---	---
Campbell (1997)	Worldwide	$4.7 < M_w < 8.1$	$3 \leq r_{seis} \leq 60$	3	F_1	D
Abrahamson and Silva (1997)	California with some others	$4.4 < M_w < 7.4$	$0.1 < r_{rup} < 220$	2	F_2	HW
Boore *et al*. (1997)	Western North America	$5.5 < M_w < 7.5$	$r_{jb} \leq 80$	1 ($V_{s,30}$)	F_3	---
Spudich *et al*. (1999) *	Worldwide extensional tectonic regimes	$5.0 < M_w < 7.7$	$r_{jb} \leq 70$	2	---	---
Toro *et al*. (1997) **	Central and Eastern North America	$5.0 < M_w < 8.0$	$r_{jb} \leq 100$	---	---	---
Youngs *et al*. (1997) ***	Worldwide subduction zones	$5 \leq M_w < 8.2$	$10 < r_{rup} < 500$	2	---	H, Z_T

D. Depth to basement rock.
F_1. Strike-slip faulting or otherwise.
F_2. Reverse, reverse/oblique or otherwise.
F_3. Strike-slip, reverse-slip or otherwise.
HW. For sites over the hanging wall or otherwise.
H. Focal depth.
Z_T. Source type: interface or intraslab
* Relationship for spectral velocity.
** Relationship for stable continental regions.
*** Relationship for subduction zones

The equations of the attenuation relationships presented in Table 4.1 are described in Annex 1.

4.2.1. Magnitude

There is a clear dependency of the spectral shape on magnitude for the attenuation relationships of Ambraseys *et al.* (1996). This can be observed from the normalised spectral shapes for a given distance.

The other three attenuation relationships for response spectral acceleration in active tectonic regions considered in this work show also a dependency of the spectral shape on magnitude in all the periods, except for the attenuation relationship of Campbell (1997), in which the dependence is for periods greater than 0.35 s. This can be observed in Figures 4.5 and 4.6.

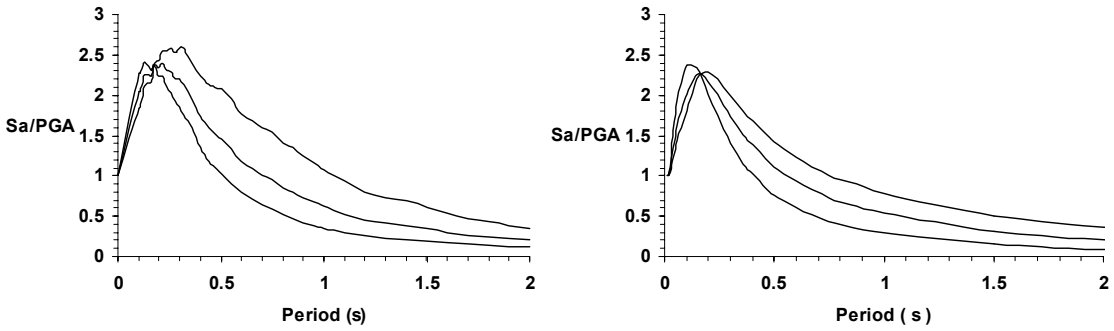

Figure 4.5. Normalised spectral shapes for rock sites at 10 km from earthquakes of M 5, 6 and 7. *Left* - from the attenuation equations of Ambraseys *et al.* (1996), *right* – from the attenuation equations of Abrahamson and Silva (1997).

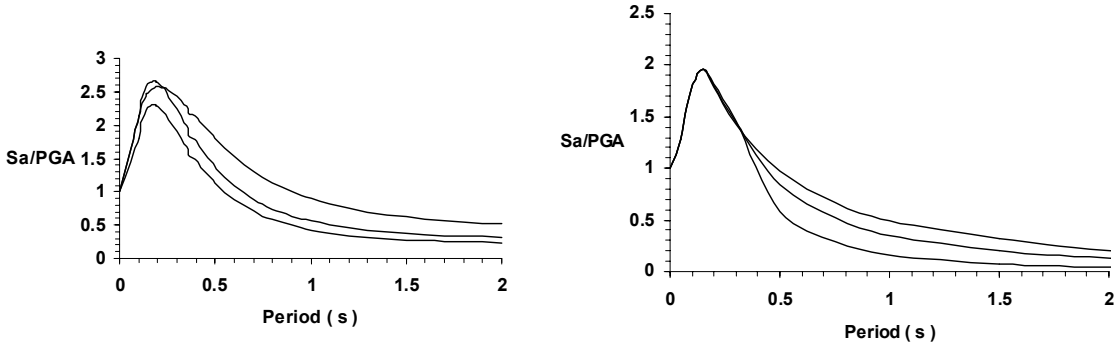

Figure 4.6. Normalised spectral shapes for rock sites at 10 km. *Left* - from earthquakes of M_w 5.5, 6 and 7 from the attenuation equations of Boore *et al.* (1997) with V_s = 620 m/s, *right* – from earthquakes of M_w 5, 6 and 7 from the attenuation equations of Campbell (1997).

4.2.2. Distance

The shape of the spectra obtained with the attenuation relationships of Ambraseys *et al.* (1996) are relatively insensitive to distance as shown in Figure 4.7. The same can be observed for the attenuation relationships of Campbell (1997) in the same figure. Therefore, it should be possible to scale

amplitudes to compensate for large distance mismatches and obtain reasonable estimates of the spectrum for the target distance.

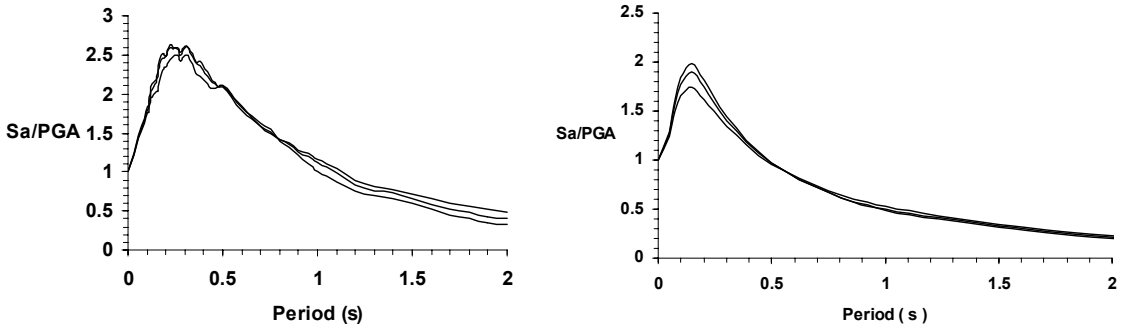

Figure 4.7. Normalised spectral shapes for rock sites at 5, 20 and 50 km from a M 7 earthquake. *Left* - from the attenuation equations of Ambraseys *et al.* (1996), *right* – from the attenuation equations of Campbell (1997).

In the attenuation relationships of Boore *et al*. (1997) and Abrahamson and Silva (1997), the spectral shapes are more sensitive to distance, as indicated in Figure 4.8. It can be observed that the relation of Abrahamson and Silva (1997) shows less attenuation with distance of longer periods; the relation of Boore *et al*. (1997) shows the sensitivity at intermediate periods.

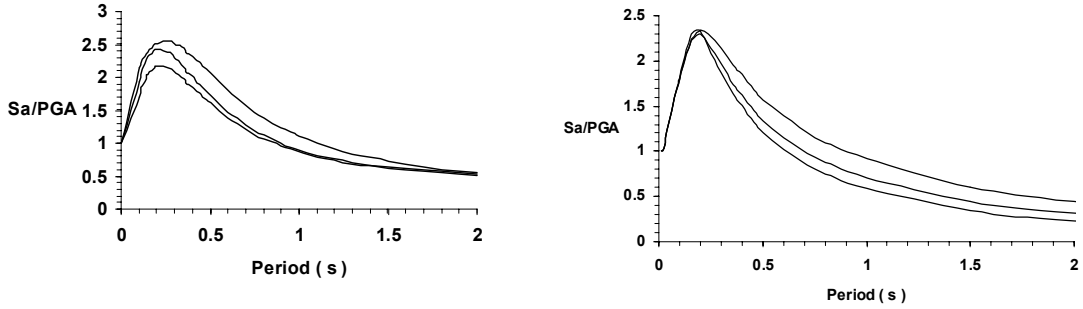

Figure 4.8. Normalised spectral shapes for rock sites at 5, 20 and 50 km from a M_w 7 earthquake. *Left* - from the attenuation equations of Boore *et al.* (1996) with V_s = 620 m/s, *right* – from the attenuation equations of Abrahamson and Silva (1997).

4.2.3. Site condition

Soil deposits can have the effect of increasing the duration of the strong shaking. The shape and amplitude of the response spectrum are also heavily influenced by the surface geology, the amplitudes of the intermediate and long period being particularly amplified, as illustrated in Figures 4.9 and 4.10.

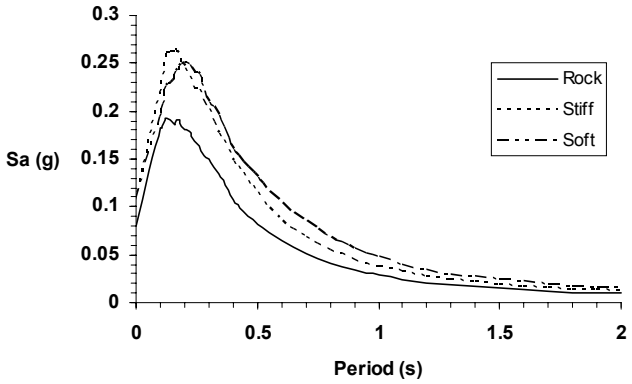

Figure 4.9. Acceleration response spectra predicted for a M_s 5.5 earthquake at 10 km according to the European equations of Ambraseys *et al.* (1996) for rock, stiff soil and soft soil sites.

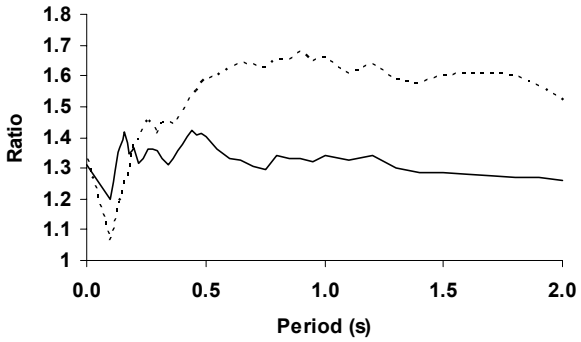

Figure 4.10. Ratios of the soil ordinates to the rock spectrum for the attenuation relationship of Ambraseys *et al.* (1996) for stiff soil (solid line) and soft soil (dashed line).

As mentioned in section 3.3.1, different attenuation relationships that include the soil condition have different outcomes, as can be observed in Figure 4.11.

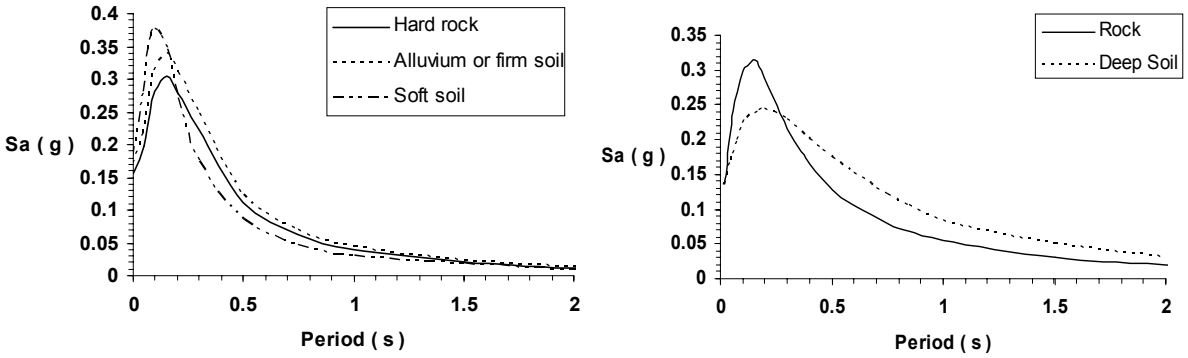

Figure 4.11. Acceleration response spectra predicted for a M_w 5.5 earthquake at 10 km. *Left* – from the attenuation relationships of Campbell (1997) for hard rock, alluvium or firm soil and soft soil, *right* – from the attenuation relationships of Abrahamson and Silva (1997) for rock and deep soil.

4.2.4. Fault mechanism

Not all attenuation relationships include the influence of the fault mechanism. Nevertheless, observation from the Northridge earthquake and other reverse faulting events indicate that this type of mechanism produce stronger motions than those from strike-slip events (e.g., Campbell, 1982; Somerville *et al*., 1996).

Some attenuation relationships that include the fault mechanism model its contribution as a period-dependent, distance-dependent and/or magnitude-dependent. In the attenuation relationships developed by Campbell (1997), the fault mechanism depends on both magnitude and distance. For the relations of Abrahamson and Silva (1997) this parameter is magnitude-dependent. For the relations of Boore *et al*. (1997), the fault effect is independent of magnitude and distance.

All the attenuation relationships that include the rupture mechanism suggest that reverse faults produce higher ground motions than strike-slip faults (about 20 to 40 percent larger) as can be observed in Figures 4.12 and 4.13 for the attenuation relationships of Campbell (1997) and Abrahamson and Silva (1997). This effect is most pronounced at short distances. Because the number of normal faulting earthquakes in most strong motion data sets is small, it has not been possible to distinguish between strike-slip and normal faulting earthquakes. Therefore, it is usual to use strike-slip attenuation relationships to predict the ground motion from normal faults. However, recent evaluations of normal faulting earthquakes have found that the ground motions from normal faulting earthquakes are smaller than for strike-slip earthquakes (Abrahamson, 2000).

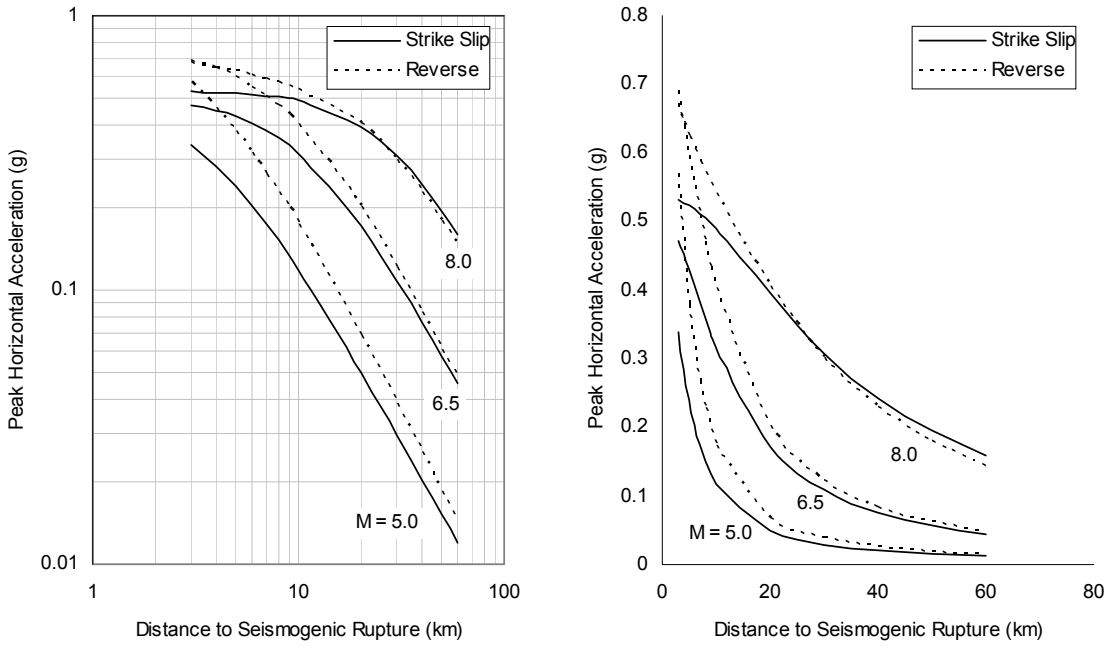

Figure 4.12. Scaling of PGA with magnitude, distance and source mechanism form the attenuation relationship of Campbell (1997) for rock.

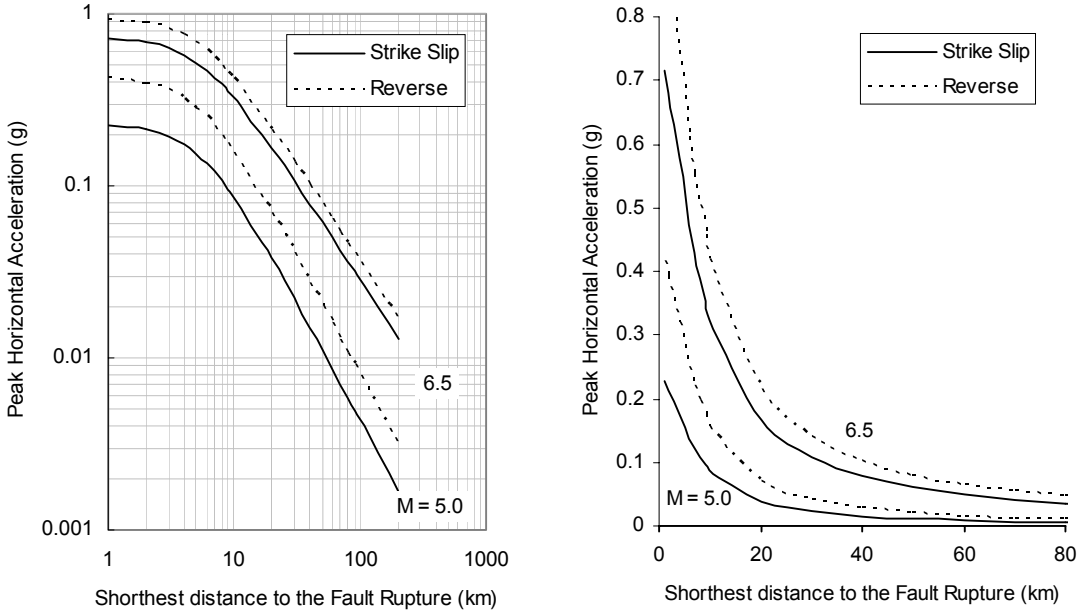

Figure 4.13. Scaling of PGA with magnitude, distance and source mechanism form the attenuation relationship of Abrahamson and Silva (1997) for rock.

The spectral ordinates given by the attenuation relationships of Campbell (1997) and Abrahamson and Silva (1997) for an event of magnitude 7 at distances of 5 and 20 km are presented in Figure 4.14 for strike-slip and reverse mechanisms.

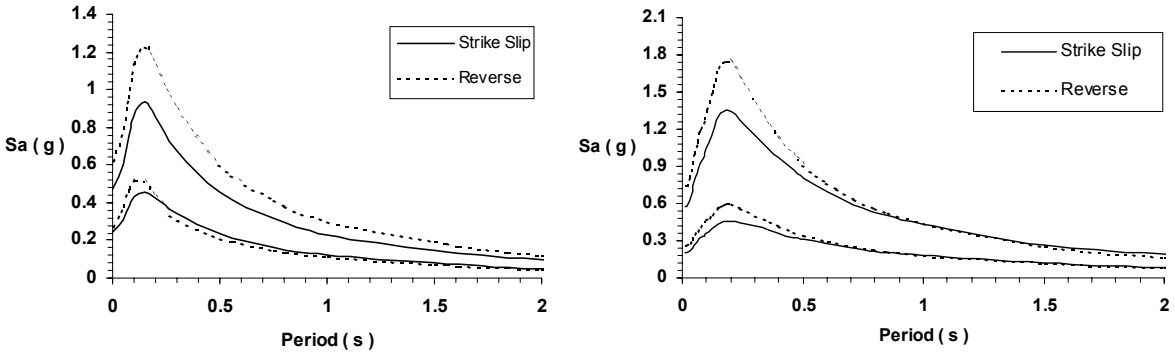

Figure 4.14. Pseudo-absolute acceleration response spectra for an earthquake of magnitude M_w 7 at 5 and 20 km for strike-slip and reverse mechanisms. *Left* – from the attenuation relationship of Campbell (1997) for firm soil, *right* – from the attenuation relationship of Abrahamson and Silva (1997) for rock.

The attenuation relationship of Abrahamson and Silva (1997) includes the effect of the hanging wall (which is considered to be primarily a geometric effect that results from the distance definition used in their study). Figure 4.15 shows the PGA values for a strike-slip event of magnitude M_w 6.5 and a reverse event with the same magnitude with and without the hanging wall effect. It can be noticed that the hanging wall effect decreases attenuation with distance for $r_{rup} < 25$ km.

The effect of the hanging wall for a reverse event in the acceleration response spectra for an earthquake with magnitude M_w 6.5 at 10 km from the source can be observed in Figure 4.16.

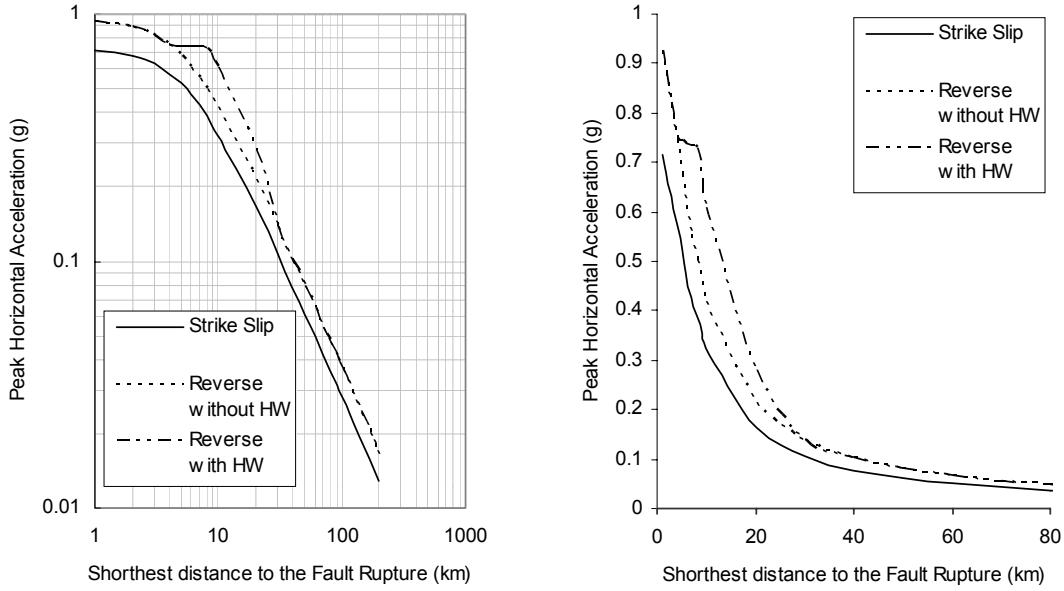

Figure 4.15. Attenuation of PGA with distance for an event of magnitude M_w 6.5 for a strike-slip event and a reverse event from the attenuation relationship of Abrahamson and Silva (1997) for rock with and without the hanging wall effect.

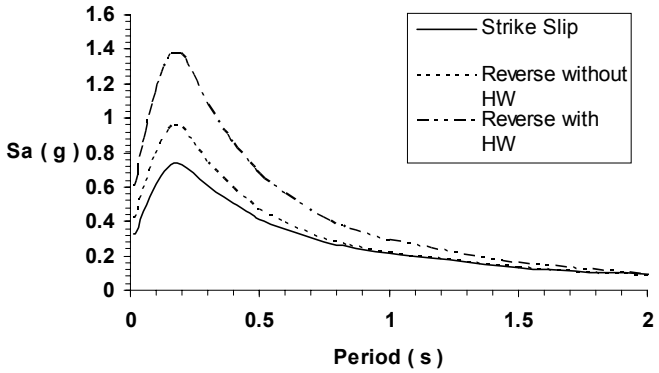

Figure 4.16. Acceleration response spectra for an earthquake at 10 km for rock sites with a magnitude M_w 6.5 for a strike-slip event and a reverse event from the attenuation relationship of Abrahamson and Silva (1997) with and without the hanging wall effect.

4.2.5. Focal depth

Ambraseys and Bommer (1991) and Ambraseys (1995) have developed depth-dependent attenuation relationships. From the equations of Ambraseys and Bommer (1991), it can be observed that the influence of the focal depth on PGA is very pronounced at short distances, but at 15 km or more from the source the value of PGA is effectively independent of depth.

As stated in section 3.14, the focal depth is important only for small earthquakes where this parameter controls how far below the surface the source of energy is located.

The equation of the attenuation relationships considered are described in Annex 2.

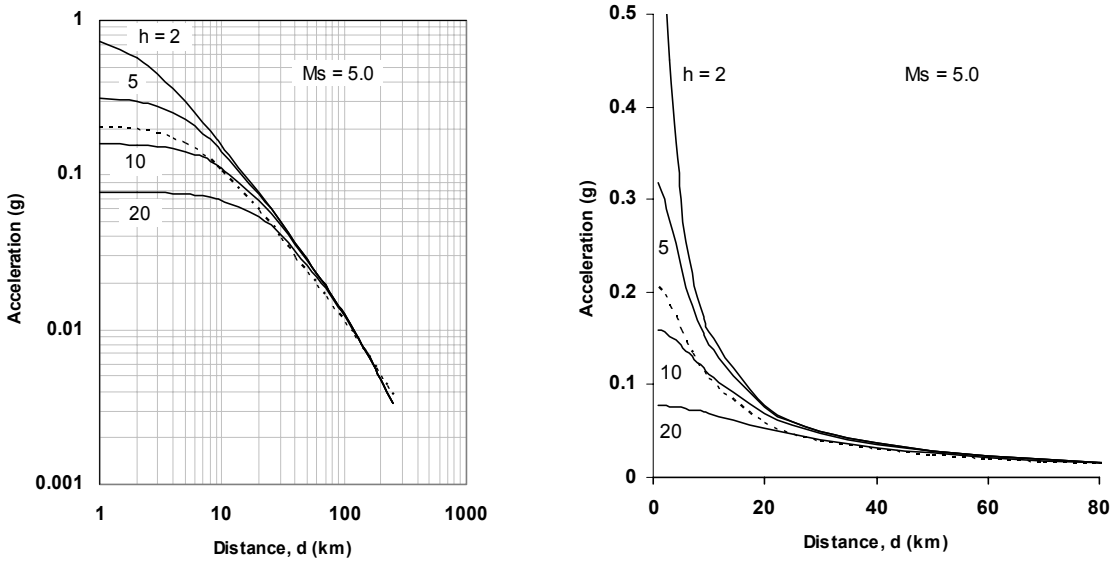

Figure 4.17. Attenuation of PGA with distance for an M_s 5 using the equations of Ambraseys and Bommer (1991) with constant depth (dashed) and explicit focal depth (solid lines).

4.2.6. Directivity

As stated in section 3.1.3, the influence of forward directivity on the spectrum leads to a pulse motion with large amplitude at intermediate to long periods and short duration. Contrary, backward directivity is characterised by motions with relatively long duration and low amplitude at long periods.

Somerville *et al*. (1997) developed modification to empirical strong-motion attenuation relationships to account for the effects of rupture directivity on strong-motion amplitudes and durations. The parameters that are modified are the average horizontal response spectral acceleration, the duration of the ground shaking and the ratio of strike-normal to strike-parallel spectral acceleration. Strike-normal refers to the horizontal component of motion normal to the strike of the fault while strike-parallel refers to the horizontal component of motion parallel to the strike of the fault. The definition of duration used is the 5-75% significant duration.

The geometric parameters used of the near-field directivity were illustrated previously in Figure 3.5. The empirical modification factors for acceleration response spectrum ordinates are illustrated in Figure 4.18, in which it can be observed that the spectral acceleration for forward directivity is larger for periods longer than 0.6 seconds.

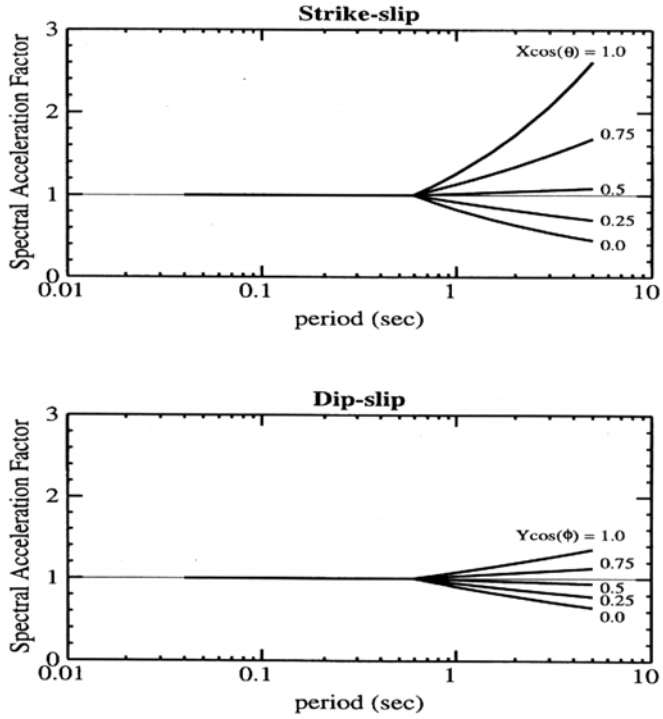

Figure 4.18. Empirical modification factors for acceleration response spectrum ordinates (Somerville *et al.*, 1997)

The models developed by Somerville *et al*. (1997) can be used to modify existing attenuation relationships to incorporate directivity effects in ground-motions used for seismic design.

4.3. Relationships for Arias intensity

Attenuation relationships have been derived the Arias Intensity. A compilation of these relationships has been done by Wilson (1993) for California and Kayen and Mitchell (1997) for active tectonic regions. An empirical relationship has recently been developed by Travasarou *et al*. (2002) to evaluate the Arias Intensity as a function of magnitude, distance, fault mechanism and site category. Since AI

contains a combination of amplitude and duration information, it is more magnitude sensitive than peak ground acceleration. The relationships mentioned are included in Table 4.2.

Table 4.2. Parameters included on some attenuation relationship for Arias Intensity.

Equation	Area	Magnitude	Distance (km)	Site considerations	Fault mechanism
Kayen and Mitchell (1997)	Active tectonic regions	M_w	r^*	Equations for rock, alluvium and soft soil.	---
Travasarou *et al*. (2002)	Worldwide	$4.7 \leq M_w \leq 7.6$	$0.1 \leq r_{jb} \leq 250$	Site classification proposed in Rodriguez-Marek *et al*. (2001). See section 3.3.1	F_1
Wilson (1993)	California	M_w	r_{jb}	---	---

r*. Source distance defined as the Pythagorean distance between a seismometer site and the closest distance to the fault rupture plane at the earthquake focal depth, Δ. $r^* = \sqrt{r_{jb}^2 + \Delta^2}$

F_1. Strike slip faults, normal faults and reverse/reverse-oblique faults.

The equations of the relationships considered for Arias Intensity are described in Annex 3. Figure 4.19 presents the attenuation relationship proposed by Travasarou *et al*. (2002).

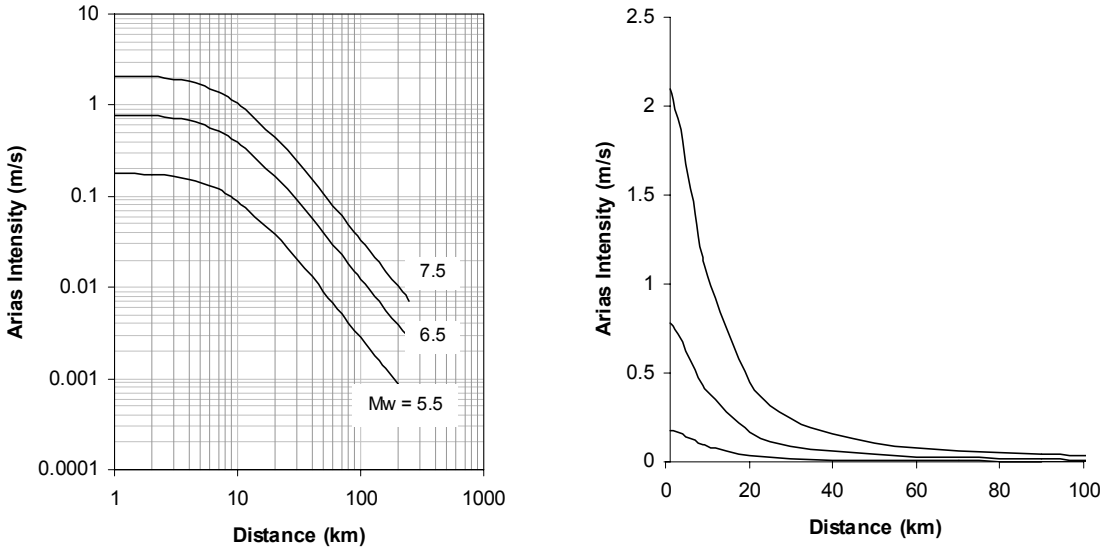

Figure 4.19. Median value of Arias Intensity for rock sites using the equations of Travasarou *et al.* (2002) for earthquakes with magnitude M_w = 5.5, 6.5 and 7.5.

4.4. Relationships for duration

It is not easy to make direct comparisons amongst attenuation relationships for duration. Besides the use of different magnitude scales and source-site distance definitions, there are many differing definitions of duration that have been employed.

Different authors have developed attenuation relationships for bracketed duration, D_B. Some of these relations for a treshold level of acceleration of 0.05g are shown in Figure 4.20. This measure of duration increases with the magnitude and decreases with distance.

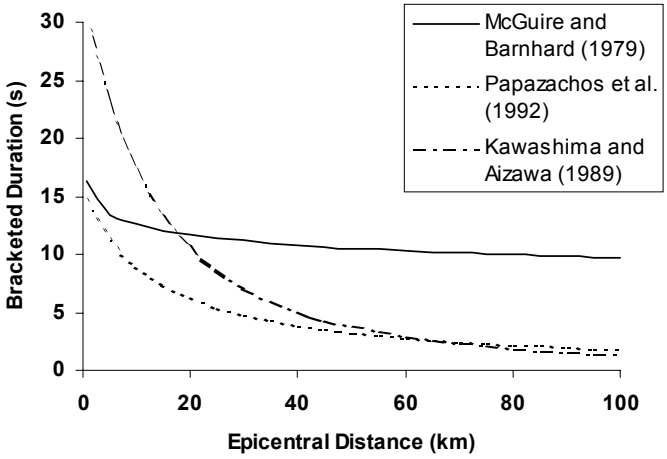

Figure 4.20. Predicted values of bracketed duration (a_0 = 0.05g) as a function of distance for a magnitude 6.5 earthquake according to the attenuation relationships of McGuire and Barnhard (1979) and Papazachos *et al.* (1992) for rock sites, and Kawasima and Aizawa (1989), which is independent of site condition.

The study of McGuire and Barnhard (1997) used a set of 50 strong-motion records, each one with three components. The record were classified as "alluvium" or "rock" and the distances used were the closest distance to the rupture surface or the epicentral distance. The records used correspond to the strong-motion records published by the California Institute of Technology in 1971.

In the work of Papazachos *et al*. (1992) 107 horizontal accelerogram components from 39 shallow earthquakes in Greece were used. They ere classified as "alluvium" or "rock" and the source-site distance used was the epicentral distance.

Kawashima and Aizawa (1989) used 197 set of two orthogonal horizontal components of strong-motion acceleration records from Japan. The epicentral distance was used. Three site conditions were considered: “rock”, “alluvium” and “soft alluvium”.

Relationships are available for significant duration, D_s, in active tectonic regions. From Figure 4.21 showing the attenuation relationship form Abrahamson and Silva (1996), it can been observed that significant duration is magnitude sensitive, and increases with distance for $r > 10$km (r_c).

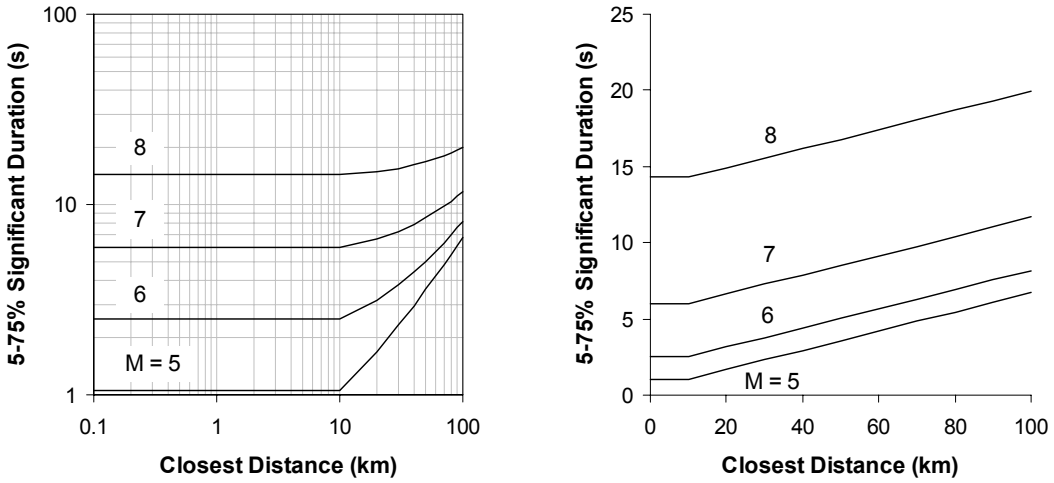

Figure 4.21. Prediction of 5-75% significant duration for rock sites using the equations of Abrahamson and Silva (1996).

The study of Abrahamson and Silva (1996) is based on a worldwide database of 655 recordings from 58 earthquakes. Relations are derived for the average horizontal and vertical component. The source-site distance definition used is the shortest distance to the fault rupture.

In Figure 4.22 predicted values of significant duration (5-95% of AI) from three different studies is presented.

It is interesting to notice that, since the significant duration is related only to the geometry of the accelerogram, regardless of its absolute amplitude, this relation predicts increasing duration with distance from the source. However, to speak of earthquake strong-motion at 100 km from an event of magnitude 5 is meaningless.

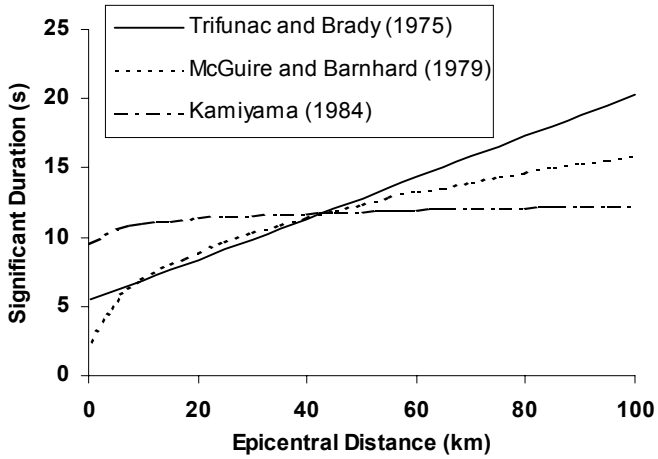

Figure 4.22. Prediction of 5-95% significant duration for rock sites using the equations of Trifunac and Brady (1975), McGuire and Barnhard (1979) and the Kamiyama (1984) for focal depth of 10 km.

In the work of Trifunac and Brady (1975) 118 acceleration records from Western USA were used (563 components). They were classified as "soft", "hard" and "intermediate" soil. The epicentral distance was used.

Kamiyama (1984) employed 192 horizontal components of strong-motion earthquakes records obtained in Japan. The source-site distance definition employed is the epicentral distance.

The dataset used by McGuire and Barnhard (1979) is the same as that used for the bracketed duration.

The details of the equations for duration included in this section are in Annex 4.

4.5. Relationships for the equivalent number of uniform stress cycles (N)

Relationships for the equivalent number of uniform stress cycles dependent on magnitude, distance and soil conditions have been proposed by Liu *et al*. (2001). As for the duration parameter, N is highly magnitude sensitive, and increases with distance like the relationship for the significant duration.

The relationship of Liu *et al*. (2001) is presented in Annex 4.

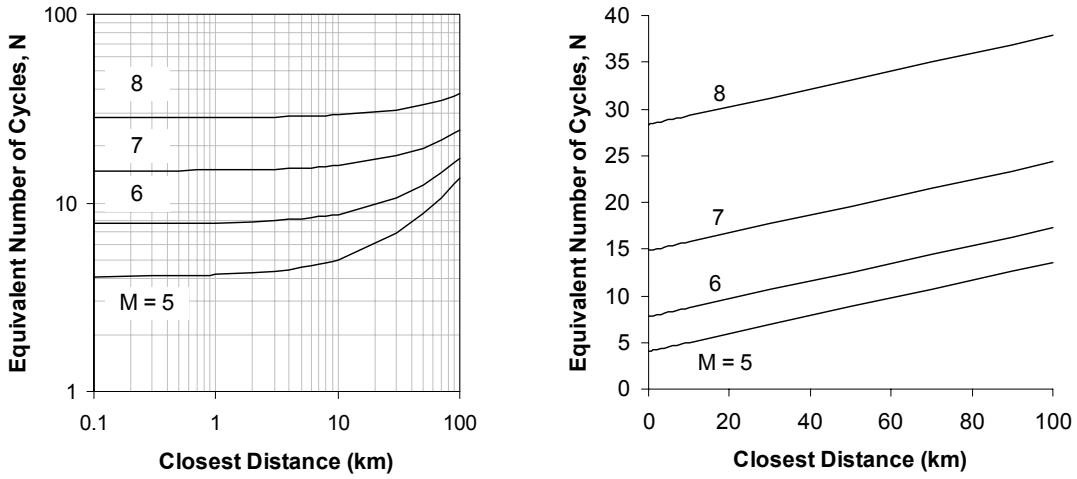

Figure 4.23. Equivalent number of uniform stress cycles for rock sites, using the equations of Liu *et al.* (2001).

4.6. Uncertainty in attenuation relationships.

The scatter in attenuation relationships is partly the result of modelling a very complex physical process with a very simple equation. It is usual to distinguish between two types of uncertainty: epistemic uncertainty and aleatory uncertainty.

Aleatory uncertainty is the inter-event uncertainty or temporal variability of strong motion. It refers to the uncertainty that is inherent due to the unpredictable nature of future earthquakes and there is no scope for its reduction. For most of the ground-motion models, the distribution of ground motion amplitude is assumed to be lognormal, characterized by a median (μ) and a logarithmic standard deviation (σ). This σ quantifies the scatter, which is considered to be entirely aleatory.

The epistemic uncertainty refers to the uncertainty arising from incomplete knowledge about earthquakes processes and therefore in principle it could be reduced by the collection of additional information. There is epistemic uncertainty, due to the limited data, in the values of μ and σ for a given magnitude and distance. The epistemic uncertainty is denoted σ_μ and σ_σ.

Probabilistc assessments that use logic trees for multiple models of the input treat aleatory and epistemic uncertainty in different ways. Aleatory uncertainty is accounted for directly in the integrations performed in the probabilistic seismic hazard analysis (PSHA). Epistemic uncertainty is

treated by development of multiple models of the PSHA which are subsequently weighted according to some estimate of the probability of each (Anderson and Brune, 1999).

The epistemic uncertainty can be appreciated by comparison of the median predicted values from different attenuation relationships for a single region. Figure 4.24 compares the response spectra for earthquakes at 10 km sites of magnitudes M_w 6 and 7 for California by two different equations.

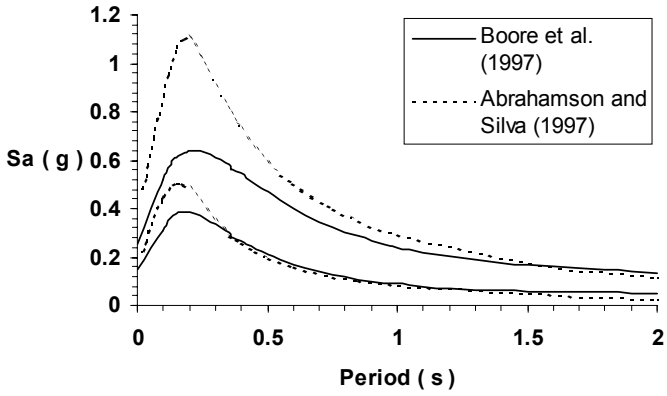

Figure 4.24. Response spectra for rock sites at 10 km for earthquakes of magnitude M_w 6 and 7 from the attenuation relationships of Boore *et al.* (1997) with V_s = 620 m/s and the equation of Abrahamson and Silva (1997).

5. INFLUENCE OF DIFFERENT FACTORS AFFECTING STRONG-MOTION

5.1. Relationships for Spectral Ordinates

5.1.1. Magnitude

As stated in Section 4.2.1, the dependency of the spectral shape on magnitude is important. This is clear when the normalised spectrum for a given distance are considered (Figures 4.5 and 4.6).

The maximum ratio of the Sa(T) values for the scenarios considered in Figures 4.3 and 4.4 increases with the period. For the periods considered (less than 2.0 seconds), the attenuation relationship of Campbell (1997) gives the biggest ratio (4.81), while the attenuation relationship of Abrahamson and Silva (1997) gives the smallest ratio (2.77).

The importance of the magnitude on the spectral shape and amplitude can also be noticed by the observation of the spectrum with the standard deviation associated with them (Figures 5.1 and 5.2).

In the spectral shapes of Figures 5.1 and 5.2 it is possible to observe the increase in the values of the spectral ordinates due to the increase of magnitude. For the scenarios considered, when the increment of half a unit of magnitude is added (from M_s = 6 to M_s = 6.5), the ordinates of the spectra for the median are lower than the ordinates of the original magnitude plus one standard deviation, but if the increment is of one unit of magnitude (from M_s = 6 to M_s = 7), the majority of the spectral ordinates for the median are higher than the ordinates of the original magnitude plus one standard deviation.

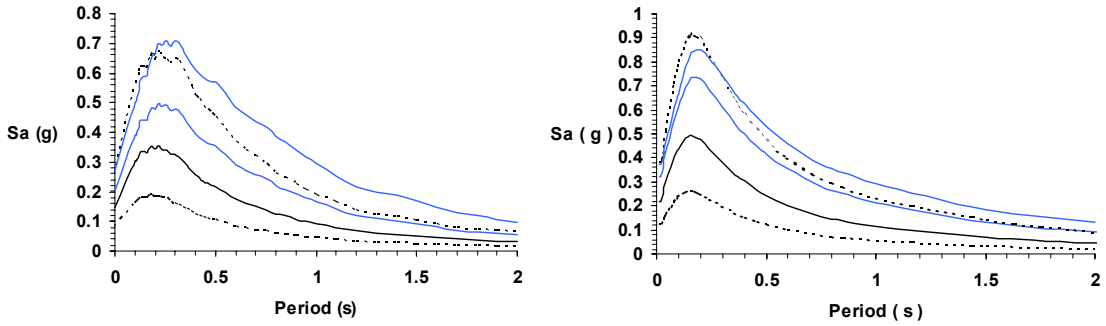

Figure 5.1. Spectral shapes for rock sites at 10 km from earthquakes of M 6, 6.5 and 7 for median values (solid lines) and median plus/minus the standard deviation for the earthquake of M = 6 (dashed). *Left* - from the attenuation equations of Ambraseys *et al.* (1996), *right* – from the attenuation equations of Abrahamson and Silva (1997).

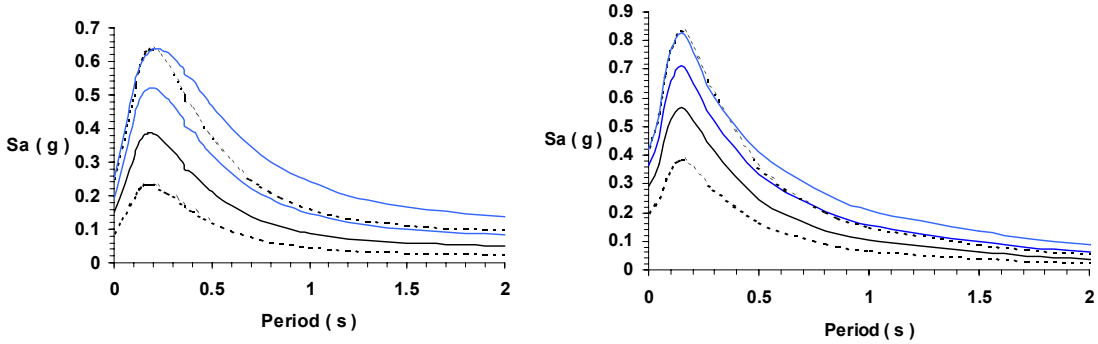

Figure 5.2. Spectral shapes for rock sites at 10 km from earthquakes of M_w 6, 6.5 and 7. *Left* - for median values (solid lines) and median*$10^{\sigma logy}$ and median/$10^{\sigma logy}$ for the earthquake of M_w = 6 (dashed) from the attenuation equations of Boore *et al.* (1997) with V_s = 620 m/s, *right* - for median values (solid lines) and median plus/minus the standard deviation for the earthquake of M_w = 6 (dashed) from the attenuation equations of Campbell (1997).

5.1.2. Distance

The relative insensitivity of the shape to distance (while being sensitive to magnitude) is clearer by the comparison of the maximum ratio of the Sa(T) values for the scenarios considered in Figures 4.5 and 4.6 (same distance for different magnitudes) and the scenarios considered in Figures 4.7 and 4.8 (same magnitude for different distances), shown in Table 5.1.

Table 5.1. Comparison of the maximum ratio of the Sa(T) values for the normalised spectra considered in Figures 4.5 and 4.6 with the scenarios of Figures 4.7 and 4.8.

Attenuation relationship	Max ratio (same distance, different magnitudes)	Max ratio (same magnitude, different distances)
Ambraseys *et al*. (1996)	3.28 at T = 1.5 s	1.47 at T = 2.0 s
Abrahamson and Silva (1997)	2.77 at T = 2.0 s	2.06 at T = 2.0 s
Boore *et al*. (1997)	2.23 at T = 1.5 s	1.30 at T = 0.7 s
Campbell (1997)	4.81 at T = 2.0 s	1.14 at T = 2.0 s

Figures 5.3 and 5.4 present the influence of the standard error on the spectral ordinates of an earthquake with magnitude M_s = 7 for a rock site at 10 km.

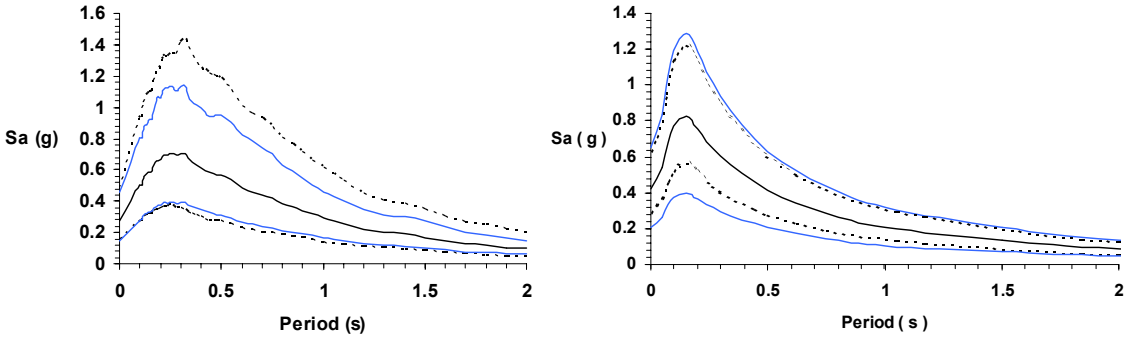

Figure 5.3. Spectral shapes for rock sites from a M 7 earthquake at 5, 10 and 20 km for median values (solid lines) and median plus/minus the standard deviation at 10 km (dashed). *Left* - from the attenuation equations of Ambraseys *et al.* (1996), *right* – from the attenuation equations of Campbell (1997).

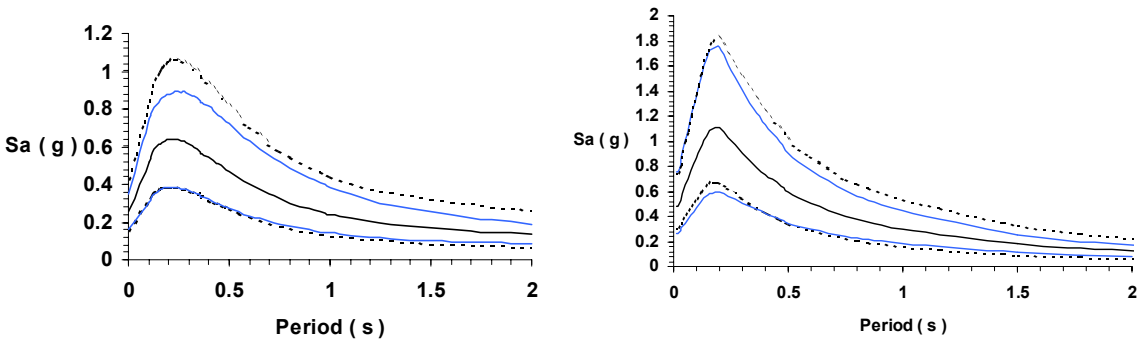

Figure 5.4. Spectral shapes for rock sites from a M_w 7 earthquake at 5, 10 and 20 km. *Left* - for median values (solid lines) and median*$10^{\sigma \log y}$ and median/$10^{\sigma \log y}$ at 10 km (dashed) from the attenuation equations of Boore *et al.* (1997) with V_s = 620 m/s, *right* - for median values (solid lines) and median plus/minus the standard deviation at 10 km (dashed) from the attenuation equations of Abrahamson and Silva (1997).

From Figures 5.3 and 5.4 it can be noticed that for a given distance (10 km) the ordinates of the spectra including the standard deviation cover the increment of distance by a factor of 2 (only in the equations by Campbell (1997) is it not covered but for an almost insignificant amount). When the distance of 5 km is considered (factor of 0.5) the spectral ordinates for the median have similar ordinates than the spectral ordinates minus one standard deviation at 10 km. The biggest difference is observed again on the attenuation relationship of Campbell (1997).

By the comparison of Figures 5.3 and 5.4 for distance and Figures 5.1 and 5.2 for magnitude, it can be observed that the degree of epistemic uncertainty reflected by a change in distance of 10 km (from d = 10 km to d = 20 km) is slightly bigger than the degree of epistemic uncertainty reflected by a change of one unit of magnitude (from M = 6 to M = 7).

5.1.3. Soil condition

In the attenuation relationships of Ambraseys *et al*. (1996) and Boore *et al*. (1997) the effect of the soil deposits is reflected in the higher values of the spectral ordinates. Even thought both equations use the same site classification, the relationship of Boore *et al*. (1997) presents a stronger dependence. From Figure 5.5, by the comparison of the spectral ordinates for soft soils for an earthquake of magnitude M 5.5 at 10 km from the site with those of a rock site at the same distance for an earthquake of magnitude M 6, it can be observed for the scenario considered that for the relationship of Ambraseys *et al*. (1996) the spectral ordinates for soft soils are very similar to those for a rock site. For the relationship of Boore *et al*. (1997) the spectral ordinates for soft soils are greater than those for a rock site for periods lower than ~ 3.0 s and lower for periods greater than ~ 3.0 s.

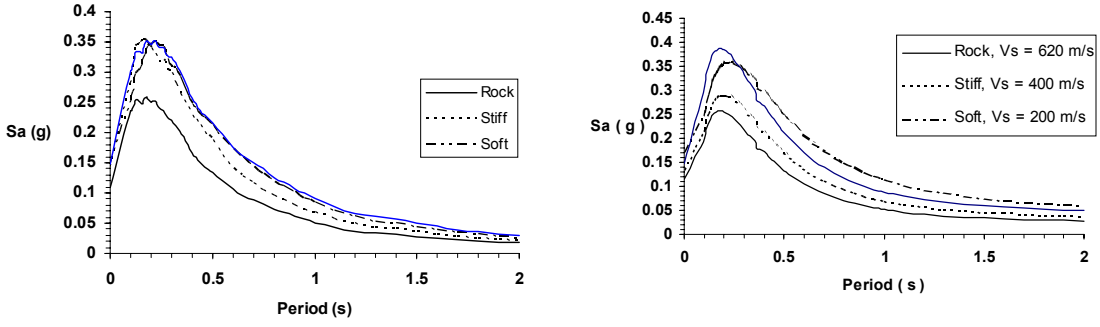

Figure 5.5. Response spectra for earthquakes at 10 km sites of magnitude M 5.5 and 6 for rock sites (solid lines) and for an earthquake of magnitude M 5.5 for stiff and soft sites (dashed lines). *Left* - from the attenuation relationship of Ambraseys *et al.* (1996), *right* - from the attenuation relationship of Boore *et al.* (1997).

In the attenuation relationships of Campbell (1997) and Abrahamson and Silva (1997), the soil effects can be observed in Figure 5.6. Contrary to the attenuation relationship of Ambraseys *et al*. (1996), the spectral ordinates of an event with a magnitude M_w 5.5 for soil sites at 10 km distances are lower than the ordinates of an event of M_w 6 for rock site at the same distance. Only for short periods in the attenuation relationship of Campbell (1997) the spectral ordinates of the scenarios considered are similar.

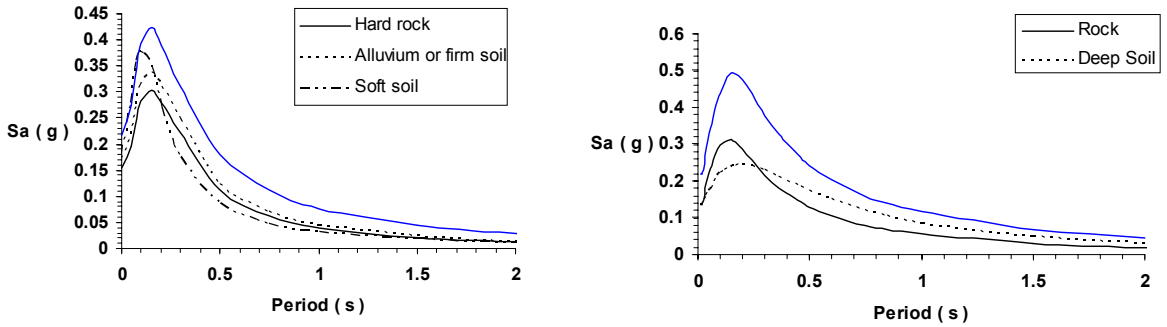

Figure 5.6. Response spectra for earthquakes at 10 km sites of magnitude M_w 5.5 and 6 for rock sites (solid lines) and for an earthquake of magnitude M_w 5.5 for soil sites (dashed lines). *Left* – from the attenuation relationship of Campbell (1997), *right* – from the attenuation relationship of Abrahamson and Silva (1997).

The effect of uncertainty in the equations of Ambraseys *et al*. (1996) and Abrahamson and Silva (1997) is presented in Figure 5.7. It can be observed that the change of soil type for rock a softer soil is cover by the standard deviation for all the periods.

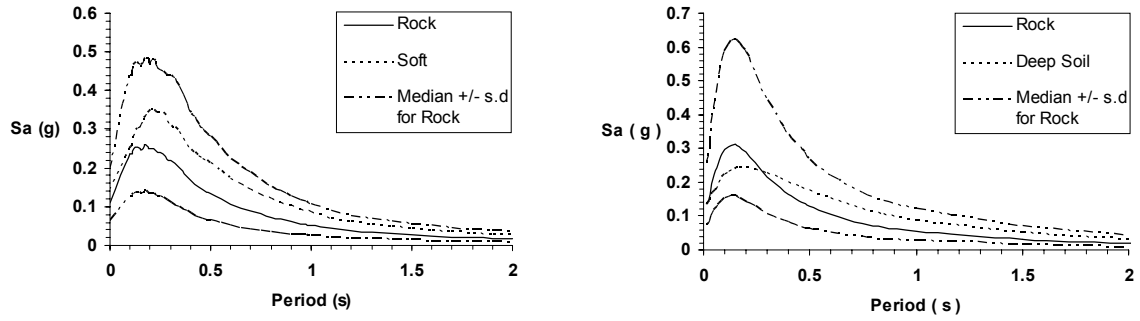

Figure 5.7. Spectral shapes of an earthquake with magnitude M 5.5 at 10 km sites for the median values for rock and soil sites and median plus/minus the standard deviation for rock sites. *Left* – from the attenuation equations of Ambraseys *et al.* (1996), *right* – from the attenuation equations of Abrahamson and Silva (1997).

5.1.4. Fault mechanism

The effect of the fault mechanism on the response spectra can be observed in Figure 5.8 for the attenuation relationships of Campbell (1997) and Abrahamson and Silva (1997). For short periods the ordinates of the spectra given by the attenuation relationship of Campbell (1997) for an event at short distances of magnitude 5.5 and with a reverse fault mechanism are relatively similar to the spectral ordinates of an event at the same distance with a magnitude of 6.5 and a strike-slip mechanism. In the attenuation relationship of Abrahamson and Silva (1997) the same is observed but for shorter periods.

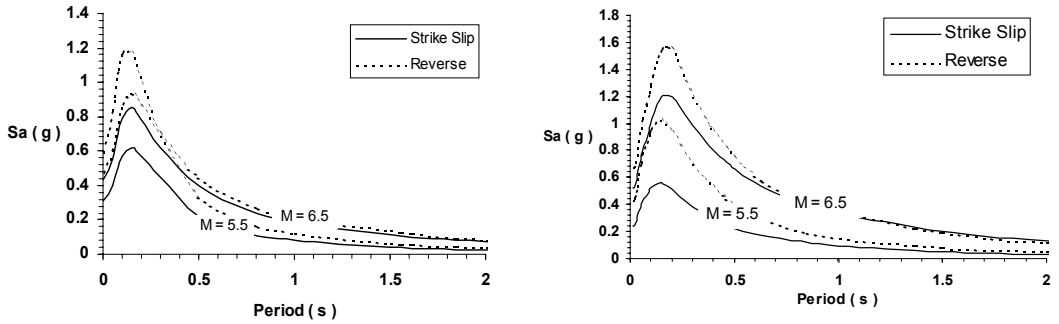

Figure 5.8. Pseudo-absolute acceleration response spectra for earthquakes of magnitudes M_w 5.5 and 6.5 *Left* - from the attenuation equations of Campbell (1997) for firm soil at 5 km with strike slip and reverse faults, *right* – from the attenuation equations of Abrahamson and Silva (1997) for rock soil at 5 km sites and reverse faults.

It is also important to notice that the differences of ordinates for events with different fault mechanism are covered by the standard error as can be observed on Figure 5.9. The spectral ordinates for the median values plus one standard deviation of a strike slip mechanism have higher values than the spectral ordinates for the median values of a reverse mechanism for the attenuation relationships of Campbell (1997) and Abrahamson and Silva (1997).

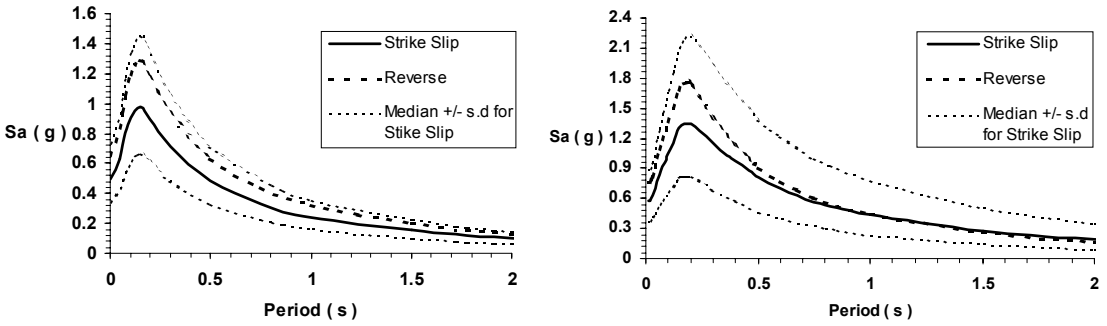

Figure 5.9. Influence of the standard error on pseudo-absolute acceleration response spectra for earthquakes of magnitude M_w 7 for rock soils at 5 km sites. *Left* - from the attenuation relationship of Campbell (1997), *right* – from the attenuation relationship of Abrahamson and Silva (1997).

5.1.5. Focal depth

The influence of the focal depth on the PGA values can be observed in Figure 4.17 for an earthquake with magnitude M_s = 5 for the attenuation relationships of Ambraseys and Bommer (1991). For the considered scenarios, at a distance of 1 km, the ratio of the PGA for depths of 2 and 20 km has a value of 9, while at a distance of 5 km this ratio has a value of 4.

The influence of the magnitude in the PGA for a given focal depth can be observed in Figure 5.10. For an increment of one unit of magnitude, the PGA value increases by a factor of 1.65 for the attenuation relationship of Ambraseys and Bommer (1991). For the attenuation relationships of Ambraseys (1995) the factor is 1.76.

The influence of the standard deviation on the equation of Ambraseys and Bommer (1991) is shown in Figure 5.11 for an event of M_s 5 and a focal depth of 5 km. The median values of PGA for focal depths of 2, 10 and 20 are presented for comparison.

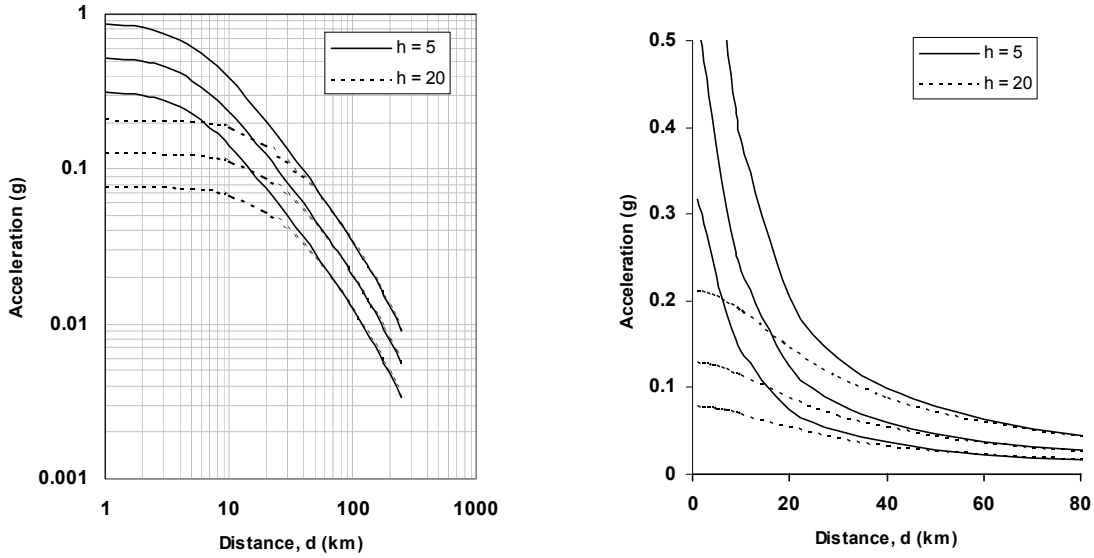

Figure 5.10. Attenuation of PGA with distance for earthquakes with M_s 5, 6 and 7 using the equations of Ambraseys and Bommer (1991) with a focal depth of 5 (solid lines) and 20 km (dashed lines).

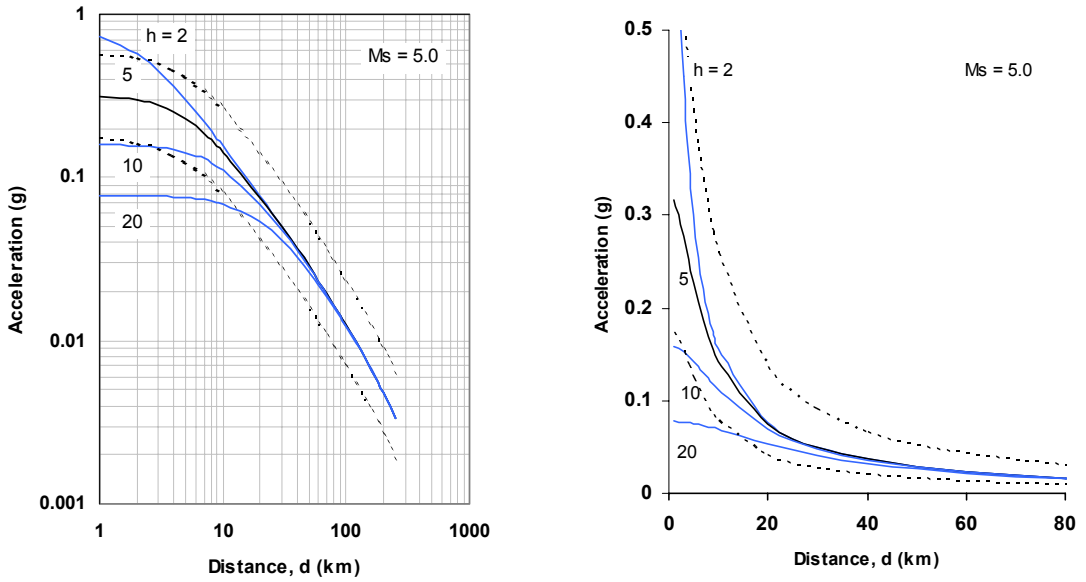

Figure 5.11. Attenuation of PGA with distance for earthquakes with M_s 5 using the equations of Ambraseys and Bommer (1991) for the median values for focal depths of 2, 5, 10 and 20 km (solid lines) and the median plus/minus one standard deviation for a focal depth of 5 km (dashed lines).

5.1.6. Directivity

According to Somerville *et al*. (1997), the variation of the spectral ordinates due to rupture directivity depends on two geometrical parameters: the angle between the direction of rupture propagation and the direction of waves travelling from the fault to the site (the smaller the angle the larger the amplitude) and the fraction of the fault rupture length that lies between the hypocentre and the site (the larger the fraction the larger the amplitude). The strike-slip is controlled by the azimuth angle, θ, while the dip-slip is controlled by the zenith angle, ϕ.

For strike-slip faulting, maximum directivity conditions ($X\cos\theta = 1$) cause an amplitude about 1.8 times larger that the median values at 2 second period, while minimum directivity conditions causes an amplitude about 0.6 of the median. For dip-slip faulting the effects lies in the range of about 1.2 to 0.8 at 2 second period.

The effect of rupture directivity (using the Somerville *et al*. (1997) factors) on the attenuation relationship of Abrahamson and Silva (1997) for an earthquake with magnitude $M_w = 6.5$ at 10 km for the site can be observed for both strike-slip and dip-slip faulting in Figure 5.12. It can be appreciated that the influence of the directivity as implied by these factors is very small. Much larger effects are implied by the near-source factors N_a and N_v from UBC97 where for closest distances to the seismic source ≤ 2 km, N_a varies between 1.5 and 1.0, while N_v varies from 2.0 to 1.0. No variation is present for distances ≥ 10 km for N_a and for distances ≥ 15 km for N_v.

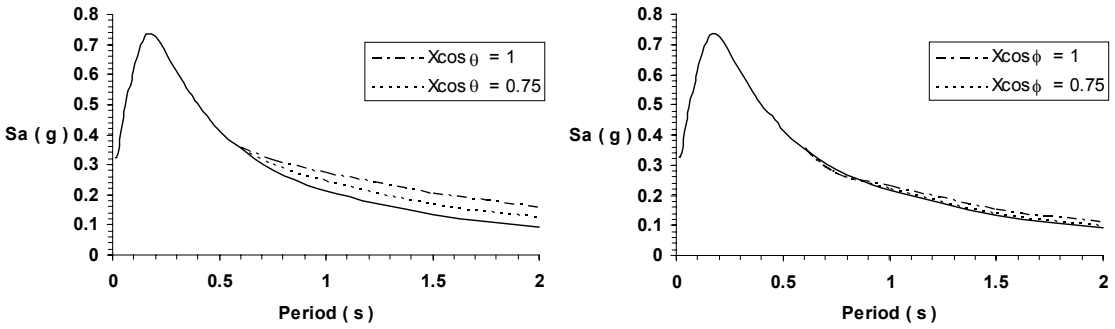

Figure 5.12. Effect of rupture directivity on the acceleration response spectra for an earthquake of magnitude $M_w = 6.5$ for rock soil at 10 km sites form the attenuation relationship of Abrahamson and Silva (1997). *Left* – for strike-slip faulting, *right* – for dip-slip faulting.

5.2. Relationships for Arias intensity

The attenuation relationship of Travasarou *et al*. (2002) includes the soil condition and the fault mechanism. The influence of these parameters can be observed in Figures 5.13 and 5.14.

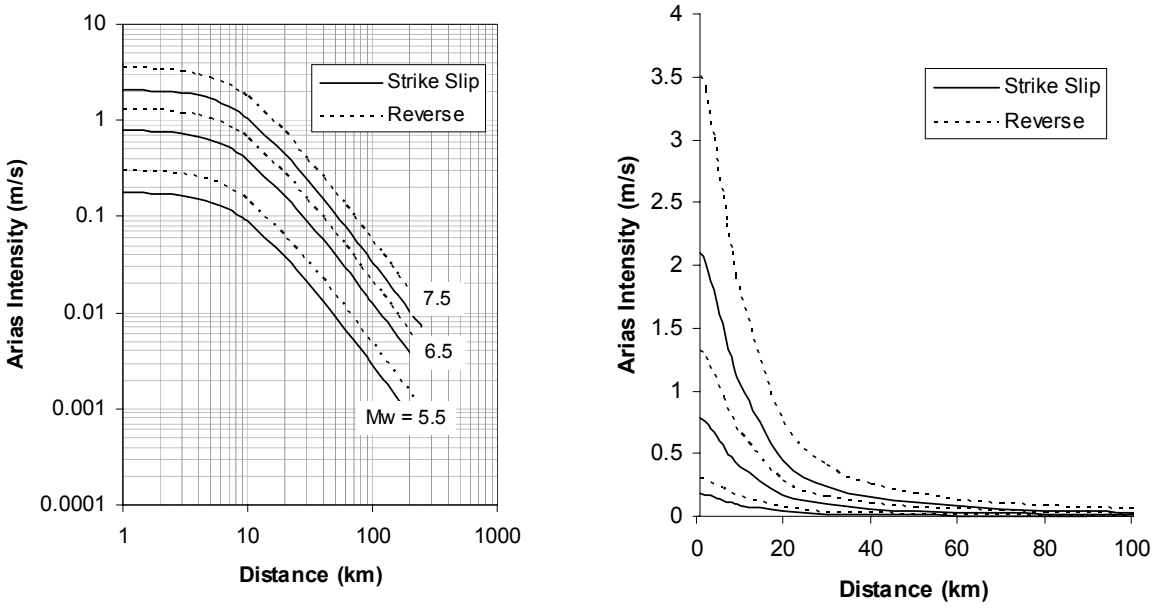

Figure 5.13. Median value of Arias intensity from earthquakes of M_w 5.5, 6.5 and 7.5 using the equations of Travasarou *et al*. for site category B (rock) and for strike slip and reverse faults.

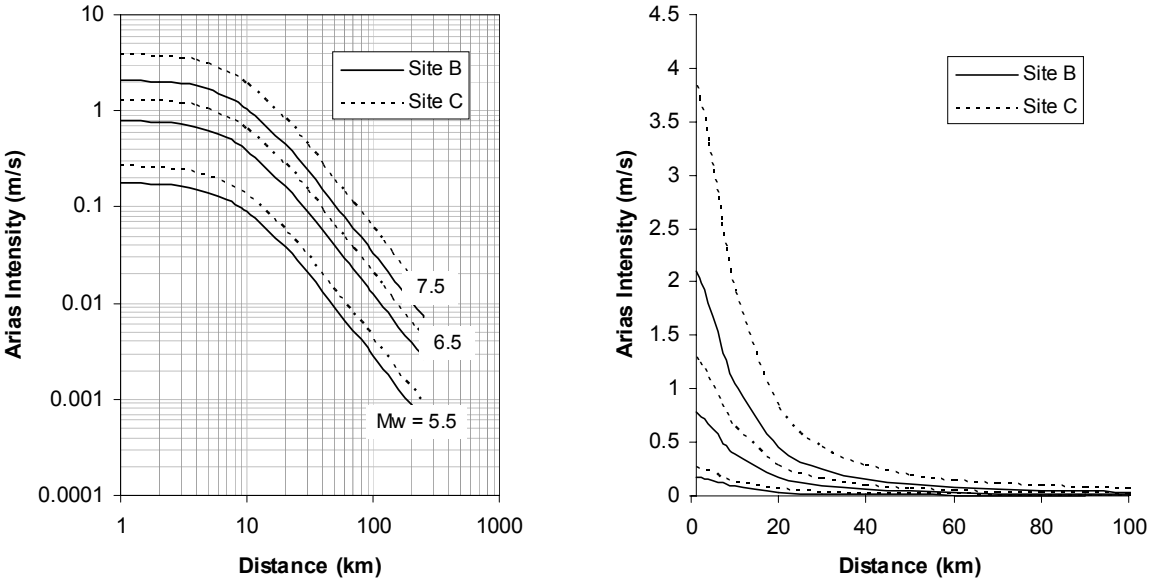

Figure 5.14. Median value of Arias intensity from earthquakes of M_w 5.5, 6.5 and 7.5 using the equations of Travasarou *et al*. for strike-slip faults and for site category B (rock) and C (deep stiff soil).

For the scenarios considered in Figure 5.13, the ratio of the AI values between the event with M_w = 5.5 and the event of M_w = 7.5 (with the same fault mechanism) is constant for all the distances, with a value of 11.7. For the scenarios considered in Figure 5.14, the ratio is also constant for all distances, with a value of 11.7 for rock sites and 14.41 for deep stiff soil.

5.3. Relationships for duration

Although all the relationships developed for bracketed duration, D_B, agree that this measure increases with the magnitude and decreases with distance, the amount by which D_B increases with the increase of one unit of magnitude is very different for each attenuation used, as can be observed on Figures 5.15 and 5.16. The same can be observed for the distance variation.

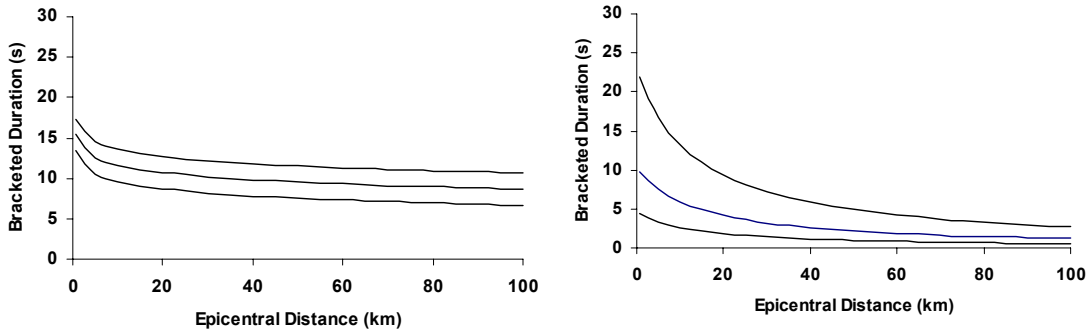

Figure 5.15. Median value of the bracketed duration (a_0 = 0.05g) for earthquakes with magnitude 5, 6 and 7 and rock sites. *Left* – from the attenuation relationship of McGuire and Barnhard (1979), *right* – from the attenuation relationship of Papazachos et al. (1992)

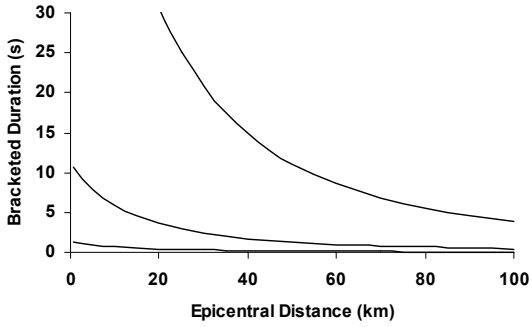

Figure 5.16. Median value of the bracketed duration (a_0 = 0.05g) for earthquakes with magnitude 5, 6 and 7 from the attenuation relationship of Kawasima and Aizawa (1989).

The significant duration increases with both magnitude and distance. Figure 4.21 shows the predicted values of 5-75% significant duration from the equation of Abrahamson and Silva (1996) for earthquakes with magnitude 5, 6, 7 and 8. For the 5-95% significant duration, Figures 5.17 and 5.18 present the predicted values for events with magnitude 5, 6 and 7 by the three equations addressed in this study.

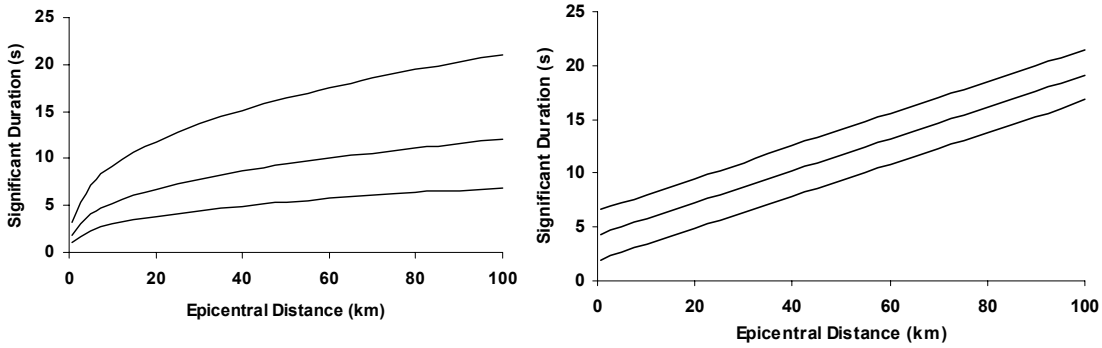

Figure 5.17. Median values for the prediction of 5-95% significant duration for rock sites for earthquakes with magnitude 5, 6 and 7 and rock sites. *Left* – McGuire and Barnhard (1979), *right* – Trifunac and Brady (1975).

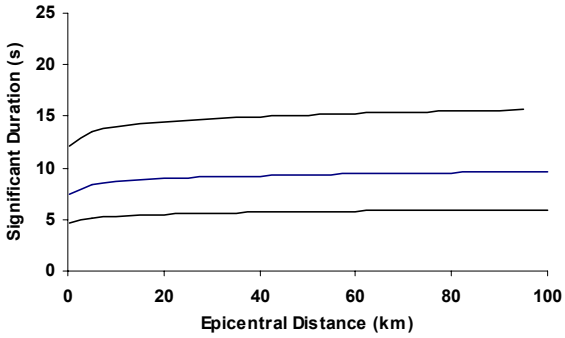

Figure 5.18. Median values for the prediction of 5-95% significant duration for rock sites for earthquakes with magnitude 5, 6 and 7 and rock sites from the attenuation relationship of Kamiyama (1984) for a focal depth of 10 km.

5.4. Relationships for the equivalent number of uniform stress cycles (N)

In Figure 4.23 the dependency on the Equivalent Number of Uniform Stress Cycles (N) on magnitude and distance can be clearly observed. The value of N given by the relationship of Liu *et al*. (2001) is

slightly higher for deep soil sites than for shallow stiff soil or rock sites, as can be observed in Figure 5.19.

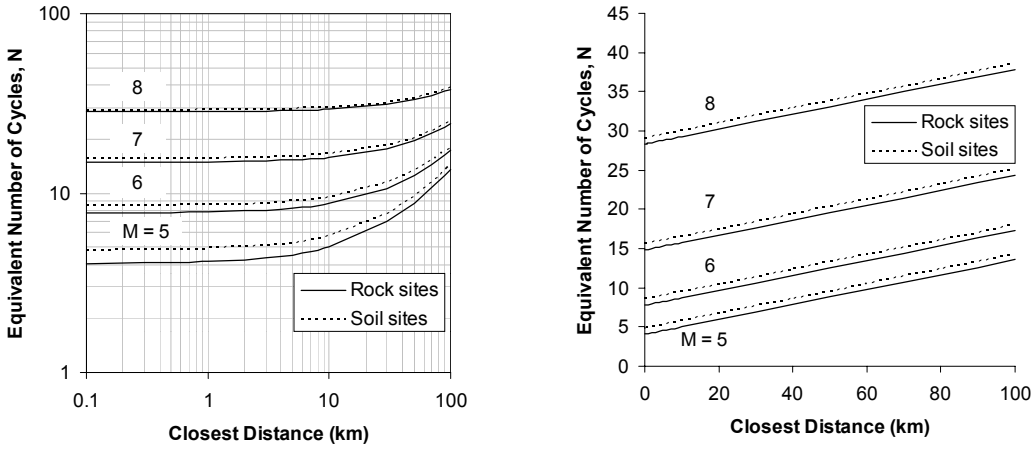

Figure 5.19. Equivalent number of uniform stress cycles using the equations of Liu *et al.* (2001) for earthquakes of magnitude 5, 6, 7 and 8 for deep soil sites (dashed lines) and shallow stiff soil or rock sites (solid lines).

5.5. Relative influence of explanatory parameters on response parameters.

In order to compare the relative influences of different explanatory parameters on different response (i.e. strong motion) parameters, four scenarios were considered. For each scenario, four attenuation relationships were used to calculate the values of the median, the median plus one standard deviation and the median plus half a standard deviation for the PGA and the spectral ordinates for periods of 0.3, 1.0 and 2.0 s.

The scenarios considered are one event with high magnitude and one event with low magnitude. For each case two source-site distances were considered. In all the cases, a rock site and a strike-slip mechanism was assumed. The scenarios are:

Scenario 1: Magnitude 7, distance 10 km
Scenario 2: Magnitude 7, distance 25 km
Scenario 3: Magnitude 5, distance 10 km
Scenario 4: Magnitude 5, distance 25 km

The attenuation relationships used for the spectral ordinates are those proposed by Ambraseys *et al*. (1996), Campbell (1997), Abrahamson and Silva (1997) and Boore *et al*. (1997). The Arias intensity was calculated by the equation of Travasarou *et al*. (2002) and the significant duration $D_{s\ 5\text{-}75\%}$ by the equation of Abrahamson and Silva (1996). From the base case studied, different changes were made to each of the factors included in the attenuation relationship. The results are presented in Figures 5.20 to Figure 5.23.

The explanatory parameters considered are distance (from 10 to 5 km and from 25 to 20 km), magnitude (from M = 7.0 to M = 7.5 and from M = 5 to M = 5.5), site condition (from rock to soil), fault mechanism (from strike-slip to reverse) and directivity (without directivity effect and with directivity effect).

The influence of ***distanc*e** is more pronounced at close sites. The attenuation relationships of Campbell (1997) and Abrahamson and Silva (1997) present a stronger influence for the event with lower magnitude (M = 5) while in the equations of Ambraseys *et al*. (1996) and Boore *et al*. (1996) the influence of the distance is independent of the magnitude. The amplification of the spectral ordinates is relatively similar for the different periods considered. The biggest difference is observed in the attenuation relationship of Boore *et al*. (1997) where the spectral ordinate corresponding to T = 1.0 s presents a larger amplification with respect to the other periods for events at close sites. The Arias intensity is independent of magnitude but dependent on distance, being greater for closer distances. The significant duration remains the same for the event at 10 km distance, independent on the magnitude, while it is deamplified for the events at bigger distances (d = 25 km), being more pronounced for the lower magnitude event.

The influence of ***magnitude*** on the spectral ordinates is greater for longer periods for both distances considered d = 10 km and d = 25 km for the attenuation relationships of Ambraseys *et al*. (1996) and Abrahamson and Silva (1997). The relationship of Campbell (1997) presents a smaller amplification on the spectral ordinates for T = 0.3 s than the amplification at T = 0 s (PGA). Nevertheless, the difference in amplifications is almost zero. For the other periods considered, amplification is greater as the period increases. In the attenuation relationship of Boore *et al*. (1997) for the event with magnitude 7, the amplification does not present a tendency with period. For the event with magnitude 5, amplification increases with increasing period. The influence of magnitude is almost independent of source-site distance. The Arias intensity presents a bigger amplification for the event of magnitude 5. The value is independent on source-site distance. The significant duration presents bigger amplification for the closest event, having the same amplification regardless of the magnitude. For the event at 25 km, bigger amplification takes place for the event with magnitude 7 while for the event at 10 km the amplification is independent of magnitude.

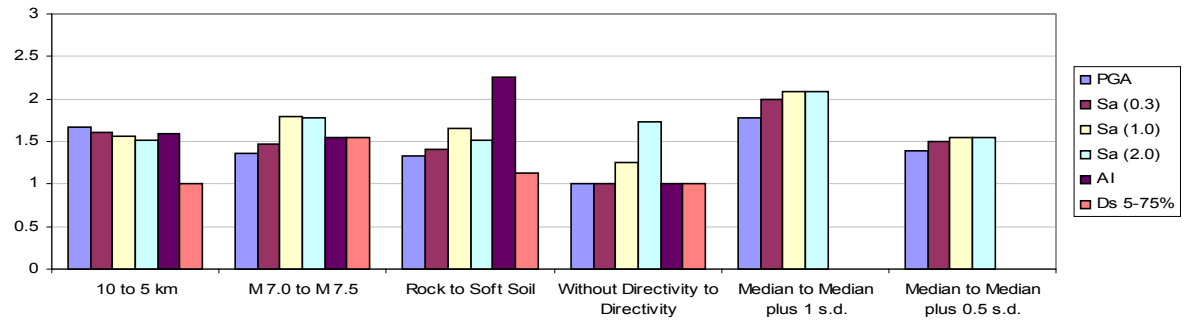

a. Scenario 1 (M = 7, d = 10 km)

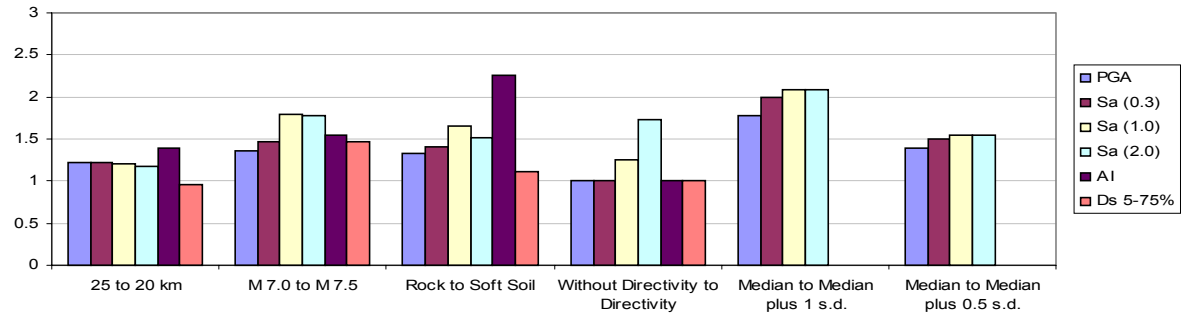

b. Scenario 2 (M = 7, d = 25 km)

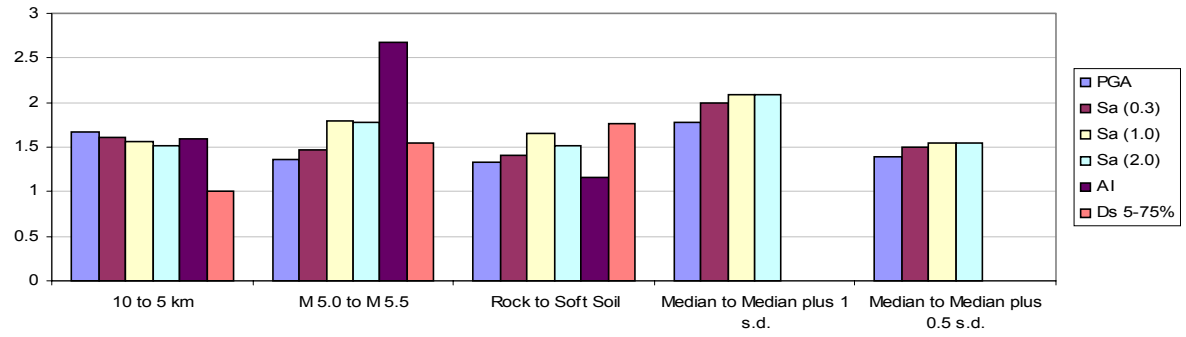

c. Scenario 3 (M = 5, d = 10 km)

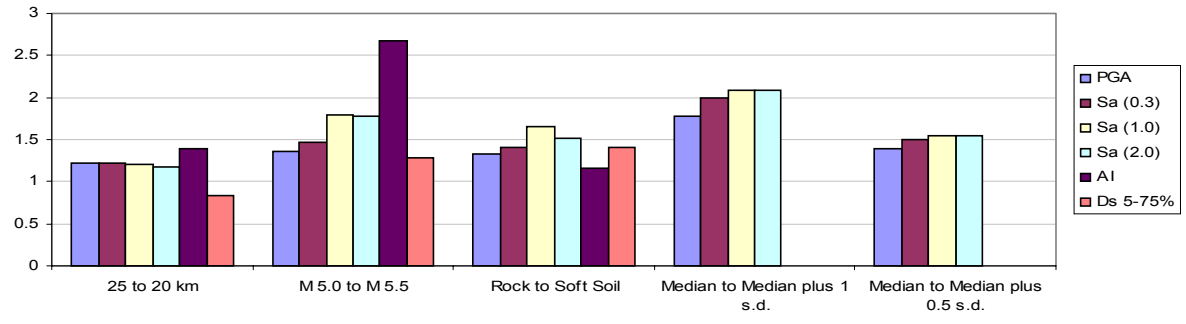

d. Scenario 4 (M = 5, d = 25 km)

Figure 5.20. Relative influence of explanatory parameters on response parameters by the attenuation relationship of Ambraseys *et al.* (1996).

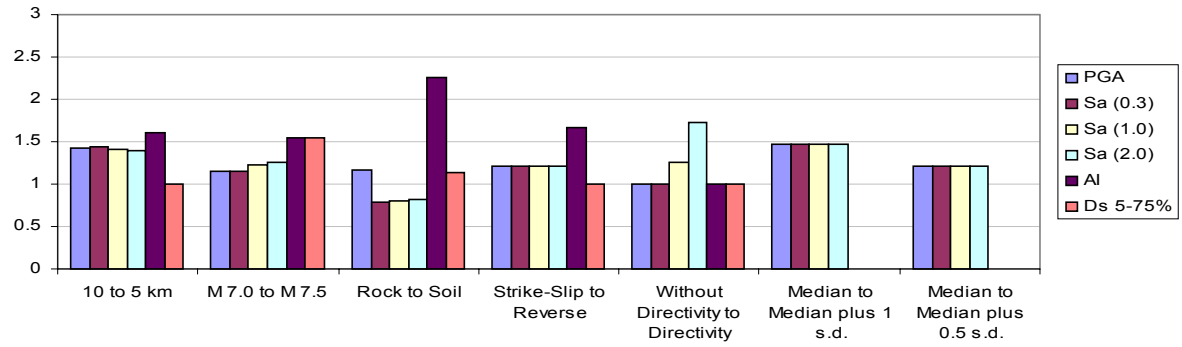

a. Scenario 1 (M = 7, d = 10 km)

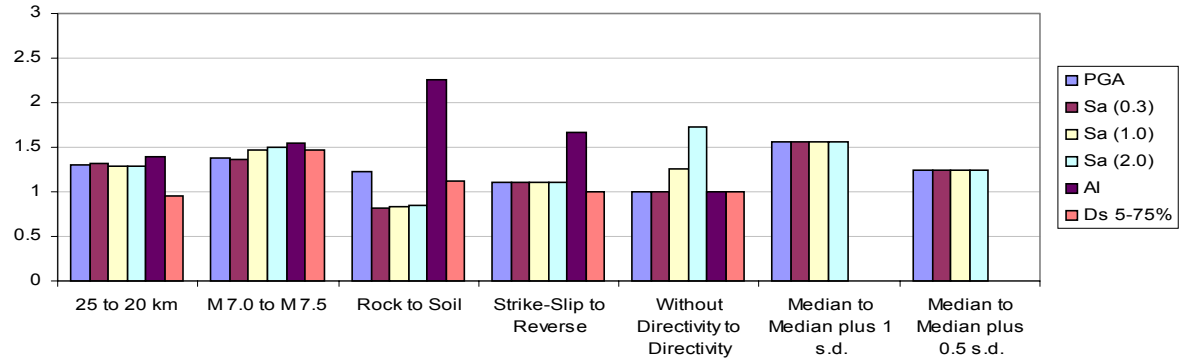

b. Scenario 2 (M = 7, d = 25 km)

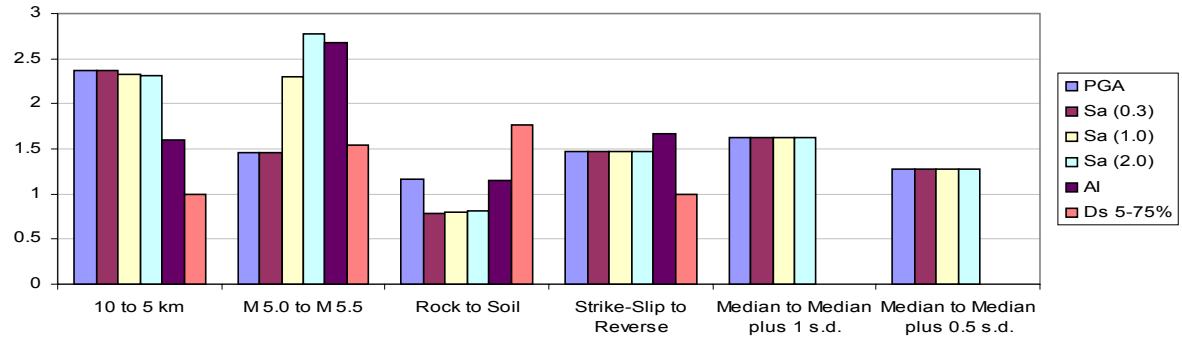

c. Scenario 3 (M = 5, d = 10 km)

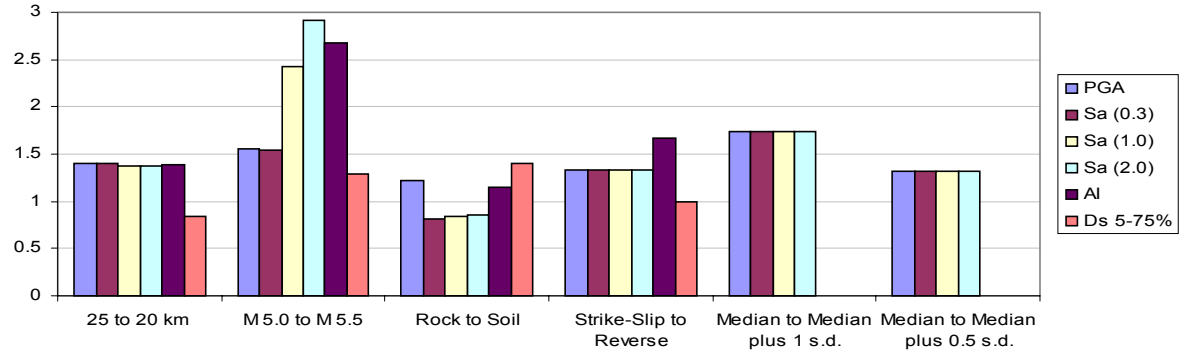

d. Scenario 4 (M = 5, d = 25 km)

Figure 5.21. Relative influence of explanatory parameters on response parameters by the attenuation relationship of Campbell. (1997).

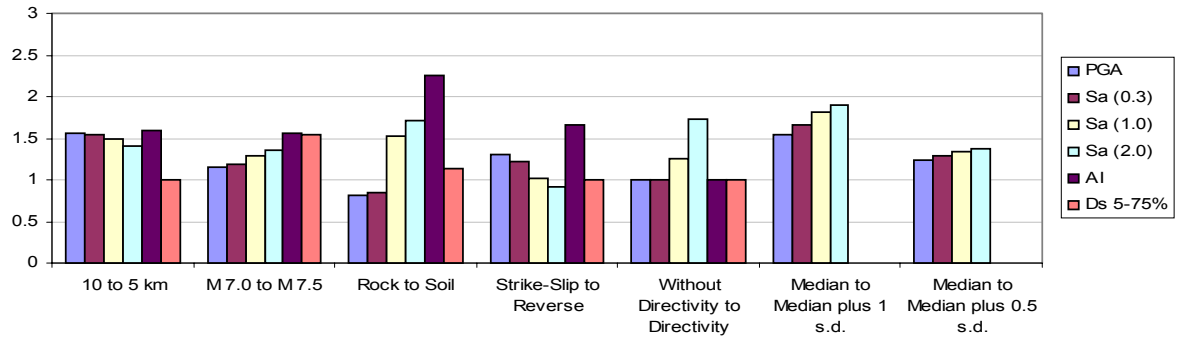

a. Scenario 1 (M = 7, d = 10 km)

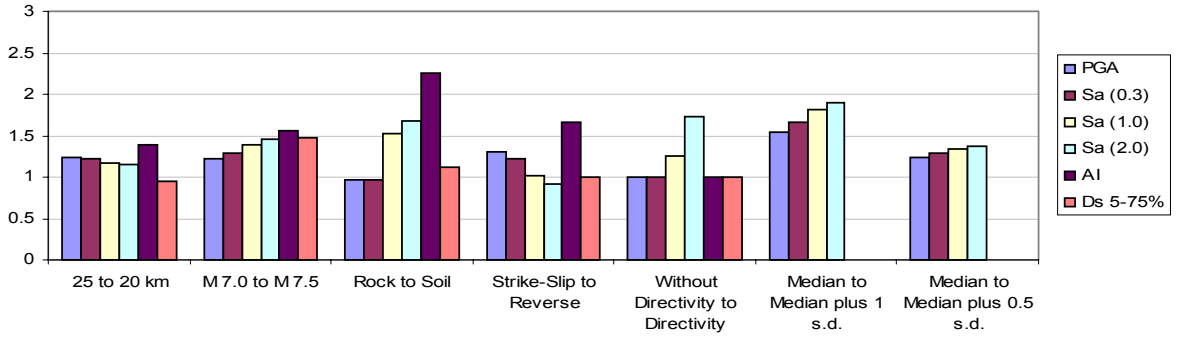

b. Scenario 2 (M = 7, d = 25 km)

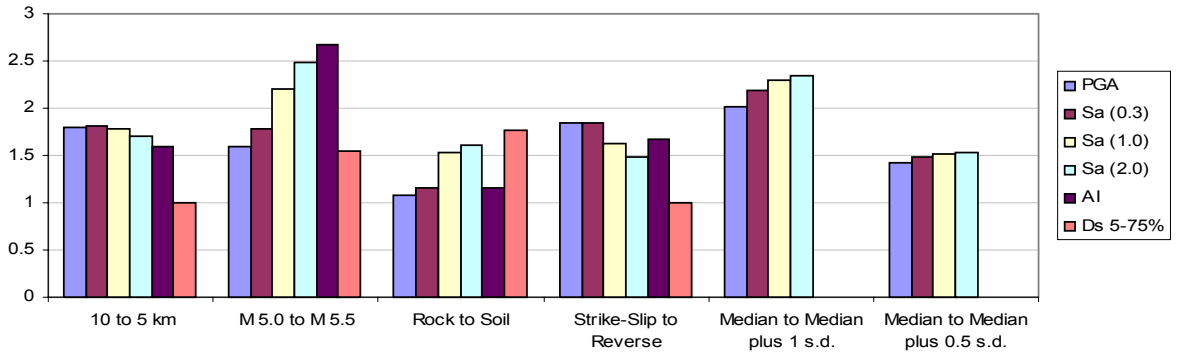

c. Scenario 3 (M = 5, d = 10 km)

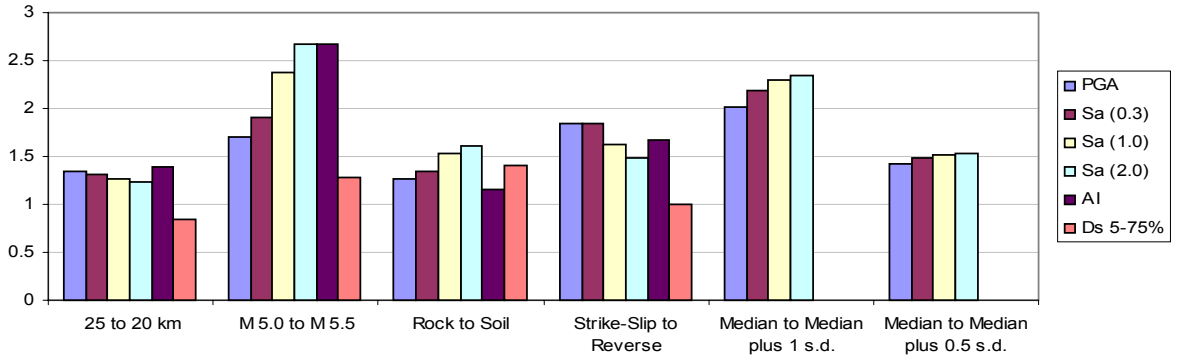

d. Scenario 4 (M = 5, d = 25 km)

Figure 5.22. Relative influence of explanatory parameters on response parameters by the attenuation relationship of Abrahamson and Silva. (1997).

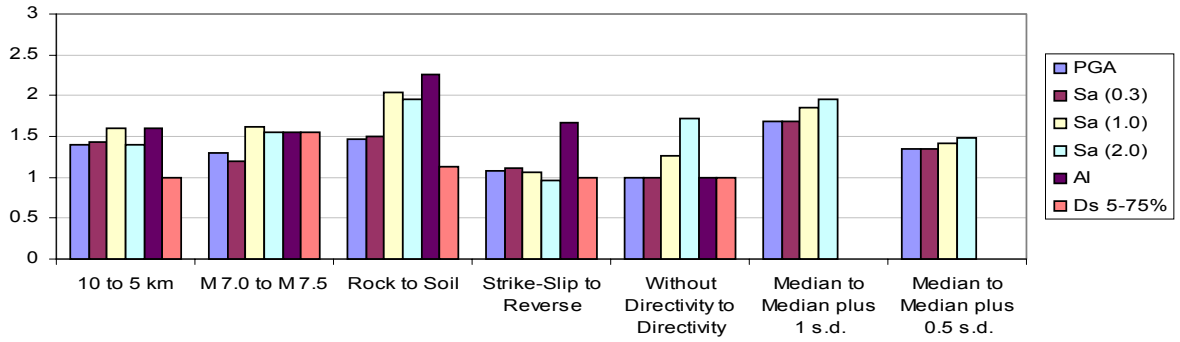

a. Scenario 1 (M = 7, d = 10 km)

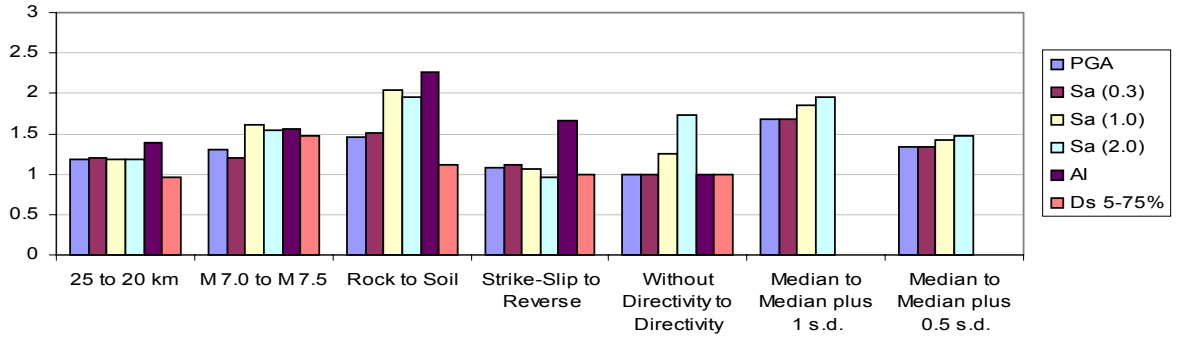

b. Scenario 2 (M = 7, d = 25 km)

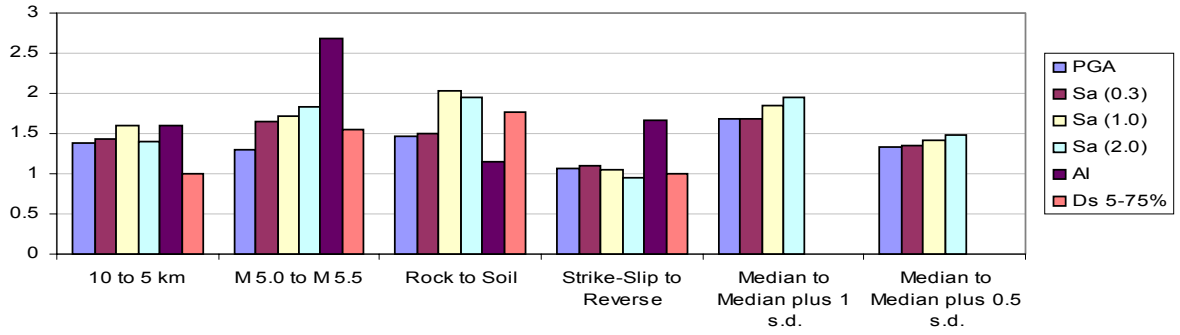

c. Scenario 3 (M = 5, d = 10 km)

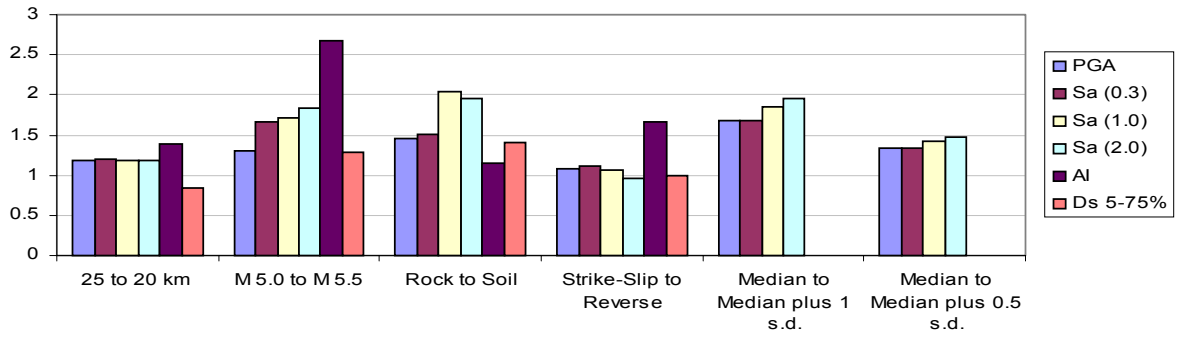

d. Scenario 4 (M = 5, d = 25 km)

Figure 5.23. Relative influence of explanatory parameters on response parameters by the attenuation relationship of Boore *et al.* (1997).

Site conditions produce different outcomes in each attenuation relationship as clearly observed in Figures 5.20 to 5.23. Some relationships present amplification in the spectral ordinates for all the periods considered, like the attenuation relationships of Ambraseys *et al*. (1996) and Boore *et al*. (1997). In both cases the amplification of the spectral ordinates increases with the period, except for T = 2.0 s where the amplification is slightly less than the amplification for T = 1.0 s. For these two equations there is no influence of the magnitude and the source-site distance, and soil non-linearity is ignored. The attenuation relationship of Campbell (1997) presents amplification of the spectral ordinates only for the PGA value and deamplification for the other periods considered. For the periods where deamplification takes place, the deamplification decreases with increasing period. As for the two previous equations, there is no influence of the magnitude and the source-site distance. For the attenuation relationship of Abrahamson and Silva (1997), which does model the non-linear behaviour of the soil, deamplification is presented for the event with magnitude 7 for the PGA and Sa (0.3), for the other spectral ordinates considered, Sa (1.0) and Sa (2.0), amplification takes place. For the event with magnitude 5, amplification always takes place, being greater for the bigger periods. Arias intensity increases considerably when the magnitude of the event is 7, but it is almost the same for the event with magnitude 5. A similar observation can be made for duration.

The ***fault mechanism*** effect is included in three of the attenuation relationship considered. Although the influence of this parameter on the spectral ordinates is different for each relationship, they all agree that amplification takes place when a reverse event is considered. Only for the spectral ordinates for T = 2.0 s deamplification takes place in the attenuation relationships of Boore *et al*. (1997) for all the scenarios considered and in the equation of Abrahamson and Silva (1997) for the scenarios with the event of magnitude 7. In the attenuation relationship of Abrahamson and Silva (1997) the fault mechanism effect is greater for the smaller periods and it is magnitude dependent, being more pronounced for the smaller magnitudes. For the attenuation relationship of Boore *et al*. (1997) the amplification is almost similar for PGA, Sa (0.3) and Sa (0.1), all being close to unity. The fault mechanism effect in this last relationship is independent of magnitude and distance. The attenuation relationship of Campbell (1997) presents a constant amplification of the spectral ordinates for all periods. The fault mechanism depends on magnitude and distance, being greater for the scenario with the smaller magnitude and distance. Arias intensity is increased by this parameter independent on magnitude and distance. The significant duration is unchanged.

Full forward ***directivity*** was applied to the attenuation relationships by using the Somerville *et al*. (1997) factors. This parameter affects only the spectral ordinates for periods greater than 0.6 s. The amplification is independent of magnitude and distance. Arias intensity and significant duration are not affected by this parameter.

The ***standard deviation*** is magnitude dependent, being greater for events with smaller magnitude for the attenuation relationship of Abrahamson and Silva (1997). For the attenuation relationship of Ambraseys *et al*. (1996) and Boore *et al*. (1997), the standard deviation is period dependent but it is independent on magnitude and distance. For the attenuation relationship of Campbell (1997) the standard deviation is independent on period, magnitude and distance.

5.6. Examples of variation of parameters with scaling

For this section three time-histories recorded on rock were selected in order to explore the variation of the characteristic parameters of the accelerograms with scaling. The scaling was done first in amplitude by factors of 0.5, 0.75, 1.25, 1.50, 1.75 and 2.00 and then in time by a factors of 0.8 and 1.2. The scaling procedures are addressed in the following chapter; in this part a specific scaling procedure was not followed because the aim is only to evaluate the variation of the parameters. The influence of the scaling procedures is addressed in Chapter 6. The magnitude of the events ranges between 6.2 and 6.6 and their source-site distances between 22.7 and 38.8 km. They were selected by comparison whit the spectral shape given by the attenuation relationship of Ambraseys *et al*. (1996) for an event with magnitude 6.5 and distance 30 km, in order to have three different types of spectral shapes. The 1984 Morgan Hill time-history presents a relatively good agreement with the spectral shape given by the attenuation relationship. The 1983 Coalinga time-history presents higher spectral ordinates for all the periods, specially between T ~ 0.1 s and T ~ 0.6 and for periods T > 0.8 s. The 1971 San Fernando time-history present higher spectral ordinates until T ~ 0.3 s and smaller values up to T ~ 1.7 s. The time histories of the record selected are specified in Table 5.2 and they are illustrated in Figure 5.24.

Table 5.2. Time-histories selected.

Eq.	YR	MDY	HRMN	M	Station	Closest Dist (km)	PGA (g)	PGV (g)	PGD (cm/s)
Morgan Hill	1984	0424	2115	6.2	Corralitos	22.7	0.081	6.4	1.17
Coalinga	1983	0502	2342	6.4	Parkfield-Gold Hill 3 W	38.8	0.137	11.0	2.76
San Fernando	1971	0209	1400	6.6	Lake Hughes #4	24.2	0.164	6.4	0.93

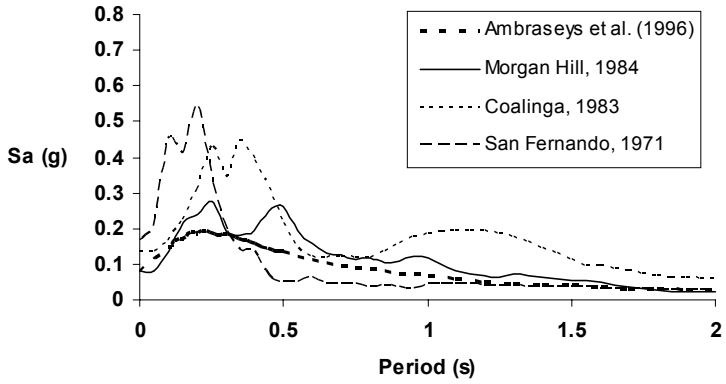

Figure 5.24. Comparison of the acceleration response spectra for the 1984 Morgan Hill, 1983 Coalinga and 1971 San Fernando earthquakes with the acceleration response spectra given by the attenuation relationship of Ambraseys *et al.* (1996) for rock sites for an event of magnitude 6.5 and source-site distance 30 km.

For each time-history the parameters analysed are Arias intensity, AI, uniform duration, D_u, bracketed duration (a_0 = 0.05g), D_b, 5-75% significant duration, $D_{s\ 5\text{-}75}$, 5-95% significant duration, $D_{s\ 5\text{-}95}$, spectral intensity, SI, root-mean-square acceleration (time interval = $t_{95} - t_5$), a_{rms}, and equivalent number of stress cycles, N (calculated by the relationship of Liu *et al*. (2001)).

Most of the changes in parameters could be directly estimated from the scaling factors: some are unaffected, like the equivalent number of stress cycles, N, for both types of scaling (on amplitude and time), significant duration, D_s, when scaling on amplitude is done and a_{rms} when scaling on time is done; others are scaled in proportion to the scaling factor, such as the spectral intensity, SI, and the a_{rms} when scaling in amplitude is done, and the Arias intensity, AI, and the three duration considered when scaling in time is done; other scale to the square of the scaling factor, such as the Arias intensity, AI, for the scaling on amplitude.

Only changes like the change in uniform and bracketed duration (D_u and D_b) for amplitude scaling and spectral intensity, SI, for time-axis scaling, are not predictable.

Tables 5.3, 5.4 and 5.5 present the values of these parameters after the scaling is performed. Figures 5.25, 5.26 and 5.27 contain the acceleration response spectra resulting from the scaling.

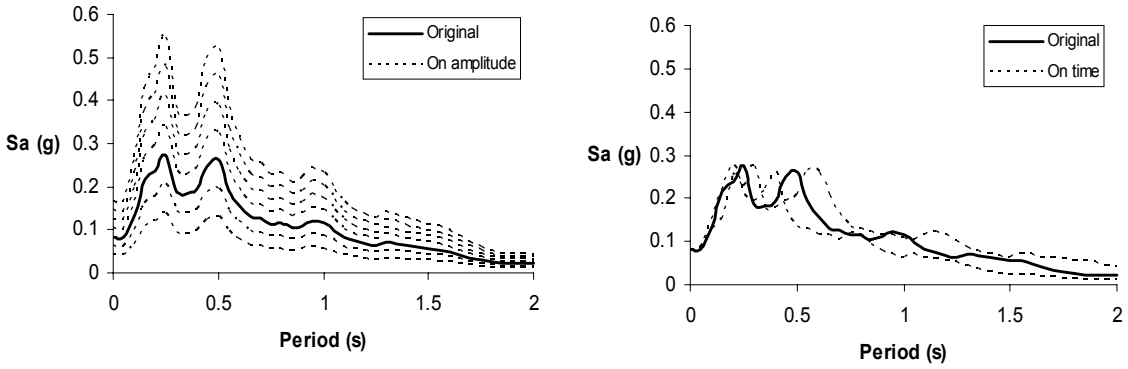

Figure 5.25. Variation of the acceleration response spectra with scaling for the 1984 Morgan Hill earthquake. *Left* - by scaling on amplitude, *right* – by scaling on time.

Table 5.3. Variation of the strong-motion parameters with scaling on amplitude and time for the 1984 Morgan Hill earthquake.

Scaling on amplitude								
Factor	AI (m/s)	D_b (s)	D_u (s)	$D_{s\ 5\text{-}75}$ (s)	$D_{s\ 5\text{-}95}$ (s)	SI (m/s)	$a_{rms\ 5\text{-}95}$ (m/s^2)	N
0.5	0.016	-------	-------	4.6	11.6	0.142	0.042	11.0
0.75	0.038	0.06	0.04	4.6	11.6	0.213	0.063	11.0
1	0.067	2.54	0.20	4.6	11.6	0.284	0.084	11.0
1.25	0.105	2.60	0.54	4.6	11.6	0.355	0.104	11.0
1.5	0.151	3.66	1.08	4.6	11.6	0.426	0.125	11.0
1.75	0.206	4.92	1.56	4.6	11.6	0.497	0.146	11.0
2	0.269	6.14	1.92	4.6	11.6	0.569	0.167	11.0
Scaling on time								
Factor	AI (m/s)	D_b (s)	D_u (s)	$D_{s\ 5\text{-}75}$ (s)	$D_{s\ 5\text{-}95}$ (s)	SI (m/s)	$a_{rms\ 5\text{-}95}$ (m/s^2)	N
0.8	0.054	2.03	0.16	3.68	9.3	0.212	0.084	11.0
1	0.067	2.54	0.2	4.60	11.6	0.284	0.084	11.0
1.2	0.082	3.05	0.24	5.52	14.0	0.364	0.084	11.0

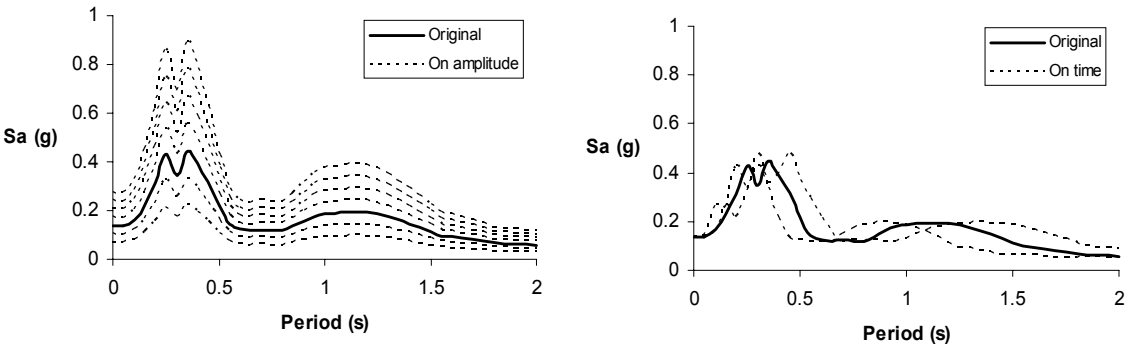

Figure 5.26. Variation of the acceleration response spectra with scaling for the 1983 Coalinga earthquake. *Left* - by scaling on amplitude, *right* – by scaling on time.

Table 5.4. Variation of the strong-motion parameters with scaling on amplitude and time for the 1983 Coalinga earthquake.

Scaling on amplitude								
Factor	AI (m/s)	D_b (s)	D_u (s)	$D_{s\ 5\text{-}75}$ (s)	$D_{s\ 5\text{-}95}$ (s)	SI (m/s)	$a_{rms\ 5\text{-}95}$ (m/s^2)	N
0.5	0.040	0.58	0.1	2.8	11.00	0.274	0.065	13.7
0.75	0.091	2.86	0.56	2.8	11.00	0.411	0.098	13.7
1	0.163	3.44	1.06	2.8	11.00	0.548	0.130	13.7
1.25	0.255	7.14	1.52	2.8	11.00	0.685	0.163	13.7
1.5	0.367	7.84	2.02	2.8	11.00	0.822	0.195	13.7
1.75	0.499	7.86	2.52	2.8	11.00	0.959	0.228	13.7
2	0.652	10.16	2.96	2.8	11.00	1.096	0.260	13.7
Scaling on time								
Factor	AI (m/s)	D_b (s)	D_u (s)	$D_{s\ 5\text{-}75}$ (s)	$D_{s\ 5\text{-}95}$ (s)	SI (m/s)	$a_{rms\ 5\text{-}95}$ (m/s^2)	N
0.8	0.131	2.75	0.85	2.24	8.80	0.417	0.130	13.7
1	0.163	3.44	1.06	2.80	11.00	0.548	0.130	13.7
1.2	0.196	4.13	1.27	3.36	13.20	0.666	0.130	13.7

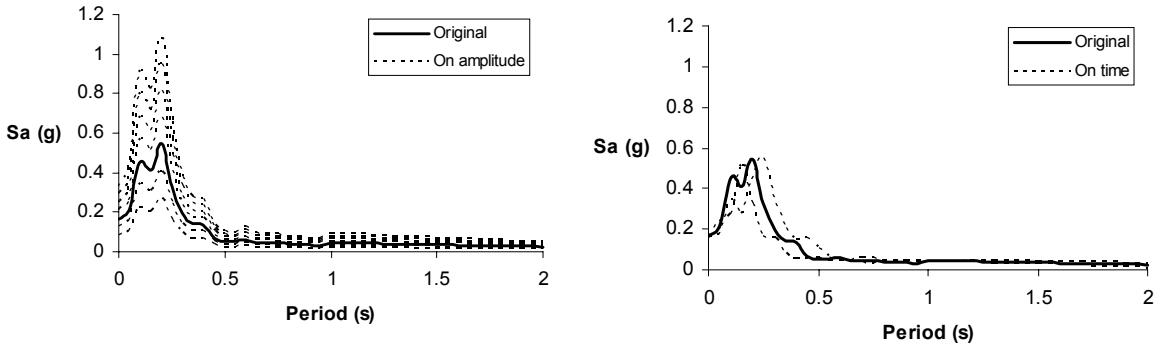

Figure 5.27. Variation of the acceleration response spectra with scaling for the 1971 San Fernando earthquake. *Left* - by scaling on amplitude, *right* – by scaling on time.

Table 5.5. Variation of the strong-motion parameters with scaling on amplitude and time for the 1971 San Fernando earthquake.

Scaling on amplitude								
Factor	AI (m/s)	D_b (s)	D_u (s)	$D_{s\ 5\text{-}75}$ (s)	$D_{s\ 5\text{-}95}$ (s)	SI (m/s)	$a_{rms\ 5\text{-}95}$ (m/s^2)	N
0.5	0.049	0.70	0.16	4.36	12.5	0.110	0.091	13.7
0.75	0.111	5.42	0.64	4.36	12.5	0.165	0.136	13.7
1	0.196	5.88	1.22	4.36	12.5	0.220	0.181	13.7
1.25	0.306	9.50	1.64	4.36	12.5	0.275	0.227	13.7
1.5	0.441	9.54	2.3	4.36	12.5	0.330	0.272	13.7
1.75	0.601	13.08	2.82	4.36	12.5	0.385	0.317	13.7
2	0.784	15.66	3.52	4.36	12.5	0.440	0.363	13.7
Scaling on time								
Factor	AI (m/s)	D_b (s)	D_u (s)	$D_{s\ 5\text{-}75}$ (s)	$D_{s\ 5\text{-}95}$ (s)	SI (m/s)	$a_{rms\ 5\text{-}95}$ (m/s^2)	N
0.8	0.157	4.70	0.98	3.49	10.02	0.165	0.181	13.7
1	0.196	5.88	1.22	4.36	12.50	0.220	0.181	13.7
1.2	0.236	7.06	1.46	5.23	15.02	0.266	0.181	13.7

6. REVIEW OF SELECTION AND SCALING PROCEDURES

When time-history analysis is performed, the non-linear response of a structure cannot be reliably determined by the use of only one ground motion. It is necessary to use different time-histories with phasing and spectral shapes according to the earthquake source, wave propagation path and site conditions that control the design spectrum.

In building codes, there is not a general number of records required to perform a time-history analysis. In fact, some of the codes do not even specify this number. In those codes where there is a required number of time histories, the specification ranges from three (e.g. Eurocode 8) to seven (IBC 2000) (Bommer and Ruggeri, 2002).

The *selection* criterion of the ground motion records is to choose records that agree with the characteristics of the design earthquake scenario. Bolt (1978) showed that if a previous record matches all the characteristics of the design earthquake in terms of source, path and site parameters, the probability of the characteristics of the selected record matching the design ground-motion would be unity. Since the design earthquake is usually defined in terms of only a few parameters, it is difficult to guarantee that the chosen records would closely model all the characteristics of the design earthquake and site. However, Bolt (1978) also demonstrated that if the characteristics of the previous record matching those of the design earthquake increases, then the probability of the records matching increases rapidly (Bommer *et al*., 2000).

The number of strong-motion records available is a very important factor in choosing the number of characteristics that can be included in the selection, as indicated in the work of Bommer and Scott (2000) and referred to in the following section.

The selection of the records to be used is generally made on the basis of only a few characteristics, neglecting other important parameters that characterise the ground motion. Because of this and the lack of real earthquakes matching the conditions of those of the design earthquake scenario, *scaling* of ground motion records has to be done in order to obtain a sufficient number of records to perform the time-history analysis.

The selection of the records is made in terms of seismological parameters, while the scaling procedure can be based on either strong-motion parameters or on seismological parameters.

6.1. SELECTION PROCEDURES.

The procedures for the selection of strong-motion records are summarized in Figure 6.1.

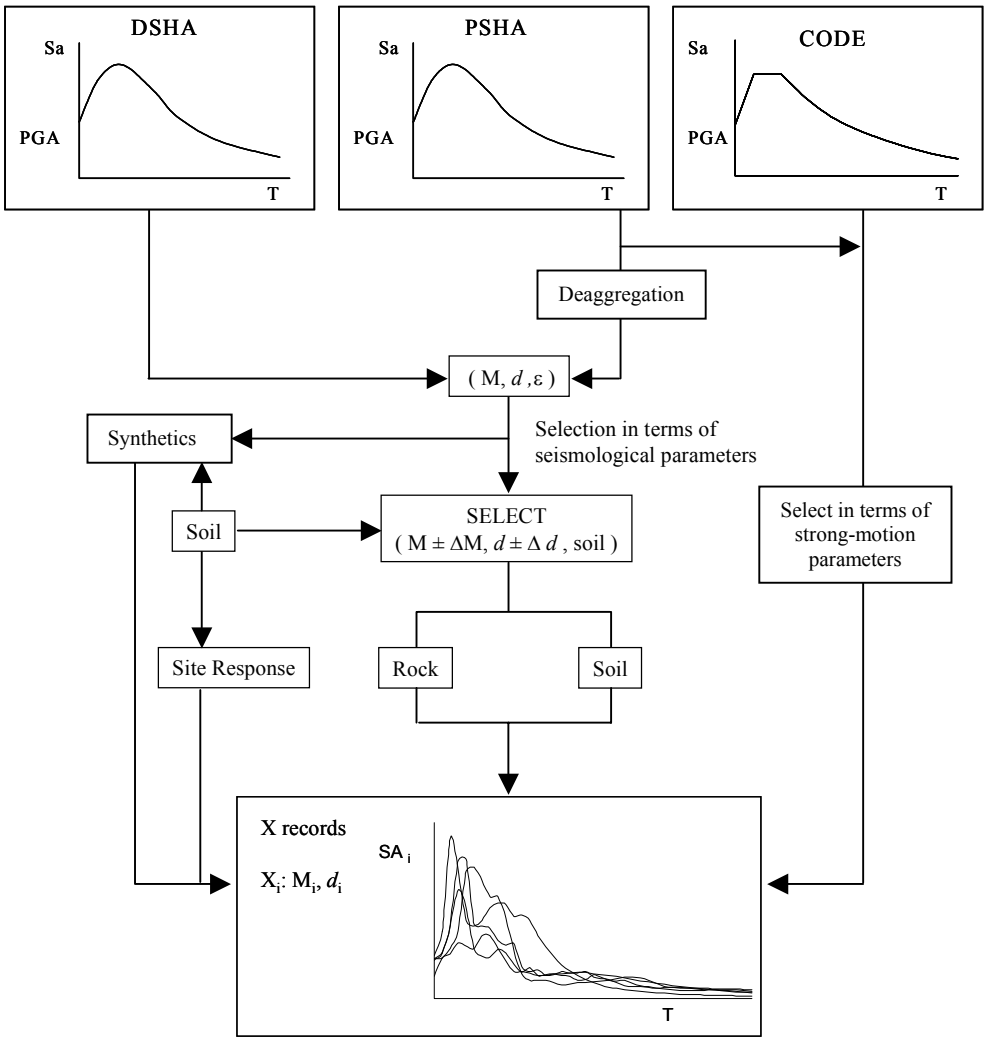

Figure 6.1. Selection procedures for strong-motion records.

The earthquakes loads at a particular site can be estimated either by a deterministic seismic hazard analysis (DSHA) or by a probabilistic seismic hazard analysis (PSHA). In the case of the DSHA, one or more earthquake scenarios (earthquake magnitude and distance) are defined as part of the process. The earthquake producing the most severe motions at the site will normally be taken as the basis of the design. In the case that one earthquake dominates at short-period spectral ordinates and another at long-period ordinates, both scenarios may need to be considered to determine which is controlling for any particular structure. These scenarios can be used directly to select the accelerograms to use in the analysis (Bommer *et al*., 2000).

Probabilistic seismic hazard assessment (PSHA) does not consider specified individual earthquakes but rather looks at all of the possible earthquakes (all possible magnitude and distance combinations) that could occur, and includes the effect of random variability in the ground motions for a given magnitude and distance (Bommer, 2001). The result of a PSHA is a hazard curve, giving the probability of exceeding various ground motion values. In order to perform the selection of real records it is necessary to define a unique earthquake scenario. Therefore, deaggregation of seismic hazards, which is the process of determining the earthquake scenarios that control the results of PSHA, needs to be done.

Deaggregation is performed by the definition of magnitude-distance bins, and their individual contribution to the hazard. Different deaggregation procedures are described and compared in the work of Bazzurro and Cornell (1999). The method of McGuire (1995) has been widely adopted. This method defines the earthquake scenario in terms of magnitude, distance and ε (defined as the number of standard deviations above the median value predicted by the relevant attenuation relationship). If different sources dominate the hazard for different periods then the distributions will be different and a scenario must be defined for each. The results of the deaggregation will be different for different probability levels and for different spectral periods (Figure 6.2). Weaknesses in the approach of McGuire (1995) have been identified by Bazzurro and Cornell (1999). The McGuire (1995) deaggregation procedure lumps the hazard contributions only in those M, R and ε bins that ensure that the target S_a value is equalled (not exceeded). This matching requirement affects the deaggregation results. In the work of Bazzurro and Cornell (1999) an alternative deaggregation approach that displays hazard contribution in terms of latitude and longitude (instead of distance), as well as M and ε, is proposed to overcome the weakness previously addressed.

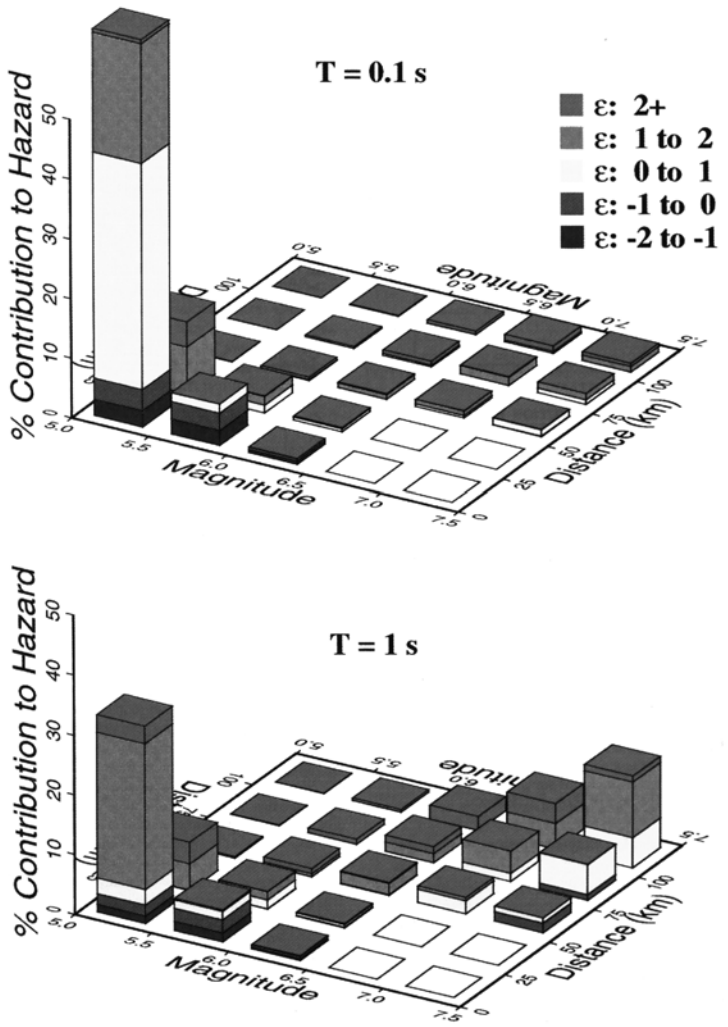

Figure 6.2. Contributions to the 100,000-year seismic hazard at Colorado (USA) by magnitude, distance and ε for the ordinate of spectral acceleration at a period of 0.1 second (top) and at 1.0 second (bottom) (McGuire, 1995).

Once the earthquake scenario is specified, the selection of the records has to be performed. The basic factors that influence the ground motion are the earthquake source, the travel path and the site effects. Their parameters were discussed in Section 3.

By evaluation of the attenuation relationships, it can be observed that the dominant parameters are magnitude, distance and site geology. In many cases, it would also be possible to assume focal depth and possibly a rupture mechanism (Bommer *et al*., 1998).

Nevertheless, the number of parameters included in the selection is strongly related to the number of strong-motion records available. In the work of Bommer and Scott (2000) a databank of almost 1600 accelerograms recorded between 1993 and 1995 was used, with the smallest magnitude M_s = 4.0 and two thirds of the records obtained at distances of less than 50 km from the source. The authors performed a search of records in terms of a window defined by an interval of magnitude and source-site distance. The result of this search without taking into account the site geology is presented on Figure 6.3.

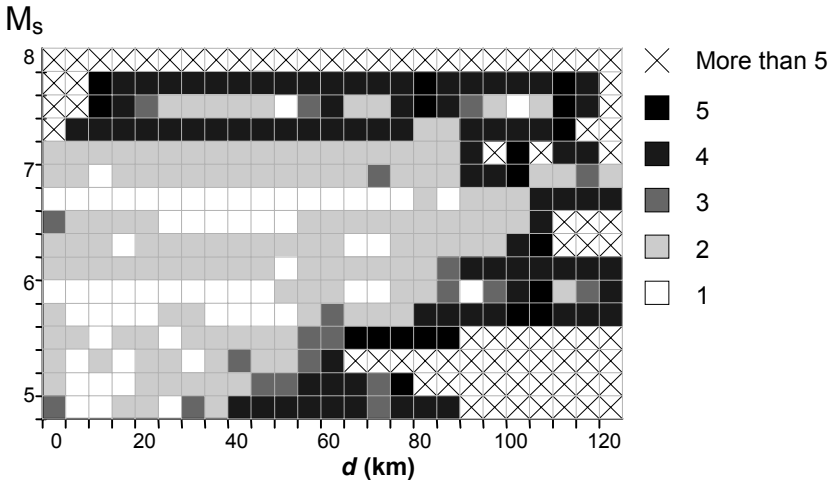

Figure 6.3. Magnification factor required on basic search window (0.1 M_s and 4 km distance) for each magnitude-distance pair in order to obtain at least three accelerograms (Bommer and Scott, 2000).

As pointed out by Bommer and Scott (2000), for most of the scenarios with M_s less than 7.2, in the range of distances of engineering interest, at least three accelerograms can be obtained with a search window of 0.2 on magnitude and 8 km on distance.

When the site geology is included, the size of the search window needs to be extended in order to obtain the required number of ground motions, as can be observed in Figure 6.4. In this case, for many scenarios, three records are obtained by increasing the size of search window to 0.3 units of magnitude and 12 km distance.

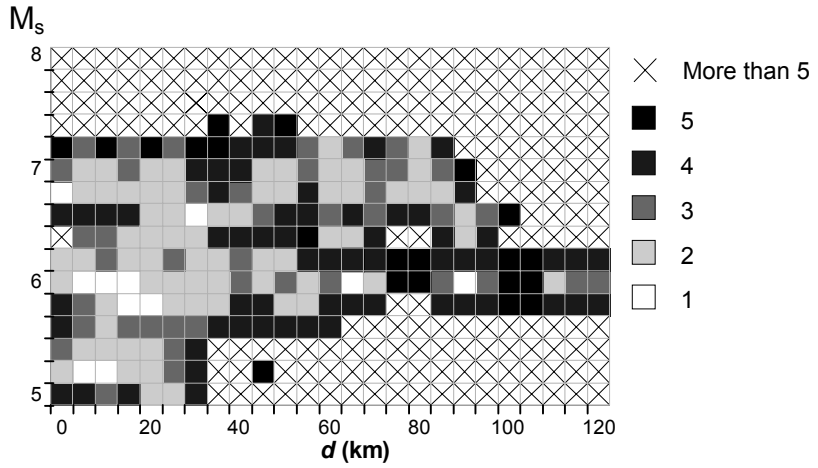

Figure 6.4. Amplification factor required on basic search window (0.1 M_s and 4 km distance) for each magnitude-distance pair in order to obtain at least three accelerograms from rock sites (Bommer and Scott, 2000).

From the attenuation relationships of Ambraseys *et al*. (1996), the strong dependency of the spectral shape on magnitude can be observed, whereas it is relatively insensitive to distance. The spectral shape cannot be adjusted by scaling the amplitude of the record, therefore the main parameter for the selection is the magnitude. Furthermore the duration of the ground motion is related to the magnitude. The influence on the duration of the record if scaled in amplitude depends on the definition of duration used.

The shape of the response spectrum is also heavily influenced by the surface geology. The records selected should match the site conditions. Alternatively, records from rock sites can be chosen and site response analyses can be performed (Bommer and Ruggeri, 2002).

The effects of directivity cannot be compensated for the current scaling techniques; therefore, if this is a relevant part of the design scenario, directivity needs to be included as a criterion for record selection (Bommer and Scott, 2000).

In contrast to these statements, in the work of Shome *et al*. (1998) on the estimation of MDOF non-linear structural response given an earthquake of magnitude M and distance R, they concluded that any group of ground-motion records can be used (any magnitude and distance) if they are scaled to the correct intensity level such as the median spectral acceleration, S_a, predicted by an attenuation relationship. For their study, four magnitude and distances groups or "bins", each with 20 accelerograms, were used for the analysis of a five-storey, four-bay steel moment-resisting frame, with

a fundamental period of 0.95 Hz. Two of the bins were selected in order to consider two alternative scenario events at some site: one for closer, smaller magnitudes and other for more distant, larger magnitudes. These two bins have approximately the same median S_a. The other two bins selected presented a median spectral acceleration much higher than those of the previous bins in order to investigate larger scaling factors.

In their work "local" and "global" measures of MDOF non-linear behaviour were used to define the influence of the different magnitude and distances associated with the records. The local measures used were displacement ductility, μ, normalised hysteretic energy, NHE (defined as the total hysteretic energy absorbed in all the cycles normalised by twice the yield strain energy) and damage index, ID (defined as a linear combination of normalised displacement and NHE). For the entire structure the measures used were global ductility, μ, global NHE (defined as the sum of the non-normalised hysteretic energies, HE, absorbed in all the stories, normalised by the product of the global-yield displacement and the global force at which it occurs) and global damage index (defined as a weighted sum of the local damage indices for each story).

The influence of the different magnitude and distance associated with the records was not significant on the displacement ductility and damage index. Nevertheless, the global normalized hysteretic energy (NHE) does not follow the same behaviour. For the bins with higher magnitude (about 7) the NHE results are similar between them, but they are substantially higher than those of the bin with the smallest magnitude (5.5). The median bracketed duration (defined by Trifunac and Brady, 1975) for the higher magnitude bins is about twice the duration of the low magnitude bin (1.73 and 15.2 for magnitudes ~ 7 and 7.3 for magnitude 5.5). The difference on duration suggests that this may be a factor influencing the cumulative NHE measure (but apparently not the ductility or the damage index).

Another procedure for the selection of earthquake ground-motion is the selection of real time histories whose spectral ordinates are comparable to those of the target spectrum for the period range of interest (Idriss, 1993) in a way that scaling is not required. In the work of Naeim and Anderson (1993) 120 time histories, with their plots of constant strength inelastic response spectra, constant ductility inelastic response spectra, elastic and inelastic input energy spectra and hysteretic energy spectra, are presented. These ground motions are the most significant for engineering interest and they are recommended to be used for analysis purposes. These 120 ground-motions were carefully selected from a database of 1500 records of earthquake ground-motion.

The use of synthetic accelerograms generated from simulation techniques can be used to represent the earthquake ground-motions at the rock site of interest. Nevertheless, since this work is focused on the use of real accelerograms, no attention will be given to synthetic accelerograms in this study.

6.2. SCALING PROCEDURES.

Scaling refers to the multiplication of the accelerogram by a scale factor that makes their peak values or response spectrum match the design spectrum at the fundamental period of the structure or over a period range of interest for the structure. It could be stated that the accelerograms should only be scaled in terms of amplitude. Nevertheless, scaling on the time axis has been used to modify the frequency content of real ground-motion records (Kramer, 1996). This approach, besides changing the duration of the record, changes the frequency content over the entire spectrum.

The actual procedures for the scaling of strong-motion records are summarized on Figure 6.5.

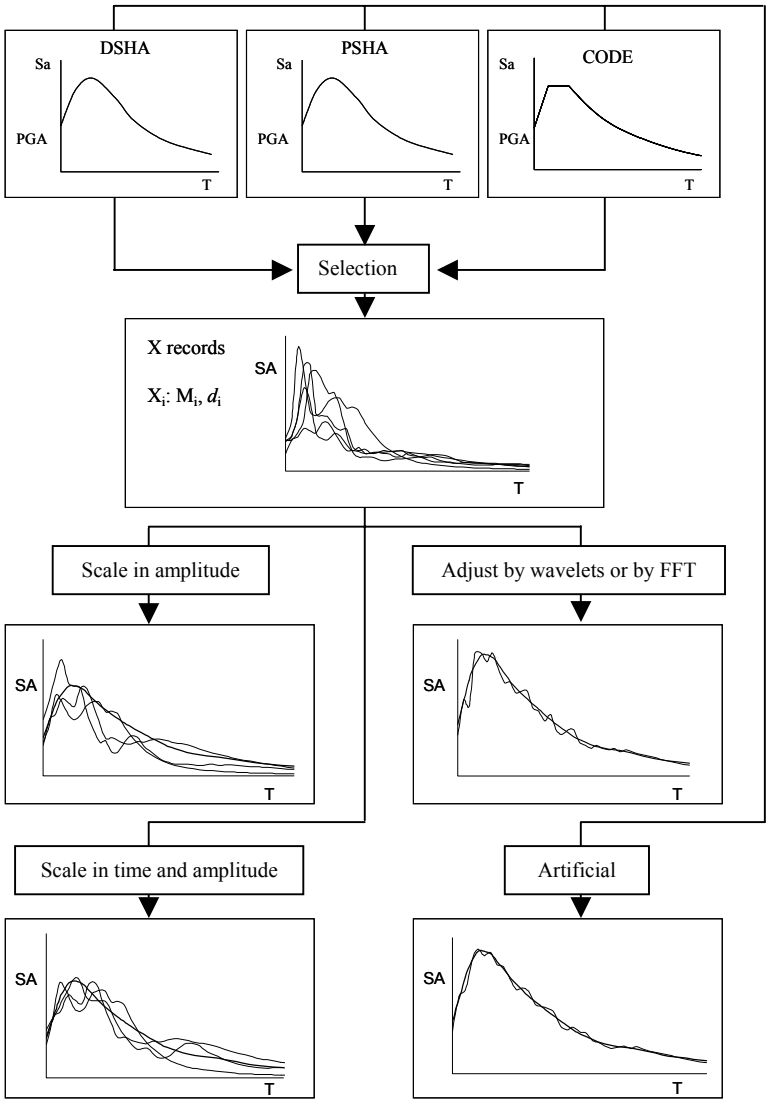

Figure 6.5. Actual scaling procedures for strong-motion records.

By scaling in terms of amplitude it is possible to adjust the peak ground-motion parameters, the spectral ordinates and the energy content. However, by scaling the amplitude, the shape of the response spectrum cannot be changed (Bommer and Scott, 2002). The influence of amplitude scaling on duration depends on the definition of duration employed. Bracketed and uniform durations, for a given acceleration threshold, will generally increase if the amplitude is increasing. Scaling of the time axis will increase all durations but not the number of cycles.

For this work it is believed that the accelerogram obtained after the scaling should be a realistic earthquake motion, an issue that is explored in the following chapters. Therefore, the scaling procedure applied should not induce changes in the record that give it characteristics that would not be expected in a real earthquake ground-motion. The rationale behind this statement is that as far as possible the benefits of using real records should be maintained even after scaling, the main benefit being the fact that the motion genuinely reflects the earthquake process.

As mentioned before, the scaling procedure can be done based either on strong motion parameters or on seismological parameters. The main focus of this work, however, is the limits on scaling that should be used.

6.2.1. Scaling on the basis of strong-motion parameters.

The majority of the actual scaling techniques are based on strong-motion parameters. Comparison between different scaling techniques can be found in the works of Nau and Hall (1984), Matsumura (1992), Martínez-Rueda (1998) and Kappos and Kyriakakis (2000). Some of these techniques are briefly describe in this section.

6.2.1.1. Scaling to the peak ground parameters (PGA and PGV).

It is very common to express the design criterion in terms of maximum ground acceleration (PGA). As consequence, it has been common to scale ground motions to a PGA value. However, the peak ground velocity (PGV) is also important in determining the severity of seismic response.

The response of short period structures (typically less than 0.5 seconds) is proportional to the values of ground motion acceleration. Structures of moderate-long period (0.5 to 3.0 seconds) are proportional to the values of ground motion velocity. Long period structures (more than 3.0 seconds) are

proportional to the values of ground motion displacement. Scaling to the PGA will generally produce a reasonable match with the response spectrum at very short periods.

To reflect the dependency on acceleration and velocity, scaling can be done to the PGA value on the short period range and to the PGV for the moderate-long period range, depending on the natural period of the structure.

Although scaling to PGV at moderate-long period range is an improvement over using only the value of PGA for the complete range period, previous studies (e.g. Nau and Hall, 1984; Matsumura, 1992) have shown that PGA and PGV are not adequate values for scaling over a wide range of frequencies since they are parameters that are essentially independent of the frequency of the ground motion. They conclude that it is more appropriate scaling to intensity measures related to the natural period of a structure.

6.2.1.2. Scaling to AI (Arias intensity).

Since the peak ground motion values do not characterise satisfactorily the intensity of the ground motion, the Arias Intensity, defined in section 2.2.2, has been proposed as a scaling parameter by Arias (1969) and by Housner and Jennings (1977).

In the study carried out by Nau and Hall (1984) it is concluded that the use of this normalising factor (based on a response quantity) does not constitute a great advantage over the use of peak ground motions since it provides only minor reductions in scatter within limited ranges of frequency. Besides, it is also quite unusual to produce AI as part of the output of a hazard study.

6.2.1.3. Scaling to the RMS (root-mean-square) acceleration.

Another scaling parameter based on ground motion data is the root-mean-square acceleration, a_{rms}, defined in section 2.2.3.

As for the scaling to the Arias Intensity, the study carried out by Nau and Hall (1984) also concludes that scaling to the RMS acceleration does not represent significant advantage over the use of peak ground motion. Furthermore, a_{rms} is very unlikely to be part of the output from a seismic hazard study.

6.2.1.4. Scaling to the SI (spectrum intensity).

Scaling to the SI is based on the assumption that the seismic energy imparted by the scaled record is equal to that implied by the design spectrum. Housner spectrum intesity, SI (defined in section 2.2.7), has been adopted as a scaling parameter.

There are several modifications to the limits proposed by Housner suggested in the literature. A review of some of them is presented by Martínez-Rueda (1998) and they are briefly described next.

In the work of Hidalgo and Clough (1974) the upper limit of the Housner intensity was modified to 1.0 second. Nau and Hall (1984) proposed a three parameter system of spectrum intensities accounting for the sensitivity of the response to acceleration, velocity or displacement. The limits (in the period domain) for the acceleration region are 0.028-0.185, for the velocity region 0.285-2.0 and for the displacement region 4.167-12.5. The spectrum intensity proposed by Kappos (1990) has limits of $0.8T_n$–$1.2T_n$, where T_n is the natural period of vibration of the structure. Matsumura (1992) proposed limits of T_y-$2T_y$, where T_y is the yield period of the structure. Finally Martínez-Rueda (1996) modified the limits of the Housner intensity to T_y-T_h, where T_y is the yield period and T_h is the hardening period of the structure.

A combined criterion to define spectrum intensity is described by Martínez-Rueda (1998) by the selection of regions for which it is possible to identify within a group of existing spectrum intensity scales the one with the best performance. The structural parameters considered included the yield seismic coefficient, C_y, the yield natural period, T_y, and the post-yield stiffness, α, of SDOF systems. The spectrum intensity scales included in the combined criterion are the Housner intensity, SI, the Matsumura intensity, SI_M and the Martínez-Rueda intensity, SI_{yh}. The effectiveness of the spectrum intensity scales was evaluated in terms of their correlation with displacement ductility demand. It was concluded that in general the most stable spectrum intensity is SI_M, followed by SI_{yh} and SI in that order. However, the combined criterion presents a possibility of taking advantage of the better performance exhibited by the SI_{yh} and SI intensity scales in regions of the space T_y-C_y-α where SI_M is not the best option.

6.2.1.5. Scaling to the I_v index.

The I_v index defined in section 2.2.8 was developed by Fajfar *et al*. (1990) because the previous methods of scaling do not satisfactorily take into account the duration of the ground motion. This scaling factor includes only two of the basic ground motion parameters (peak ground velocity and

duration of the strong shaking). Nevertheless, these two parameters are rarely available from seismic hazard studies.

The scaling parameter was evaluated by using inelastic relative displacement and input energy spectra (input energy is defined as the work of the equivalent loading on relative displacements). This intensity parameter is applicable to ground motions of different durations and of different frequency content, as well as for different soil conditions. It was found that the use of the I_v index represents a reduction in scatter of the relative displacement and input energy spectra when scaling is done only to the PGV value.

6.2.1.6. Scaling to S_a (spectral acceleration).

In the study of Shome *et al*. (1998), a five-DOF model of a steel structure was used, considering global and non-linear damage measures. The records used were scaled to the same "intensity" measured by the mean S_a, at the fundamental period of the structure. The study concludes that when scaling to the median spectral acceleration predicted by an attenuation equation is done, the MDOF response does not depend on the magnitude and distance (see Section 5.1).

Scaling to S_a at the natural period of the structure is fundamental to code approaches. For the dynamic analysis most of the seismic design codes do not provide targets of records in terms on strong-motion parameters. When matching of real records is included, it is generally specified with regard to the ordinates of the acceleration response spectrum in the code. Bommer and Ruggeri (2002) summarise in their work the guidelines in current seismic design codes for the use of time-histories in dynamic analysis. The New Zeland code specifies the matching in a descriptive manner over the period range of interest of the structure being analysed. The requirements of the Argentinian code are more specific with conditions of matching the areas of the two spectra between 0.05 s and the fundamental period of the structure. In the French code the matching is done over the entire period for the value of the mean spectrum. For the UBC97 the scaling is done by comparison of the average ordinates of the individual spectra with the design-basis earthquakes for a range of periods neighbouring the fundamental period. More details about the requirements of the code mentioned previously are presented in Bommer and Ruggeri (2002).

6.2.1.7. Scaling in time.

As stated before, scaling of the time axis changes the duration of the record and the frequency content over the entire spectrum. Another important issue of this type of scaling is that the relation between duration and number of cycles is lost if scaling is applied to the time axis. Scaling on the time axis should be used carefully to avoid unintended consequences.

For the three earthquakes addressed in Section 5.6 the equivalent number of uniform stress cycles (N) was found using the relationship of Liu *et al*. (2001) (Tables 6.1, 6.2 and 6.3). Figures 6.6, 6.7 and 6.8 present the variation of the time-histories with the scaling on the time axis.

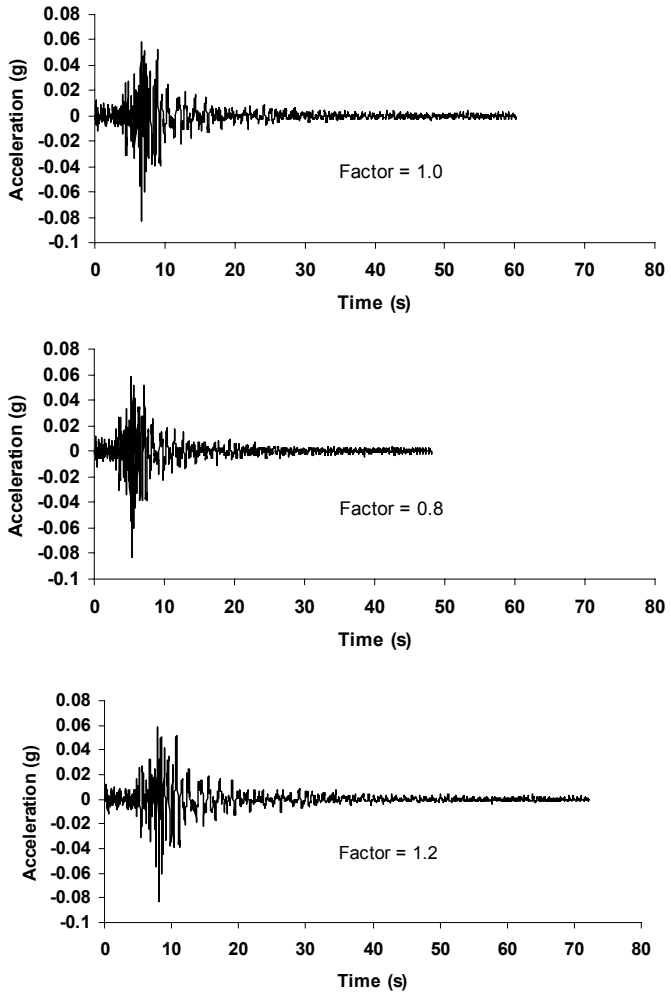

Figure 6.6. Variation of the time-history of the 1984 Morgan Hill earthquake when scaling in time axis.

Table 6.1. Variation of the duration and Equivalent Number of Uniform Stress Cycles (N) for the 1984 Morgan Hill earthquake (magnitude 6.2).

Scaling on time axis					
Factor	D_b (s)	D_u (s)	$D_{s\ 5\text{-}75}$ (s)	$D_{s\ 5\text{-}95}$ (s)	N
0.8	2.03	0.16	3.68	9.3	11.0
1	2.54	0.2	4.60	11.6	11.0
1.2	3.05	0.24	5.52	14.0	11.0

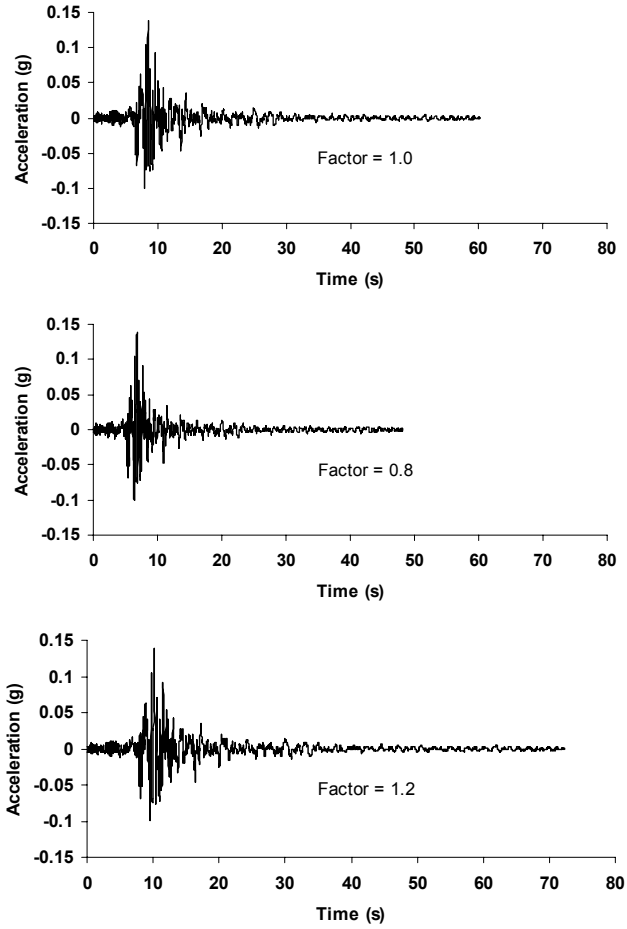

Figure 6.7. Variation of the time-history of the 1983 Coalinga earthquake when scaling in time axis.

Table 6.2. Variation of the duration and Equivalent Number of Uniform Stress Cycles (N) for the 1983 Coalinga earthquake (magnitude 6.4).

Scaling on time axis					
Factor	D_b (s)	D_u (s)	$D_{s\ 5\text{-}75}$ (s)	$D_{s\ 5\text{-}95}$ (s)	N
0.8	2.75	0.85	2.24	8.80	13.7
1	3.44	1.08	2.80	10.78	13.7
1.2	4.13	1.27	3.36	13.20	13.7

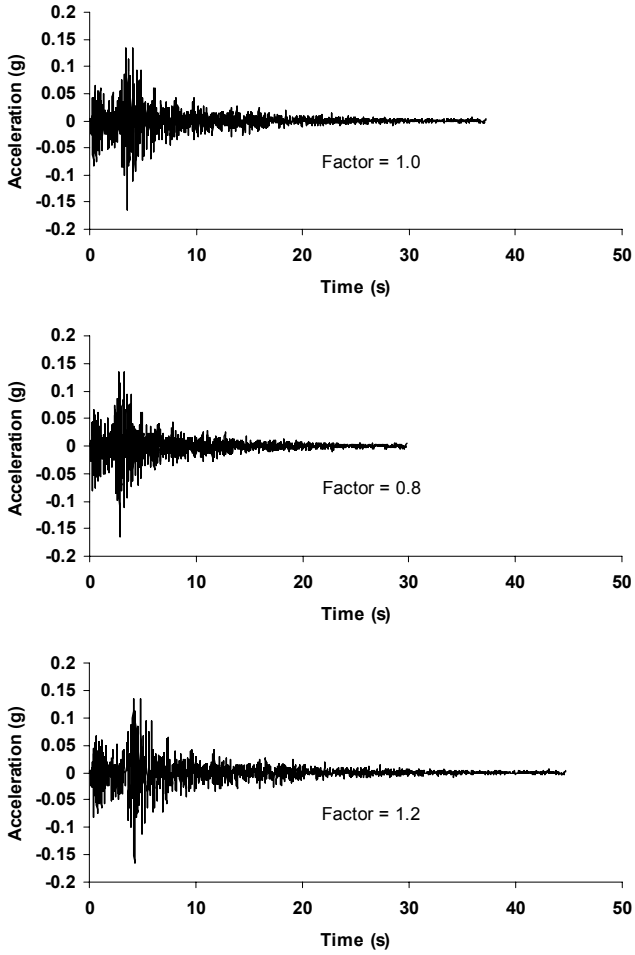

Figure 6.8. Variation of the time-history of the 1971 San Fernando earthquake when scaling in time axis.

Table 6.3. Variation of the duration and Equivalent Number of Uniform Stress Cycles (N) for the 1971 San Fernando earthquake (magnitude 6.6).

Scaling on time axis					
Factor	D_b (s)	D_u (s)	$D_{s\ 5\text{-}75}$ (s)	$D_{s\ 5\text{-}95}$ (s)	N
0.8	4.70	0.98	3.49	10.02	13.7
1	5.88	1.22	4.36	12.50	13.7
1.2	7.06	1.46	5.23	15.02	13.7

To generate motions of long duration without significantly changing the frequency content some authors like Seed and Idriss (1969) have proposed to modify portions of existing accelerograms and assemble them in a series to obtain the desired duration. As with scaling on the time axis, careful examination of this type of motion is required. Besides, using such scaling, the time history obtained is unlikely to be realistic.

6.2.2. Scaling by wavelets or Fourier transform.

The amplitude of a recorded time history can be modified in a way that the response spectrum matches the target spectrum. This modification is usually called *spectrum matching*. Applying the Fourier Transform or wavelets theory can perform this modification.

The computer program RASCAL, developed by Silva and Lee (1987), modifies the records in the frequency domain by the Fourier Transform, while the computer program RSPMATCH, developed by Abrahamson (1993), modifies the records in the time domain by adding wavelets to the reference time history.

For both modifications (in the time or frequency domain) the recorded accelerogram is decomposed into a finite number of time-histories with energy in non-overlapping frequencies bands. These time-histories are iteratively scaled such that the assembled time-history is compatible with the target spectrum. A detail explanation of the way this analysis is done in the time domain is given by Mukherjee and Gupta (2002).

Since the spectral amplitudes of the input record are modified but their phases are retained, the adjusted time-history resembles the original one. In this way the temporal variations in the record frequency content is retained in the synthesized accelerogram.

Even if the initial record is a real one, the results of this scaling can no longer be considered a real ground-motion in the strict sense. Therefore, this type of scaling will not be addressed in the following chapters of this work, although this is not to imply that the author rejects these methods as a viable alternative. For illustration of this scaling procedure the three records addressed in Section 5.5 were adjusted using the programs RASCAL and RSPMATCH to a given target spectrum. The acceleration and velocity response spectra obtained after the scaling can be observed in Figures 6.9, 6.10 and 6.11. Figures 6.12 to 6.17 present the time-history variation due to the spectrum matching, the Husid plots for the accelerograms before and after the scaling and the ratio of the Arias intensity between the records after scaling and the original records.

Two observations can be made, the first being that the time-domain adjustment using RSPMATCH consistently yields a closer match with the target spectrum than the frequency-domain method embodied in the RASCAL program. The second observation, which is particularly important from the perspective of this study, is that the change in shape of the Arias intensity, as indicated in Figures 6.13, 6.15 and 6.17, is small, which implies that the adjustments to the original time-history have very little

impact on the total energy content. Nevertheless, the ratio of the Arias intensity between the records after scaling and the original records shows that the energy in not uniformly distributed in time. Here again, RSPMATCH gives better results than RASCAL, and in the time-history plots in Figures 6.12, 6.14 and 6.16, the accelerograms adjusted using RSPMATCH are almost indistinguishable from the originals, whereas the RASCAL adjusted records are clearly different.

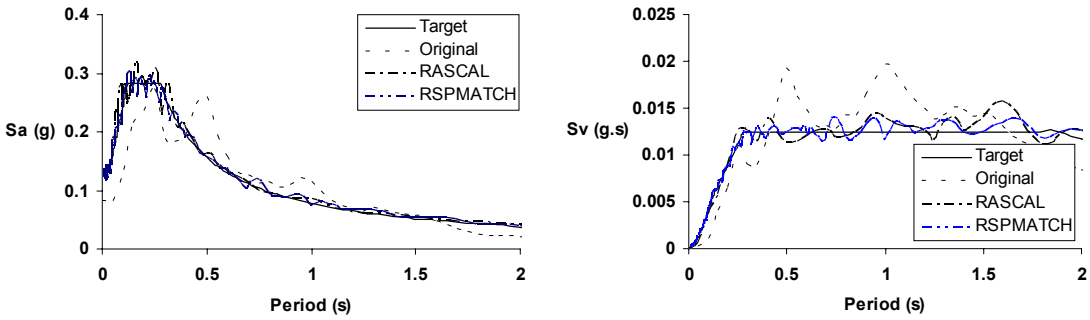

Figure 6.9. Variation of the response spectra when adjusting by RASCAL and RSPMATCH programs is performed for the 1984 Morgan Hill earthquake. *Left* – acceleration response spectra, *right* – velocity response spectra.

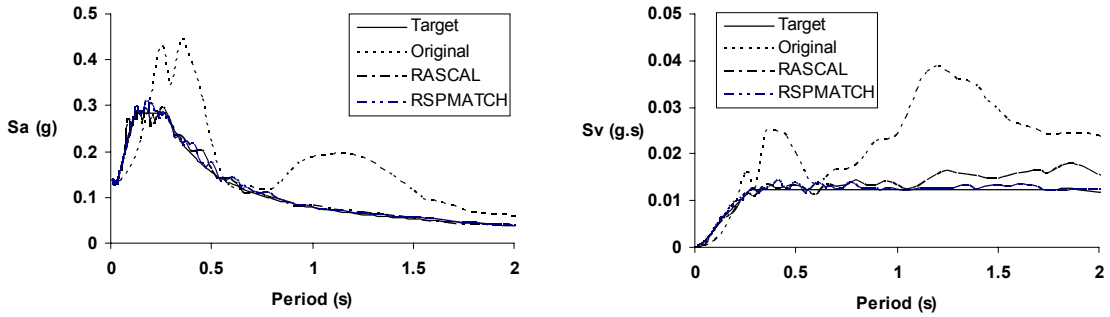

Figure 6.10. Variation of the response spectra when adjusting by RASCAL and RSPMATCH programs is performed for the 1983 Coalinga earthquake. *Left* – acceleration response spectra, *right* – velocity response spectra.

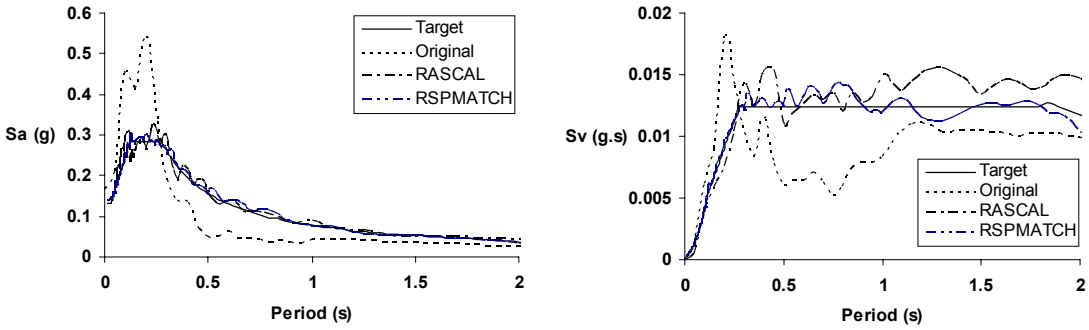

Figure 6.11. Variation of the response spectra when adjusting by RASCAL and RSPMATCH programs is performed for the 1971 San Fernando earthquake. *Left* – acceleration response spectra, *right* – velocity response spectra.

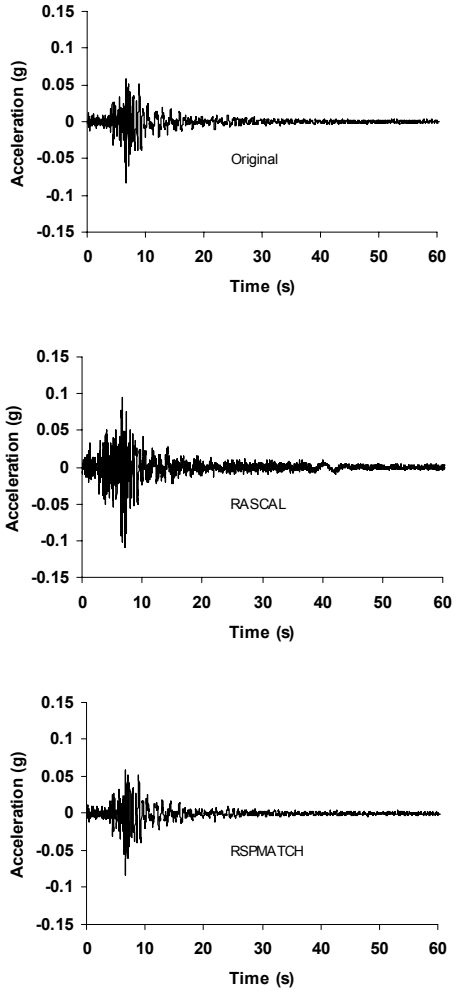

Figure 6.12. Variation of the time-history of the 1984 Morgan Hill earthquake when adjusting by RASCAL and RSPMATCH programs is performed.

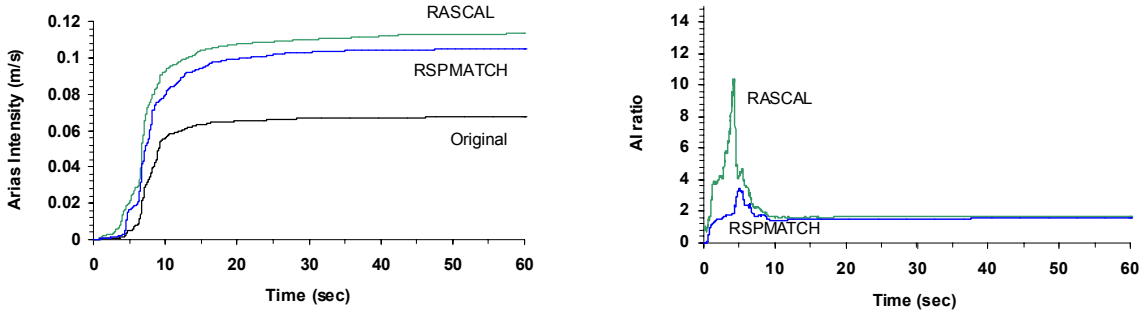

Figure 6.13. Variation of the Arias intesity of the 1984 Morgan Hill earthquake when adjusting by RASCAL and RSPMATCH programs is performed. *Left* – Husid plots, *right* – ratio between adjusted records and original record.

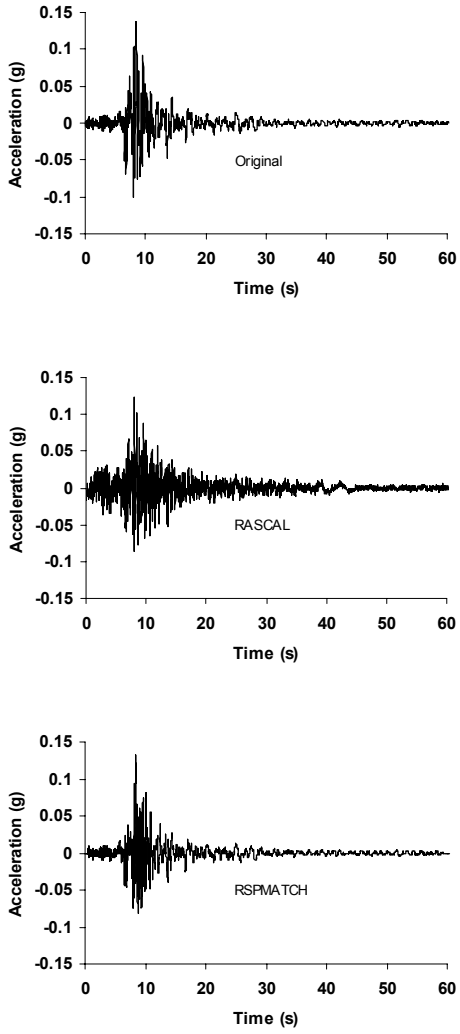

Figure 6.14. Variation of the time-history of the 1983 Coalinga earthquake when adjusting by RASCAL and RSPMATCH programs is performed.

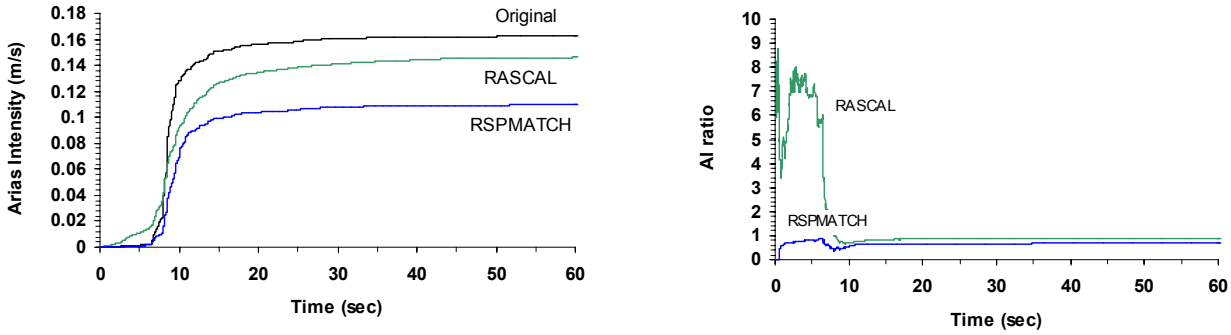

Figure 6.15. Variation of the Arias intensity of the 1983 Coalinga earthquake when adjusting by RASCAL and RSPMATCH programs is performed. *Left* – Husid plots, *right* – ratio between adjusted records and original record.

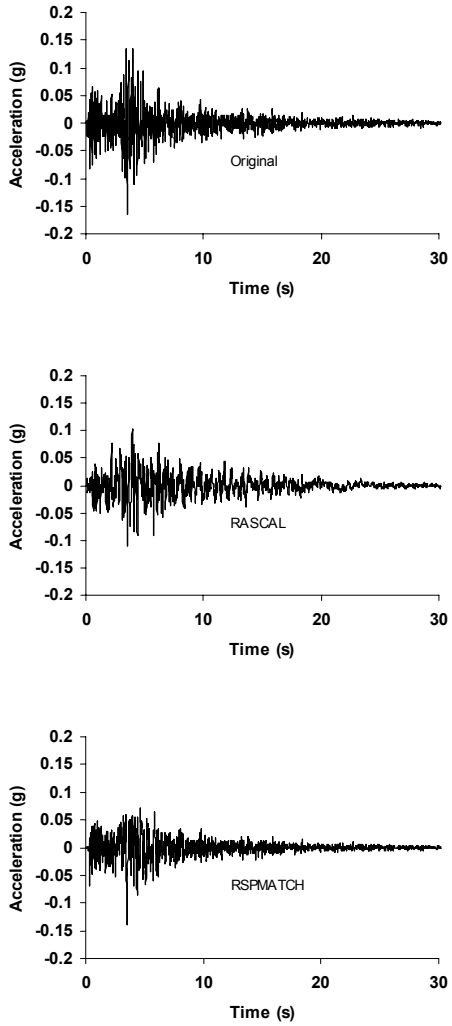

Figure 6.16. Variation of the time-history of the 1971 San Fernando earthquake when adjusting by RASCAL and RSPMATCH programs is performed.

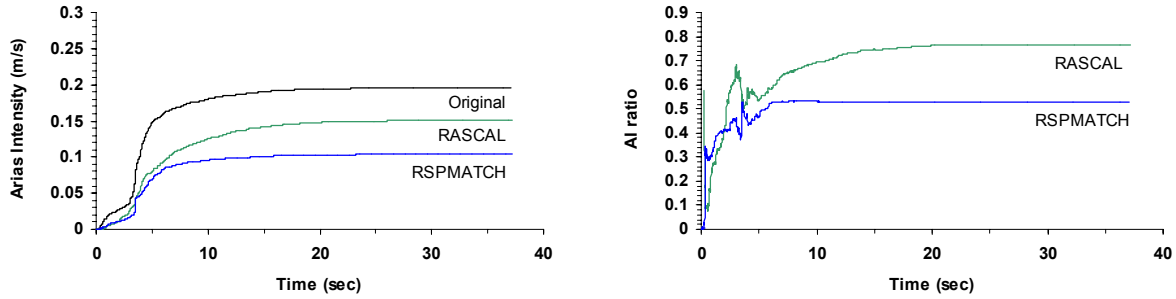

Figure 6.17. Variation of the Arias intensity of the 1971 San Fernando earthquake when adjusting by RASCAL and RSPMATCH programs is performed. *Left* – Husid plots, *right* – ratio between adjusted records and original record.

6.2.3. Scaling on the basis of seismological parameters.

Scaling by seismological parameters is hardly addressed in technical literature. The possibilities for performing seismological scaling will be explored in Chapters 7 and 8.

Additionally, the limits that should be placed on amplitude and time scaling in order to maintain realistic records have been barely mentioned, apart from the study by Vanmarke (1979) proposing a lower limit of 0.5 and an upper limit of 2.0 for liquefaction and 4 for linear elastic analysis of structures. These approximate limits were proposed almost 25 years ago and they were based on limited data, nevertheless they have been widely adopted in practice. Furthermore, spectral shape is relatively insensitive to distances, suggesting that scaling amplitude by factor much higher than 2 for mismatched distances may be acceptable (Bommer and Ruggeri, 2002). In this work seismological criteria will be considered to establish the limits for permissible scaling.

7. DEFINITION OF SELECTION AND SCALING CRITERIA

7.1. Selection of real records.

The principal parameters for the selection of the records will be the magnitude, M, and the distance, *d*. Although in the study of Shome *et al*. (1998) it is concluded that if their scaling procedure is followed, magnitude and distance can be ignored, it is assumed herein that the selection of the records requires appropriate M-*d* pairs. Another important parameter for the selection is the site conditions. This parameter, along with M and *d*, will be the parameters used for the records selection in this study.

Because of the current lack of data, the use of M-*d* bins becomes necessary in order to find sufficient records for the analysis. From the attenuation relationship of Ambraseyes *et al*. (1996), as mentioned before, the strong dependency of the spectral shape on magnitude can be observed, whereas it is relatively insensitive to distance. In consequence, the magnitude values covered by a bin need to be closely spaced, while the distance value can have a bigger range within the bin. It is worth bearing in mind, however, that the standard deviation on magnitude determinations is generally not less than 0.2, so a minimum window on magnitude could be 0.4 units. However, for the purposes of this study, smaller windows will be considered. The site conditions will be taken into account by the appropriate selection of the records according to this parameter.

The scaling procedures studied in this work are summarised in Figure 7.1.

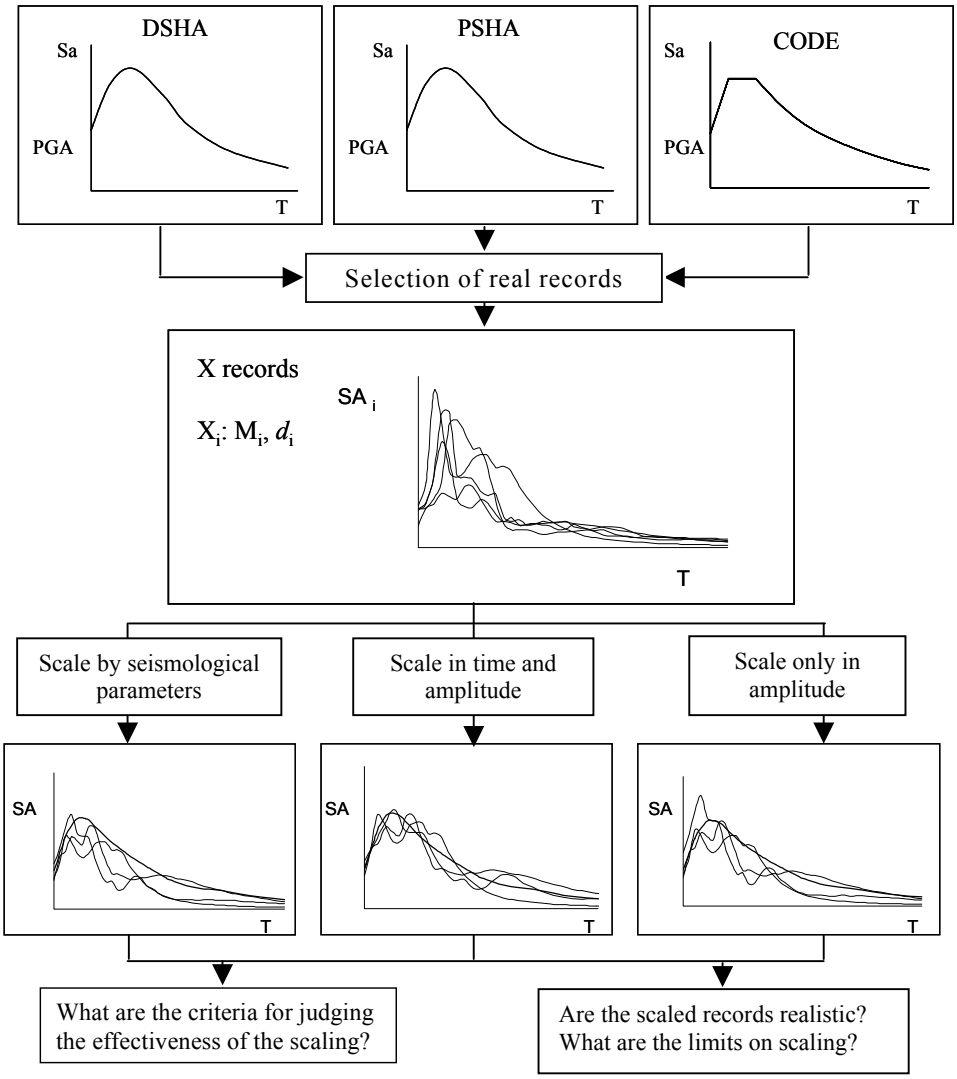

Figure 7.1. Scaling procedures studied in this work.

In this work, the database presented by McGuire *et al*. (2001) will be used. The assembled database of strong-motion records presents suitable records for spectral matching as well for scaling. The database is provided for both soft and hard rock site conditions and the records are separated for western US (WUS) and central and eastern US (CEUS)

The database is organised into M and *d* bins which were selected to preserve significant differences in spectral composition and time domain characteristics. The distance bins are separated into near-source (0 to 10 km fault rupture distance) and beyond (>10 km). For the WUS there are an extended number of recorded ground-motions, while for the CEUS many of the records are synthetic.

Because of the presence of synthetic accelerograms in the CEUS bins, they will not be used and in this work only the real ground-motion records of the WUS for distances up to 50 km will be used. Details of the earthquakes studied are presented in Annex 5.

7.2. Criteria for judging effectiveness of scaling procedures.

Regardless of the scaling procedure, the resultant spectrum should reflect that of a realistic earthquake ground motion. This is achieved when the scaled records have characteristics consistent with real records.

The effectiveness of the scaling is determined by the spectra obtained with the scaled time-histories and their "match" to the design spectrum, as well by the scatter presented among the scaled records within a bin. Matching criteria must be established to judge the degree to which the scaled records are compatible with the design criteria, for which it is judged that at least two of the following should be considered: divergence, over a given period range, between the mean of the scaled records and the design spectrum; covariance of the scaled spectra; maximum residual between a scaled record and the design spectrum. In this work the scatter among the scaled records and the relative error, defined as the residual between scaled and target spectra divided by the target ordinate are considered.

The target spectrum does not have to be matched across all the period range, but to those periods close to the natural period of the structure considered. The differences between the spectra resulting from the scaling and the design spectra are analysed for the individual records and for the average of each bin.

7.3. Scaling on the basis of seismological parameters.

For this type of scaling the target spectrum is defined by the attenuation relationship of Ambraseys *et al*. (1996):

$$\log(y) = C_1' + C_2 M + C_4 \log(r) + C_A S_A + C_S S_S + \sigma P \qquad (7.1)$$

The scaling factor is defined as:

$$\frac{Y_d}{Y_{di}} = 10^{C_2(M-M_i)}\left(\frac{d^2+h_0^2}{d_i^2+h_0^2}\right)^{\frac{C_4}{2}} \tag{7.2}$$

where M and d are the magnitude and distance of the target spectrum and M_i and d_i are the magnitude and distance of the record to scale.

For the scaling factor, the average of the results of Equation (7.2) over the periods of interest (0 -2.0 s) will be considered. The average is used because the variation of the factor within these periods is not significant, as can be observed in Figures 7.2 and 7.3 for the scaling factor for the 1984 Morgan Hill, 1983 Coalinga and 1971 San Fernando earthquakes considered in Section 5.5. The target magnitude and distance used on this scaling are M = 6.5 and d = 30 km.

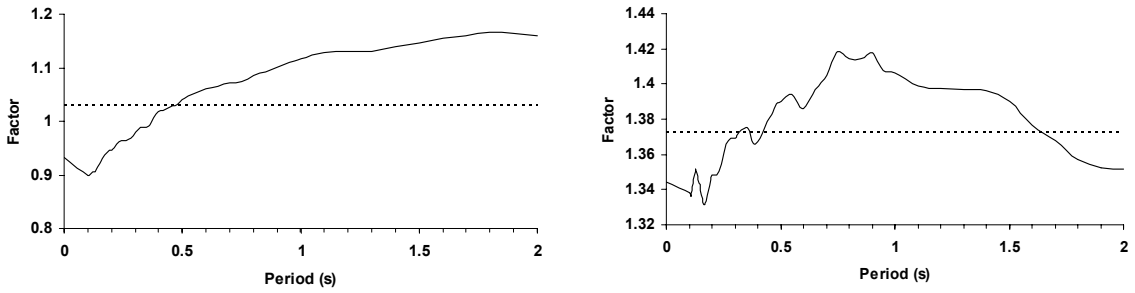

Figure 7.2. Scaling factor for a target earthquake with magnitude M = 6.5 and distance d = 30 km. *Left* – for the 1984 Morgan Hill earthquake (M = 6.2, d = 22.7 km), *right* – for the 1983 Coalinga earthquake (M = 6.4, d = 38.8 km).

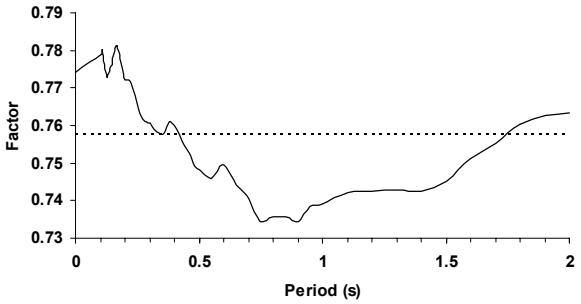

Figure 7.3. Scaling factor for a target earthquake with magnitude M = 6.5 and distance d = 30 km for the 1971 San Fernando earthquake (M = 6.6, d = 24.2 km).

From what can be observed from the analysis in Chapter 8, scaling on the basis of seismological parameters gives a very poor result: it does not present any tendency along the periods of the spectrum and in most of the cases the resultant spectra after the scaling do not agree with the target spectrum. Therefore, scaling by seismological parameters is rejected and should not be used as a scaling technique.

7.4. Scaling in amplitude.

The spectrum given by the attenuation relationship of Ambraseys *et al*. (1996) for the specified magnitude and distance defines the target spectrum. Since this attenuation relationship is only defined up to a period of T = 2.0 sec, the limits of the Housner spectrum intensity will be modified. In addition to this modification, others are explored to see if an improved scaling parameter can be obtained, the modifications being to alter the upper limit of integration and to use the acceleration rather than velocity spectrum.

Six different scaling factors will be used:

$$SI_{V2.0} = \int_{0.1}^{2.0} SV(T,\xi)dT \tag{7.3}$$

$$SI_{V1.5} = \int_{0.1}^{1.5} SV(T,\xi)dT \tag{7.4}$$

$$SI_{V1.0} = \int_{0.1}^{1.0} SV(T,\xi)dT \tag{7.5}$$

$$SI_{A2.0} = \int_{0.1}^{2.0} SA(T,\xi)dT \tag{7.6}$$

$$SI_{A1.5} = \int_{0.1}^{1.5} SA(T,\xi)dT \tag{7.7}$$

$$SI_{A1.0} = \int_{0.1}^{1.0} SA(T,\xi)dT \tag{7.8}$$

Where SV and SA are the velocity and acceleration spectrum respectively and ξ is the damping coefficient taken as 5%.

7.5. Scaling in time and amplitude.

Scaling in time axis changes the duration and the frequency content over the entire spectrum. As a consequence, it is very unlikely to yield realistic motions when scaling in time is perform, as presented in sections 5.6 and 6.2. The approach of scaling both in time and amplitude will alter the duration without changing the number of cycles of motion. Therefore, this type of scaling will not be studied in this work and its used is discouraged.

7.6. Limits on scaling.

The limits on scaling will be explored in each scaling procedure by the match between the scaled time-history and the design spectrum and the issue if the resultant spectrum corresponds to a realistic earthquake ground motion.

In order to explore better this point, the selected bins will also be scaled to match a design spectrum with magnitude values greater (or smaller) than the centre of the bin.

An exercise is performed in the next chapter to explore the limits that may be permissible on scaling factors applied to the amplitudes of recorded motions. Accelerograms are selected from earthquakes recorded at several stations distributed over a wide range of distances from the seismic source. From each suite of records from a single earthquake, sub-sets are selected for which all the records are recorded at sites with the same classification; where possible, the records will also be selected having a similar azimuth with respect to the source. As was shown in Section 5.1.2, spectral amplitudes decay very rapidly with distance from the source, although the spectral shape is relatively insensitive to the distance. As a result, the hypothesis is that it may be possible to scale a record from a distance of, say, 40 km, by a factor of 7 or more, to obtain a record for a scenario defined by the same magnitude but a distance of 10 km. The scaled record obtained at greater distance can then be compared to the actual record obtained at that distance, and the degree of similarity in their peak values, spectral ordinates, durations and Arias energy investigated to verify whether scaling amplitudes by such large factors may indeed be acceptable. Exact matches between the recorded and scaled records would not be expected, because of spatial variability of the ground motion (and the fact that it is unlikely that the two records will have a common azimuth), the fact that two sites with the same classification may

have significant differences in stiffness, profile and topography, and the fact that the more distance recording will include more indirect wave arrivals than the near source records, whereas the latter may be affected by directivity effects not identifiable in the distant record. Notwithstanding these possible limitations, if the Husid plots and response spectra of the recorded and scaled accelerograms match to within acceptable limits, the results would support the idea that the scaling limits of 0.5 to 2.0 may be unnecessarily restrictive.

8. EXPLORATORY ANALYSES

Eleven bins were used for the study. The first eight bins are analysed in section 8.1 to explore the performance of different scaling factors; three of these bins correspond to multiply-recorded earthquakes (bins BF, BG and BH). The maximum magnitude size of the bins corresponding to section 8.1 is of M ± 0.2; for the distance the maximum bin size is d ± 20. Bins BI, BJ and BK are analysed in section 8.2 to explore the limits on scaling. They correspond to multiply-recorded earthquakes with a maximum distance size of the bin of 37 km.

8.1. Scaling performance

Table 8.1 presents the bins selected and their characteristics, as well as the corresponding bins of the McGuire *et al*. (2001) classification.

Table 8.1. Characteristics of the bins.

BIN	Magnitude, M	Distance, d	Target spectrum	Number of records	McGuire *et al*. (2001). classification
BA	[5.2 – 5.4]	[10 – 22]	M = 5.3, d = 15	12	M = 5 – 6, d = 0 - 50
BB	[6.1 – 6.2]	[8 – 12]	M = 6.1, d = 10	8	M = 6 – 7, d = 0 - 10
BC	[6.0 – 6.4]	[11 – 44]	M = 6.2, d = 25	20	M = 6 – 7, d = 10 - 50
BD	[6.9 – 7.3]	[0 – 9]	M = 7.1, d = 5	8	M > 7, d = 0 - 10
BE	[7.1 – 7.4]	[17 – 43]	M = 7.3, d = 25	10	M > 7, d = 10 - 50
BF	6.4	[28 – 41]	M = 6.4, d = 35	8	M = 6 – 7, d = 10 - 50
BG	7.6	[4 – 10]	M = 7.6, d = 6	10	M > 7, d = 0 - 10
BH	7.6	[14 – 49]	M = 7.6, d = 30	8	M > 7, d = 10 - 50

Each bin was scaled to the target spectrum (given by the attenuation relationship of Ambraseys *et al*. (1996) for the specified magnitude and distance) by six different scaling factors coming from the scaling by seismological parameters and scaling in amplitude to the maximum peak ground acceleration (PGA) and to the modified spectrum intensities defined in section 7.4. For all of the bins the two horizontal components of each recorded earthquake were considered.

The performance of the different scaling factors is analysed in terms of the scatter among the scaled records, defined as the ratio between the standard deviation and the arithmetic average, and the relative error of the average scaled record with respect to the target spectrum, obtained by dividing the residual between scaled and target spectra by the target ordinate.

8.1.1. Different recorded earthquakes

Bins BA to BE include different earthquakes. When the scatter among the scaled records is considered, it is observed that the scaling factor that gives the smallest scatter varies along the period. In general the PGA gives the best performance for the smaller periods $T < \sim 0.2$ s. For the longest periods $T > \sim 1.0$ s scaling to SI_V, especially $SI_{V2.0}$, gives the best performance, while scaling to the other parameters present a rather poor behaviour. For the intermediate periods the best performance is obtained when scaling is done either to SI_A or to SI_V.

When the "match" of the average scaled record to the target spectrum is considered, the results obtained are different according to the bin under study. Even if the behaviour is not as clear as when the scatter is considered, it is observed that for the short periods the best match to the target spectrum is given when scaling is done to the PGA. For the long periods, the error in the matching is smaller when scaling is done to SI_V. The greater errors are concentrated in the intermediate period region, especially when scaling to PGA is performed. The performance of the seismological scaling is very poor for both types of criteria: scatter among the records and difference in shape to the target spectrum.

Tables 8.2 to 8.6 presents the scaling factor applied to each record according to the different scaling criteria. Table 8.7 presents the convention used to indicate the scaling performance according to the scatter among the records and the fit to the target spectrum for the following graphs. Figures 8.1 to 8.10 present the average scaled records for each scaling factor with their corresponding coefficient of variation and the relative error in the matching to the target spectrum, and the performance of the resultant scaled records (for each scaling factor) across the period in terms of the scatter among the average scaled records and the relative error of the average spectra with respect to the target spectrum.

Table 8.2. Scaling factors for bin BA.

Scaling criteria	Lytle Creek M = 5.4 *d* = 21.9 St. Devil's Canyon		Lytle Creek M = 5.4 *d* = 15.4 St. Wrightwood-6074 Park Dr.		Coalinga M = 5.2 *d* = 11.0 St. Anticline Ridge Free-Field	
Seism.	1.26	1.26	0.93	0.93	0.85	0.85
PGA	0.42	0.42	0.48	0.34	0.25	0.18
$SI_{V2.0}$	0.84	1.12	0.35	0.46	0.56	0.29
$SI_{V1.5}$	0.81	1.02	0.32	0.41	0.48	0.26
$SI_{V1.0}$	0.78	0.89	0.28	0.35	0.39	0.22
$SI_{A2.0}$	0.67	0.84	0.38	0.43	0.40	0.23
$SI_{A1.5}$	0.59	0.72	0.33	0.37	0.34	0.20
$SI_{A1.0}$	0.56	0.67	0.32	0.35	0.31	0.19

Scaling criteria	Coalinga M = 5.2 *d* = 11.0 St. Anticline Ridge Pad		Coalinga M = 5.2 *d* = 10.0 St. Oil City		Coalinga M = 5.2 *d* = 10.4 St. Transmitter Hill	
Seism.	0.85	0.85	0.79	0.79	0.81	0.81
PGA	0.26	0.16	0.18	0.19	0.39	0.35
$SI_{V2.0}$	0.47	0.30	0.41	0.28	0.37	0.30
$SI_{V1.5}$	0.41	0.27	0.38	0.26	0.33	0.28
$SI_{V1.0}$	0.35	0.24	0.32	0.24	0.29	0.26
$SI_{A2.0}$	0.35	0.24	0.32	0.25	0.35	0.31
$SI_{A1.5}$	0.30	0.21	0.28	0.21	0.30	0.27
$SI_{A1.0}$	0.27	0.20	0.26	0.21	0.28	0.27

Table 8.3. Scaling factors for bin BB.

Scaling criteria	Helena, Montana M = 6.2 *d* = 8.0 St. Carroll College		Parkfield M = 6.1 *d* = 9.2 St. Cholame #8		Parkfield M = 6.1 *d* = 9.9 St. Temblor pre-1969		Morgan Hill M = 6.2 *d* = 11.8 St. Gilroy Array #6	
Seism.	0.77	0.77	0.94	0.94	0.99	0.99	1.04	1.04
PGA	1.11	1.05	0.61	0.58	0.58	0.43	0.54	0.69
$SI_{V2.0}$	1.94	0.75	0.85	0.74	0.69	0.61	0.75	2.59
$SI_{V1.5}$	1.91	0.76	0.85	0.74	0.70	0.55	0.64	2.19
$SI_{V1.0}$	1.63	0.90	0.91	0.72	0.76	0.55	0.51	1.72
$SI_{A2.0}$	1.73	0.91	0.90	0.72	0.69	0.58	0.64	1.77
$SI_{A1.5}$	1.56	0.85	0.83	0.66	0.63	0.51	0.55	1.52
$SI_{A1.0}$	1.44	0.93	0.85	0.65	0.64	0.51	0.50	1.36

Table 8.4. Scaling factors for bin BC.

Scaling criteria	Mammoth Lakes M = 6.0 *d* = 19.7 St. Long Valley Dam (L. Abut.)		Mammoth Lakes M = 6.0 *d* = 43.7 St. Bishop-Paradise Lodge		Coalinga M =6.4 *d* = 28.4 St. Parkfield-Fault Zone 11	
Seism.	0.97	0.97	1.96	1.96	0.94	0.94
PGA	1.01	0.85	0.66	0.84	0.86	0.97
$SI_{V2.0}$	1.10	0.69	1.47	1.19	0.58	0.47
$SI_{V1.5}$	1.17	0.67	1.70	1.26	0.55	0.46
$SI_{V1.0}$	1.40	0.69	1.72	1.43	0.52	0.53
$SI_{A2.0}$	1.27	0.76	1.47	1.40	0.65	0.60
$SI_{A1.5}$	1.21	0.71	1.41	1.34	0.60	0.57
$SI_{A1.0}$	1.29	0.72	1.36	1.43	0.60	0.63

Scaling criteria	Coalinga M = 6.4 *d* = 38.8 St. Parkfield-Gold Hill 3W		Coalinga M = 6.4 *d* = 40.5 St. Parkfield-Cholame 2E		Coalinga M = 6.4 *d* = 34.6 St. Parkfield-Vineyard Cany 4W	
Seism.	1.23	1.23	1.28	1.28	1.11	1.11
PGA	0.60	0.55	1.90	3.01	1.90	1.33
$SI_{V2.0}$	0.43	0.35	0.79	1.35	0.90	0.65
$SI_{V1.5}$	0.40	0.36	1.03	1.41	0.87	0.60
$SI_{V1.0}$	0.51	0.50	1.54	1.85	1.00	0.63
$SI_{A2.0}$	0.51	0.45	1.24	1.84	1.15	0.82
$SI_{A1.5}$	0.47	0.43	1.36	1.78	1.08	0.75
$SI_{A1.0}$	0.53	0.51	1.74	2.12	1.21	0.81

Scaling criteria	Morgan Hill M = 6.2 *d* = 22.7 St. Corralitos		Morgan Hill M = 6.2 *d* = 11.8 St. Gilroy Array #6		Morgan Hill M = 6.2 *d* = 16.2 St. Gilroy-Gavilan Coll		Whittier Narrows M = 6.0 *d* = 32.6 St. LA-Chalon Rd #	
Seism.	0.92	0.92	0.53	0.53	0.69	0.69	1.51	1.51
PGA	0.68	0.90	0.26	0.33	0.64	0.78	4.25	2.02
$SI_{V2.0}$	0.47	0.63	0.13	0.40	1.70	1.93	4.35	2.57
$SI_{V1.5}$	0.42	0.60	0.12	0.36	1.78	1.95	3.98	2.22
$SI_{V1.0}$	0.45	0.62	0.15	0.34	1.85	1.84	3.41	1.89
$SI_{A2.0}$	0.54	0.71	0.16	0.38	1.63	1.63	4.04	2.31
$SI_{A1.5}$	0.48	0.65	0.15	0.33	1.51	1.48	3.59	2.02
$SI_{A1.0}$	0.52	0.67	0.18	0.32	1.49	1.39	3.34	1.88

Table 8.5. Scaling factors for bin BD.

Scaling criteria	Loma Prieta M = 6.9 *d* = 5.1 St. Corralitos		Cape Mendocino M = 7.1 *d* = 8.5 St. Cape Mendocino #		Landers M = 7.3 *d* = 1.1 St. Lucerne		Kobe M = 6.9 *d* = 0.2 St. Kobe University	
Seism.	1.21	1.21	1.42	1.42	0.55	0.55	0.76	0.76
PGA	1.00	0.76	0.47	0.32	0.76	0.84	1.57	1.75
$SI_{V2.0}$	0.89	1.02	1.31	0.67	1.79	0.91	1.26	0.81
$SI_{V1.5}$	0.83	0.97	1.51	0.66	1.74	1.03	1.32	0.84
$SI_{V1.0}$	0.78	0.85	1.59	0.64	1.79	1.35	1.63	1.39
$SI_{A2.0}$	0.97	0.95	1.32	0.62	1.65	1.09	1.55	1.14
$SI_{A1.5}$	0.90	0.87	1.30	0.58	1.53	1.10	1.52	1.15
$SI_{A1.0}$	0.89	0.81	1.28	0.56	1.50	1.23	1.73	1.62

Table 8.6. Scaling factors for bin BE.

Scaling criteria	Tabas, Iran M = 7.4 *d* = 17.0 St. Dayhook		Cape Mendocino M = 7.1 *d* = 33.8 St. Shelter Cove Airport #		Landers M = 7.3 *d* = 42.2 St. Twentynine Palms#	
Seism.	0.66	0.66	1.56	1.56	1.59	1.59
PGA	0.48	0.38	0.84	0.65	2.45	1.84
$SI_{V2.0}$	0.69	0.58	4.08	4.37	5.57	5.73
$SI_{V1.5}$	0.69	0.60	3.77	3.91	5.88	5.78
$SI_{V1.0}$	0.66	0.55	3.05	2.82	5.73	5.05
$SI_{A2.0}$	0.63	0.59	2.42	2.15	4.75	4.56
$SI_{A1.5}$	0.59	0.56	2.14	1.88	4.48	4.21
$SI_{A1.0}$	0.56	0.54	1.82	1.54	4.18	3.77

Scaling criteria	Kocaeli, Turkey M = 7.4 *d* = 17.0 St. Gebze		Kocaeli, Turkey M = 7.4 *d* = 35.5 St. Goynuk	
Seism.	0.66	0.66	1.25	1.25
PGA	0.63	1.11	1.09	1.26
$SI_{V2.0}$	0.89	1.11	1.62	1.26
$SI_{V1.5}$	0.88	1.18	1.80	1.30
$SI_{V1.0}$	0.80	1.22	1.67	1.49
$SI_{A2.0}$	0.89	1.17	1.53	1.35
$SI_{A1.5}$	0.84	1.14	1.48	1.31
$SI_{A1.0}$	0.79	1.14	1.38	1.37

Table 8.7. Convention to indicate scaling performance.

	COV	Relative Error (%)
	$COV \leq 0.20$	$R.E \leq 25$
	$0.20 < COV \leq 0.40$	$25 < R.E \leq 50$
	$0.40 < COV \leq 0.60$	$50 < R.E \leq 75$
	$0.60 < COV \leq 0.80$	$75 < R.E \leq 100$
	$COV \geq 0.80$	$R.E \geq 100$

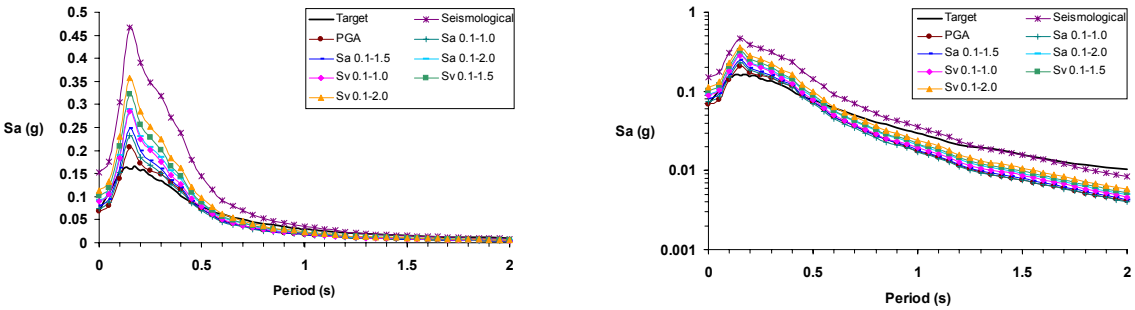

a. Average of the scaled records.

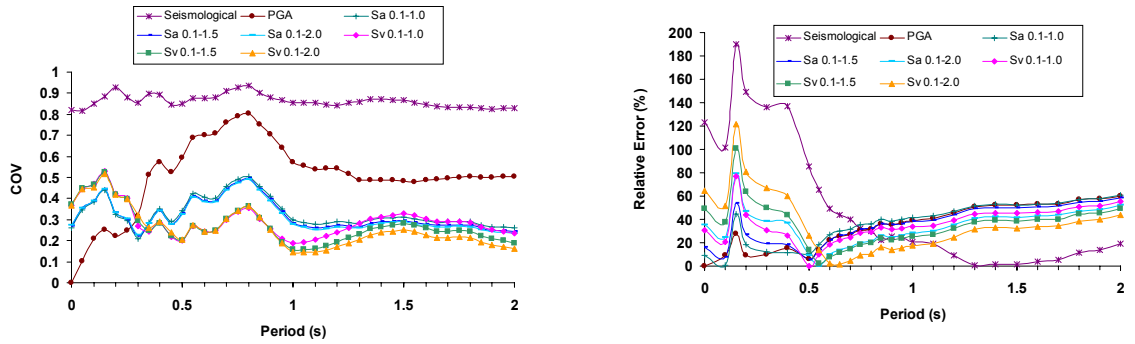

b. *Left* – scatter among the records (COV), *right* – relative error for the average.

Figure 8.1. Scaled records for bin BA.

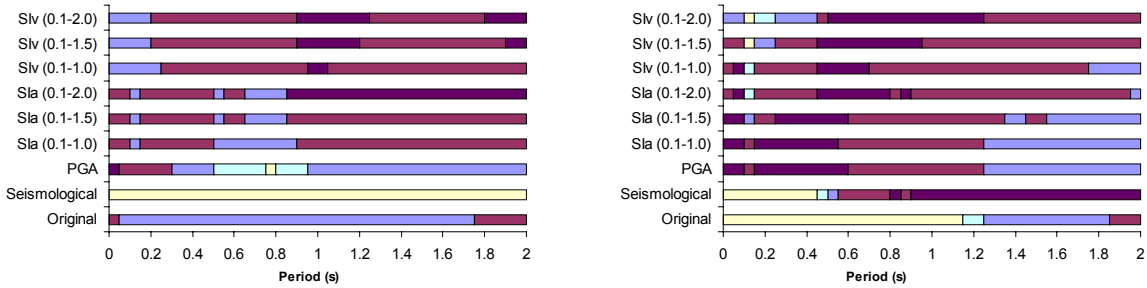

Figure 8.2. Performance of the scaling factors for bin BA. *Left* – considering the scatter among the scaled records, *right* – considering the relative error with respect to the target spectrum.

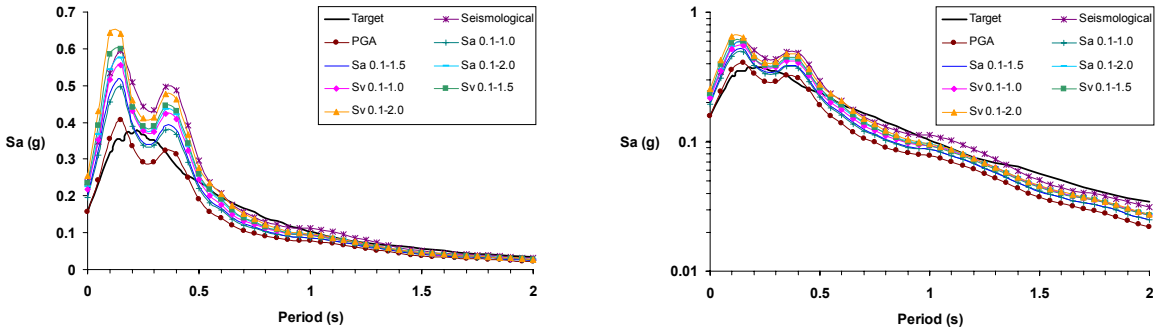

a. Average of the scaled records.

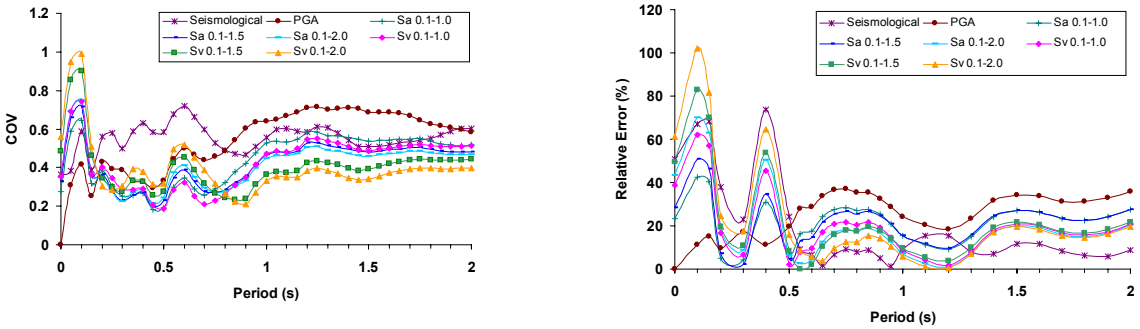

b. *Left* – scatter among the records (COV), *right* – relative error for the average.

Figure 8.3. Scaled records for bin BB.

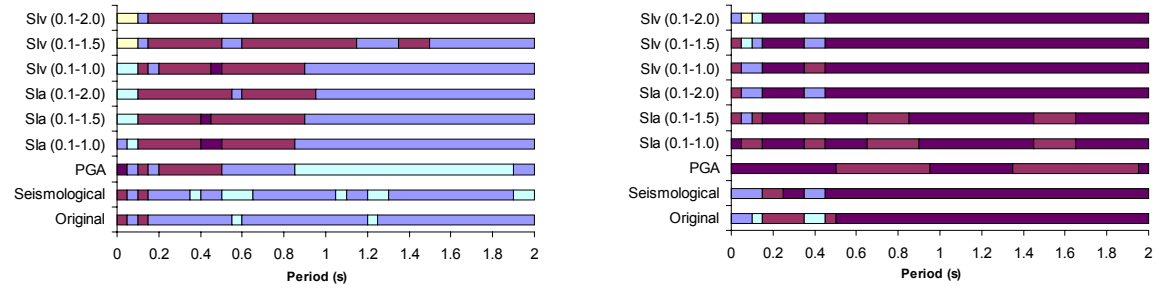

Figure 8.4. Performance of the scaling factors for bin BB. *Left* – considering the scatter among the scaled records, *right* – considering the relative error with respect to the target spectrum.

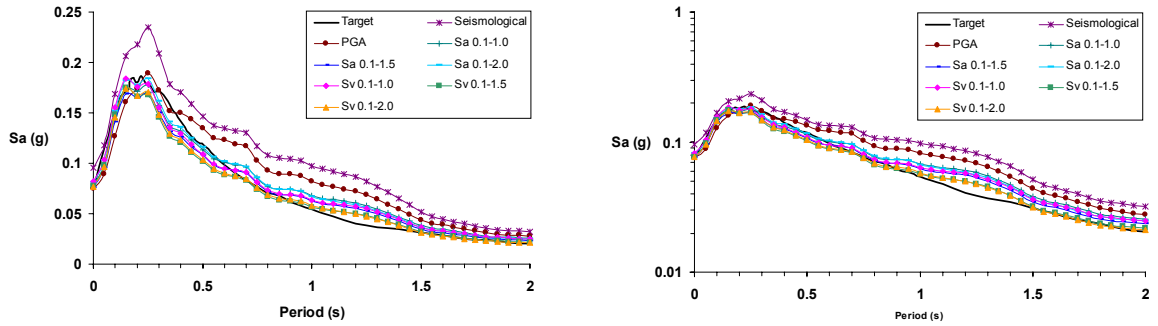

a. Average of the scaled records.

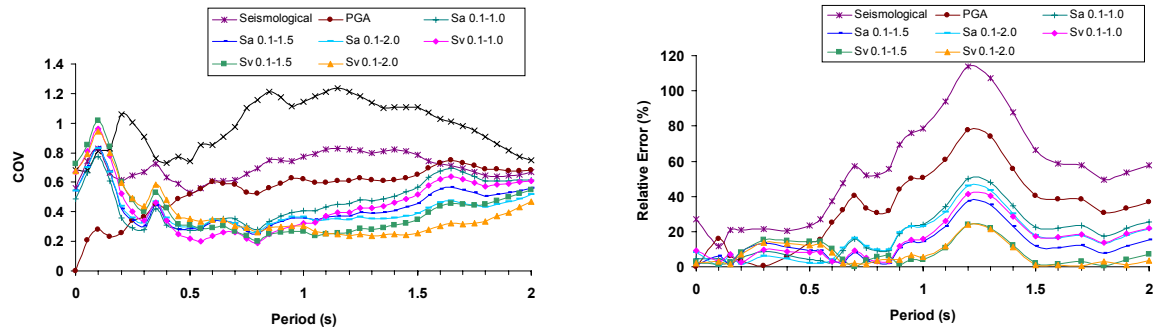

b. *Left* – scatter among the records (COV), *right* – relative error for the average.

Figure 8.5. Scaled records for bin BC. Scatter among the records (COV) and relative error for the average.

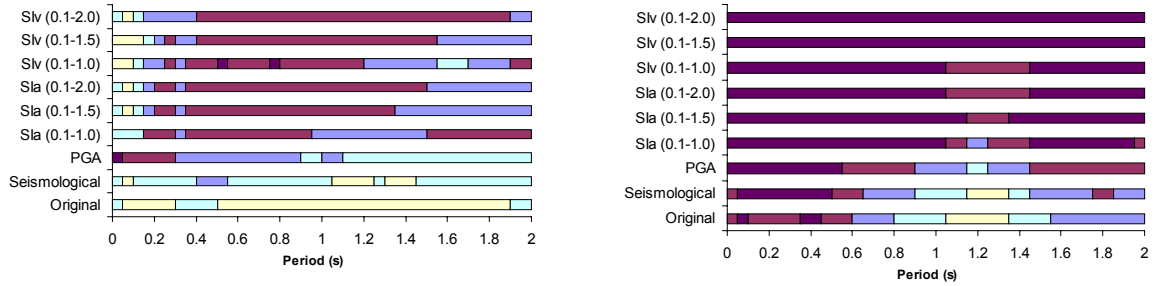

Figure 8.6. Performance of the scaling factors for bin BC. *Left* – considering the scatter among the scaled records, *right* – considering the relative error with respect to the target spectrum.

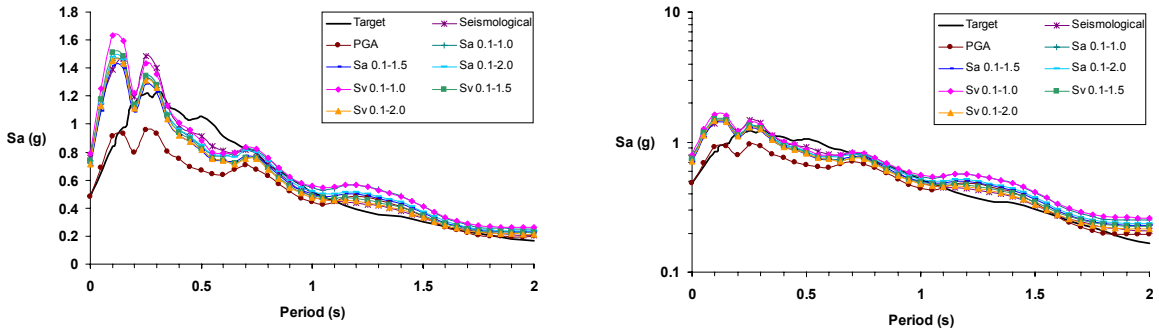

a. Average of the scaled records.

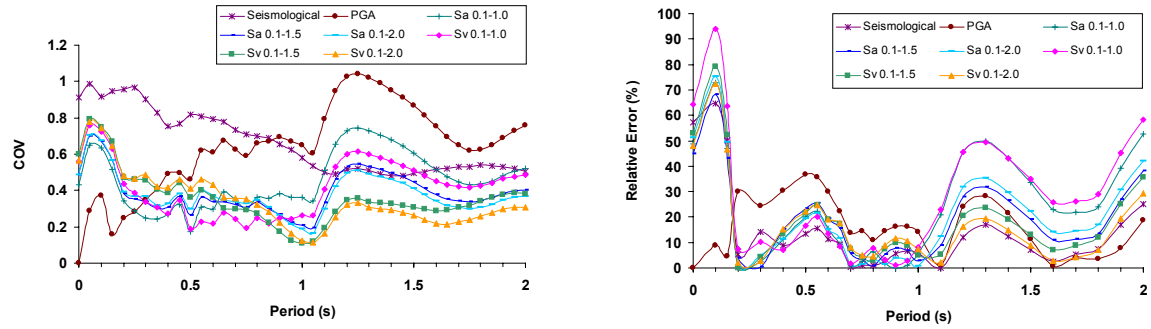

b. *Left* – scatter among the records (COV), *right* – relative error for the average.

Figure 8.7. Scaled records for bin BD.

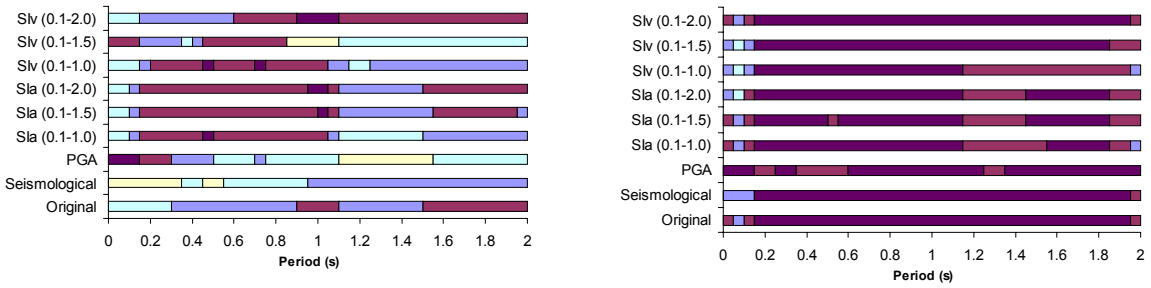

Figure 8.8. Performance of the scaling factors for bin BD. *Left* – considering the scatter among the scaled records, *right* – considering the relative error with respect to the target spectrum.

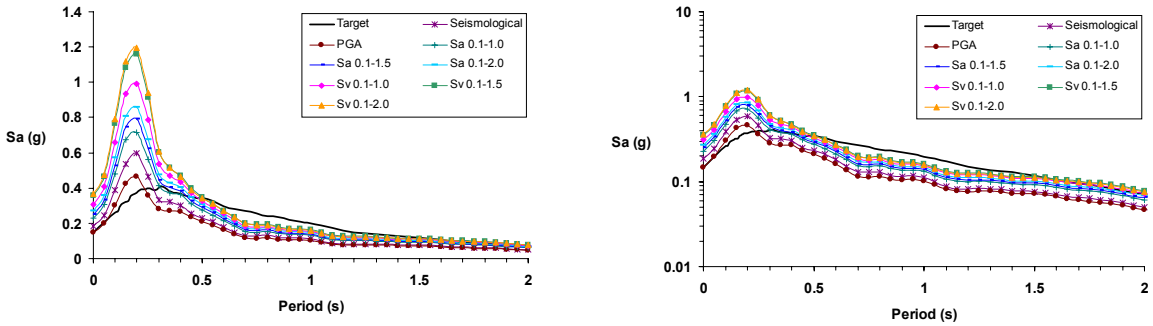

a. Average of the scaled records.

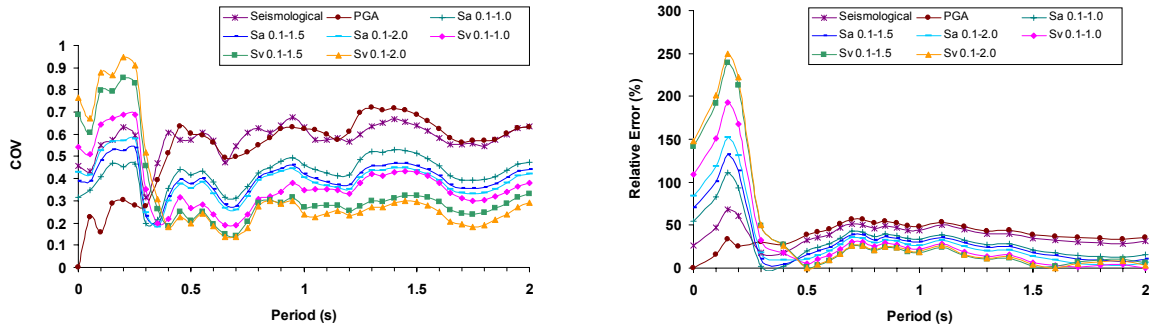

b. *Left* – scatter among the records (COV), *right* – relative error for the average.

Figure 8.9 Scaled records for bin BE.

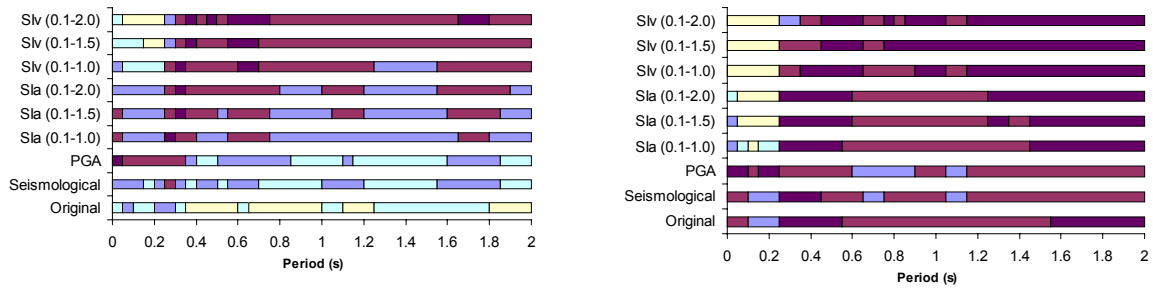

Figure 8.10. Performance of the scaling factors for bin BE. *Left* – considering the scatter among the scaled records, *right* – considering the relative error with respect to the target spectrum.

8.1.2. Multiply-recorded earthquakes

For this case two different earthquakes were studied: the Coalinga event of 1983 with a magnitude of 6.4 as an example of near source records (bin BF), and the Chi-Chi, Taiwan event of 1999, with a magnitude of 7.6. For this case two scenarios were considered: close events (near fault) in bin BG, and far events in bin BH.

For all the components, when the scatter among the scaled records is considered, the scaling factor with the best performance varies along the period in the same mode as in the previous case studied (when different recorded earthquakes are considered within a bin): for the shortest periods scaling to the PGA gives the smaller scatter; for the intermediate periods, the best performance is given by either SI_A or SI_V; for the longer periods the best performance is obtained when scaling is done to SI_V.

When the "match" of the average scaled record to the target spectrum is considered, the tendency presented when the scatter is considered is conserved for the records of the Coalinga earthquake (bin BF). For the Chi-Chi, Taiwan earthquake, very good agreement was found for the close events (bin BG) for periods T ~ < 1.0 s for all the scaling factors, excluding the seismological factor. For the far events of the same earthquake, a very good agreement with the target spectrum shape was found for all the periods.

Tables 8.8 to 8.10 present the scaling factor applied to each record according to the different scaling criteria. Figures 8.11 to 8.16 present the average scaled records for each scaling factor with their corresponding coefficient of variation and the relative error in the matching to the target spectrum, and the performance of the resultant scaled records (for each scaling factor) across the period in terms of the scatter among the average scaled records and the relative error of the average spectra with respect to the target spectrum.

Table 8.8. Scaling factors for bin BF.

Scaling criteria	Coalinga M =6.4 *d* = 28.4 St. Parkfield-Fault Zone 11		Coalinga M = 6.4 *d* = 38.8 St. Parkfield-Gold Hill 3W		Coalinga M = 6.4 *d* = 40.5 St. Parkfield-Cholame 2E		Coalinga M = 6.4 *d* = 34.6 St. Parkfield-Vineyard Cany 4W	
Seism.	0.94	0.94	1.23	1.23	1.28	1.28	1.11	1.11
PGA	0.86	0.97	0.60	0.55	1.90	3.01	1.90	1.33
$SI_{V2.0}$	0.58	0.47	0.43	0.35	0.79	1.35	0.90	0.65
$SI_{V1.5}$	0.55	0.46	0.40	0.36	1.03	1.41	0.87	0.60
$SI_{V1.0}$	0.52	0.53	0.51	0.50	1.54	1.85	1.00	0.63
$SI_{A2.0}$	0.65	0.60	0.51	0.45	1.24	1.84	1.15	0.82
$SI_{A1.5}$	0.60	0.57	0.47	0.43	1.36	1.78	1.08	0.75
$SI_{A1.0}$	0.60	0.63	0.53	0.51	1.74	2.12	1.21	0.81

Table 8.9. Scaling factors for bin BG.

Scaling criteria	Chi-Chi, Taiwan M = 7.6 *d* = 3.1 St. TCU087		Chi-Chi, Taiwan M = 7.6 *d* = 8.2 St. TCU089	
Seism.	0.72	0.72	1.24	1.24
PGA	2.64	4.68	2.64	1.74
$SI_{V2.0}$	2.71	3.66	2.71	2.02
$SI_{V1.5}$	2.77	4.31	2.77	2.09
$SI_{V1.0}$	3.33	5.04	3.33	2.15
$SI_{A2.0}$	2.86	4.42	2.86	2.06
$SI_{A1.5}$	2.77	4.62	2.77	1.99
$SI_{A1.0}$	2.98	5.00	2.98	1.99

Scaling criteria	Chi-Chi, Taiwan M = 7.6 *d* = 8.1 St. TCU120		Chi-Chi, Taiwan M = 7.6 *d* = 9.7 St. TCU128		Chi-Chi, Taiwan M = 7.6 *d* = 8.9 St. TCU136	
Seism.	1.23	1.23	1.41	1.41	1.32	1.32
PGA	3.23	2.93	3.72	5.34	3.66	3.62
$SI_{V2.0}$	2.88	1.76	2.76	3.23	2.67	2.38
$SI_{V1.5}$	3.50	2.24	3.41	3.70	2.70	2.47
$SI_{V1.0}$	3.71	2.72	3.70	5.75	3.07	2.83
$SI_{A2.0}$	3.30	2.34	3.52	4.22	3.32	2.94
$SI_{A1.5}$	3.44	2.58	3.79	4.44	3.26	2.92
$SI_{A1.0}$	3.51	2.96	4.05	5.74	3.75	3.31

Table 8.10. Scaling factors for bin BH.

Scaling criteria	Chi-Chi, Taiwan M = 7.6 *d* = 47.3 St. TCU015		Chi-Chi, Taiwan M = 7.6 *d* = 14.3 St. TCU046		Chi-Chi, Taiwan M = 7.6 *d* = 33.0 St. TCU047		Chi-Chi, Taiwan M = 7.6 *d* = 43.4 St. TCU095	
Seism.	1.50	1.50	0.53	0.53	1.09	1.09	1.39	1.39
PGA	1.41	1.44	1.28	1.17	0.37	0.50	0.23	0.50
$SI_{V2.0}$	1.18	1.07	1.41	1.34	0.63	0.49	0.62	0.49
$SI_{V1.5}$	1.43	1.17	1.58	1.43	0.59	0.43	0.55	0.43
$SI_{V1.0}$	1.53	1.37	1.64	1.41	0.50	0.46	0.46	0.46
$SI_{A2.0}$	1.41	1.26	1.51	1.39	0.56	0.53	0.44	0.53
$SI_{A1.5}$	1.50	1.28	1.52	1.36	0.51	0.48	0.39	0.48
$SI_{A1.0}$	1.56	1.41	1.52	1.33	0.46	0.52	0.35	0.52

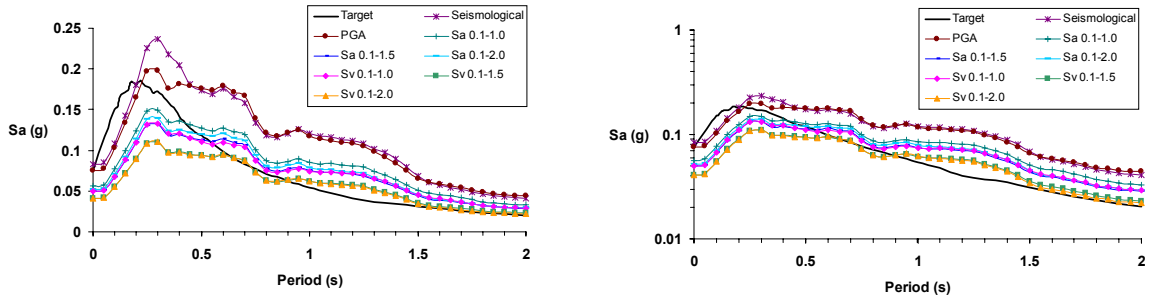

a. Average of the scaled records.

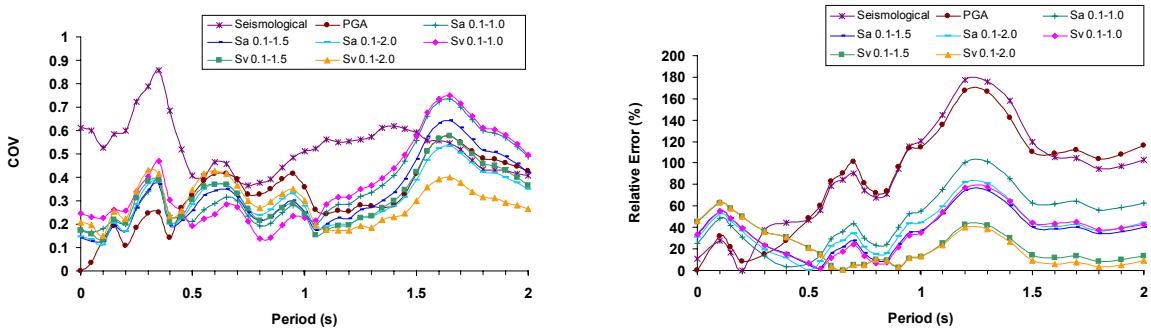

b. *Left* – scatter among the records (COV), *right* – relative error for the average.

Figure 8.11. Scaled records for bin BF.

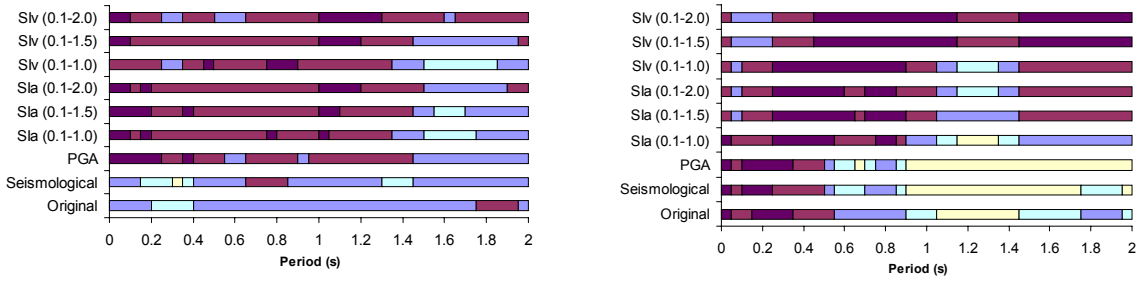

Figure 8.12. Performance of the scaling factors for bin BF. *Left* – considering the scatter among the scaled records, *right* – considering the relative error with respect to the target spectrum.

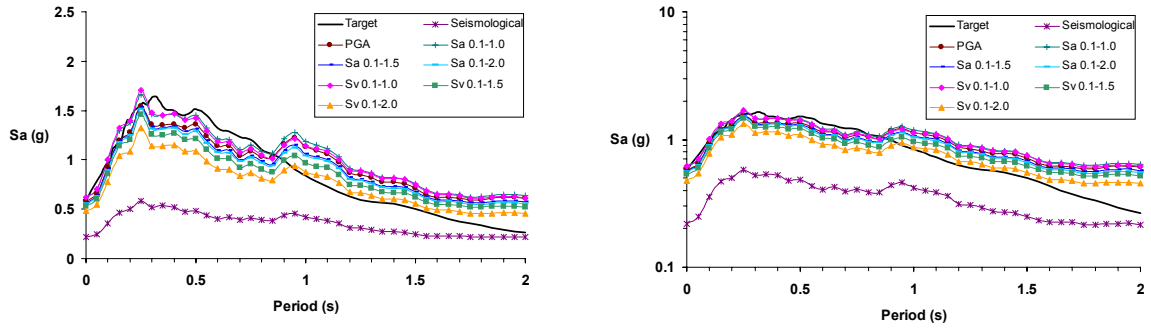

a. Average of the scaled records.

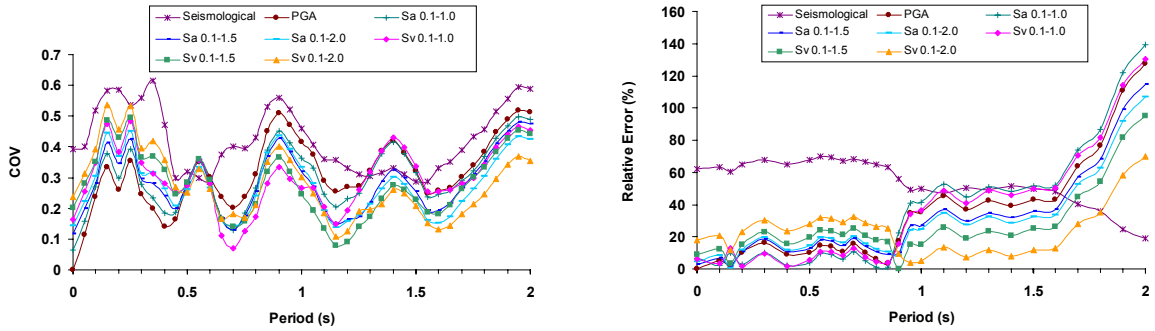

b. *Left* – scatter among the records (COV), *right* – relative error for the average.

Figure 8.13. Scaled records for bin BG.

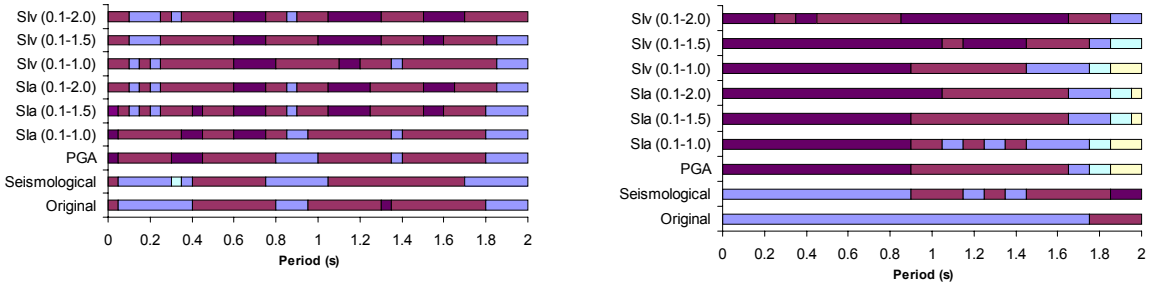

Figure 8.14. Performance of the scaling factors for bin BG. *Left* – considering the scatter among the scaled records, *right* – considering the relative error with respect to the target spectrum.

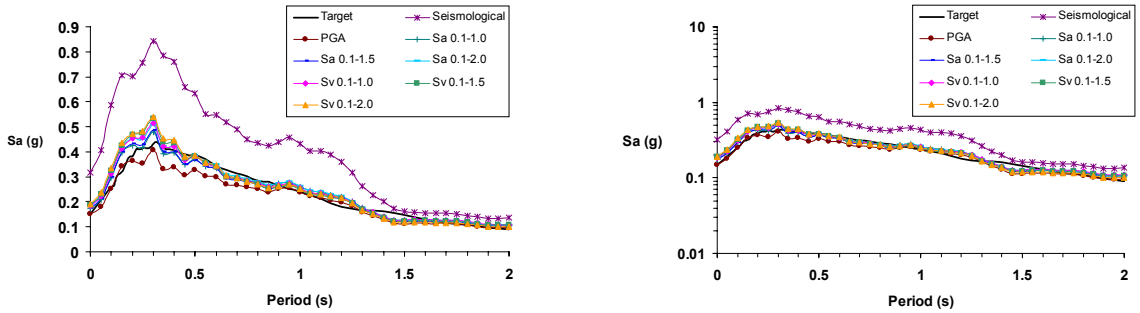

a. Average of the scaled records.

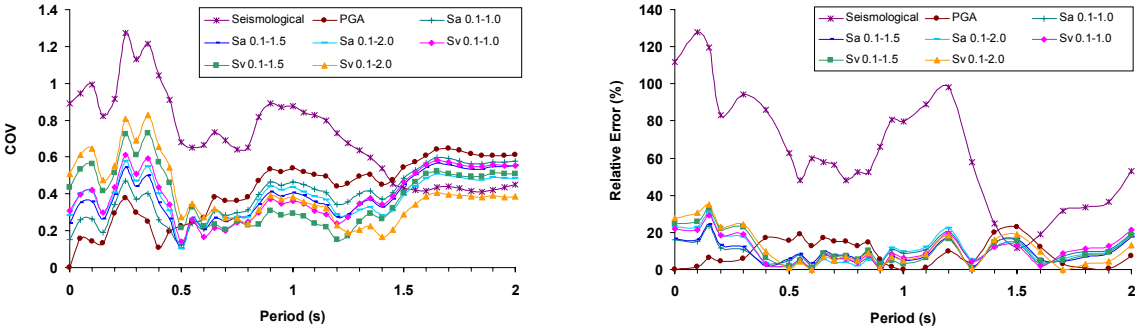

b. *Left* – scatter among the records (COV), *right* – relative error for the average.

Figure 8.15. Scaled records for bin BH.

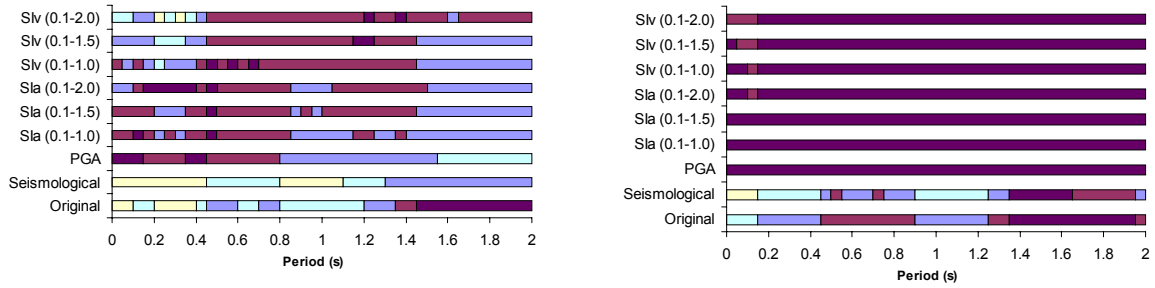

Figure 8.16. Performance of the scaling factors for bin BH. *Left* – considering the scatter among the scaled records, *right* – considering the relative error with respect to the target spectrum.

8.1.3. Bins scaled to a smaller distance

To initially explore the limits on scaling, the records from bins BA, BC and BE are scaled to a distance of one third of that one of the centre of the bin. Table 8.11 presents the characteristics of the bins and the new target spectrum. The bins for the new distances are renamed as BA*, BC* and BE*. The target spectrum considered for these bins is the spectrum given by the attenuation relationship of Ambraseys *et al*. 1996 for the median plus half standard deviation as an approximation of the results of a probabilistic seismic hazard assessment (PSHA), which includes a number of standard deviations above the median value predicted by the attenuation relationship.

To scale the records to the target spectrum corresponding to a distance of one third of the centre of the bin implies greater scaling factors. Nevertheless, it is observed that the scatter among the records remains the same for each bin, since the scatter is a characteristic of the group of records considered. When the fit to the target spectrum is considered, the behaviour is practically the same as the one presented when the bins are scaled to a distance corresponding to the centre of the bin.

This initial exploration of the scaling limits indicates that when bins are scaled to distances outside the centre of the bin, the behaviour of the scaling factors is practically the same, indicating that set of records from far distances could be scaled to shorter distances when the match to the target spectrum is considered. This issue is explored further in section 8.2, where it is also considered the fact that the resultant scaled motions should be realistic and consistent with the earthquake scenario considered.

Tables 8.12 to 8.14 present the scaling factor applied to each record to the different scaling criteria. Figures 8.17 to 8.22 present the average scaled records for each scaling factor with their corresponding coefficient of variation and the relative error in the matching to the target spectrum, as well as the performance of the resultant scaled records across the period in terms of the scatter among the average records and the relative error of the average spectra with respect to the target spectrum.

Table 8.11. Characteristics of bins BA*, BC* and BE*.

BIN	Magnitude, M	Distance, *d*	Target spectrum	Number of records	McGuire *et al*. (2001). classification
BA*	[5.2 – 5.4]	[10 – 22]	M = 5.3, *d* = 5	12	M = 5 – 6, *d* = 0 - 50
BC*	[6.0 – 6.4]	[11 – 44]	M = 6.2, *d* = 8	20	M = 6 – 7, *d* = 10 - 50
BE*	[7.1 – 7.4]	[17 – 43]	M = 7.3, *d* = 8	10	M > 7, *d* = 10 - 50

Table 8.12. Scaling factors for bin BA*.

Scaling criteria	Lytle Creek M = 5.4 *d* = 21.9 St. Devil's Canyon		Lytle Creek M = 5.4 *d* = 15.4 St. Wrightwood-6074 Park Dr.		Coalinga M = 5.2 *d* = 11.0 St. Anticline Ridge Free-Field	
Seism.	4.24	4.24	3.14	3.14	2.85	2.85
PGA	1.38	1.36	1.55	1.13	0.81	0.58
$SI_{V2.0}$	2.87	3.80	1.20	1.56	1.92	0.97
$SI_{V1.5}$	2.80	3.51	1.10	1.41	1.67	0.89
$SI_{V1.0}$	2.73	3.12	0.98	1.23	1.38	0.79
$SI_{A2.0}$	2.26	2.84	1.29	1.45	1.34	0.79
$SI_{A1.5}$	1.99	2.46	1.13	1.26	1.14	0.68
$SI_{A1.0}$	1.90	2.30	1.09	1.19	1.04	0.64

Scaling criteria	Coalinga M = 5.2 *d* = 11.0 St. Anticline Ridge Pad		Coalinga M = 5.2 *d* = 10.0 St. Oil City		Coalinga M = 5.2 *d* = 10.4 St. Transmitter Hill	
Seism.	2.85	2.85	2.64	2.64	2.73	2.73
PGA	0.86	0.53	0.60	0.62	1.27	1.16
$SI_{V2.0}$	1.61	1.03	1.40	0.97	1.27	1.03
$SI_{V1.5}$	1.42	0.95	1.29	0.90	1.14	0.96
$SI_{V1.0}$	1.22	0.85	1.12	0.84	1.01	0.91
$SI_{A2.0}$	1.17	0.82	1.08	0.84	1.18	1.05
$SI_{A1.5}$	1.01	0.71	0.94	0.73	1.02	0.93
$SI_{A1.0}$	0.93	0.67	0.87	0.70	0.97	0.91

Table 8.13. Scaling factors for bin BC*.

Scaling criteria	Mammoth Lakes M = 6.0 *d* = 19.7 St. Long Valley Dam (L. Abut.)		Mammoth Lakes M = 6.0 *d* = 43.7 St. Bishop-Paradise Lodge		Coalinga M =6.4 *d* = 28.4 St. Parkfield-Fault Zone 11	
Seism.	3.73	3.73	7.51	7.51	3.58	3.58
PGA	3.73	3.16	2.43	3.11	3.20	3.60
$SI_{V2.0}$	4.21	2.62	5.63	4.53	2.20	1.79
$SI_{V1.5}$	4.58	2.63	6.67	4.95	2.16	1.82
$SI_{V1.0}$	5.62	2.75	6.89	5.72	2.10	2.11
$SI_{A2.0}$	4.90	2.96	5.70	5.43	2.53	2.34
$SI_{A1.5}$	4.72	2.76	5.52	5.24	2.35	2.22
$SI_{A1.0}$	5.10	2.84	5.37	5.62	2.35	2.49

Scaling criteria	Coalinga M = 6.4 *d* = 38.8 St. Parkfield-Gold Hill 3W		Coalinga M = 6.4 *d* = 40.5 St. Parkfield-Cholame 2E		Coalinga M = 6.4 *d* = 34.6 St. Parkfield-Vineyard Cany 4W	
Seism.	4.73	4.73	4.91	4.91	4.27	4.27
PGA	2.23	2.02	7.04	11.12	7.01	4.91
$SI_{V2.0}$	1.63	1.35	3.03	5.17	3.45	2.48
$SI_{V1.5}$	1.58	1.40	4.03	5.52	3.41	2.36
$SI_{V1.0}$	2.02	1.99	6.18	7.40	4.02	2.52
$SI_{A2.0}$	1.98	1.74	4.79	7.10	4.46	3.18
$SI_{A1.5}$	1.85	1.67	5.34	6.95	4.20	2.94
$SI_{A1.0}$	2.10	2.01	6.84	8.35	4.75	3.19

Scaling criteria	Morgan Hill M = 6.2 *d* = 22.7 St. Corralitos		Morgan Hill M = 6.2 *d* = 11.8 St. Gilroy Array #6		Morgan Hill M = 6.2 *d* = 16.2 St. Gilroy-Gavilan Coll		Whittier Narrows M = 6.0 *d* = 32.6 St. LA-Chalon Rd #	
Seism.	3.52	3.52	2.03	2.03	2.63	2.63	5.79	5.79
PGA	2.53	3.34	0.95	1.22	2.38	2.87	15.71	7.46
$SI_{V2.0}$	1.79	2.41	0.48	1.53	6.50	7.36	16.59	9.80
$SI_{V1.5}$	1.65	2.34	0.48	1.40	6.96	7.65	15.60	8.69
$SI_{V1.0}$	1.82	2.50	0.61	1.37	7.43	7.35	13.65	7.58
$SI_{A2.0}$	2.09	2.73	0.63	1.46	6.31	6.30	15.60	8.94
$SI_{A1.5}$	1.90	2.53	0.59	1.30	5.92	5.79	14.06	7.90
$SI_{A1.0}$	2.05	2.63	0.70	1.28	5.86	5.46	13.16	7.43

Table 8.14. Scaling factors for bin BE*.

Scaling criteria	Tabas, Iran M = 7.4 *d* = 17.0 St. Dayhook		Cape Mendocino M = 7.1 *d* = 33.8 St. Shelter Cove Airport #		Landers M = 7.3 *d* = 42.2 St. Twentynine Palms#	
Seism.	2.51	2.51	5.98	5.98	6.08	6.08
PGA	1.77	1.42	3.09	2.41	9.05	6.80
$SI_{V2.0}$	2.63	2.20	15.51	16.63	21.18	21.81
$SI_{V1.5}$	2.68	2.35	14.75	15.30	23.00	22.61
$SI_{V1.0}$	2.64	2.23	12.27	11.35	23.05	20.29
$SI_{A2.0}$	2.43	2.27	9.35	8.32	18.36	17.63
$SI_{A1.5}$	2.30	2.21	8.40	7.36	17.59	16.52
$SI_{A1.0}$	2.21	2.13	7.24	6.12	16.57	14.98

Scaling criteria	Kocaeli, Turkey M = 7.4 *d* = 17.0 St. Gebze		Kocaeli, Turkey M = 7.4 *d* = 35.5 St. Goynuk	
Seism.	2.51	2.51	4.77	4.77
PGA	2.34	4.10	4.05	4.65
$SI_{V2.0}$	3.38	4.21	6.15	4.79
$SI_{V1.5}$	3.44	4.60	7.03	5.10
$SI_{V1.0}$	3.20	4.91	6.73	6.00
$SI_{A2.0}$	3.44	4.52	5.90	5.21
$SI_{A1.5}$	3.30	4.46	5.82	5.12
$SI_{A1.0}$	3.16	4.54	5.49	5.42

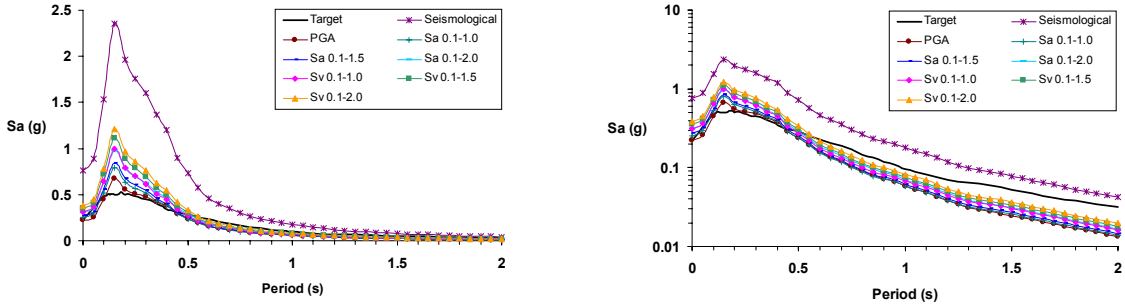

a. Average of the scaled records.

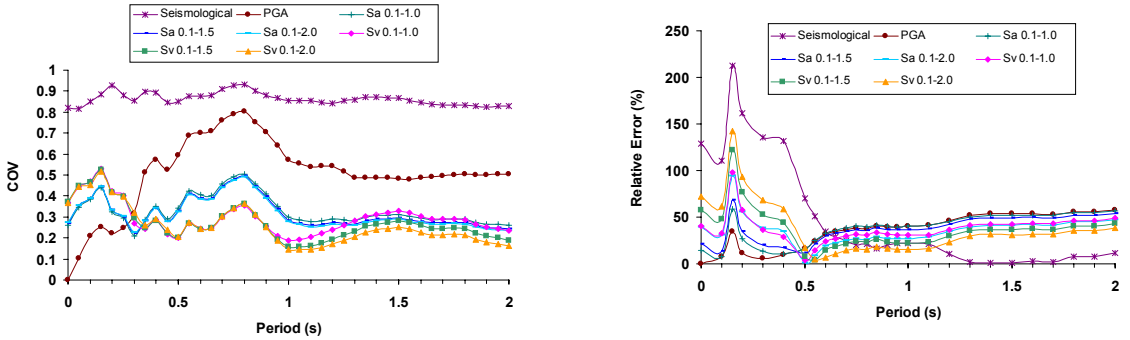

b. *Left* – scatter among the records (COV), *right* – relative error for the average.

Figure 8.17. Scaled records for bin BA*.

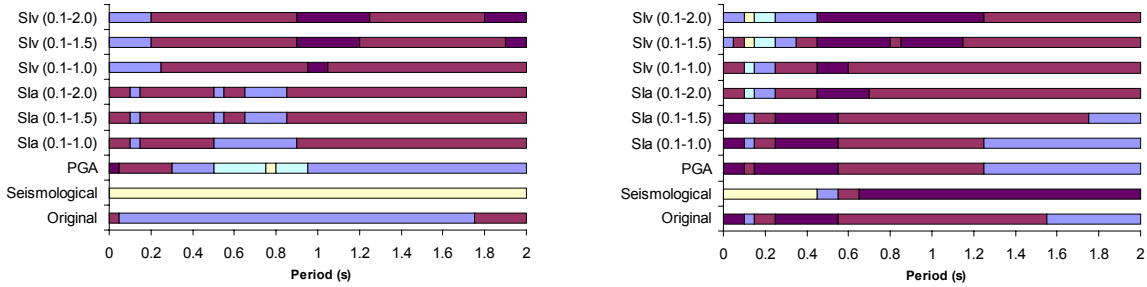

Figure 8.18. Performance of the scaling factors for bin BA*. *Left* – considering the scatter among the scaled records, *right* – considering the relative error with respect to the target spectrum.

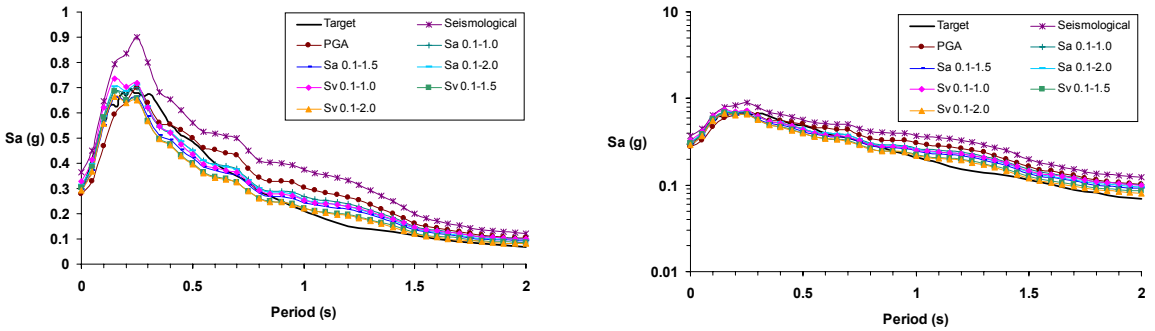

a. Average of the scaled records.

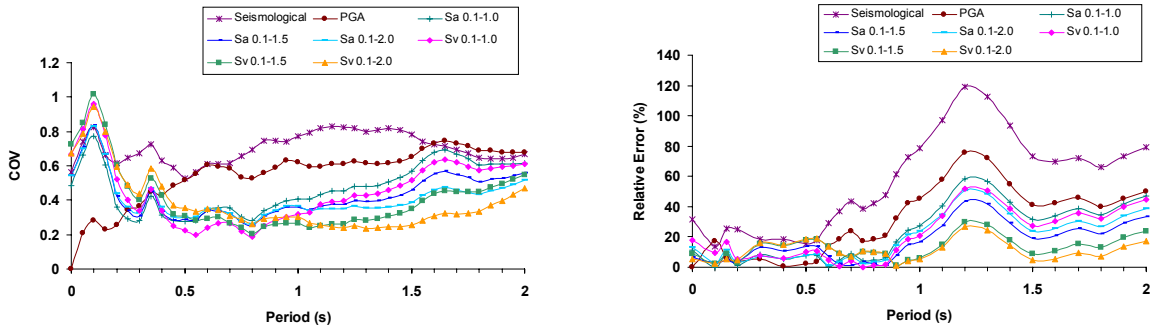

b. *Left* – scatter among the records (COV), *right* – relative error for the average.

Figure 8.19. Scaled records for bin BC*.

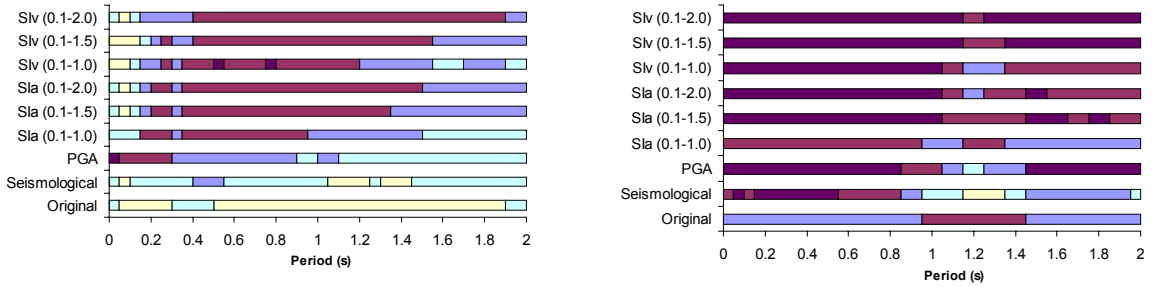

Figure 8.20. Performance of the scaling factors for bin BC*. *Left* – considering the scatter among the scaled records, *right* – considering the relative error with respect to the target spectrum.

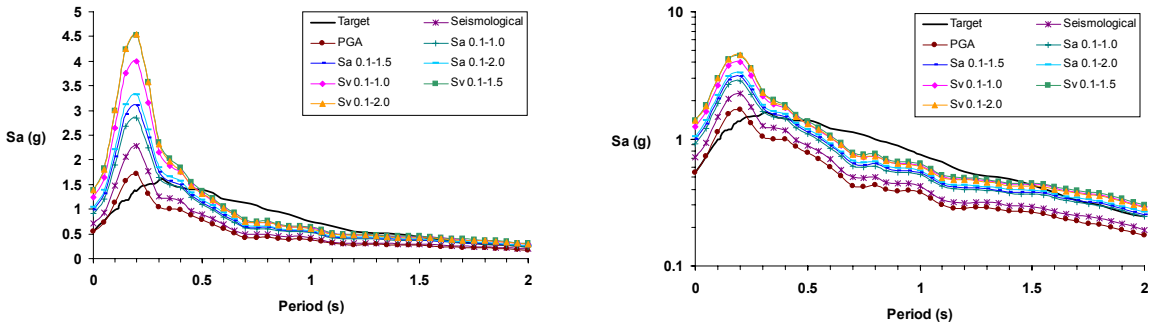

a. Average of the scaled records.

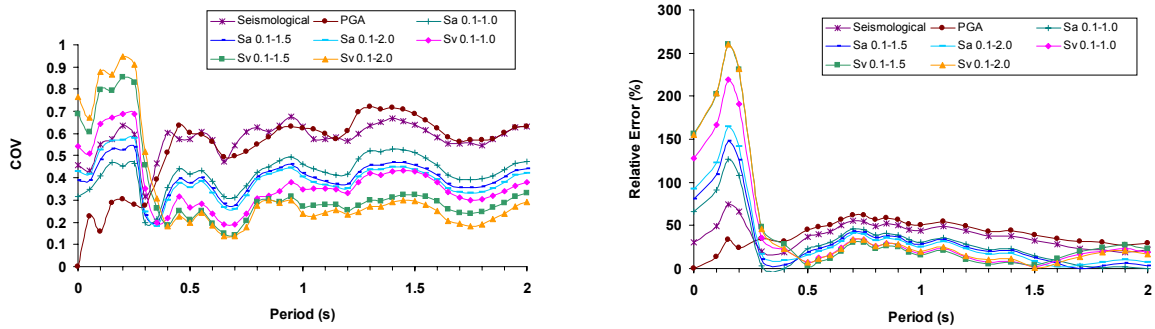

b. *Left* – scatter among the records (COV), *right* – relative error for the average.

Figure 8.21. Scaled records for bin BE*.

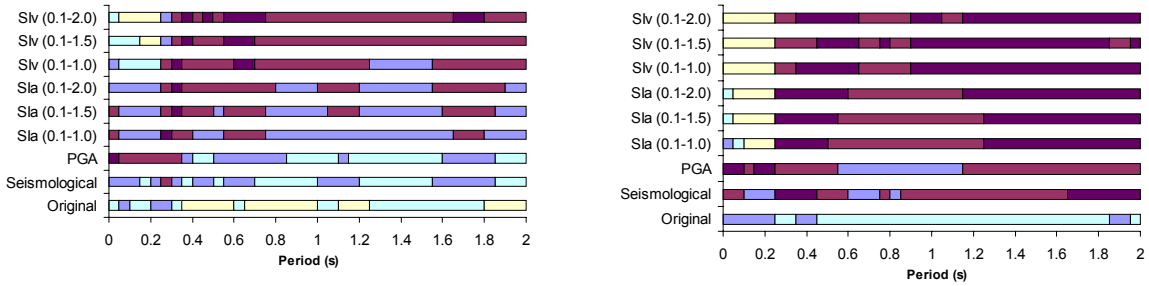

Figure 8.22. Performance of the scaling factors for bin BE*. *Left* – considering the scatter among the scaled records, *right* – considering the relative error with respect to the target spectrum.

8.2. Exploration of limits on scaling

In Chapter 4 it was shown that the form of the elastic response spectrum of absolute acceleration is relatively insensitive to distance from the source, but strongly dependent on the magnitude of the earthquake. On this basis it was inferred that provided the magnitude of the earthquake generating the selected real accelerograms is close to the magnitude of the target earthquake scenario – and provided that the recording sites are comparable with the site under consideration in the hazard assessment – it may be possible to scale records by factors significantly greater than the factor of 2 proposed by Vanmarcke (1979) without creating unrealistic acceleration time-histories. In this section, this issue is explored further by using suites of real recordings and in particular multiply-recorded earthquakes for which records at similar sites are obtained at various distances from the source. The procedure followed is as follows:

- For each multiply-recorded earthquake, suites of records are selected from stations that have the same site classification.
- To the extent that this is possible, records from each suite will then be selected that have similar path azimuths with respect to the source.
- For each suite of records, those from greater distances will be scaled – using one of the spectral intensity options – in order to obtain the best possible match with the individual spectra of records from close distances. The goodness of fit will need to be assessed by criteria similar, but not necessarily the same, as those used to evaluate scaling procedures in section 8.1.
- The Husid plots of the scaled and target records will then also be compared; if, within acceptable limits, both the spectra and the Husid plots "match", then it can be concluded that the scaled records from greater distances could be used for cases where the close-in records are not available.
- If the match of spectral shapes and Husid plots is acceptable, despite using scaling factors greater than 2, it may be concluded that the Vanmarcke limits should be revised.
- A further exercise that can be carried out is to scale the distant records to the average spectrum obtained from a group of spectra at relatively short distances, in order to remove some of the aleatory variation and obtain a smoother and more representative target for scaling and comparison. Conceivably, the "average" of the close-in Husid plots could be used as targets.

There are several factors that from the outset need to be kept in mind since they will clearly mitigate against obtaining very good matches in this exercise:

- If records from very close distances (< 10 km) are used as the target, these may contain near-source rupture effects (directivity, polarisation, etc.) that cannot be recreated by linearly scaling distant records.
- There is inherently a large spatial variability in earthquake ground motion (Boore, 2003), hence this aleatory variation will reduce the possibilities of obtaining very good matches between target and scaled spectra.
- The fact that the distant and close stations have the same classification, does not mean that they will be identical, and this further limits the possibilities of a good match. Even using the NEHRP classification scheme, $V_{s,30}$ values can vary by at least 200 m/s within a single class, and furthermore this gives no indication of the deeper geological structure, which can also exert a significant influence on the surface motions.

The earthquakes selected to perform this analyses are the horizontal components of the Whittier Narrows event of 1987 with a magnitude of 6.0, the Loma Prieta event of 1989 with a magnitude of 6.9 and the Northridge event of 1994 with a magnitude of 6.7. All the time-histories used for the analysis are recorded on rock. The records were grouped in bins BI (Whittier Narrows earthquake), BJ (Loma Prieta earthquake) and BK (Northridge earthquake). Table 8.15 presents the bins selected and their characteristics, with the corresponding bins of the McGuire *et al*. (2001) classification.

Table 8.15. Characteristics of the bins.

BIN	Magnitude, M	Distance, *d*	Target spectrum	Number of records	McGuire *et al*. (2001). classification
BI	6.0	[9 – 47]	M = 6.0, *d* = 9.0	8	M = 6 – 7, *d* = 10 – 50
BJ	6.9	[5 – 50]	M = 6.9, *d* = 5.1	8	M = 6 – 7, *d* = 10 – 50
BK	6.7	[8 – 35]	M = 6.7, *d* = 8.0	8	M = 6 – 7, *d* = 10 – 50

Tables 8.16 to 8.18 present in more detail the characteristics of each of the bins. The target spectrum for each bin corresponds to the larger horizontal component of motion at each response period for the records to the closest station to the fault.

Tables 8.19 to 8.21 present the scaling factors applied to each record for the scaling criteria related to the spectral intensity. As can be observed, none of the scaling factors present a good agreement with the target spectrum for all the periods. As stated before, the large spatial variability in earthquake ground motion reduces the possibilities of obtaining a very good match between target and scaled spectra. However, it is observed that for most of the cases, a good match between target and scaled spectra can be obtained for a range of period. The definition of the periods for which the best fit with

the target spectrum is required is determinant to the value of the scaling factor. Since this analysis is not focused on a specific period, the scaling given by the six spectral intensity options are presented and a good match for all the periods is never achieved.

Figures 8.23 to 8.28 present the Husid plots for the relative and absolute value of the records selected and the average scaled records for the scaling factors related to the spectral intensity, with their corresponding coefficient of variation and the relative error in the matching to the target spectrum. Not all the records presented in tables 8.15 to 8.17 were considered to obtain the average of the scaled records. Only those with Husid plots for the relative value of Arias intensity reasonably similar to those of the two components of the target spectrum were considered. They correspond to the shaded values on the tables. Tables 8.22 to 8.24 present the values of the strong motion parameters of Arias intensity and root-mean-square acceleration (time interval = $t_{95} - t_5$) of the ground-motion in order to appreciate better the differences between the records.

From the resultant scaled records, it is observed that it is possible to linear scale records for mismatched distances for scaling factors greater than the value of 2 proposed by Vanmarcke (1979), obtaining a good agreement with the target spectrum for the range of period of interest. This indicates that the limits proposed by Vanmarcke should be revised. The resultant ground motion is considered a realistic one when the Husid plots of the scaled records are consistent to those of the target spectrum.

Table 8.16. Characteristics of bins BI (Whittier Narrows earthquake)

Station	Magnitude, M	Distance, *d*	Number of records	McGuire *et al*. (2001). classification
San Gabriel – E Grand Ave#	6.0	9.0	2	M = 6 – 7, *d* = 0 - 10
LA-N Faring Rd#	6.0	28.5	2	M = 6 – 7, *d* = 10 - 50
LA-Chalon Rd#	6.0	32.6	2	M = 6 – 7, *d* = 10 - 50
Malibu-Las Flores Canyon #	6.0	46.3	2	M = 6 – 7, *d* = 10 - 50

Table 8.17. Characteristics of bins BJ (Loma Prieta earthquake)

Station	Magnitude, M	Distance, *d*	Number of records	McGuire *et al*. (2001). classification
Corralitos	6.9	5.1	2	M = 6 – 7, *d* = 0 - 10
Belmont-Envirotech	6.9	49.9	2	M = 6 – 7, *d* = 10 - 50
SAGO South – Surface	6.9	34.7	2	M = 6 – 7, *d* = 10 - 50
Woodside	6.9	39.9	2	M = 6 – 7, *d* = 10 - 50

Table 8.18. Characteristics of bins BK (Northridge earthquake)

Station	Magnitude, M	Distance, *d*	Number of records	McGuire *et al*. (2001). classification
Pacoima Dam (downstr) #	6.7	8.0	2	M = 6 – 7, *d* = 0 - 10
Burbank – Howard Rd.	6.7	20.0	2	M = 6 – 7, *d* = 10 - 50
LA-N Faring Rd	6.7	23.9	2	M = 6 – 7, *d* = 10 - 50
LA-Univ Hospital #	6.7	34.6	2	M = 6 – 7, *d* = 10 - 50

Table 8.19. Scaling factors for bin BI.

Scaling criteria	Whittier Narrows M = 6.0 *d* = 28.5 St. LA-N Faring Rd #		Whittier Narrows M = 6.0 *d* = 32.6 St. LA-Chalon Rd#		Whittier Narrows M = 6.0 *d* = 46.3 St. Malibu-Las Flores Canyon #	
$SI_{V2.0}$	10.71	12.55	24.20	14.29	15.60	18.10
$SI_{V1.5}$	10.45	12.76	24.55	13.68	16.02	17.34
$SI_{V1.0}$	11.63	12.48	23.81	13.23	17.83	15.47
$SI_{A2.0}$	9.24	11.20	21.54	12.35	12.58	12.59
$SI_{A1.5}$	8.90	10.94	21.01	11.82	12.25	11.95
$SI_{A1.0}$	9.04	10.64	20.33	11.48	12.21	11.07

Table 8.20. Scaling factors for bin BJ.

Scaling criteria	Loma Prieta M = 6.9 *d* = 49.9 St. Belmont-Envirotech		Loma Prieta M = 6.9 *d* = 34.7 St. SAGO South - Surface		Loma Prieta M = 6.9 *d* = 39.9 St. Woodside	
$SI_{V2.0}$	5.18	3.99	5.07	5.26	4.42	4.36
$SI_{V1.5}$	5.53	4.09	5.52	5.75	5.42	5.31
$SI_{V1.0}$	5.81	4.49	6.62	6.83	6.95	6.98
$SI_{A2.0}$	5.82	4.73	6.62	6.84	6.14	5.84
$SI_{A1.5}$	5.88	4.73	6.87	7.10	6.76	6.37
$SI_{A1.0}$	6.08	5.10	7.94	8.11	8.06	7.54

Table 8.21. Scaling factors for bin BK.

Scaling criteria	Northridge M = 6.7 *d* = 20.0 St. Burbank – Howard Rd.		Northridge M = 6.7 *d* = 23.9 St. LA – N Faring Rd		Northridge M = 6.7 *d* = 34.6 St. LA – Univ Hospital #	
$SI_{V2.0}$	3.55	3.61	1.79	1.21	1.37	2.81
$SI_{V1.5}$	3.64	3.83	1.78	1.26	1.33	3.06
$SI_{V1.0}$	3.41	3.46	1.51	1.34	1.17	2.90
$SI_{A2.0}$	3.70	3.33	1.85	1.44	1.23	2.74
$SI_{A1.5}$	3.64	3.27	1.80	1.45	1.18	2.73
$SI_{A1.0}$	3.56	3.09	1.69	1.53	1.11	2.63

Table 8.22. Strong-motion parameters for the Whittier Narrows records (bin BI).

Station	Longitudinal component		Transversal component	
	AI (m/s)	$a_{rms\ 5\text{-}95}$ (m/s^2)	AI (m/s)	$a_{rms\ 5\text{-}95}$ (m/s^2)
San Gabriel – E Grand Ave#	0.831	0.424	0.375	0.285
LA-N Faring Rd#	0.035	0.099	0.024	0.082
LA-Chalon Rd#	0.006	0.049	0.011	0.065
Malibu-Las Flores Canyon #	0.024	0.100	0.026	0.105

Table 8.23. Strong-motion parameters for the Loma Prieta records (bin BJ).

Station	Longitudinal component		Transversal component	
	AI (m/s)	$a_{rms\ 5\text{-}95}$ (m/s^2)	AI (m/s)	$a_{rms\ 5\text{-}95}$ (m/s^2)
Corralitos	3.237	0.725	2.530	0.641
Belmont-Envirotech	0.120	0.139	0.177	0.169
SAGO South - Surface	0.084	0.117	0.094	0.124
Woodside	0.107	0.132	0.127	0.143

Table 8.24. Strong-motion parameters for the Northridge records (bin BK).

Station	Longitudinal component		Transversal component	
	AI (m/s)	$a_{rms\ 5\text{-}95}$ (m/s^2)	AI (m/s)	$a_{rms\ 5\text{-}95}$ (m/s^2)
Pacoima Dam (downstr) #	0.935	0.550	0.731	0.487
Burbank – Howard Rd.	0.216	0.216	0.329	0.266
LA-N Faring Rd	0.667	0.379	0.844	0.427
LA-Univ Hospital #	1.371	0.471	0.538	0.295

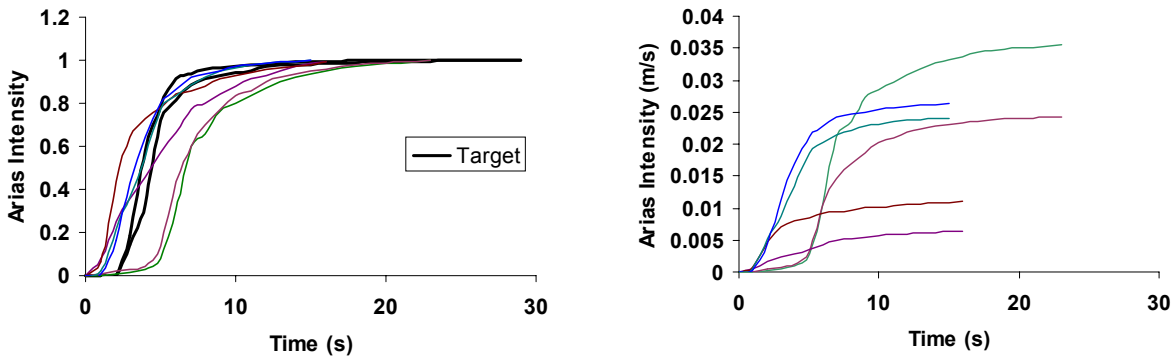

Figure 8.23. Husid plot for the records of bin BI (Whittier Narrows earthquake). *Left* – relative value of AI, *right* – absolute value of AI

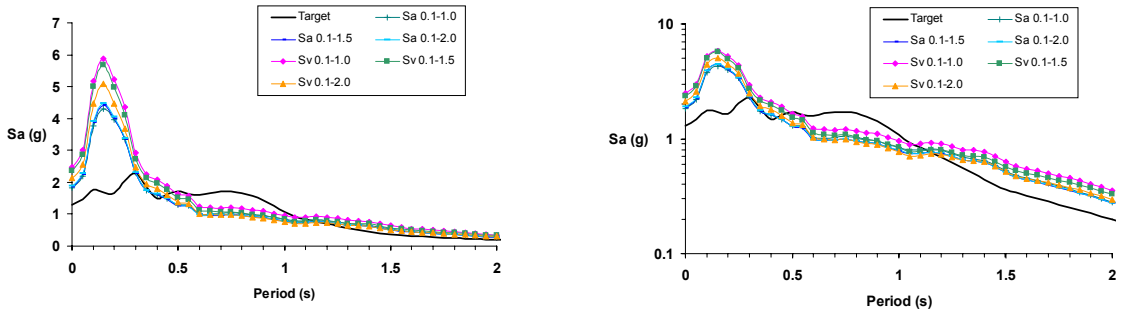

a. Average of the scaled records.

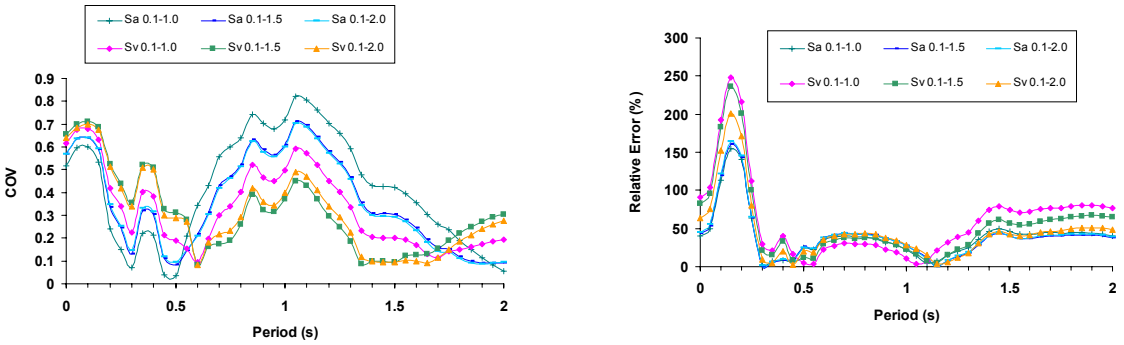

b. *Left* – scatter among the records (COV), *right* – relative error for the average.

Figure 8.24. Scaled records for bin BI (Whittier Narrows earthquake).

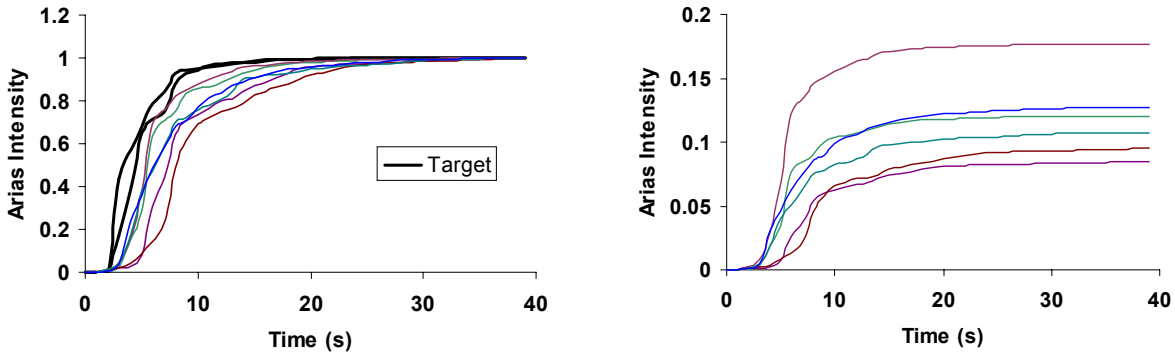

Figure 8.25. Husid plot for the records of bin BJ (Loma Prieta earthquake). *Left* – relative value of AI, *right* – absolute value of AI

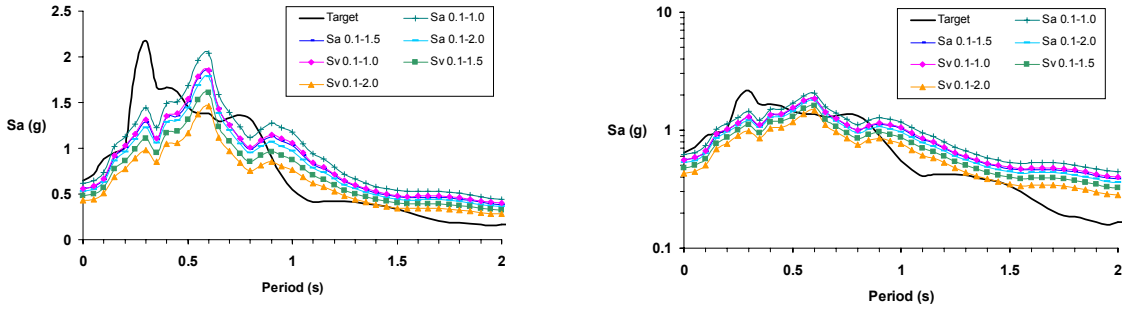

a. Average of the scaled records.

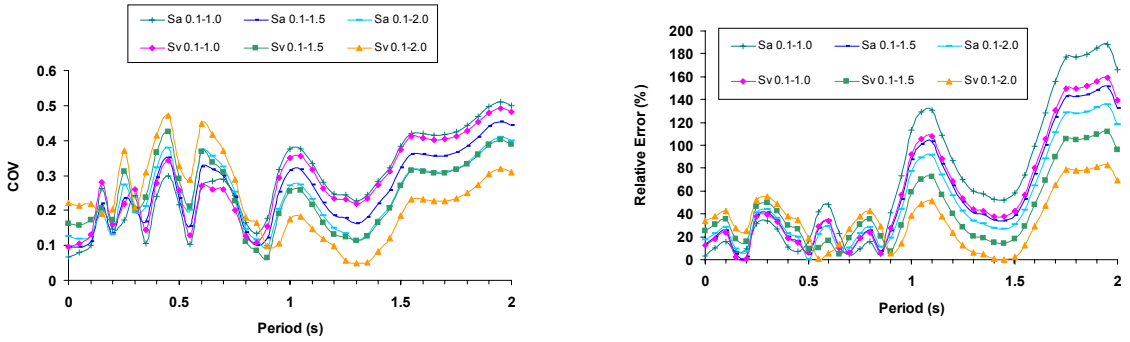

b. *Left* – scatter among the records (COV), *right* – relative error for the average.

Figure 8.26. Scaled records for bin BJ (Loma Prieta earthquake).

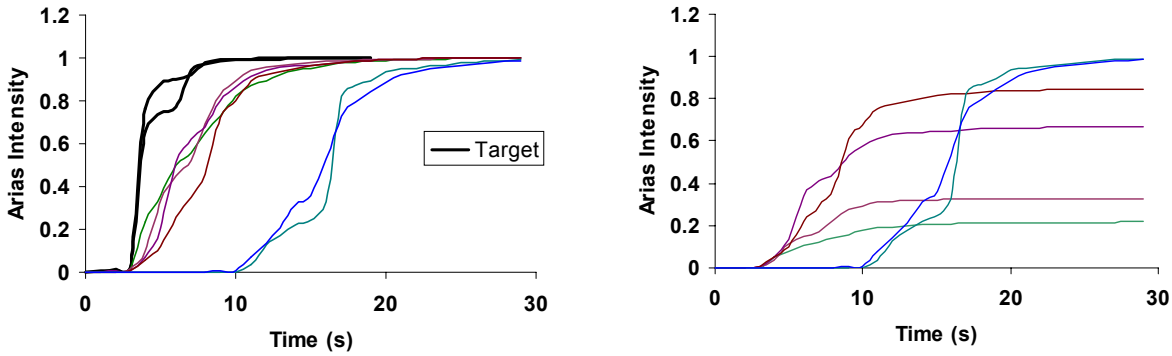

Figure 8.27. Husid plot for the records of bin BK (Northridge earthquake). *Left* – relative value of AI, *right* – absolute value of AI

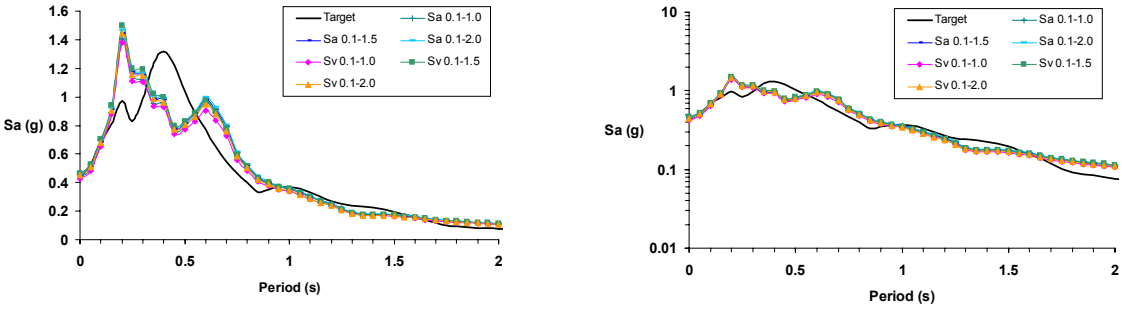

a. Average of the scaled records.

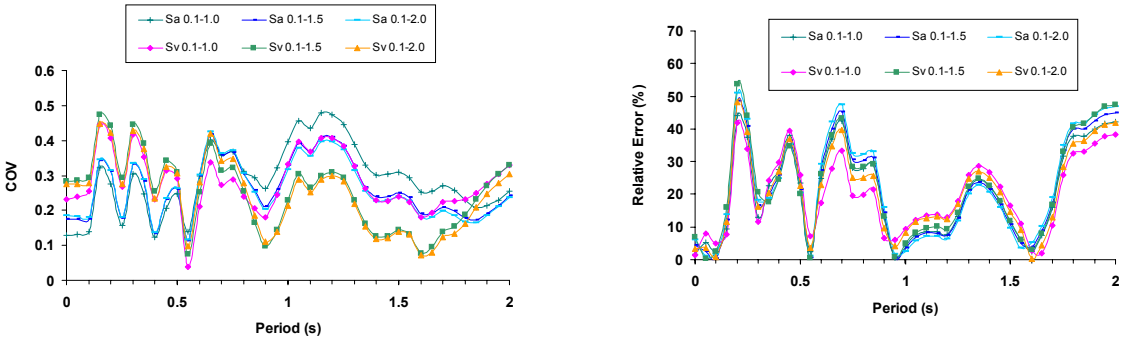

b. *Left* – scatter among the records (COV), *right* – relative error for the average.

Figure 8.28. Scaled records for bin BK (Northridge earthquake).

9. DISCUSSION and CONCLUSIONS

This dissertation has addressed the issue the defining acceleration time-histories for use in engineering analysis and design. Earthquake actions need to be defined in terms of time-histories of acceleration whenever dynamic analysis is required, which is generally for the assessment or checking of critical or complex structures.

There are three fundamental types of acceleration time-histories available to the engineer: artificial spectrum-compatible records, synthetic records obtained from seismological models, and real accelerograms recorded in earthquakes. There are various problems associated with the first group, generally related to the unrealistically high number of cycles of motion that such records require in order to match the target spectrum across the entire period range, particularly when they are applied to inelastic or non-linear analyses. Point and finite source seismological models offer a viable alternative and can yield acceleration records with characteristics that are consistent with those expected for the design earthquake scenario. The difficulty that these synthetic records present for the practising structural or geotechnical engineer is that their generation requires knowledge of earthquake source, path and site parameters, which can only be competently defined by a seismologist. The complexity of the input parameters, and the possible variations that these can have (with significant effects on the resulting motions), increases significantly in passing from point to finite source models, although the latter would generally be required for simulating ground motions from larger magnitude events.

Due to the shortcomings of artificial records and the problems presented by the generation of synthetic records, the dissertation has focussed on the most accessible solution for engineering applications, that of selecting, and when necessary scaling, real accelerograms. An issue that has not been addressed, but

which requires further investigation to produce more definitive guidelines, is the availability and distribution of real accelerograms. This would involve reviewing existing strong-motion databanks and the distribution of the records within these databanks with respect to the parameters used for their selection, primarily magnitude, distance and site classification. Another issue that warrants investigation, which would require a separate study, is whether records obtained from one region can be applied in another. This issue has not been addressed in this dissertation, but the implicit assumption is that ground motions from shallow crustal earthquakes in tectonically active areas are essentially similar, although it is acknowledged that shaking in extensional regimes may well be lower (Spudich *et al*., 1999).

The parameters used to characterise ground motions have been briefly described, with the main emphasis placed on the elastic response spectrum of acceleration, since this is the tool most frequently used in engineering analysis and is the fundamental representation of earthquake actions in all seismic design codes. Future development of this research will need to address matching of the selected ground motions to displacement response spectra as well, in recognition of the trend away from force-based seismic design towards displacement-based approaches for design and assessment (Priestley, 2003). The other ground-motion parameters that have been given particular attention are the duration of the shaking, notwithstanding the ambiguity in the definition of this parameter, and the Arias intensity, since these are essentially complementary to the elastic response spectrum but also related to the damage capacity of the motion. The factors influencing ground motions, organised into groups related to source, path and site, have also been briefly described, in order to then identify the effect of each of these on the ground-motion parameters. A key conclusion from this analysis is that the shape of the response spectrum is strongly influenced by both magnitude and site classification but is relatively insensitive to distance. The basic options for linear scaling of accelerograms are to uniformly adjust one or both of the time scale and the acceleration scale. Scaling the records in time causes a shift in the entire frequency content and furthermore changes the duration of the motion without changing the number of cycles of motion, all of which is likely to produce scaled records with characteristics that are not representative of real earthquake motions. For this reason, the option of scaling in time is discarded – and it use discouraged – whence it is assumed that the spectral shape will not be adjusted by linear scaling of the records. Therefore, one of the first conclusions of the work is that records need to be selected either to match the spectral shape or, preferably, to match the site classification and the magnitude of the design earthquake scenario.

This conclusion would need to be incorporated into further exploration of the availability of real records, by looking at records in different site classes and identifying the number of recordings available in different (narrow) magnitude bins. This also requires a response to the still unanswered question of how many real records are actually required to produce stable and reliable results in

structural analysis. The minimum of three inferred from current code guidelines may be too small. However, for the current work the focus has been on the issue of obtaining realistic accelerograms – by which it is meant that the selected and scaled records correspond to physically realisable earthquake motions in all their characteristics – for use as input to risk assessments. A specific issue that has been addressed in this context is the factor by which the records may be scaled, since the rule-of-thumb used widely in engineering practice is that the factor should not exceed 2. The origin of this figure is in the work of Vanmarcke (1979), which is now more than 20 years old and the basis for which is certainly worthy of re-evaluation. From the outset, the question has been re-phrased in this study: if the real records are selected from a narrow range of magnitudes around the target magnitude and from the same site category as that of interest for the engineering project, by what factor can the records be scaled to compensate for mismatch in distance? The work has demonstrated that as far as the shape of the elastic acceleration spectrum is concerned, the permissible factor may be significantly larger than 2. Further validation of this conclusion is provided by examination of records from multiply-recorded earthquakes, although a perfect reproduction of the spectral shape at close distances from scaling the records obtained at greater distances should not be expected due to the inherent spatial variability of ground motion and the considerable variation amongst sites grouped into the same classification (Boore, 2003b). However, matching of the spectral shape alone is insufficient, for which reason, the form of the scaled and recorded Arias intensities (Husid plots) have also been examined. The conclusion from this is that it is possible to obtained a good agreement with the spectral shape around the period of interest when records with similar Husid plots are considered, but not over the entire range of periods; the range of periods of interest thus controlling the value of the scaling factor. A further limitation that needs to be kept in mind, and explored further, is that records obtained near to the rupture of large earthquakes often display features such as high-energy pulses that are not encountered in records from greater distances, and these features cannot be introduced by linear scaling.

A major component of the work undertaken in this thesis has been to explore the effectiveness of different procedures for scaling real accelerograms to match a target response spectrum, defined in this case by a single earthquake scenario rather than a genuine uniform hazard spectrum (UHS) that would normally be obtained from a probabilistic seismic hazard assessment. There are obvious inherent difficulties in matching a scaled record to a UHS, which would complicate the analysis and perhaps distract from the more fundamental issues addressed in this work. The scaling procedures are essentially related to using different features of the record and target spectra to derive the factor to be applied to the amplitude of the acceleration. The options explored include using PGA and spectral intensities defined using both acceleration and velocity response ordinates integrated over different period ranges. In order to judge how well each scaling method works, it was first necessary to define criteria for measuring the match between the scaled and target spectra, although there is no consensus

as to what these should be, at least in current code guidelines. The two options used in this work are the covariance of the scaled spectra, as a measure of the dispersion amongst the records, and the relative error, which is a measure of the actual matching obtained by dividing the residual between scaled and target spectra by the target ordinate. The results show that none of the scaling factors present the best performance in terms of scatter among the records and best fit to the target spectrum over the entire range of periods. Nevertheless, for small periods ($T < \sim 0.2$), scaling to the PGA gives the best performance, whereas for the longest periods ($T > \sim 1.0$) scaling to a spectral intensity option related to the velocity gives the best performance. For intermediate periods the used of a spectral intensity option, related either to velocity or acceleration gives the best perform. Another criterion that could be considered is to limit the maximum individual deviations between scaled and target spectra. Another issue that may be considered, and indeed which is reflected in several codes, is to concentrate on matching the ordinates only over a limited range of periods that are of particular relevance to the structure to be analysed. There are potential problems with such an approach, one of these being that it provides no control over the ordinates elsewhere in the spectrum, which may affect higher mode responses. Another possible problem is that structures of different natural periods at a single site, for which the same risk level is required, could be subjected to completely different ground motions although the hazard is assumed to be the same. Some would argue that unless the objective of the study is to estimate total loss to the group of structures this is unimportant, but intuitively it would be expected that the same acceleration time-histories would be applicable to all of the structures. As mentioned above, the trend towards using displacement-based design may lead to the need to match displacement ordinates, and probably at longer periods, which should also be considered in the further development of this work.

The issue of by exactly how much records can be scaled in amplitude has been examined by looking at the change of spectral shape and Husid plots with distance, to determine whether or not it is possible to scale linearly to compensate for differences in distance between record and target scenario. The work has also looked at alternative procedures in which records are adjusted to match spectral ordinates rather than linearly scaled. The two techniques examined make these adjustments in the frequency- and time-domains respectively, easily being applied after linear scaling to “fine tune” the match to the target spectrum. These techniques, however, have been developed without consideration of whether or not the adjustments made to the records could have any geophysical basis, for which reason there is additional work to be done to investigate this issue. The changes in the spectral shapes, and more particularly in the Husid plot and the number of cycles, need to be subjected to examination of their physical consistency with real earthquake motions.

The next phase of the work will address two issues in particular that may be of particular significance for engineering analysis. The first is the inclusion of the vertical components of motion, which have

been neglected in this phase of the work. The second, which is of fundamental importance if definitive guidelines on input to dynamic analysis is to be provided, is to consider the match of the scaled records not only to the elastic spectral ordinates but also, and perhaps more importantly, to the inelastic response.

10. BIBLIOGRAPHY

1. Abrahamson, N. A. and W. J. Silva [1996] "Empirical ground motion models," Report to Brookhaven National Laboratoty.

2. Abrahamson, N. A. and W. J. Silva [1997] "Empirical response spectral attenuation relations for shallow crustal earthquakes," *Seismological Research Letters*. **68**, 94-127.

3. Abrahamson, N. A. and K. M. Shedlock [1997] "Overview," *Seismological Research Letters* **68**(1), 9-23.

4. Abrahamson, N. A. [2000] "State of the practice of seismic hazard evaluation," *Geotechnical Earthquake Engineering*, Melbourne, Australia, 19-24 November.

5. Abrahamson, N. A. [1993] "Non-Stationary Spectral Matching Program RSPMATCH".

6. Ambraseys, N. N. and J. J. Bommer [1990] "Uniform magnitude re-evaluation of European earthquakes associated with strong-motion records," *Earthquake Engineering and Structural Dynamics*. **19**, 1-20.

7. Ambraseys, N. N. and J. J. Bommer [1991] "The attenuation of ground accelerations in Europe," *Earthquake Engineering and Structural Dynamics*. **20**, 1179-1202.

8. Ambraseys, N. N. [1995] "The prediction of earthquake peak ground acceleration in Europe," *Earthquake Engineering and Structural Dynamics*. **24**(4), 467-490.

9. Ambraseys, N. N., K. A. Simpson and J. J. Bommer [1996] "The prediction of horizontal response spectra in Europe," *Earthquake Engineering and Structural Dynamics*. **25**, 371-400.

10. Anderson, J. G. and J. N. Brune [1999] "Probabilistic seismic hazard analysis without the ergodic assumption," *Seismological Research Letters* **79**(1), 19-28.

11. Arias, A. [1969] "A measure of earthquake intensity," In Hansen, R. J. (ed.), *Seismic Design of Nuclear Reactors*, MIT Press, 438-483.

12. Atkinson, G. M. and D. M. Boore [1997a] "Some comparisons between recent ground motion relations," *Seismological Research Letters* **68**, 24-40.

13. Atkinson, G. M. and D. M. Boore [1997b] "Stochastic point-source modeling of ground motions in the Cascadia region," *Seismological Research Letters* **68**, 74-85.

14. Atkinson, G. M. and D. M. Boore [2003] "Empirical relations for subduction zone earthquakes and their application to Cascadia and other regions," for submission to *Bull. Seis. Soc. Am*. October 04, 2002.

15. Bazzurro P. and C. A. Cornell [1999] "Disaggregation of seismic hazard," *Bulletin of Seismological Society of America* **89**, 501-520.

16. Bolt, B. A. [1978] "Fallacies in current ground motion prediction," Proceedings, Second International Conference on Microzonation, San Francisco, **vol.II**, 617-633.

17. Bommer, J. J. [1991] "The design and engineering application of an earthquake strong-motion database," *PhD Thesis*, Imperial College, University of London.

18. Bommer, J. J. [2001] *Basics of Seismology and Seismic Hazard Assessment*. Imperial College, London.

19. Bommer, J. J. and A. S. Elnashai [1999] "Displacement spectra for seismic design," *Journal of Earthquake Engineering* **3**(1), 1-32.

20. Bommer, J. J. and A. Martínez-Pereira [1999] "The effective duration of earthquake strong motion," *Journal of Earthquake Engineering*. **3**, 127-172.

21. Bommer, J. J. and C. Ruggeri [2002] "The specification of acceleration time-histories in seismic design codes," *European Earthquake Engineering*. **1**, 3-17.

22. Bommer, J. J. and S. G. Scott [2000] "The feasibility of using real accelerograms for seismic design," *In* Implications of Recent Earthquakes on Seismic Risk, *eds*. Elnashai and Antoninou, Imperial College Press, 115-126.

23. Bommer, J. J., S. G. Scott, and S. K. Sarma [1998] "Time-history representation of seismic hazard," 11th European Conference on Earthquake Engineering, Rotterdam, ISBN 90 5410 982 3.

24. Bommer, J. J., S. G. Scott, and S. K. Sarma [2000] "Hazard-consistent earthquake scenarios," *Soil Dynamics and Earthquake Engineering*. **19**, 219-231.

25. Boore, D. M. [2003a] "Simulation of ground motion using the stochastic method," *Pure and Applied Geophysics*. **160**, 635-676.

26. Boore, D. M. [2003b] "Can site response be predicted?," Third International ROSE School Seminar, Pavia, Italy, 23-24 June.

27. Boore, D. M., W. B. Joyner and T. E. Fumal [1993] "Estimation of response spectra and peak accelerations from western North American earthquakes: an interim report. *US Geological Survey Open-File Report* 93-509.

28. Boore, D. M., W. B. Joyner and T. E. Fumal [1997] "Equations for estimating horizontal response spectra and peak acceleration from western North American earthquakes: a summary of recent work. *Seismological Research Letters* **68**(1), 128-153.

29. Campbell, K. W. [1979] "Preliminary evaluation of near-source attenuation of peak acceleration in the United States. *Earthquake Notes*. **50**, 16-17.

30. Campbell, K. W. [1982] "Near-source scaling characteristics of peak horizontal acceleration for moderate-to-large earthquakes," in *The Dynamic Characteristics of Faulting Inferred from*

Recordings of Strong Ground Motion. **Vol. I**, Open-File Report 82-591, U.S. Geological Survey, Menlo Park, California, 120-184.

31. Campbell, K. W., [1983] "The effects of site characteristics on near-source recordings of strong ground motion," Proceedings of Conference XXII – A Workshop on Site Specific Effects of Soil and Rock on Ground Motion and their Implications for Earthquake Resistant Design, Santa Fe, New Mexico, 1983. *U.S. Geological Survey*, Open-File Report 83-845, 280-309.

32. Campbell, K. W. [1984] "Observed structural modification of recorded strong ground motion. Proceedings of Seminar and Workshop on Earthquake Ground Motion and Building Damage Potential, San Francisco, California, 1984. *Applied Technology Council Report ATC-10-1*, Palo Alto, California.

33. Campbell, K. W. [1997] "Empirical near-source attenuation relationships for horizontal and vertical components of peak ground acceleration, peal ground velocity, and pseudo-absolute acceleration response spectra," *Seismological Research Letters*. **68**, 154-179.

34. Darragh, R. B. and K. W. Campbell [1981] "Empirical assessment of the reduction in the free field ground motion due to the presence of structures (abstract)," *Earthquake Notes*. **52**, 8-19.

35. Fajfar, P., T. Vidic and M. Fischinger [1990] "A measure of earthquake motion capacity to damage medium-period structures," *Soil Dynamics and Earthquake Engineering*. **9**, 236-242.

36. Gasparini D. A. and E. H. Vanmarcke [1976] "Simulated earthquake motions compatible with prescribed response spectra," *Dept. of Civil Engineering, Research Report R76-4*, Massachussets Institute of Technology, Cambridge, Massachusetts.

37. Hidalgo, P. and R. W. Clough [1974] "Earthquake simulator study of a reinforced concrete frame," *Report UCB/EERC-74/13*, EERC, University of California, Berkeley, CA.

38. Housner, G. W and P. C. Jennings [1977] "The capacity of extreme earthquake motions to damage structures," *Structural and Geotechnical Mechanics*, W. J. Hall, ed., Prentice-Hall, Inc., Englewood Cliffs, N. J., 102-116.

39. Idriss, I. M [1993] "Procedures for selecting earthquake ground motions at rock sites," *Report to the U.S. Department of Commerce*. National Institute of Standards and Technology.

40. Kappos, A. J. [1990] "Sensitivity of calculated inelastic seismic response to input motion characteristics," *Proceedings of 4USNCEE*, **2**, 25-34.

41. Kappos, A. J. and P. Kyriakakis [2000] "A re-evaluation of scaling techniques for natural records," *Soil Dynamics and Earthquake Engineering*. **20**, 111-123.

42. Kamiyama M. [1984] "Effects of subsoil conditions and other factors on the duration of earthquake ground shakings," *Proc. Eight World Conference on Earthquake Engineering*, Vol. 2, San Francisco, pp. 793-800.

43. Kawashima K. and K. Aizawa [1989] "Bracketed and normalized durations of earthquake ground acceleration," *Earthquake Engineering and Structural Dynamics*. **18**, 1041-1051.

44. Kayen, R. E. and J. K. Mitchell [1997] "Assessment of liquefaction potential during earthquakes by Arias Intensity," *Journal of Geotech. and Geonv. Engineering*, ASCE, **123**(12), 1162-1174.

45. Kramer, S. L. [1996] *Geotechnical Earthquake Engineering*. Prentice Hall.

46. Liu, A. H., J. P. Stewart, N. A. Abrahamson and Y. Moriwaki [2001] "Equivalent number of uniform stress cycles for soil liquefaction analysis," *Journal of Geotech. and Geoenv. Engineering*. ASCE, **127**(12), 1017-1026.

47. McCann, W. M., Jr. and D. M. Boore [1983] "Variability in ground motions: root-mean-square acceleration and peak acceleration for the 1971 San Fernando, California earthquake," *Bulletin of the Seismological Society of America*. **73**, 615-632.

48. McGuire, R. K. [1995] "Probabilistic seismic hazard analysis and design earthquakes: closing the loop," *Bulletin of the Seismological Society of America*. **85**, 1275-1284.

49. McGuire, R. K. and T. P. Barnhard [1979] "The usefulness of ground motion duration in predicting the severity of seismic shaking," *Proc. Second US National Conference on Earthquake Engineering*, Stanford, pp. 713-722.

50. McGuire, R. K., W. J. Silva and C. J. Costantino [2001] "Technical basis for revision of regulatory guidance on design ground motions: hazard- and risk- consistent ground motion spectra guidelines," U.S Nuclear Regulatory Commission Office of Nuclear Regulatory Research, NUREG/CR-6728 Washington.

51. Martínez-Rueda, J. E. [1996] "Application of passive devices for the retrofitting of reinforced concrete structures," *CD ROM, Proceedings of 11WCEE*.

52. Martínez-Rueda, J. E. [1998] "Scaling procedure for natural accelerograms based on a system of spectrum intensity scales," *Earthquake Spectra*. **14**(1), 135-152.

53. Matsumura, K. [1992] "On the intensity measure of strong motions related to structural failures," *Proceedings of 10WCEE*, **1**, 375-380.

54. Mukherjee, S. and V. K. Gupta [2002] "Wavelet-based generation of spectrum-compatible time-histories," *Soil Dynamics and Earthquake Engineering*. **22**, 799-804.

55. Naeim, F. and J. C. Anderson [1993] "Classification and evaluation of earthquake records for design."

56. Nau, J. M. and W. J. Hall [1984] "Scaling methods for earthquake response spectra," *Journal of Structural Engineering*. **110**, 1533-1548.

57. Papazachos, B. C., Ch. A. Papaioannou, V. N. Margaris and N. P. Theodulidis [1992] "Seismic hazard assessment in Greece based on strong motion duration," *Proc. Tenth World Conference on Earthquake Engineering*, Vol. 2, Madrid, pp. 425-430.

58. Priestly, M. J. N. [2003] "Myths and fallacies in earthquake engineering, revisited," The Mallet Milne Lecture. *IUSS Press*, Istituto Universitario di Studi Superiori di Pavia.

59. Reiter, L. [1990] *Earthquake Hazard Analysis: issues and insights*. Columbia University Press.

60. Rodriguez-Marek, A., J. D. Bray and N. A. Abrahamson [2001] "An empirical geotechnical seismic site response procedures," *Earthquake Spectra*. **17**(1), 65-87.

61. Seed, H. B. and I. M. Idriss [1969] "Rock motion accelerograms for high magnitude earthquakes," *EERC Report* 69-7, Earthquake Engineering Research Center, University of California, Berkeley.

62. Seed, H. B., R. V. Whitman, H. Dezfulian, R. Dorby and I. M. Idriss [1972] "Soil conditions and building damage in the 1967 Caracas earthquake," *Journal of the Soil Mechanics and Foundation Division*, ASCE, **98** (SM8), 787-806.

63. Shearer, P. M. [1999]. *Introduction to Seismology*. Cambridge University Press.

64. Shome, N., Cornell, C. A., Bazzurro, P. and Carballo, J. E. [1998] "Earthquakes, records, and nonlinear responses," *Earthquake Sepectra*. **14**(3), 469-500.

65. Silva, W. J and K. Lee. [1987] "WES RASCAL code for synthesizing earthquake ground motions". *State-of-the-Art for Assessing Earthquake Hazard in the United States. Report* 24. US Army Corps of Engineers.

66. Silva, W. J., and R. B. Darragh [1995] "Engineering characterization of earthquake strong ground motion recorded at rock sites," *Report TR-102261*, Electric Power Research Institute, Palo Alto, CA.

67. Somerville, P. G., R. W. Graves and C. K. Saikia [1995] "Characterization of ground motions during the Northridge earthquake of January 17, 1994*," Program to reduce the Earthquake Hazards of Steel Moment Frame Buildings*, SAC Reèprt 95-03.

68. Somerville, P. G., C. K. Saikia, D. Wald and R. W. Graves [1996] "Implications of the Northridge earthquake for strong ground motions from thrust faults*," Bull. Seism. Soc. Am*., 86, S115-S125.

69. Somerville, P. G., N. F. Smith, R. W. Graves and N. A. Abrahamson [1997] "Modification of empirical strong ground motion attenuation relations to include the amplitude and duration effects of rupture directivity," *Seismological Research Letters* **68**, 199-222.

70. Spudich, P., W. B. Joyner, A. G. Lindh, D. M. Boore, B. M. Margaris and J. B. Fletcher [1999] "SEA99 - A Revised Ground Motion Prediction Relation for Use in Extensional Tectonic Regimes," *Bulletin of the Seismological Society of America*, v. 89, pp. 1156 - 1170.

71. Stewart, J. P., S-J. Chiou, J. D. Bray, R. W. Graves, P. G. Somerville and Abrahamson N. A. [2001] *Ground Motion Evaluation Procedures for Performance-Based Design*. Pacific Earthquake Engineering Research Center. September.

72. Toro, G. R., N. A. Abrahamson and J. F. Schneider [1997] "Model of strong ground motions from earthquakes in central and eastern North America: best estimates and uncertainties," *Seismological Research Letters* **68**, 41-57.

73. Travasarou, T., J. D. Bray, N. A. Abrahamson [2002] "Empirical attenuation relationship for Arias intensity," Accepted for publication in *Earthquake Engineering and Structural Dynamics.*

74. Trifunac, M. D. and A. G. Brady [1975] "A study on the duration of strong earthquake ground motion," *Bull. Seis. Soc. Am*. **65**, 581-626.

75. Tsangaris, M. [1996] "Application of EC8 elastic design spectra," *M.Sc. Dissertation*, Imperial College, London.

76. Vanmarcke, E. H. [1979]. "State-of-the-art for assessing earthquake hazards in the United States: Representation of earthquake ground motions – scaled accelerograms and equivalent response spectra*. Miscellaneous Paper S-73-1, Report 14*, US Army Corps of Engineers Waterways Experiment Station, Vicksburg, Mississippi.

77. Wilson, R. C. [1993] "Relation of Arias intensity to magnitude and distance in California," Open File Report, 93-0556. *U.S. Geological Survey*, Menlo Park, CA, 42 p.

78. Youngs, R. R., S. –J. Chiou, W. J. Silva and J. R. Humphrey [1997] "Strong ground motion attenuation relationships for subductuion zone earthquakes," *Seismological Research Letters* **68**, 58-73.

ATTENUATION EQUATIONS FOR RESPONSE SPECTRAL ORDINATES.

Ambraseys *et al*. (1996)

$$\log Y = C_1' + C_2 M_S + C_4 \log r + C_A S_A + C_S S_S \tag{A.1.1}$$

where

$$r = \sqrt{r_{jb}^2 + h_0^2} \tag{A.1.2}$$

Site parameters:

Four site conditions are defined but only three are retained (because there are only three records from very soft soil which are combined with soft soil category).

Rock soils: $V_s > 750$ m/s, $S_A = 0$, $S_S = 0$.
Stiff soil: $360 < V_s \leq 750$ m/s, $S_A = 1$, $S_S = 0$.
Soft soil: $180 < V_s \leq 360$ m/s, $S_A = 0$, $S_S = 1$.
Very soft soil: $V_s \leq 180$ m/s, $S_A = 0$, $S_S = 1$.

Standard deviation:

$$\sigma = 0.25 \tag{A.1.3}$$

Campbell (1997)

$$\begin{aligned} \ln SA_H = {} & \ln A_H + c_1 + c_2 \tanh\left[c_3 (M_W - 4.7)\right] + (c_4 + c_5 M_W) R_{SEIS} \\ & + 0.5 c_6 S_{SR} + c_6 S_{HR} + c_7 \tanh(c_8 D)(1 - S_{HR}) + f_{SA}(D) \end{aligned} \tag{A.1.4}$$

where

$$\begin{aligned} \ln A_H = {} & -3.512 + 0.904 M_W - 1.328 \ln \sqrt{R_{SEIS}^2 + \left[0.149 \exp(0.647 M_W)\right]^2} \\ & + \left[1.125 - 0.112 \ln R_{SEIS} - 0.0957 M_W\right] F \\ & + \left[0.440 - 0.171 \ln R_{SEIS}\right] S_{SR} + \left[0.405 - 0.222 \ln R_{SEIS}\right] S_{HR} \end{aligned} \tag{A.1.5}$$

$$f_{SA}(D) = \begin{cases} 0 & D \geq 1km \\ c_6(1-S_{HR})(1-D) + 0.5c_6(1-D)S_{SR} & D < 1km \end{cases} \quad \text{(A.1.6)}$$

Site parameters:

Three sites categories are used: hard rock, alluvium or firm soil and soft soil.

Hard rock: primary Cretaceous and older sedimentary deposits, metamorphic rock, crystalline rock and hard volcanic deposits (e.g. basalt).
Alluvium or firm soil: firm or stiff Quaternary deposits with depths greater than 10m.
Soft soil: primarily Tertiary sedimentary deposits and soft volcanic deposits (e.g. ash deposits).

Hard rock: $S_{SR} = 0$, $S_{HR} = 1$
Alluvium or firm soil: $S_{SR} = 0$, $S_{HR} = 0$
Soft soil: $S_{SR} = 1$, $S_{HR} = 0$
Fault mechanism:

Strike-slip: F=0
Otherwise: F=1

Standard deviation:

$$\sigma = \begin{cases} 0.55 & A_H < 0.068g \\ 1.73 - 0.140 \ln A_H & 0.068g \leq A_H \leq 0.21g \\ 0.39 & A_H > 0.21g \end{cases} \quad \text{(A.1.7)}$$

Abrahamson and Silva (1997)

$$\ln Sa(g) = f_1(M_W, r_{rup}) + Ff_3(M_W) + HWf_4(M_W, r_{rup}) + Sf_5(\overline{pga}_{rock}) \quad \text{(A.1.8)}$$

where

$$f_1(M_W, r_{rup}) = \begin{cases} a_1 + a_2(M_W - c_1) + a_{12}(8.5 - M_W)^n \\ \quad + \left[a_3 + a_{13}(M_W - c_1)\right]\ln R & M_w \le c_1 \\ a_1 + a_4(M_W - c_1) + a_{12}(8.5 - M_W)^n \\ \quad + \left[a_3 + a_{13}(M_W - c_1)\right]\ln R & M_w > c_1 \end{cases} \quad \text{(A.1.9)}$$

$$f_4(M_W, r_{rup}) = f_{HW}(M_W) f_{HW}(r_{rup}) \quad \text{(A.1.10)}$$

$$R = \sqrt{r_{rup}^2 + c_4^2} \quad \text{(A.1.11)}$$

$$f_3(M_W) = \begin{cases} a_5 & M_w \le 5.8 \\ a_5 + \dfrac{(a_6 - a_5)}{c_1 - 5.8} & 5.8 < M_w < c_1 \\ a_6 & M_w \ge c_1 \end{cases} \quad \text{(A.1.12)}$$

$$f_{HW}(M_W) = \begin{cases} 0 & M_w \le 5.5 \\ M_w - 5.5 & 5.5 < M_w < 6.5 \\ 1 & M_w \ge 6.5 \end{cases} \quad \text{(A.1.13)}$$

$$f_{HW}(r_{rup}) = \begin{cases} 0 & r_{rup} < 4 \\ a_9 \dfrac{r_{rup} - 4}{4} & 4 < r_{rup} < 8 \\ a_9 & 8 < M_w < 18 \\ a_9\left(1 - \dfrac{r_{rup} - 18}{7}\right) & 18 < r_{rup} < 24 \\ 0 & r_{rup} > 25 \end{cases} \quad \text{(A.1.14)}$$

$$f_5(\overline{PGA}_{rock}) = a_{10} + a_{11}\ln(\overline{PGA}_{rock} + c_5) \quad \text{(A.1.15)}$$

where $\overline{PGA}$ is expected acceleration on rock as predicted by the attenuation equation with S = 0

Site parameters:

Two categories are use: rock and deep soil.

Rock: rock (Vs > 600 m/s), very thin soil (< 5m) over rock or soil 5 to 20m thick over rock.
Deep soil: deep soil in narrow canyon (soil > 20m thick and canyon < 2 km wide) or deep soil in broad canyon (soil > 20m thick and canyon > 2 km wide).

Rock: S = 0
Deep soil: S = 1

Fault mechanism:

Reverse: F= 1
Reverse/oblique: F = 0.5
Strike-slip and normal: F = 0

Hanging wall:

Over hanging wall: HW = 1
Otherwise: HW = 0

Total standard error:

$$\sigma_{total}(M_w) = \begin{cases} b_5 & M_w \le 5.5 \\ b_5 - b_6 (M_w - 5) & 5.5 < M_w < 7.0 \\ b_5 - 2b_6 & M_w \ge 7 \end{cases} \quad \text{(A.1.16)}$$

Boore *et al.* (1997)

$$\ln Y = b_1 + b_2 (M_W - 6) + b_3 (M_W - 6)^2 + b_5 \ln r + b_v \ln \frac{V_S}{V_A} \quad \text{(A.1.17)}$$

where

$$r = \sqrt{r_{jb}^2 + h^2} \quad \text{(A.1.18)}$$

Site parameters:

V_S = average shear-wave velocity to 30 m

Fault mechanism:

Strike-slip: $b_1 = b_{1SS}$
Reverse-slip: $b_1 = b_{1RS}$
Not specified: $b_1 = b_{1ALL}$

Standard deviation:

$\sigma_{\ln Y}$ varies with period and it is given by the regression.

Spudich *et al.* (1999)

$$\log_{10} Y = 0.299 + 0.229(M_W - 6) - 1.052 \log_{10} R + 0.112\Gamma \qquad \text{(A.1.19)}$$

where

$$R = \sqrt{r_{jb}^2 + h^2} \qquad \text{(A.1.20)}$$

Site parameters:

Two site categories are used: rock and soil.

Rock: includes hard rock (plutonic igneous rocks, lava flows, welded tuffs and metamorphic rocks unless severely weathered when they are soft rock), soft rock (all sedimentary rocks unless there was some special characteristic noted in description, such as crystalline limestone or massive cliff-forming sandstone when they are hard rock) and unknown rock.

Soil (alluvium, sand, gravel, clay, silt, mud, fill or glacial outwash of more than 5m deep): included shallow soil (5 to 20m deep), deep soil (> 20m deep) and unknown soil.

Rock: $\Gamma = 0$

Soil: $\Gamma = 1$

Standard deviation:

$$\sigma = \sqrt{\sigma_1^2 + \sigma_2^2 + \sigma_3^2} \tag{A.1.21}$$

where $\sigma_1 = 0.172$ and $\sigma_2 = 0.108$. $\sigma_3 = 0.094$ for randomly oriented horizontal component and $\sigma_3 = 0$ for larger horizontal component.

Toro *et al.* (1997)

$$\begin{aligned} \ln Y = {} & C_1 + C_2(M_W - 6) + C_3(M_W - 6)^2 - C_4 \ln R_M \\ & -(C_5 - C_4)\max\left[\ln\left(\frac{R_M}{100}, 0\right)\right] - C_6 R_M \end{aligned} \tag{A.1.22}$$

where

$$R_M = \sqrt{R_{jb}^2 + C_7^2} \tag{A.1.23}$$

Standard deviation:

$$\sigma_{a,\text{modelling}} = \begin{cases} 0.32 & f > 9 \text{ Hz} \\ 0.63 - 0.14 \ln(f) & 2 < f \leq 9 \text{ Hz} \\ 0.53 & f \leq 2 \text{ Hz} \end{cases} \tag{A.1.24}$$

$$\sigma_{e,\text{modelling}} = 0.27 \tag{A.1.25}$$

Youngs *et al.* (1997)

For rock:

$$\begin{aligned} \ln Y = {} & 0.2418 + 1.414 M_W + C_1 + C_2 (10 - M_W)^3 \\ & + C_3 \ln(r_{rup} + 1.7818 e^{0.554 M_W}) + 0.00607 H + 0.3846 Z_T \end{aligned} \tag{A.1.26}$$

For soil:

$$\ln Y = -0.6687 + 1.438M_W + C_1 + C_2(10 - M_W)^3 + C_3 \ln(r_{rup} + 1.097e^{0.617M_W}) + 0.00648H + 0.3643Z_T \quad \text{(A.1.27)}$$

Site parameters:

Three site categories are used to do the regression but only the result for rock and deep soil are reported.

Rock: consists of at most about a metre of soil over weathered rock.
Deep soil: depth to bedrock is greater than 20m.
Shallow soil: depth to bedrock is less than 20m and a significant velocity contrast may exist within 30m of surface.

Rock: $Z_r = 1$, $Z_{ds} = 0$, $Z_{ss} = 0$
Deep soil: $Z_r = 0$, $Z_{ds} = 1$, $Z_{ss} = 0$
Shallow soil: $Z_r = 0$, $Z_{ds} = 0$, $Z_{ss} = 1$

Tectonic type:

Interface (assumed to be thrust): $Z_t = 0$
Intraslab (assumed to be normal): $Z_t = 1$

Standard deviation:

$$\sigma = C_4 + C_5 M_w \quad \text{(A.1.28)}$$

ATTENUATION EQUATIONS FOR PGA INCLUDING EXPLICIT TREATMENT OF FOCAL DEPTH.

Ambraseys and Bommer (1991) for horizontal component

$$\log(a_h) = -0.87 + 0.217 M_s - 0.00117 r - \log r \qquad \text{(A.1.21)}$$

where

$$r = \sqrt{r_{jb}^2 + h^2} \qquad \text{(A.1.22)}$$

Standard deviation:

$$\sigma = 0.26 \qquad \text{(A.1.23)}$$

Ambraseys (1995) for horizontal component

$$\log(a_h) = -1.06 + 0.245 M_s - 0.00045 r - 1.016 \log r \qquad \text{(A.1.24)}$$

where

$$r = \sqrt{r_{jb}^2 + h^2} \qquad \text{(A.1.25)}$$

Standard deviation:

$$\sigma = 0.25 \qquad \text{(A.1.26)}$$

ATTENUATION EQUATIONS FOR ARIAS INTENSITY.

Kayen and Mitchell (1997)

For rock sites:

$$\log I_h = M_W - 4.0 - 2\log r^* \tag{A.3.1}$$

For alluvium sites:

$$\log I_h = M_W - 3.8 - 2\log r^* \tag{A.3.2}$$

For soft soil sites:

$$\log I_h = M_W - 3.4 - 2\log r^* \tag{A.3.3}$$

where

$$r^* = \sqrt{r_{jb}^2 + \Delta^2} \tag{A.3.4}$$

Δ = earthquake focal depth.

Site parameters:

Three site categories are used: rock, alluvium and soft sites.

Standard deviation:

For rocks sites

$$\sigma = 0.63 \tag{A.3.5}$$

For alluvium sites

$$\sigma = 0.61 \tag{A.3.6}$$

The number of samples was insufficient to determine σ for soft soil sites.

Travasarou (2002)

$$\begin{aligned} \ln I_a &= c_1 + c_2(M_W - 6) + c_3 \ln(M_W / 6) + c_4 \ln\sqrt{r_{jb}^2 + h^2} \\ &+ (s_{11} + s_{12}(M_W - 6))S_C + (s_{21} + s_{22}(M_W - 6))S_D \\ &+ f_1 F_N + f_2 F_R \end{aligned} \tag{A.3.7}$$

Site parameters:

The local site conditions were categorised using the classification scheme proposed in Rodríguez-Marek *et al*. (2001) but only three retained: B, C and D (see section 3.3.1).

Site category B: $S_C = 0$, $S_D = 0$
Site category C: $S_C = 1$, $S_D = 0$
Site category D: $S_C = 0$, $S_D = 1$

Fault mechanism:

Strike-slip: $F_N = 0$, $F_R = 0$
Normal: $F_N = 1$, $F_R = 0$
Reverse or reverse-oblique faults: $F_N = 0$, $F_R = 1$

Standard error:

$$\sigma_{tot}(M_W, I_a, site) = \sqrt{\sigma(I_a, site)^2 + \tau(M_W)^2} \tag{A.3.8}$$

where

$$\tau(M_W) = \quad 0.611 - 0.0466\,(M_w - 4.7) \qquad 4.7 \le M_w \le 7.6 \tag{A.3.9}$$

$$\sigma(I_a, site) = \begin{cases} \sigma_1 & I_a \le 0.0132 \text{ m/s} \\ \sigma_1 - 0.1064(\ln I_a - \ln 0.0132) & 0.0132 < I_a < 0.1245 \text{ m/s} \\ \sigma_2 & I_a \ge 0.1245 \text{ m/s} \end{cases} \quad \text{(A.3.10)}$$

Wilson (1993)

$$\log I_a = M_W - 2\log\sqrt{r_{jb}^2 + h^2} - 4.1 \quad \text{(A.3.11)}$$

ATTENUATION EQUATIONS FOR DURATION AND EQUIVALENT NUMBER OF UNIFORM STRESS CYCLES (N).

McGuire and Barnhard (1979)[1] for the horizontal component

$$\ln D = c_1 + c_2 M + c_3 S + c_5 \ln R \qquad \text{(A.4.1)}$$

where R is the closest distance to the rupture surface.

Site parameters:

Two site categories are used: rock and alluvium sites.

Rock: S = 1
Alluvium: S = 0

Standard deviation:

$$\sigma = c_5 \ln R \qquad \text{(A.4.2)}$$

Papazachos *et al.* (1992)

$$\ln D_B = 1.84 + 0.81 M_s - 1.04 \ln(R + 15) - 0.19 S - 27.7 L \qquad \text{(A.4.3)}$$

where R is the epicentral distance and L is the threshold level of acceleration ($L \geq 0.02g$)

Site parameters:

Two site categories are used: rock and soil sites.

Rock: S = 1
Soil: S = 0

[1] It is assumed that the equation is in terms of *D* rather than ln(*D*) as presented in the original paper for bracketed duration, D_B.

Standard deviation:

$$\sigma = 0.76 \tag{A.4.4}$$

Kawasima and Aizawa (1989)

$$Braketed\ duration\ \ t_{50} = a \times 10^{bM} \times (\Delta + 30)^{c} \tag{A.4.5}$$

where Δ is the epicentral distance.

Standard deviation:

$$\sigma = 0.71 \tag{A.4.6}$$

Trifunac and Brady (1975) for horizontal acceleration

$$D_s = -4.88S + 2.33M + 0.149\Delta \tag{A.4.7}$$

where Δ is the epicentral distance.

Site parameters:

Three site categories are used: soft, intermediate and hard sites.

Soft: all accelerograph stations recorded on alluvium or otherwise “soft” sedimentary deposits.
Hard: sites located on “hard” basement rocks.
Intermediate: sites located on “intermediate” type rocks or in a complex environment which could not be identify as either soft or hard.

Soft: S = 0
Intermediate: S = 1
Hard: S = 2

Standard deviation:

$$\sigma = 10.67 \tag{A.4.8}$$

Kamiyama (1984) for rock sites

$$Significant\ duration\ \ t_p = 0.444 \times 10^{0.21 M_{JMA}} \times 10^{-0.0019 H} \times \Delta^{0.048} \tag{A.4.9}$$

where Δ is the epicentral distance and H is the focal depth.

Abrahamson and Silva (1996) for significant duration and Liu et *al*. (2001) for equivalent number of uniform stress cycles (N)

Significant duration

$$\ln(SD) = \ln\left[\frac{\left(\frac{\exp(b_1 + b_2(M_W - m^*))}{10^{1.5M_W + 16.05}}\right)^{-\frac{1}{3}}}{4.9 \cdot 10^6 \beta} + Sc_1 + c_2(r_{rup} - r_c)\right] + D_{rat},\ r_{rup} \geq r_c$$

$$\ln(SD) = \ln\left[\frac{\left(\frac{\exp(b_1 + b_2(M_W - m^*))}{10^{1.5M_W + 16.05}}\right)^{-\frac{1}{3}}}{4.9 \cdot 10^6 \beta} + Sc_1\right] + D_{rat},\ r_{rup} < r_c \tag{A.4.10}$$

Equivalent number of uniform stress cycles (N)

$$\ln(N) = \ln\left[\frac{\left(\frac{\exp(b_1 + b_2(M_W - m^*))}{10^{1.5M_W + 16.05}}\right)^{-\frac{1}{3}}}{4.9 \cdot 10^6 \beta} + Sc_1 + r_{rup} c_2\right] \tag{A.4.11}$$

where β, b_1, b_2, m^*, c_1, c_2, D_{rat} and r_c are regression coefficients.

Site parameters:

Two categories are use: rock/shallow stiff soil sites and deep soil sites.

Rock/shallow stiff soil: rock (Vs > 600 m/s), very thin soil (< 5m) over rock or soil 5 to 20m thick over rock.
Deep soil: deep soil in narrow canyon (soil > 20m thick and canyon < 2 km wide) or deep soil in broad canyon (soil > 20m thick and canyon > 2 km wide).

Rock: S = 0
Soil: S = 1

Standard deviation:

σ is a constant given by the regression.

McGuire *et al* (2001) STRONG-MOTION DATABASE

TABLE B-1: WUS, ROCK, M = 5-6, D = 0-50 km

Earthquake	YR	MODY	HRMN	Mag	Station	Closest Dist (km)	PGA (g)	PGV (g)	PGD (cm/s)	Dur (s)
Lytle Creek	1970	0912	1430	5.4	Devil's Canyon	21.9	.084	1.8	0.10	1.1
Lytle Creek	1970	0912	1430	5.4	Devil's Canyon	21.9	.146	3.3	.18	1.1
Lytle Creek	1970	0912	1430	5.4	Devil's Canyon	21.9	.151	5.6	.23	1.2
Lytle Creek	1970	0912	1430	5.4	Wrightwood-6074 Park Dr	15.4	.078	2.3	.25	2.0
Lytle Creek	1970	0912	1430	5.4	Wrightwood-6074 Park Dr	15.4	.162	10.1	1.02	1.8
Lytle Creek	1970	0912	1430	5.4	Wrightwood-6074 Park Dr	15.4	.200	10.5	.62	1.7
Fruili, Italy	1976	0911	1631	5.5	San Rocco	17.9	.013	1.8	.34	5.7
Fruili, Italy	1976	0911	1631	5.5	San Rocco	17.9	.029	2.3	.48	3.7
Fruili, Italy	1976	0911	1631	5.5	San Rocco	17.9	.072	4.3	.90	.8
Santa Barbara	1978	0813		6.0	Cachuma Dam Toe	36.6	.024	1.6	.40	5.5
Santa Barbara	1978	0813		6.0	Cachuma Dam Toe	36.6	.072	6.3	1.26	1.4
Santa Barbara	1978	0813		6.0	Cachuma Dam Toe	36.6	.034	2.6	.55	3.4
Livermore	1980	0127	0233	5.4	APEEL 3E Hayward CSUH	31.0	.014	.9	.09	5.2
Livermore	1980	0127	0233	5.4	APEEL 3E Hayward CSUH	31.0	.053	4.5	.58	1.2
Livermore	1980	0127	0233	5.4	APEEL 3E Hayward CSUH	31.0	.028	1.4	.30	3.9
Livermore	1980	0127	0233	5.4	San Ramon-Eastman Kodak	17.6	.037	4.0	.50	7.0
Livermore	1980	0127	0233	5.4	San Ramon-Eastman Kodak	17.6	.301	19.1	2.82	.7
Livermore	1980	0127	0233	5.4	San Ramon-Eastman Kodak	17.6	.097	5.6	.62	5.8
Mammoth Lakes	1980	0611	0441	5.0	USC Convict Lakes	9.1	.038	.4	.02	1.2
Mammoth Lakes	1980	0611	0441	5.0	USC Convict Lakes	9.1	.030	.6	.02	1.7
Mammoth Lakes	1980	0611	0441	5.0	USC Convict Lakes	9.1	.046	.6	.02	.8
Coalinga	1983	0709	0740	5.2	Anticline Ridge Free-Field	11.0	.115	3.7	.43	2.1
Coalinga	1983	0709	0740	5.2	Anticline Ridge Free-Field	11.0	.330	16.1	1.20	2.0
Coalinga	1983	0709	0740	5.2	Anticline Ridge Free-Field	11.0	.275	8.9	.46	1.8
Coalinga	1983	0709	0740	5.2	Anticline Ridge Pad	11.0	.137	4.7	.34	2.1
Coalinga	1983	0709	0740	5.2	Anticline Ridge Pad	11.0	.378	16.1	1.03	1.9
Coalinga	1983	0709	0740	5.2	Anticline Ridge Pad	11.0	.261	9.2	.53	1.8
Coalinga	1983	0709	0740	5.2	Oil City	10.0	.210	4.6	.29	2.7
Coalinga	1983	0709	0740	5.2	Oil City	10.0	.387	13.8	1.59	1.7
Coalinga	1983	0709	0740	5.2	Oil City	10.0	.370	12.4	.89	2.0
Coalinga	1983	0709	0740	5.2	Transmitter Hill	10.4	.114	3.3	.35	3.0
Coalinga	1983	0709	0740	5.2	Transmitter Hill	10.4	.205	12.0	1.34	2.2
Coalinga	1983	0709	0740	5.2	Transmitter Hill	10.4	.194	9.9	.87	2.4
Coalinga	1983	0722	0239	5.8	Oil City	8.2	.568	12.5	1.20	2.7
Coalinga	1983	0722	0239	5.8	Oil City	8.2	.866	42.2	6.14	1.6
Coalinga	1983	0722	0239	5.8	Oil City	8.2	.447	24.8	2.23	1.8
Coalinga	1983	0722	0239	5.8	Palmer Ave	12.2	.201	6.9	1.35	3.5
Coalinga	1983	0722	0239	5.8	Palmer Ave	12.2	.272	12.8	3.31	2.0
Coalinga	1983	0722	0239	5.8	Palmer Ave	12.2	.290	21.5	3.31	1.8
N. Palm Springs	1986	0708	0920	6.0	Hurkey Creek Park	34.9	.097	3.6	.55	5.5
N. Palm Springs	1986	0708	0920	6.0	Hurkey Creek Park	34.9	.240	7.4	.45	2.4
N. Palm Springs	1986	0708	0920	6.0	Hurkey Creek Park	34.9	.187	9.1	.89	1.4
Whittier Narrows	1987	1001	1442	6.0	Garvey Res.-Control Bldg	12.1	.362	9.9	.75	2.6
Whittier Narrows	1987	1001	1442	6.0	Garvey Res.-Control Bldg	12.1	.384	15.8	2.49	2.5
Whittier Narrows	1987	1001	1442	6.0	Garvey Res.-Control Bldg	12.1	.457	19.0	4.31	2.1

TABLE B-1: WUS, ROCK, M = 6-7, D = 0-10 km

Earthquake	YR	MODY	HRMN	Mag	Station	Closest Dist (km)	PGA (g)	PGV (g)	PGD (cm/s)	Dur (s)
Helena, Montana	1935	1031	1838	6.2	Carroll College	8.0	.102	7.3	2.29	1.1
Helena, Montana	1935	1031	1838	6.2	Carroll College	8.0	.150	5.8	1.00	1.3
Helena, Montana	1935	1031	1838	6.2	Carroll College	8.0	.173	16.5	2.37	1.1
Parkfield	1966	0628	0426	6.1	Cholame #8	9.2	.116	4.3	1.48	4.0
Parkfield	1966	0628	0426	6.1	Cholame #8	9.2	.246	10.2	3.60	5.9
Parkfield	1966	0628	0426	6.1	Cholame #8	9.2	.273	11.3	3.20	3.7
Parkfield	1966	0628	0426	6.1	Temblor pre-1969	9.9	.136	4.4	1.10	3.2
Parkfield	1966	0628	0426	6.1	Temblor pre-1969	9.9	.357	21.5	3.87	1.3
Parkfield	1966	0628	0426	6.1	Temblor pre-1969	9.9	.272	15.0	3.40	1.3
San Fernando	1971	0209	1400	6.6	Pacoima Dam	2.8	.699	56.5	18.25	5.5
San Fernando	1971	0209	1400	6.6	Pacoima Dam	2.8	1.226	112.5	35.50	5.4
San Fernando	1971	0209	1400	6.6	Pacoima Dam	2.8	1.160	54.3	11.73	5.8
Gazli, USSR	1976	0517		6.8	Karakyr	3.0	1.264	54.2	30.15	5.1
Gazli, USSR	1976	0517		6.8	Karakyr	3.0	.608	65.4	25.29	4.5
Gazli, USSR	1976	0517		6.8	Karakyr	3.0	.718	71.6	23.71	5.4
Morgan Hill	1984	0424	2115	6.2	Coyote Lake Dam (SW Abut)	.1	.388	15.6	2.65	3.0
Morgan Hill	1984	0424	2115	6.2	Coyote Lake Dam (SW Abut)	.1	.711	51.6	12.00	3.0
Morgan Hill	1984	0424	2115	6.2	Coyote Lake Dam (SW Abut)	.1	1.298	80.8	9.63	1.7
Morgan Hill	1984	0424	2115	6.2	Gilroy Array #6	11.8	.405	14.1	1.86	.5
Morgan Hill	1984	0424	2115	6.2	Gilroy Array #6	11.8	.222	11.4	2.45	3.1
Morgan Hill	1984	0424	2115	6.2	Gilroy Array #6	11.8	.292	36.7	6.12	4.5
Whittier Narrows	1987	1001	1442	6.0	San Gabriel – E Grand Ave #	9.0	.227	5.5	.44	2.5
Whittier Narrows	1987	1001	1442	6.0	San Gabriel – E Grand Ave #	9.0	.304	23.0	3.34	2.4
Whittier Narrows	1987	1001	1442	6.0	San Gabriel – E Grand Ave #	9.0	.199	11.0	1.04	2.8
Loma Prieta	1989	1018	0005	6.9	Corralitos	5.1	.455	17.7	7.11	3.5
Loma Prieta	1989	1018	0005	6.9	Corralitos	5.1	.644	55.2	10.88	3.4
Loma Prieta	1989	1018	0005	6.9	Corralitos	5.1	.479	45.2	11.37	4.6
Loma Prieta	1989	1018	0005	6.9	LGPC	6.1	.890	54.9	17.56	4.5
Loma Prieta	1989	1018	0005	6.9	LGPC	6.1	.563	94.8	41.18	5.5
Loma Prieta	1989	1018	0005	6.9	LGPC	6.1	.605	51.0	11.50	5.5
Northridge	1994	0117	1231	6.7	Pacoima Dam (downstr) #	8.0	.190	14.2	1.35	3.9
Northridge	1994	0117	1231	6.7	Pacoima Dam (downstr) #	8.0	.415	45.6	5.06	.6
Northridge	1994	0117	1231	6.7	Pacoima Dam (downstr) #	8.0	.434	31.3	4.80	2.0
Northridge	1994	0117	1231	6.7	Pacoima Dam (upper left) #	8.0	1.229	49.6	11.75	3.0
Northridge	1994	0117	1231	6.7	Pacoima Dam (upper left) #	8.0	1.585	55.7	6.06	2.5
Northridge	1994	0117	1231	6.7	Pacoima Dam (upper left) #	8.0	1.285	103.9	23.80	3.8
Northridge	1994	0117	1231	6.7	Pacoima Kagel Canyon #	8.2	.169	15.1	4.14	6.9
Northridge	1994	0117	1231	6.7	Pacoima Kagel Canyon #	8.2	.301	31.4	10.87	5.7
Northridge	1994	0117	1231	6.7	Pacoima Kagel Canyon #	8.2	.433	51.5	7.21	5.6
Kobe	1995	0116	2046	6.9	Kobe University	.2	.380	20.2	6.48	2.8
Kobe	1995	0116	2046	6.9	Kobe University	.2	.290	54.8	13.61	3.3
Kobe	1995	0116	2046	6.9	Kobe University	.2	.310	34.2	7.14	3.7
Kobe	1995	0116	2046	6.9	KJMA	.6	.343	38.3	10.29	4.7
Kobe	1995	0116	2046	6.9	KJMA	.6	.821	81.3	17.68	4.2
Kobe	1995	0116	2046	6.9	KJMA	.6	.599	74.3	19.95	4.3

TABLE B-1: WUS, ROCK, M = 6-7, D = 10-50 km

Earthquake	YR	MODY	HRMN	Mag	Station	Closest Dist (km)	PGA (g)	PGV (g)	PGD (cm/s)	Dur (s)
San Fernando	1971	0209	1400	6.6	Lake Hughes #4	24.2	.164	6.4	.93	4.1
San Fernando	1971	0209	1400	6.6	Lake Hughes #4	24.2	.192	5.6	.92	3.6
San Fernando	1971	0209	1400	6.6	Lake Hughes #4	24.2	.153	8.4	1.85	4.1
San Fernando	1971	0209	1400	6.6	Santa Felita Dam (Outlet)	27.5	.065	4.1	2.36	8.9
San Fernando	1971	0209	1400	6.6	Santa Felita Dam (Outlet)	27.5	.148	9.4	7.02	7.4
San Fernando	1971	0209	1400	6.6	Santa Felita Dam (Outlet)	27.5	.152	6.5	3.46	5.0
Imperial Valley	1979	1015	2316	6.5	Superstition Mtn Camera	26.0	.077	2.3	1.14	5.8
Imperial Valley	1979	1015	2316	6.5	Superstition Mtn Camera	26.0	.109	5.2	2.21	6.3
Imperial Valley	1979	1015	2316	6.5	Superstition Mtn Camera	26.0	.195	8.8	2.78	2.2
Mammoth Lakes	1980	0525	1944	6.0	Long Valley Dam (L Abut)	19.7	.068	4.0	.45	4.6
Mammoth Lakes	1980	0525	1944	6.0	Long Valley Dam (L Abut)	19.7	.104	6.6	1.06	4.2
Mammoth Lakes	1980	0525	1944	6.0	Long Valley Dam (L Abut)	19.7	.077	5.4	1.69	4.8
Mammoth Lakes	1980	0525	1944	6.0	Bishop-Paradise Lodge	43.7	.084	3.0	.77	4.6
Mammoth Lakes	1980	0525	1944	6.0	Bishop-Paradise Lodge	43.7	.091	5.5	1.48	4.9
Mammoth Lakes	1980	0525	1944	6.0	Bishop-Paradise Lodge	43.7	.114	5.3	1.41	4.3
Victoria, Mexico	1980	0609	0328	6.1	Cerro Prieto	34.8	.304	12.1	4.90	5.1
Victoria, Mexico	1980	0609	0328	6.1	Cerro Prieto	34.8	.621	31.6	13.20	4.4
Victoria, Mexico	1980	0609	0328	6.1	Cerro Prieto	34.8	.587	19.9	9.40	4.2
Coalinga	1983	0502	2342	6.4	Parkfield-Fault Zone 11	28.4	.042	4.8	1.80	8.9
Coalinga	1983	0502	2342	6.4	Parkfield-Fault Zone 11	28.4	.097	11.9	2.35	4.5
Coalinga	1983	0502	2342	6.4	Parkfield-Fault Zone 11	28.4	.087	6.6	1.83	3.6
Coalinga	1983	0502	2342	6.4	Parkfield-Gold Hill 3W	38.8	.067	7.5	1.77	9.0
Coalinga	1983	0502	2342	6.4	Parkfield-Gold Hill 3W	38.8	.137	11.0	2.76	2.8
Coalinga	1983	0502	2342	6.4	Parkfield-Gold Hill 3W	38.8	.122	9.0	1.74	3.8
Coalinga	1983	0502	2342	6.4	Parkfield-Cholame 2E	40.5	.017	2.3	.52	12.1
Coalinga	1983	0502	2342	6.4	Parkfield-Cholame 2E	40.5	.026	2.9	.62	8.8
Coalinga	1983	0502	2342	6.4	Parkfield-Cholame 2E	40.5	.037	5.4	1.40	7.6
Coalinga	1983	0502	2342	6.4	Parkfield-Vineyard Cany 4W	34.6	.024	2.8	.64	8.2
Coalinga	1983	0502	2342	6.4	Parkfield-Vineyard Cany 4W	34.6	.064	6.5	1.37	4.3
Coalinga	1983	0502	2342	6.4	Parkfield-Vineyard Cany 4W	34.6	.046	4.2	.95	5.9
Morgan Hill	1984	0424	2115	6.2	Corralitos	22.7	.040	4.0	.54	4.9
Morgan Hill	1984	0424	2115	6.2	Corralitos	22.7	.081	6.4	1.17	4.4
Morgan Hill	1984	0424	2115	6.2	Corralitos	22.7	.109	10.8	2.13	3.4
Morgan Hill	1984	0424	2115	6.2	Gilroy Array #6	11.8	.405	14.1	1.86	.5
Morgan Hill	1984	0424	2115	6.2	Gilroy Array #6	11.8	.222	11.4	2.45	3.1
Morgan Hill	1984	0424	2115	6.2	Gilroy Array #6	11.8	.292	36.7	6.12	4.5
Morgan Hill	1984	0424	2115	6.2	Gilroy – Gavilan Coll.	16.2	.081	2.3	.41	3.6
Morgan Hill	1984	0424	2115	6.2	Gilroy – Gavilan Coll.	16.2	.114	3.6	.87	5.0
Morgan Hill	1984	0424	2115	6.2	Gilroy – Gavilan Coll.	16.2	.095	2.9	.93	4.7
N. Palm Springs	1986	0708	0920	6.0	Santa Rosa Mountain	43.8	.051	1.5	.10	6.6
N. Palm Springs	1986	0708	0920	6.0	Santa Rosa Mountain	43.8	.102	2.2	.10	6.0
N. Palm Springs	1986	0708	0920	6.0	Santa Rosa Mountain	43.8	.103	2.2	.10	6.6
Chalfant Valley	1986	0721	1442	6.2	Long Valley Dam (L Abut)	33.4	.074	3.3	1.45	6.4
Chalfant Valley	1986	0721	1442	6.2	Long Valley Dam (L Abut)	33.4	.082	7.0	1.34	5.3
Chalfant Valley	1986	0721	1442	6.2	Long Valley Dam (L Abut)	33.4	.071	7.9	3.06	7.9
Chalfant Valley	1986	0721	1442	6.2	Tinemaha Res. Free Field	40.5	.023	1.7	.54	11.3
Chalfant Valley	1986	0721	1442	6.2	Tinemaha Res. Free Field	40.5	.037	3.6	1.12	6.7
Chalfant Valley	1986	0721	1442	6.2	Tinemaha Res. Free Field	40.5	.037	6.3	1.21	5.6
Whittier Narrows	1987	1001	1442	6.0	LA-Chalon Rd #	32.6	.019	.7	.07	5.1
Whittier Narrows	1987	1001	1442	6.0	LA-Chalon Rd #	32.6	.036	2.3	.21	3.5
Whittier Narrows	1987	1001	1442	6.0	LA-Chalon Rd #	32.6	.020	1.1	.12	5.6
Whittier Narrows	1987	1001	1442	6.0	LA-N Faring Rd #	28.5	.034	1.6	.13	6.1
Whittier Narrows	1987	1001	1442	6.0	LA-N Faring Rd #	28.5	.048	2.2	.26	4.4
Whittier Narrows	1987	1001	1442	6.0	LA-N Faring Rd #	28.5	.053	3.0	.29	4.1
Whittier Narrows	1987	1001	1442	6.0	Malibu-Las Flores Canyon #	46.3	.015	1.0	.13	4.4
Whittier Narrows	1987	1001	1442	6.0	Malibu-Las Flores Canyon #	46.3	.065	2.3	.14	3.3
Whittier Narrows	1987	1001	1442	6.0	Malibu-Las Flores Canyon #	46.3	.055	2.2	.32	3.5
Whittier Narrows	1987	1001	1442	6.0	Pacoima Kagel Canyon	37.9	.055	2.7	.30	7.0
Whittier Narrows	1987	1001	1442	6.0	Pacoima Kagel Canyon	37.9	.166	6.2	.68	3.7
Whittier Narrows	1987	1001	1442	6.0	Pacoima Kagel Canyon	37.9	.164	6.8	.87	4.3
Whittier Narrows	1987	1001	1442	6.0	Villa Park-Serrano Ave #	30.0	.033	1.3	.11	8.9
Whittier Narrows	1987	1001	1442	6.0	Villa Park-Serrano Ave #	30.0	.046	1.4	.13	6.4
Whittier Narrows	1987	1001	1442	6.0	Villa Park-Serrano Ave #	30.0	.072	2.6	.27	5.5
Spitak, Armenia	1988	1207		6.8	Gukasian	30.0	.119	8.8	4.30	6.2
Spitak, Armenia	1988	1207		6.8	Gukasian	30.0	.199	28.6	9.80	6.3
Spitak, Armenia	1988	1207		6.8	Gukasian	30.0	.715	15.1	4.30	4.4
Loma Prieta	1989	1018	0005	6.9	Belmont-Envirotech	49.9	.041	4.5	2.46	7.1
Loma Prieta	1989	1018	0005	6.9	Belmont-Envirotech	49.9	.108	11.8	3.30	4.7
Loma Prieta	1989	1018	0005	6.9	Belmont-Envirotech	49.9	.110	16.2	5.71	3.8
Loma Prieta	1989	1018	0005	6.9	Gilroy Array #6	19.9	.101	9.5	4.10	5.1
Loma Prieta	1989	1018	0005	6.9	Gilroy Array #6	19.9	.126	12.8	4.74	4.5
Loma Prieta	1989	1018	0005	6.9	Gilroy Array #6	19.9	.170	14.2	3.79	4.5

TABLE B-1: WUS, ROCK, M = 6-7, D = 10-50 km (Cont…)

Earthquake	YR	MODY	HRMN	Mag	Station	Closest Dist (km)	PGA (g)	PGV (g)	PGD (cm/s)	Dur (s)
Loma Prieta	1989	1018	0005	6.9	SAGO South - Surface	34.7	.060	7.8	5.86	5.9
Loma Prieta	1989	1018	0005	6.9	SAGO South - Surface	34.7	.073	10.5	6.40	5.4
Loma Prieta	1989	1018	0005	6.9	SAGO South - Surface	34.7	.067	9.6	6.42	7.8
Loma Prieta	1989	1018	0005	6.9	Woodside	39.9	.050	6.2	2.80	6.5
Loma Prieta	1989	1018	0005	6.9	Woodside	39.9	.080	13.7	8.47	6.2
Loma Prieta	1989	1018	0005	6.9	Woodside	39.9	.082	16.7	8.89	6.3
Northridge	1994	0117	1231	6.7	Burbank – Howard Rd.	20.0	.085	3.6	1.48	7.0
Northridge	1994	0117	1231	6.7	Burbank – Howard Rd.	20.0	.120	9.5	2.25	5.9
Northridge	1994	0117	1231	6.7	Burbank – Howard Rd.	20.0	.163	8.5	1.81	5.1
Northridge	1994	0117	1231	6.7	LA – Chalon Rd	23.7	.174	8.0	1.09	5.8
Northridge	1994	0117	1231	6.7	LA – Chalon Rd	23.7	.225	16.6	3.39	5.7
Northridge	1994	0117	1231	6.7	LA – Chalon Rd	23.7	.185	27.1	5.77	5.0
Northridge	1994	0117	1231	6.7	LA – N Faring Rd	23.9	.191	8.9	1.65	5.9
Northridge	1994	0117	1231	6.7	LA – N Faring Rd	23.9	.273	15.8	3.29	4.8
Northridge	1994	0117	1231	6.7	LA – N Faring Rd	23.9	.242	29.8	4.74	5.8
Northridge	1994	0117	1231	6.7	LA – Univ Hospital #	34.6	.119	6.4	1.37	7.6
Northridge	1994	0117	1231	6.7	LA – Univ Hospital #	34.6	.493	31.1	2.39	5.6
Northridge	1994	0117	1231	6.7	LA – Univ Hospital #	34.6	.214	10.8	2.37	6.7

TABLE B-1: WUS, ROCK, M > 7, D = 0-10 km

Earthquake	YR	MODY	HRMN	Mag	Station	Closest Dist (km)	PGA (g)	PGV (g)	PGD (cm/s)	Dur (s)
Gazli, USSR	1976	0517		6.8	Karakyr	3.0	1.264	54.2	30.15	5.1
Gazli, USSR	1976	0517		6.8	Karakyr	3.0	.608	65.4	25.29	4.5
Gazli, USSR	1976	0517		6.8	Karakyr	3.0	.718	71.6	23.71	5.4
Loma Prieta	1989	1018	0005	6.9	Corralitos	5.1	.455	17.7	7.11	3.5
Loma Prieta	1989	1018	0005	6.9	Corralitos	5.1	.644	55.2	10.88	3.4
Loma Prieta	1989	1018	0005	6.9	Corralitos	5.1	.479	45.2	11.37	4.6
Loma Prieta	1989	1018	0005	6.9	LGPC	6.1	.890	54.9	17.56	4.5
Loma Prieta	1989	1018	0005	6.9	LGPC	6.1	.563	94.8	41.18	5.5
Loma Prieta	1989	1018	0005	6.9	LGPC	6.1	.605	51.0	11.50	5.5
Loma Prieta	1989	1018	0005	6.9	BRAN	10.3	.507	17.9	4.17	6.2
Loma Prieta	1989	1018	0005	6.9	BRAN	10.3	.453	51.3	8.37	5.6
Loma Prieta	1989	1018	0005	6.9	BRAN	10.3	.501	44.6	4.86	6.9
Cape Mendocino	1992	0425	1806	7.1	Cape Mendocino #	8.5	.754	63.0	109.48	2.2
Cape Mendocino	1992	0425	1806	7.1	Cape Mendocino #	8.5	1.497	127.4	41.01	2.5
Cape Mendocino	1992	0425	1806	7.1	Cape Mendocino #	8.5	1.039	42.0	12.39	2.9
Landers	1992	0628	1158	7.3	Luceme	1.1	.818	45.9	22.23	7.4
Landers	1992	0628	1158	7.3	Luceme	1.1	.721	97.6	70.31	8.4
Landers	1992	0628	1158	7.3	Luceme	1.1	.785	31.9	16.42	8.4
Kobe	1995	0116	2046	6.9	Kobe Univeristy	.2	.380	20.2	6.48	2.8
Kobe	1995	0116	2046	6.9	Kobe Univeristy	.2	.290	54.8	13.61	3.3
Kobe	1995	0116	2046	6.9	Kobe Univeristy	.2	.310	34.2	7.14	3.7
Kobe	1995	0116	2046	6.9	KJMA	.6	.343	38.3	10.29	4.7
Kobe	1995	0116	2046	6.9	KJMA	.6	.821	81.3	17.68	4.2
Kobe	1995	0116	2046	6.9	KJMA	.6	.599	74.3	19.95	4.3
Kocaely, Turkey	1999	0817		7.4	Izmit	7.7	.149	11.9	4.99	8.4
Kocaely, Turkey	1999	0817		7.4	Izmit	7.7	.152	22.6	9.81	8.2
Kocaely, Turkey	1999	0817		7.4	Izmit	7.7	.220	29.8	17.12	6.3
Chi-Chi, Taiwan	1999	0920		7.6	CHY080	6.9	.724	49.0	27.82	5.9
Chi-Chi, Taiwan	1999	0920		7.6	CHY080	6.9	.902	102.4	33.97	5.7
Chi-Chi, Taiwan	1999	0920		7.6	CHY080	6.9	.968	107.5	18.60	7.0
Chi-Chi, Taiwan	1999	0920		7.6	TCU087	3.1	.108	61.5	51.32	9.8
Chi-Chi, Taiwan	1999	0920		7.6	TCU087	3.1	.122	37.1	25.54	16.1
Chi-Chi, Taiwan	1999	0920		7.6	TCU087	3.1	.128	40.8	62.62	14.9
Chi-Chi, Taiwan	1999	0920		7.6	TCU089	8.2	.191	22.3	24.36	18.0
Chi-Chi, Taiwan	1999	0920		7.6	TCU089	8.2	.248	31.0	32.37	21.8
Chi-Chi, Taiwan	1999	0920		7.6	TCU089	8.2	.333	30.9	18.48	19.3
Chi-Chi, Taiwan	1999	0920		7.6	TCU120	8.1	.162	32.1	22.34	19.5
Chi-Chi, Taiwan	1999	0920		7.6	TCU120	8.1	.192	36.9	33.30	21.7
Chi-Chi, Taiwan	1999	0920		7.6	TCU120	8.1	.225	63.1	54.09	19.7
Chi-Chi, Taiwan	1999	0920		7.6	TCU128	9.7	.097	46.0	34.77	18.1
Chi-Chi, Taiwan	1999	0920		7.6	TCU128	9.7	.170	68.8	41.87	10.6
Chi-Chi, Taiwan	1999	0920		7.6	TCU128	9.7	.139	73.0	90.62	13.5
Chi-Chi, Taiwan	1999	0920		7.6	TCU136	8.9	.123	27.3	30.19	17.6
Chi-Chi, Taiwan	1999	0920		7.6	TCU136	8.9	.171	55.8	66.48	17.4
Chi-Chi, Taiwan	1999	0920		7.6	TCU136	8.9	.177	47.5	44.82	19.2

TABLE B-1: WUS, ROCK, M > 7, D = 10-50 km

Earthquake	YR	MODY	HRMN	Mag	Station	Closest Dist (km)	PGA (g)	PGV (g)	PGD (cm/s)	Dur (s)
Tabas, Iran	1978	0916		7.4	Dayhook	17.0	.183	12.0	4.97	8.3
Tabas, Iran	1978	0916		7.4	Dayhook	17.0	.328	20.6	12.56	6.7
Tabas, Iran	1978	0916		7.4	Dayhook	17.0	.406	26.5	8.75	6.9
Cape Mendocino	1992	0425	1806	7.1	Shelter Cove Ariport #	33.8	.054	2.0	.33	15.5
Cape Mendocino	1992	0425	1806	7.1	Shelter Cove Ariport #	33.8	.229	7.1	.39	13.6
Cape Mendocino	1992	0425	1806	7.1	Shelter Cove Ariport #	33.8	.189	6.6	.57	14.8
Landers	1992	0628	1158	7.3	Twentynine Palms #	42.2	.040	3.3	1.93	22.7
Landers	1992	0628	1158	7.3	Twentynine Palms #	42.2	.080	3.7	2.34	21.6
Landers	1992	0628	1158	7.3	Twentynine Palms #	42.2	.060	4.9	4.30	20.4
Kocaeli, Turkey	1999	0817		7.4	Arcelik	17.0	.086	2.6	.22	8.7
Kocaeli, Turkey	1999	0817		7.4	Arcelik	17.0	.180	10.5	.90	7.7
Kocaeli, Turkey	1999	0817		7.4	Arcelik	17.0	.108	6.2	.63	4.4
Kocaeli, Turkey	1999	0817		7.4	Gebze	17.0	.151	6.3	.59	5.6
Kocaeli, Turkey	1999	0817		7.4	Gebze	17.0	.244	50.3	42.74	5.3
Kocaeli, Turkey	1999	0817		7.4	Gebze	17.0	.137	29.7	27.54	5.7
Kocaeli, Turkey	1999	0817		7.4	Goynuk	35.5	.114	11.5	7.59	6.6
Kocaeli, Turkey	1999	0817		7.4	Goynuk	35.5	.132	8.8	3.05	5.5
Kocaeli, Turkey	1999	0817		7.4	Goynuk	35.5	.119	10.5	3.94	4.4
Kocaeli, Turkey	1999	0817		7.4	Iznik	29.7	.083	7.7	1.70	9.9
Kocaeli, Turkey	1999	0817		7.4	Iznik	29.7	.103	16.5	7.00	12.7
Kocaeli, Turkey	1999	0817		7.4	Iznik	29.7	.136	28.8	17.44	10.7
Chi-Chi, Taiwan	1999	0920		7.6	HWA056	48.7	.062	7.1	10.35	10.7
Chi-Chi, Taiwan	1999	0920		7.6	HWA056	48.7	.107	10.8	10.36	9.5
Chi-Chi, Taiwan	1999	0920		7.6	HWA056	48.7	.107	11.7	17.64	9.2
Chi-Chi, Taiwan	1999	0920		7.6	TCU015	47.3	.068	17.2	14.85	19.1
Chi-Chi, Taiwan	1999	0920		7.6	TCU015	47.3	.114	29.5	24.14	12.7
Chi-Chi, Taiwan	1999	0920		7.6	TCU015	47.3	.119	49.8	49.79	15.7
Chi-Chi, Taiwan	1999	0920		7.6	TCU046	14.3	.104	32.3	37.74	9.5
Chi-Chi, Taiwan	1999	0920		7.6	TCU046	14.3	.116	30.9	23.18	10.8
Chi-Chi, Taiwan	1999	0920		7.6	TCU046	14.3	.133	39.8	37.37	11.5
Chi-Chi, Taiwan	1999	0920		7.6	TCU047	33.0	.270	26.9	17.88	11.6
Chi-Chi, Taiwan	1999	0920		7.6	TCU047	33.0	.413	40.2	22.22	9.8
Chi-Chi, Taiwan	1999	0920		7.6	TCU047	33.0	.301	41.6	51.08	10.1
Chi-Chi, Taiwan	1999	0920		7.6	TCU095	43.4	.255	21.8	21.95	13.0
Chi-Chi, Taiwan	1999	0920		7.6	TCU095	43.4	.712	49.1	24.45	8.3
Chi-Chi, Taiwan	1999	0920		7.6	TCU095	43.4	.378	62.0	51.75	8.3
Duzce, Turkey	1999	1112		7.1	Bolu	16.0	.203	17.3	14.29	6.0
Duzce, Turkey	1999	1112		7.1	Bolu	16.0	.728	56.4	23.07	2.6
Duzce, Turkey	1999	1112		7.1	Bolu	16.0	.822	62.1	13.55	1.5
Duzce, Turkey	1999	1112		7.1	Mudumu	34.6	.060	10.6	7.33	19.5
Duzce, Turkey	1999	1112		7.1	Mudumu	34.6	.120	9.3	7.63	17.1
Duzce, Turkey	1999	1112		7.1	Mudumu	34.6	.056	16.3	15.37	18.6
Duzce, Turkey	1999	1112		7.1	Sakarya	42.7	.011	3.2	4.00	17.4
Duzce, Turkey	1999	1112		7.1	Sakarya	42.7	.023	5.5	5.80	16.9
Duzce, Turkey	1999	1112		7.1	Sakarya	42.7	.016	5.5	7.34	17.1

TABLE B-2: WUS, SOIL, M = 5-6, D = 0-50 km

Earthquake	YR	MODY	HRMN	Mag	Station	Closest Dist (km)	PGA (g)	PGV (g)	PGD (cm/s)	Dur (s)
Northern Calif	1967	1210	1206	5.6	Ferndale City Hall	30.8	.032	3.3	.46	8.7
Northern Calif	1967	1210	1206	5.6	Ferndale City Hall	30.8	.283	9.2	1.23	1.3
Northern Calif	1967	1210	1206	5.6	Ferndale City Hall	30.8	.113	11.1	1.58	6.0
Mammoth Lakes	1980	0525	1944	6.0	Convict Creek	17.4	.195	8.5	1.58	3.3
Mammoth Lakes	1980	0525	1944	6.0	Convict Creek	17.4	.219	18.5	4.87	2.8
Mammoth Lakes	1980	0525	1944	6.0	Convict Creek	17.4	.208	16.1	2.29	2.1
Mammoth Lakes	1983	0107	0138	5.2	Convict Creek	9.5	.097	7.9	1.65	3.9
Mammoth Lakes	1983	0107	0138	5.2	Convict Creek	9.5	.165	14.4	2.05	2.8
Mammoth Lakes	1983	0107	0138	5.2	Convict Creek	9.5	.153	18.7	2.88	1.9
Coalinga	1983	0509	0249	5.0	Bumett Construction	17.7	.077	2.0	.15	2.6
Coalinga	1983	0509	0249	5.0	Bumett Construction	17.7	.095	3.5	.37	3.6
Coalinga	1983	0509	0249	5.0	Bumett Construction	17.7	.095	4.5	.35	2.2
Coalinga	1983	0709	0740	5.2	CHP (temp)	14.9	.079	2.4	.22	3.7
Coalinga	1983	0709	0740	5.2	CHP (temp)	14.9	.204	8.0	.62	2.0
Coalinga	1983	0709	0740	5.2	CHP (temp)	14.9	.171	5.4	.38	2.2
N. Palm Springs	1986	0708	0920	6.0	Cabazon	16.3	.363	7.4	.84	2.0
N. Palm Springs	1986	0708	0920	6.0	Cabazon	16.3	.217	7.6	1.96	2.6
N. Palm Springs	1986	0708	0920	6.0	Cabazon	16.3	.212	16.3	2.24	1.5
N. Palm Springs	1986	0708	0920	6.0	Whitewater Trout Farm	7.3	.471	13.4	1.02	2.3
N. Palm Springs	1986	0708	0920	6.0	Whitewater Trout Farm	7.3	.492	34.7	6.38	1.7
N. Palm Springs	1986	0708	0920	6.0	Whitewater Trout Farm	7.3	.612	31.5	4.58	1.8
Chalfant Valley	1986	0721	1451	5.6	Zack Brothers Ranch	20.0	.079	2.1	.15	3.9
Chalfant Valley	1986	0721	1451	5.6	Zack Brothers Ranch	20.0	.143	7.4	.67	1.5
Chalfant Valley	1986	0721	1451	5.6	Zack Brothers Ranch	20.0	.108	5.1	.58	3.6
Whittier Narrows	1987	1001	1442	6.0	Brea Dam (Downstream)	23.3	.094	3.1	.22	5.3
Whittier Narrows	1987	1001	1442	6.0	Brea Dam (Downstream)	23.3	.163	6.2	.36	1.9
Whittier Narrows	1987	1001	1442	6.0	Brea Dam (Downstream)	23.3	.313	14.5	.77	1.4
Whittier Narrows	1987	1001	1442	6.0	Compton – Castlegate Sr #	16.9	.167	3.3	.19	3.0
Whittier Narrows	1987	1001	1442	6.0	Compton – Castlegate Sr #	16.9	.332	27.1	5.04	1.8
Whittier Narrows	1987	1001	1442	6.0	Compton – Castlegate Sr #	16.9	.333	14.1	1.48	2.1
Whittier Narrows	1987	1001	1442	6.0	Inglewood – Union Oil	25.2	.069	2.4	.24	5.9
Whittier Narrows	1987	1001	1442	6.0	Inglewood – Union Oil	25.2	.299	8.9	.78	1.6
Whittier Narrows	1987	1001	1442	6.0	Inglewood – Union Oil	25.2	.247	18.1	1.92	1.9
Whittier Narrows	1987	1001	1442	6.0	La Puente – Rimgrove Av #	11.9	.076	2.5	.19	4.0
Whittier Narrows	1987	1001	1442	6.0	La Puente – Rimgrove Av #	11.9	.143	6.2	1.04	3.8
Whittier Narrows	1987	1001	1442	6.0	La Puente – Rimgrove Av #	11.9	.118	5.9	.42	3.4
Whittier Narrows	1987	1001	1442	6.0	Pasadena-CIT Calif Blvd	15.5	.171	7.0	.58	2.8
Whittier Narrows	1987	1001	1442	6.0	Pasadena-CIT Calif Blvd	15.5	.177	8.1	.96	2.6
Whittier Narrows	1987	1001	1442	6.0	Pasadena-CIT Calif Blvd	15.5	.271	15.4	2.33	2.1
Whittier Narrows	1987	1001	1442	6.0	Pasadena-CIT Keck Lab	15.5	.096	4.0	.41	4.6
Whittier Narrows	1987	1001	1442	6.0	Pasadena-CIT Keck Lab	15.5	.152	5.1	.60	3.7
Whittier Narrows	1987	1001	1442	6.0	Pasadena-CIT Keck Lab	15.5	.188	14.1	2.63	2.6
Whittier Narrows	1987	1001	1442	6.0	Whittier N. Dam upstream	12.3	.505	7.1	.31	2.3
Whittier Narrows	1987	1001	1442	6.0	Whittier N. Dam upstream	12.3	.229	17.8	2.62	2.7
Whittier Narrows	1987	1001	1442	6.0	Whittier N. Dam upstream	12.3	.316	12.0	1.36	2.4

TABLE B-2: WUS, SOIL, M = 6-7, D = 0-10 km

Earthquake	YR	MODY	HRMN	Mag	Station	Closest Dist (km)	PGA (g)	PGV (g)	PGD (cm/s)	Dur (s)
Imperial Valley	1979	1015	2316	6.5	Bonds Corner	2.5	.425	12.2	4.02	4.5
Imperial Valley	1979	1015	2316	6.5	Bonds Corner	2.5	.588	45.2	16.78	6.1
Imperial Valley	1979	1015	2316	6.5	Bonds Corner	2.5	.775	45.9	14.89	4.7
Imperial Valley	1979	1015	2316	6.5	Brawley Airport	8.5	.146	8.4	3.49	4.8
Imperial Valley	1979	1015	2316	6.5	Brawley Airport	8.5	.160	35.9	22.44	5.2
Imperial Valley	1979	1015	2316	6.5	Brawley Airport	8.5	.220	38.9	13.46	2.9
Imperial Valley	1979	1015	2316	6.5	EC County Center FF	7.6	.246	18.1	9.70	3.5
Imperial Valley	1979	1015	2316	6.5	EC County Center FF	7.6	.213	37.5	15.98	3.7
Imperial Valley	1979	1015	2316	6.5	EC County Center FF	7.6	.235	68.8	39.35	4.7
Imperial Valley	1979	1015	2316	6.5	El Centro Array # 3	9.9	.127	8.7	4.70	6.2
Imperial Valley	1979	1015	2316	6.5	El Centro Array # 3	9.9	.266	46.8	18.92	4.3
Imperial Valley	1979	1015	2316	6.5	El Centro Array # 3	9.9	.221	39.9	23.31	5.1
Imperial Valley	1979	1015	2316	6.5	El Centro Array # 5	1.0	.537	38.5	19.69	2.3
Imperial Valley	1979	1015	2316	6.5	El Centro Array # 5	1.0	.519	46.9	35.35	3.5
Imperial Valley	1979	1015	2316	6.5	El Centro Array # 5	1.0	.379	90.5	63.03	3.7
Imperial Valley	1979	1015	2316	6.5	El Centro Array # 6	1.0	1.655	57.5	26.41	1.0
Imperial Valley	1979	1015	2316	6.5	El Centro Array # 6	1.0	.410	64.9	27.69	5.3
Imperial Valley	1979	1015	2316	6.5	El Centro Array # 6	1.0	.439	109.8	65.89	4.1
Imperial Valley	1979	1015	2316	6.5	El Centro Differential Array	5.3	.707	20.7	11.55	2.8
Imperial Valley	1979	1015	2316	6.5	El Centro Differential Array	5.3	.352	71.2	45.80	3.7
Imperial Valley	1979	1015	2316	6.5	El Centro Differential Array	5.3	.480	40.8	14.04	3.0
Imperial Valley	1979	1015	2316	6.5	Holtville Post Office	7.5	.230	9.9	5.69	5.1
Imperial Valley	1979	1015	2316	6.5	Holtville Post Office	7.5	.253	48.8	31.54	4.7
Imperial Valley	1979	1015	2316	6.5	Holtville Post Office	7.5	.221	49.8	31.96	4.7
Mammoth Lakes	1980	0525	1634	6.3	Convict Creek	9.0	.388	20.5	5.93	6.0
Mammoth Lakes	1980	0525	1634	6.3	Convict Creek	9.0	.416	23.3	4.66	6.6
Mammoth Lakes	1980	0525	1634	6.3	Convict Creek	9.0	.442	23.1	5.42	7.1
Coalinga	1983	0502	2342	6.4	Pleasant Valley P.P - yard	8.5	.353	16.1	2.35	5.1
Coalinga	1983	0502	2342	6.4	Pleasant Valley P.P - yard	8.5	.592	60.2	8.77	4.1
Coalinga	1983	0502	2342	6.4	Pleasant Valley P.P - yard	8.5	.551	36.4	3.96	4.4
Chalfant Valley	1983	0502	2342	6.2	Bisho-LADWP South St	9.2	.140	6.7	2.25	5.1
Chalfant Valley	1983	0502	2342	6.2	Bisho-LADWP South St	9.2	.248	19.2	7.04	3.6
Chalfant Valley	1983	0502	2342	6.2	Bisho-LADWP South St	9.2	.175	19.4	6.72	3.1
Erzican, Turkey	1992	0313		6.9	Erzincan	2.0	.248	18.3	7.86	5.4
Erzican, Turkey	1992	0313		6.9	Erzincan	2.0	.515	83.9	27.35	1.5
Erzican, Turkey	1992	0313		6.9	Erzincan	2.0	.496	64.3	22.78	2.0
Northridge	1994	0117	1231	6.7	Arleta-Nordhoff Fire Sta #	9.2	.552	18.4	8.83	6.5
Northridge	1994	0117	1231	6.7	Arleta-Nordhoff Fire Sta #	9.2	.344	40.5	15.04	6.4
Northridge	1994	0117	1231	6.7	Arleta-Nordhoff Fire Sta #	9.2	.308	23.2	10.75	5.7
Northridge	1994	0117	1231	6.7	Jensen Filter Plant #	6.2	.400	34.1	8.89	5.2
Northridge	1994	0117	1231	6.7	Jensen Filter Plant #	6.2	.424	106.2	43.06	4.0
Northridge	1994	0117	1231	6.7	Jensen Filter Plant #	6.2	.593	99.3	24.00	3.1
Northridge	1994	0117	1231	6.7	Sepulveda V A #	8.9	.467	33.2	9.58	5.6
Northridge	1994	0117	1231	6.7	Sepulveda V A #	8.9	.753	84.8	18.68	4.5
Northridge	1994	0117	1231	6.7	Sepulveda V A #	8.9	.939	76.6	14.95	4.3
Northridge	1994	0117	1231	6.7	Sylmar-Converter Sta East #	6.1	.377	24.3	7.30	3.6
Northridge	1994	0117	1231	6.7	Sylmar-Converter Sta East #	6.1	.828	117.5	34.22	3.8
Northridge	1994	0117	1231	6.7	Sylmar-Converter Sta East #	6.1	.493	74.6	28.69	3.4
Kobe	1995	0116	2046	6.9	Takarazuka	1.2	.433	34.8	12.38	1.5
Kobe	1995	0116	2046	6.9	Takarazuka	1.2	.693	68.3	26.65	2.2
Kobe	1995	0116	2046	6.9	Takarazuka	1.2	.694	85.3	16.75	2.1
Kobe	1995	0116	2046	6.9	Takatori	.3	.272	16.0	4.47	7.5
Kobe	1995	0116	2046	6.9	Takatori	.3	.611	127.1	35.77	6.0
Kobe	1995	0116	2046	6.9	Takatori	.3	.616	120.7	32.72	4.8

TABLE B-2: WUS, SOIL, M = 6-7, D = 10-50 km

Earthquake	YR	MODY	HRMN	Mag	Station	Closest Dist (km)	PGA (g)	PGV (g)	PGD (cm/s)	Dur (s)
San Fernando	1971	0209	1400	6.6	Whittier Narrows Dam	45.1	.032	3.7	2.61	9.8
San Fernando	1971	0209	1400	6.6	Whittier Narrows Dam	45.1	.100	9.3	5.79	6.8
San Fernando	1971	0209	1400	6.6	Whittier Narrows Dam	45.1	.107	9.7	5.04	7.1
Imperial Valley	1979	1015	2316	6.5	Calexico Fire Station	10.6	.187	6.7	2.49	6.5
Imperial Valley	1979	1015	2316	6.5	Calexico Fire Station	10.6	.275	21.2	9.02	5.8
Imperial Valley	1979	1015	2316	6.5	Calexico Fire Station	10.6	.202	16.0	9.20	7.2
Imperial Valley	1979	1015	2316	6.5	El Centro Array # 1	15.5	.056	3.8	2.14	7.5
Imperial Valley	1979	1015	2316	6.5	El Centro Array # 1	15.5	.139	16.0	9.96	5.4
Imperial Valley	1979	1015	2316	6.5	El Centro Array # 1	15.5	.134	10.7	6.97	7.2
Taiwan SMART1 (5)	1981	0129		6.3	SMART1 M07	21.0	.050	1.5	.34	5.5
Taiwan SMART1 (5)	1981	0129		6.3	SMART1 M07	21.0	.111	5.6	.86	4.2
Taiwan SMART1 (5)	1981	0129		6.3	SMART1 M07	21.0	.109	10.9	1.74	4.3
N. Palm Springs	1986	0708	0920	6.0	Landers Fire Station	38.2	.055	2.4	.42	5.8
N. Palm Springs	1986	0708	0920	6.0	Landers Fire Station	38.2	.081	4.3	.42	3.9
N. Palm Springs	1986	0708	0920	6.0	Landers Fire Station	38.2	.098	4.6	.53	4.6
Whittier Narrows	1987	1001	1442	6.0	Baldwin Park – N Holly #	11.9	.080	2.2	.75	3.1
Whittier Narrows	1987	1001	1442	6.0	Baldwin Park – N Holly #	11.9	.127	8.6	2.50	2.8
Whittier Narrows	1987	1001	1442	6.0	Baldwin Park – N Holly #	11.9	.061	4.3	.54	6.9
Whittier Narrows	1987	1001	1442	6.0	Beverly Hills-14145 Mulhol #	30.3	.043	2.0	.25	7.3
Whittier Narrows	1987	1001	1442	6.0	Beverly Hills-14145 Mulhol #	30.3	.104	6.5	.58	5.7
Whittier Narrows	1987	1001	1442	6.0	Beverly Hills-14145 Mulhol #	30.3	.126	10.3	1.05	3.4
Whittier Narrows	1987	1001	1442	6.0	Northridge-17645 Saticoy St #	39.8	.084	2.4	.41	6.6
Whittier Narrows	1987	1001	1442	6.0	Northridge-17645 Saticoy St #	39.8	.161	8.5	.72	4.9
Whittier Narrows	1987	1001	1442	6.0	Northridge-17645 Saticoy St #	39.8	.118	5.1	.83	9.7
Superstition Hills (A)	1987	1124	0514	6.3	Wildlife Liquef. Array	24.7	.186	4.6	2.20	3.6
Superstition Hills (A)	1987	1124	0514	6.3	Wildlife Liquef. Array	24.7	.132	12.7	7.30	7.1
Superstition Hills (A)	1987	1124	0514	6.3	Wildlife Liquef. Array	24.7	.134	13.4	5.20	7.3
Loma Prieta	1989	1018	0005	6.9	Saratoga – Aloha Ave	13.0	.389	26.9	15.15	4.7
Loma Prieta	1989	1018	0005	6.9	Saratoga – Aloha Ave	13.0	.512	41.2	16.21	3.7
Loma Prieta	1989	1018	0005	6.9	Saratoga – Aloha Ave	13.0	.324	42.6	27.53	4.2
Georgia, USSR	1991	0615	0059	6.2	Baz	49.0	.016	1.4	.39	11.6
Georgia, USSR	1991	0615	0059	6.2	Baz	49.0	.033	2.2	.40	7.2
Georgia, USSR	1991	0615	0059	6.2	Baz	49.0	.038	2.0	.35	8.1
Northridge	1994	0117	1231	6.7	Glendale – Las Palmas	25.4	.127	4.3	.44	7.2
Northridge	1994	0117	1231	6.7	Glendale – Las Palmas	25.4	.357	12.3	1.94	6.2
Northridge	1994	0117	1231	6.7	Glendale – Las Palmas	25.4	.206	7.4	1.75	6.2
Northridge	1994	0117	1231	6.7	LA-Century City CC North #	25.7	.116	8.7	3.47	8.1
Northridge	1994	0117	1231	6.7	LA-Century City CC North #	25.7	.256	21.1	6.68	7.0
Northridge	1994	0117	1231	6.7	LA-Century City CC North #	25.7	.222	25.2	5.70	7.2
Northridge	1994	0117	1231	6.7	LA – N Westmoreland	29.0	.093	6.3	1.08	8.1
Northridge	1994	0117	1231	6.7	LA – N Westmoreland	29.0	.401	20.9	2.29	5.3
Northridge	1994	0117	1231	6.7	LA – N Westmoreland	29.0	.361	20.9	4.27	5.7
Northridge	1994	0117	1231	6.7	Leona Valley # 5 – Ritter #	38.3	.097	11.6	2.53	8.5
Northridge	1994	0117	1231	6.7	Leona Valley # 5 – Ritter #	38.3	.146	14.9	2.35	6.3
Northridge	1994	0117	1231	6.7	Leona Valley # 5 – Ritter #	38.3	.092	10.5	2.70	7.2

TABLE B-2: WUS, SOIL, M > 7, D = 0-10 km

Earthquake	YR	MODY	HRMN	Mag	Station	Closest Dist (km)	PGA (g)	PGV (g)	PGD (cm/s)	Dur (s)
Imperial Valley	1940	0519	0437	7.0	El Centro Array # 9	8.3	.205	10.7	9.16	7.6
Imperial Valley	1940	0519	0437	7.0	El Centro Array # 9	8.3	.313	29.8	13.32	11.3
Imperial Valley	1940	0519	0437	7.0	El Centro Array # 9	8.3	.215	30.2	23.91	16.9
Tabas, Iran	1978	0916		7.4	Tabas	3.0	.688	45.6	17.04	9.5
Tabas, Iran	1978	0916		7.4	Tabas	3.0	.836	97.8	36.92	8.3
Tabas, Iran	1978	0916		7.4	Tabas	3.0	.852	121.4	94.58	7.5
Erzican, Turkey	1992	0313		6.9	Erzincan	2.0	.248	18.3	7.86	5.4
Erzican, Turkey	1992	0313		6.9	Erzincan	2.0	.515	83.9	27.35	1.5
Erzican, Turkey	1992	0313		6.9	Erzincan	2.0	.496	64.3	22.78	2.0
Cape Mendocino	1992	0425	1806	7.1	Petrolia #	9.5	.163	24.5	31.78	5.8
Cape Mendocino	1992	0425	1806	7.1	Petrolia #	9.5	.590	48.4	21.74	6.5
Cape Mendocino	1992	0425	1806	7.1	Petrolia #	9.5	.662	89.7	29.55	2.7
Kobe	1995	0116	2046	6.9	Takarazuka	1.2	.433	34.8	12.38	1.5
Kobe	1995	0116	2046	6.9	Takarazuka	1.2	.693	68.3	26.65	2.2
Kobe	1995	0116	2046	6.9	Takarazuka	1.2	.694	85.3	16.75	2.1
Kobe	1995	0116	2046	6.9	Takatori	.3	.272	16.0	4.47	7.5
Kobe	1995	0116	2046	6.9	Takatori	.3	.611	127.1	35.77	6.0
Kobe	1995	0116	2046	6.9	Takatori	.3	.616	120.7	32.72	4.8
Kocaeli, Turkey	1999	0817		7.4	Yarimca	4.4	.242	30.8	29.55	6.5
Kocaeli, Turkey	1999	0817		7.4	Yarimca	4.4	.292	62.3	44.91	6.0
Kocaeli, Turkey	1999	0817		7.4	Yarimca	4.4	.340	68.2	35.86	6.4
Chi-Chi, Taiwan	1999	0920		7.6	CHY024	9.0	.152	44.8	34.80	15.5
Chi-Chi, Taiwan	1999	0920		7.6	CHY024	9.0	.175	48.9	31.04	13.7
Chi-Chi, Taiwan	1999	0920		7.6	CHY024	9.0	.278	52.9	43.62	11.5
Chi-Chi, Taiwan	1999	0920		7.6	TCU049	4.4	.171	26.1	21.82	12.5
Chi-Chi, Taiwan	1999	0920		7.6	TCU049	4.4	.251	61.2	51.29	16.5
Chi-Chi, Taiwan	1999	0920		7.6	TCU049	4.4	.293	47.9	65.28	17.6
Chi-Chi, Taiwan	1999	0920		7.6	TCU051	8.2	.114	34.6	24.56	17.3
Chi-Chi, Taiwan	1999	0920		7.6	TCU051	8.2	.225	38.4	56.52	20.0
Chi-Chi, Taiwan	1999	0920		7.6	TCU051	8.2	.186	49.3	70.26	17.4
Chi-Chi, Taiwan	1999	0920		7.6	TCU052	.2	.241	110.5	163.51	6.2
Chi-Chi, Taiwan	1999	0920		7.6	TCU052	.2	.419	118.4	246.15	5.8
Chi-Chi, Taiwan	1999	0920		7.6	TCU052	.2	.348	159.0	184.42	6.3
Chi-Chi, Taiwan	1999	0920		7.6	TCU060	9.4	.086	27.5	24.81	16.2
Chi-Chi, Taiwan	1999	0920		7.6	TCU060	9.4	.106	45.3	45.56	20.3
Chi-Chi, Taiwan	1999	0920		7.6	TCU060	9.4	.201	36.3	51.89	17.6
Chi-Chi, Taiwan	1999	0920		7.6	TCU067	.3	.225	42.7	28.48	10.6
Chi-Chi, Taiwan	1999	0920		7.6	TCU067	.3	.325	66.6	45.95	7.6
Chi-Chi, Taiwan	1999	0920		7.6	TCU067	.3	.503	79.5	93.09	11.0
Chi-Chi, Taiwan	1999	0920		7.6	TCU068	1.0	.486	187.3	266.55	2.0
Chi-Chi, Taiwan	1999	0920		7.6	TCU068	1.0	.462	263.1	430.00	7.6
Chi-Chi, Taiwan	1999	0920		7.6	TCU068	1.0	.566	176.6	324.11	6.4
Chi-Chi, Taiwan	1999	0920		7.6	TCU072	7.3	.279	35.8	27.28	14.6
Chi-Chi, Taiwan	1999	0920		7.6	TCU072	7.3	.400	56.3	41.28	15.5
Chi-Chi, Taiwan	1999	0920		7.6	TCU072	7.3	.489	71.7	38.64	14.0
Chi-Chi, Taiwan	1999	0920		7.6	TCU076	1.9	.281	34.1	17.39	16.5
Chi-Chi, Taiwan	1999	0920		7.6	TCU076	1.9	.416	64.2	35.37	16.5
Chi-Chi, Taiwan	1999	0920		7.6	TCU076	1.9	.303	62.6	31.47	17.5
Chi-Chi, Taiwan	1999	0920		7.6	TCU082	5.7	.131	40.8	25.50	15.2
Chi-Chi, Taiwan	1999	0920		7.6	TCU082	5.7	.192	40.5	53.79	19.5
Chi-Chi, Taiwan	1999	0920		7.6	TCU082	5.7	.223	58.4	71.47	17.9
Chi-Chi, Taiwan	1999	0920		7.6	TCU101	2.9	.169	55.2	39.19	15.7
Chi-Chi, Taiwan	1999	0920		7.6	TCU101	2.9	.251	49.4	35.12	16.9
Chi-Chi, Taiwan	1999	0920		7.6	TCU101	2.9	.202	67.9	75.36	16.5
Chi-Chi, Taiwan	1999	0920		7.6	TCU102	1.7	.189	56.2	48.74	11.0
Chi-Chi, Taiwan	1999	0920		7.6	TCU102	1.7	.169	77.1	44.87	15.2
Chi-Chi, Taiwan	1999	0920		7.6	TCU102	1.7	.298	112.4	89.19	13.1
Chi-Chi, Taiwan	1999	0920		7.6	TCU128	9.7	.097	46.0	34.77	18.1
Chi-Chi, Taiwan	1999	0920		7.6	TCU128	9.7	.170	68.8	41.87	10.6
Chi-Chi, Taiwan	1999	0920		7.6	TCU128	9.7	.139	73.0	90.62	13.5
Duzce, Turkey	1999	1112		7.1	Duzce	6.7	.357	22.6	19.40	11.5
Duzce, Turkey	1999	1112		7.1	Duzce	6.7	.348	60.0	42.09	14.4
Duzce, Turkey	1999	1112		7.1	Duzce	6.7	.535	83.5	51.59	13.8

TABLE B-2: WUS, SOIL, M > 7, D = 10-50 km

Earthquake	YR	MODY	HRMN	Mag	Station	Closest Dist (km)	PGA (g)	PGV (g)	PGD (cm/s)	Dur (s)
Tabas, Iran	1978	0916		7.4	Boshrooyeh	26.1	.084	11.6	8.36	15.8
Tabas, Iran	1978	0916		7.4	Boshrooyeh	26.1	.107	13.7	10.50	14.7
Tabas, Iran	1978	0916		7.4	Boshrooyeh	26.1	.089	18.0	18.27	14.8
Taiwan SMART1(45)	1986	1114		7.3	SMART1 I01	39.0	.075	7.1	4.22	10.8
Taiwan SMART1(45)	1986	1114		7.3	SMART1 I01	39.0	.132	30.5	9.05	10.4
Taiwan SMART1(45)	1986	1114		7.3	SMART1 I01	39.0	.141	29.8	10.34	12.7
Taiwan SMART1(45)	1986	1114		7.3	SMART1 M07	39.0	.106	8.6	3.19	10.0
Taiwan SMART1(45)	1986	1114		7.3	SMART1 M07	39.0	.156	26.8	9.09	9.9
Taiwan SMART1(45)	1986	1114		7.3	SMART1 M07	39.0	.160	22.5	7.62	9.4
Taiwan SMART1(45)	1986	1114		7.3	SMART1 O08	39.0	.105	9.2	4.18	11.1
Taiwan SMART1(45)	1986	1114		7.3	SMART1 O08	39.0	.142	24.5	9.33	12.8
Taiwan SMART1(45)	1986	1114		7.3	SMART1 O08	39.0	.163	30.1	13.21	10.4
Landers	1992	0628	1158	7.3	Palm Springs Airport #	37.5	.108	6.8	3.08	22.8
Landers	1992	0628	1158	7.3	Palm Springs Airport #	37.5	.076	10.9	6.95	25.5
Landers	1992	0628	1158	7.3	Palm Springs Airport #	37.5	.089	13.8	5.29	26.2
Landers	1992	0628	1158	7.3	Yermo Fire Station #	24.9	.136	12.9	4.82	13.4
Landers	1992	0628	1158	7.3	Yermo Fire Station #	24.9	.245	51.5	43.81	7.1
Landers	1992	0628	1158	7.3	Yermo Fire Station #	24.9	.152	29.7	24.69	10.9
Kocaeli, Turkey	1999	0817		7.4	Duzce	14.2	.229	20.4	17.01	2.9
Kocaeli, Turkey	1999	0817		7.4	Duzce	14.2	.312	58.8	44.11	3.0
Kocaeli, Turkey	1999	0817		7.4	Duzce	14.2	.358	46.4	17.61	1.8
Chi-Chi, Taiwan	1999	0920		7.6	WGK	11.1	.180	25.0	16.28	11.0
Chi-Chi, Taiwan	1999	0920		7.6	WGK	11.1	.334	69.0	35.70	13.3
Chi-Chi, Taiwan	1999	0920		7.6	WGK	11.1	.484	74.4	66.92	10.2
Chi-Chi, Taiwan	1999	0920		7.6	CHY036	20.3	.104	11.3	10.18	17.3
Chi-Chi, Taiwan	1999	0920		7.6	CHY036	20.3	.207	41.4	34.17	12.3
Chi-Chi, Taiwan	1999	0920		7.6	CHY036	20.3	.294	38.9	21.19	8.7
Chi-Chi, Taiwan	1999	0920		7.6	CHY101	11.1	.165	28.0	19.73	13.0
Chi-Chi, Taiwan	1999	0920		7.6	CHY101	11.1	.440	115.0	68.75	10.3
Chi-Chi, Taiwan	1999	0920		7.6	CHY101	11.1	.353	70.6	45.28	13.5
Chi-Chi, Taiwan	1999	0920		7.6	HWA006	44.0	.063	6.9	6.81	14.3
Chi-Chi, Taiwan	1999	0920		7.6	HWA006	44.0	.089	9.2	6.11	9.3
Chi-Chi, Taiwan	1999	0920		7.6	HWA006	44.0	.083	7.3	5.89	10.0
Chi-Chi, Taiwan	1999	0920		7.6	HWA030	46.3	.049	8.2	11.65	12.5
Chi-Chi, Taiwan	1999	0920		7.6	HWA030	46.3	.079	13.8	8.48	10.6
Chi-Chi, Taiwan	1999	0920		7.6	HWA030	46.3	.070	11.0	19.95	9.5
Chi-Chi, Taiwan	1999	0920		7.6	HWA035	45.8	.054	7.5	9.60	12.1
Chi-Chi, Taiwan	1999	0920		7.6	HWA035	45.8	.074	7.5	8.88	10.1
Chi-Chi, Taiwan	1999	0920		7.6	HWA035	45.8	.078	11.9	16.89	11.4
Chi-Chi, Taiwan	1999	0920		7.6	TCU038	22.4	.067	34.6	28.80	19.2
Chi-Chi, Taiwan	1999	0920		7.6	TCU038	22.4	.168	44.9	43.60	13.1
Chi-Chi, Taiwan	1999	0920		7.6	TCU038	22.4	.141	48.9	64.17	15.9
Chi-Chi, Taiwan	1999	0920		7.6	TCU042	23.3	.086	19.7	24.09	16.0
Chi-Chi, Taiwan	1999	0920		7.6	TCU042	23.3	.199	39.3	23.86	14.8
Chi-Chi, Taiwan	1999	0920		7.6	TCU042	23.3	.246	44.8	46.91	12.7